Fluctuations and nematicity in unconventional and topological superconductors

---

Zur Erlangung des akademischen Grades eines

Doktors der Naturwissenschaften

von der KIT-Fakultät für Physik
des Karlsruher Instituts für Technologie

genehmigte

Dissertation

von

Matthias Hecker, M. Sc.
aus Eppingen

Tag der mündlichen Prüfung: 24.04.2020

Referent: Prof. Dr. Jörg Schmalian
Korreferent: Prof. Dr. Markus Garst

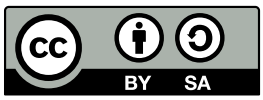

Introduction

"Imagine you want to transport oil from Vyborg in Russia to Greifswald in Germany over the Baltic sea. The oil can be transported by the means of tankers which require a relatively long shipping time, and moreover the tankers are prone to all the turbulences on the water surface: delays, detours and accidents are natural consequences thereof. In terms of transport efficiency, we would call it standard, but it is clearly far from perfect. Now, we assume there is a remarkable installation between the two cities: an underwater pipeline named North stream inside which the oil funnels constantly and undisturbed from the water surface complications, providing in that sense a perfect means for oil transportation. In the superconducting context we replace the oil by electric charge, and we imagine that the pipeline emerges spontaneously if a metal is cooled below a certain transition temperature."
In a science slam, a person aims to explain the phenomenon of superconductivity to the audience in layman's terms, sparking curiosity and, at the same time, a certain amazement... regardless of the fact that superconductivity has been around for over a century.

With the year of its discovery in 1911 by Heike Kamerlingh Onnes [1] the interest in superconductivity has been immense and has never receded. The phenomenon has kept the scientific community captivated, mostly due to its ever growing variety in superconducting materials exhibiting increasingly more fascinating physics—but also due to the enormous potential a room temperature superconductor would have for the electrical industry.

The first discovered superconductors were elemental materials like mercury or aluminum with transition temperatures of just a few Kelvin. Nowadays, these materials are called conventional superconductors—not because they have been around for so long or their critical temperature is fairly low, but because of the microscopic structure of the involved pairing state. With the development of the BCS theory [2, 3] in 1957, the emerging superconducting state could be attributed to the formation of bound pairs of electrons (Cooper pairs) and the underlying broken symmetry was identified as the $U(1)$ symmetry. The broken $U(1)$ symmetry is the origin of characteristic observations like the vanishing resistance or the transition into a perfect diamagnetic phase (Meissner phase) [4].

While conventional superconductors only break the $U(1)$ symmetry, unconventional superconductors develop a more complex pairing structure which—apart from the $U(1)$—also breaks some lattice symmetries. Interestingly, the most widespread superconductors to date fall into this category: the high-temperature superconductors. In 1986 the research interest has been boosted by the observation of a transition temperature which reached around 30 K in cuprate materials [5]. This led to an intense follow-up research effort and to the discovery of the whole family of copper-based superconductors with transition temperatures reaching as high as $\sim 140\,\mathrm{K}$ [6]. The iron-based superconductors discovered in 2008 [7] mark another family of high-temperature superconductors. These two families are just two examples of the whole class of unconventional superconductors whose physical properties are not yet fully understood. Nagging questions reach from the respective microscopic driving mechanism, over the relevance of close-by instabilities, to the role of fluctuations. Conventional superconductors are usually well characterized by a mean-field description; that is, the ground state is described by a uniform field. In contrast, unconventional superconductors are more susceptible to field variations in space and time. In the extreme cases those fluctuations can cause the collapse of the superconducting

phase-coherent state [8–10]. In this context, a central concept is the rigidity of the phase-coherent state which is quantified by the superfluid phase stiffness.

Another topic in condensed matter systems that has enjoyed a great deal of interest during the last 40 years revolves around the concept of topology. While it is often reduced to the comparison between donuts and mugs or brezels, the underlying principle is more subtle. The topological non-trivial state is equally shared between the bulk and boundary of a material - one being described by a topological index, the other hosting topologically protected gapless edge states. In 1980 the first manifestation of a topological state has been observed by van Klitzing in the form of the integer quantum Hall effect [11]. This observation sparked an intense research effort which, during the last decades, has led to the discovery of many topological materials; particularly, topological insulators [12]. Yet, the topological concept equally applies to superconducting systems. Due to the reality constraint the superconducting topological edge states have to be Majorana modes which offer, owed to their non-Abelian nature, a promising platform for quantum information applications. It has been shown that topological superconductivity can be realized on the basis of a proximitized topological insulator [13]; yet, bulk topological superconductors are scarce.

The discovery of the emergent superconducting state in the doped topological insulator Bi_2Se_3 with a $T_c \sim 3 - 4\,\mathrm{K}$ in 2009 [14] has attracted much attention with regard to its possible topological character. A few years later, the pairing state has been reported to break the C_{3z} rotational symmetry and thereby, cause a nematic distortion [15]. Follow-up experiments have consistently confirmed the finding and pointed towards the two-dimensional odd-parity pairing state. Accordingly, doped Bi_2Se_3 is a nematic superconductor. On top of that, the odd-parity pairing state is likely to be topological [16], where some experimental indications for Majorana modes have been provided [17].

It seems evident that a multitude of interesting physical aspects come together in the doped topological insulator Bi_2Se_3. As if that was not enough, its low carrier density $n \sim 10^{20}\,\mathrm{cm}^{-3}$ along with a small ratio of coherence length over Fermi wavelength $\xi_0/\lambda_F = 2..4$ make superconducting fluctuations increasingly important [14, 18, 19].

The central topic of this dissertation revolves around the concept of a fluctuation-induced nematic phase that precedes the superconducting state in the doped topological insulator Bi_2Se_3. In this scenario, the rotational C_{3z} and the superconducting $U(1)$ symmetry are separately broken at different temperatures. Using a large-N theory, we predict the existence of such a vestigial nematic phase. We study various implications thereof, and we present evidence for its existence, based on a collaboration with an experimental group [20]. This thesis is structured as follows.

The first introductory **Chapter** 1 splits into three parts. First, we provide a brief overview on the historical development of the prevailing superconducting descriptions and thereby, we introduce both, the BCS theory and the language of a Ginzburg-Landau approach. Additionally, some chosen topics including the role of the superfluid phase stiffness are discussed which are of direct relevance for the work in chapter 4. Second, the idea of a large-N theory is introduced which is the framework for the study in chapter 3. Third, we discuss the role of symmetries in condensed matter system. Thereby, we demonstrate how symmetries are imposed on a Hamiltonian, how the pairing state is classified, and how the symmetries are implemented in a free energy expansion. In various passages throughout the work, symmetry classifications are employed.

In **Chapter** 2 we introduce the concept of topology, followed by a presentation of the material, doped and undoped Bi_2Se_3. Thereby, we revisit the experimental situation, and we present the prevailing theoretical models. We derive the low-energy Hamiltonian from symmetry grounds, and we discuss the involved helical edge states. Thereafter, the emergent superconducting state in doped Bi_2Se_3 is considered. We derive the pairing state candidates, discuss their topological character and contrast

them with the experimental findings. Lastly, we study the mean-field Ginzburg-Landau theory of the two-dimensional odd-parity state and compute the relevant parameter which discriminate between the possible ground state phases.

In **Chapter** 3 we employ a vestigial nematic analysis which is designed to capture the physics in doped Bi_2Se_3. Here, the chapter splits into two large parts. In the first part, we provide an introduction on the concept of vestigial phases. Then, on the basis of a large-N theory we conduct a mean-field analysis where both, superconducting fluctuations and interactions are consistently included. The analysis is discussed on equal footing for a possible vestigial nematic or a possible vestigial chiral scenario. Then, we choose the parameters compatible with doped Bi_2Se_3, and find—depending on the z-anisotropy
—either a vestigial nematic phase where the fluctuation-induced nematic phase preempts the superconducting state, or a joint transition where both phases appear simultaneously. In the second part, the implications of a vestigial nematic phase are studied with respect to various aspects. First, we demonstrate the onset of in-plane anisotropy in the magnetic susceptibility and the conductivity together with a strong enhancement of superconducting fluctuations upon the phase transit. Then, we study the response of the underlying lattice, where the renormalization of the elastic constants due to nematic fluctuations is addressed as well as the induced lattice distortion inside the vestigial nematic phase. Lastly, we study the implications of an applied magnetic field from the viewpoint of a vestigial nematic scenario.

In **Chapter** 4 we study the role of superconducting fluctuations in a different context. The superfluid phase stiffness quantifies the strength of phase fluctuations, and its large value ensures a robust phase-coherent state. While the value has to be large in Galilean invariant systems due to the Leggett's theorem [21], the same does not hold in a Galilean non-invariant environment, like the periodic crystal lattice. In particular, the presence of a periodic lattice leads to a suppression of the phase stiffness, and in this work, we aim to quantify the magnitude of this effect. Our work has been inspired by experiments in the over-doped regime of certain cuprate superconductors [22, 23], where an unexpected suppression of the phase stiffness has been detected. Our calculations demonstrate that the suppression—mediated by superconducting fluctuations—can already for a moderate BCS coupling strength become significant. This provides a qualitative insight which may be relevant for the interpretation of some of the aforementioned data.

Contents

Chapter 1

1 Fundamentals: symmetry and spontaneous symmetry breaking

The concept of symmetries and spontaneous symmetry breaking is essential for the understanding of phase transitions. This chapter is designed to introduce the concept on the example of superconductivity.

In the first part we illustrate the historical development in the field of superconductivity. Thereby, we introduce the Ginzburg-Landau approach to phase transitions and we summarize the microscopic BCS theory. Attached is a discussion on the role of superconducting fluctuations where the relevance of the superfluid phase stiffness is emphasized. Owed to the direct relevance for the thesis at hands, in the second part we outline the general idea of the large-N approach. In the third part, we shed light on the relevant symmetries in condensed matter systems, and we derive the formalism how symmetries can be imposed on a Hamiltonian and implemented into the free energy. Additionally, we demonstrate how the superconducting pairing states can be symmetry classified.

1.1 Superconductivity

Historically, the discovery of the phenomenon of superconductivity goes back to Heike Kamerlingh Onnes [1, 24, 25], who in 1911 measured a sudden resistance drop of pure mercury at a temperature $T_c = 4.183\,\mathrm{K}$. Reaching down to those cold temperatures was a difficult task at that time. It shall be acknowledged that it was Onnes himself in 1908 who first produced liquified Helium which was essential to reach temperatures as cold as $1.5\,\mathrm{K}$. At the time he published his discovery in 1911, the theory of quantum mechanics was still in its infancy, and the scientific community simply did not have the tools to understand its origin. As we know of now, superconductivity is a quantum mechanical many-body phenomenon. From that point of view it is less surprising that it took almost half a century until theorists found a satisfying microscopical description. In 1933 Meissner and Ochsenfeld discovered a further experimental manifestation of the superconducting phenomenon, namely that a superconductor is not only a perfect electrical conductor, but also a perfect diamagnet [4]. The underlying effect became known as the Meissner effect and it is characterized by an induced current that perfectly expels external magnetic fields from its interior. The first microscopic (BCS) theory, named after its developers Bardeen, Cooper and Schrieffer, was published in 1957 [2, 3]. The BCS theory will be reviewed extensively in section 1.1.2. Here, we want to first discuss the theoretical advances made in the years prior to the development of the microscopic BCS theory. During those years

the phenomenon of superconductivity posed a core theoretical challenge. While some of the inspiring theories were disproved, others turned out to be very useful. An interesting overview on the failed theories of superconductivity can be found in Ref. [26]. Only a few years after the discovery of Meissner and Ochsenfeld, the London brothers postulated on phenomenological grounds that the superconductor should host an electrical current $\boldsymbol{j} \propto \boldsymbol{A}$ [27]. This current, also called the supercurrent counteracts the external fields and enforces an exponential magnetic field decay upon entering a superconductor. Thereby, they introduced one of the two characteristic length scales in superconductors: the London penetration depth λ_{L}. Another major advance towards the understanding of superconductivity, or more generally, towards the understanding of phase transitions, was initiated by Landau [28]. Together with Ginzburg, the two of them presented the well-known Ginzburg-Landau theory in 1950 [29, 30]. This theory provided fruitful insights and predictions, and it has an appeal in its conceptional simplicity. Moreover, its applicability reaching far beyond the realm of superconductivity. Let us pause with the history and shed some light on the ideas of this phenomenological approach.

1.1.1 Phenomenological theory

The Ginzburg-Landau theory is a phenomenological theory well-suited for the description of phase transitions. Its framework evolves around the concept of an order parameter, a quantity that is designed to be zero in the high-temperature 'disordered' phase and non-zero in the low-temperature 'ordered' phase. The phase transition is characterized through the onset of this order parameter. In a second-order phase transition the order parameter evolves continuously at the transition, whereas it jumps for a first-order transition. Implicitly, the theory assumes that the free energy is an analytical function in the vicinity of the phase transition, such that it can be expanded in terms of the order parameter to describe the behavior of the system. In the case of superconductivity, Ginzburg and Landau postulated that the order parameter is a complex number $\Delta = \Delta_0 e^{i\varphi} \in \mathbb{C}$ where $\Delta_0^2 \sim n_s \in \mathbb{R}$ measures the density of superconducting electrons, and the phase $\varphi \in \mathbb{R}$ should be of no physical significance. In other words, the free energy should be invariant under a global $U(1)$ rotation $\Delta \to \Delta e^{\mathrm{i}\varphi}$. Then, for a homogeneous superconductor the free energy expansion in terms of Δ and Δ^* reads

$$F_\Delta\left[\Delta^*, \Delta\right] = F_N + a(T)\,|\Delta|^2 + b\,|\Delta|^4 + \mathcal{O}(|\Delta|^6)\,, \tag{1.1}$$

with F_N describing the normal 'disordered' part of the system. A positive parameter b ensures the stability of the system for $\Delta \to \infty$. If it barely varies with temperature $b \neq b(T)$—as is commonly employed–the dominant temperature dependence comes from the quadratic coefficient $a(T) \approx a_0(T - T_c)$ with $a_0 > 0$ and the transition temperature T_c. An explicit derivation of a_0 (and b) is found in the appendix B.1. The key logic of the Ginzburg-Landau approach (1.1) is demonstrated in figure 1.1(a). For $T > T_c$, $a(T)$ is positive, and the expectation value Δ remains zero. Only if $a(T)$ becomes negative the system acquires a non-zero order parameter value $\Delta_0 = \sqrt{-a(T)/2b}\,\theta(-a(T))$.[1] Hence, the system undergoes a phase transition at $a(T) = 0$ where it spontaneously breaks a symmetry by picking a certain value of the phase ϕ_0 in the valley of the 'Mexican hat' potential. To be more precise, the new ground state of the system does not share the $U(1)$ symmetry of the Hamiltonian. This is known as a spontaneous symmetry breaking and will be covered in more detail in section 1.1.2. The simple form of the free energy (1.1) directly allows for a prediction of the temperature behavior of thermodynamic quantities such as the entropy $S(T)$ or the heat capacity $C_v(T)$. Indeed, the heat capacity prediction has been confirmed by an experiment in 1959 [31].

[1] We use the Heaviside step function $\theta(x)$ for a compact notation.

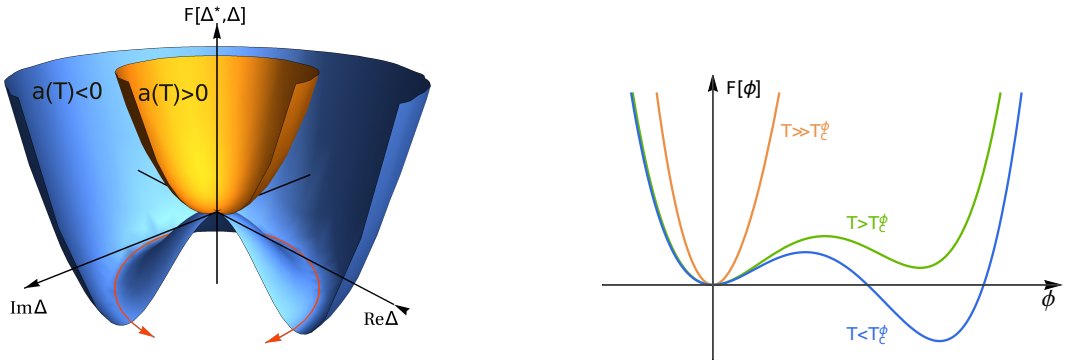

(a) **(b)**

Figure 1.1: (a) shows the free energy landscape (1.1) for a temperature above ($a(T) > 0$) and below ($a(T) < 0$) the transition temperature. The accompanying massless phase excitation is indicated along the valley of the *Mexican hat*. (b) shows a typical free energy evolution of a first-order phase transition. The phase transition happens before the quadratic expansion coefficient becomes negative.

While the initial Ginzburg-Landau version (1.1) allows for a description of a homogeneous superconductor, it can be extended to include spatial and time variations of the order parameter. To this end, one has to replace the order parameter $\Delta \to \Delta(\boldsymbol{r})$ by a field, and the free energy $F \to \int_{\boldsymbol{r}} \mathcal{F}(\boldsymbol{r})$ by a free energy density. Then, minimizations have to be carried out as functional derivatives. Focusing only on long-wavelength spatial variations, the first non-vanishing term that penalizes spatial fluctuations is of the form $(\boldsymbol{\nabla}_{\boldsymbol{r}}\Delta^*)\boldsymbol{\nabla}_{\boldsymbol{r}}\Delta$ which upon inclusion of a magnetic field becomes

$$\mathcal{F}_{\text{grad}}(\boldsymbol{r}) + \mathcal{F}_{\text{B}}(\boldsymbol{r}) = \frac{1}{2m}\Delta^*(\boldsymbol{r})\left(-\mathrm{i}\boldsymbol{\nabla}_{\boldsymbol{r}} - e^*\boldsymbol{A}(\boldsymbol{r})\right)^2\Delta(\boldsymbol{r}) + \frac{\boldsymbol{B}(\boldsymbol{r})^2}{2\mu_0}\,, \tag{1.2}$$

with the mass $m > 0$ and the charge e^* of the field $\Delta(\boldsymbol{r})$.[2] The second term represents the kinetic energy of the magnetic field with the vacuum permeability μ_0. The free energy (1.2) introduces two characteristic length scales: the correlation length ξ and the aforementioned London penetration depth λ_L. The former arises from the non-magnetic part in Eq. (1.2) and reads $\xi(T) = 1/\sqrt{2m|a(T)|}$.[3] It determines the range within which one expects a homogeneous order parameter solution. At a second-order phase transition the correlation length diverges and a homogeneous order parameter can be established over the entire sample. The remaining terms in Eq. (1.2) result from the minimal coupling of a magnetic field $\boldsymbol{B}(\boldsymbol{r}) = \boldsymbol{\nabla}_{\boldsymbol{r}} \times \boldsymbol{A}(\boldsymbol{r})$ with $\boldsymbol{A}(\boldsymbol{r})$ being the vector potential. The penetration depth

[2] In case of superconductivity the field $\Delta(\boldsymbol{r})$ describes a so-called Cooper pair with a charge $e^* = 2e$ and mass $m = 2m_e$, as will be shown in the next paragraph.

[3] The correlation length has to be distinguished from the coherence length $\xi_0 = \xi(T = 0)$. Far from the phase transition they become comparable, but at T_c only the correlation length diverges.

can be most conveniently deduced from the London equation

$$\frac{1}{V\mu_0}\nabla_{\boldsymbol{r}} \times \boldsymbol{B}(\boldsymbol{r}) = \boldsymbol{j} \approx -\frac{1}{Vm}(e^*)^2|\Delta(\boldsymbol{r})|^2\,\boldsymbol{A}(\boldsymbol{r})\,, \tag{1.3}$$

which is the result of the variation of the free energy density with respect to the vector potential $\boldsymbol{A}(\boldsymbol{r})$. The characteristic London penetration depth $\lambda_{\mathrm{L}} = \sqrt{m/\mu_0(e^*)^2\Delta_0^2}$ determines how deep a magnetic perturbation can penetrate into the superconductor. Below the transition temperature, the ratio between the two characteristic length scales, known as the Ginzburg-Landau parameter $\kappa = \lambda_{\mathrm{L}}/\xi$, becomes a characteristic of the superconductor on its own. It serves as a discriminator between type I and type II superconductors, and we refer to standard textbooks for more details [32, 33]. Let us remark a few more things on the Ginzburg-Landau theory.
First, the applicability of the Ginzburg-Landau theory is not limited to superconductivity, but can be used to study any phase transition that involves an order parameter. Popular examples involve magnetic or structural transitions which will be discussed later in section 3.4.
Second, the applicability of the Ginzburg-Landau theory is restricted to the vicinity of the phase transition as emphasized in section 3.1.
Third, although the assumption of a small order parameter around the phase transition is only justified for second-order phase transitions, the Ginzburg-Landau theory can also provide crucial insights into first-order transitions. Importantly, weak first-order transitions are still well covered. With regards to Eq. (1.1), a first order phase transition can be identified if the quartic coefficient b happens to be negative. Then, a sixth-order term $F_6 = g|\Delta|^6$ guarantees the stability of the system. A similar situation would arise for an order parameter ϕ that allows for a cubic term $F_\phi^{(3)} = g_\phi\phi^3$ in the free energy. In both examples the free energy exhibits a global minimum with a non-zero order parameter even before the quadratic coefficient $a(T)$ turns negative, as illustrated in Fig. 1.1(b). Characteristically for a first-order transition, the order parameter jumps at the transition temperature. The extent of the jump could be that pronounced such that the entire series of expansion terms would have to be included. In principle, higher-order contributions can push the additional minima above zero and thus, turn the transition back into a second-order transition. However, for a weak first-order transition, i.e. a small order parameter jump, the expanded free energy (1.1) remains its validity.
Fourth, the Ginzburg-Landau theory is a phenomenological theory in the sense that it is blind towards the microscopic origin of the order parameter and its symmetry properties. In section (1.3), we demonstrate in detail how a Ginzburg-Landau expansion can be derived on symmetry grounds. If, however, a microscopic Hamiltonian is at hands, the Ginzburg-Landau expansion parameters can be rigorously computed. Such a deduction has first been shown in the context of superconductivity by Gorkov in 1959 [34], shortly after the publication of the BCS theory.

1.1.2 Microscopic theory

While the theory by Ginzburg and Landau has provided a convincing qualitative understanding for phase transitions, it did not help to understand the mechanism of superconductivity and to unravel the question about its microscopic origin. A key advancement was achieved through the observation of the so-called isotope effect in 1950 by the groups of E. Maxwell [35] and C.A. Reynolds [36]. The experiments on different isotopes of mercury have tied the transition temperature to the mass of the nuclei, and hence, demonstrated a connection between superconductivity and the underlying lattice. Shortly before, H. Fröhlich had already predicted such a dependence [37]. He and independently, J. Bardeen [38] came to the same conclusion that the interaction between electrons and lattice vibrations

can lead to a net attraction between electrons. Later, L. Cooper has shown in 1956 [39] that the Fermi surface is unstable against the formation of a bound electron pair (now called Cooper pair) of opposite momenta and spin. In particular, he has shown that an infinitesimal attraction—such as the net attraction caused by the lattice—is sufficient to bind two such electrons in the states $(\boldsymbol{k},\uparrow)$ and $(-\boldsymbol{k},\downarrow)$. As it happens, these two constituents are exactly time-reversed partner of one another, i.e. $\mathcal{T}|\boldsymbol{k},\uparrow\rangle = |-\boldsymbol{k},\downarrow\rangle$ with the time-reversal operation $\mathcal{T}$. Thus, in a time-reversal invariant system, i.e. without any internal or external magnetic fields, the two Cooper pair constituents are guaranteed to be present at the Fermi surface. The last intellectual step has been taken by the three namesakes J. Bardeen, L. Cooper and Schrieffer of the BCS theory. They extended Cooper's instability into the environment of a many-body system where the interaction term gets decoupled in the particle-particle channel. For details on the derivations and implications we refer to standard condensed matter textbooks, such as [40]. The decoupled Hamiltonian is known as the BCS Hamiltonian

$$\hat{\mathcal{H}}_{\mathrm{BCS}} = \sum_{\boldsymbol{k},s} \epsilon_{\boldsymbol{k}} \hat{c}^{\dagger}_{\boldsymbol{k}s} \hat{c}_{\boldsymbol{k}s} + \sum_{\boldsymbol{k}} \left(\Delta \hat{c}^{\dagger}_{\boldsymbol{k}\uparrow} \hat{c}^{\dagger}_{-\boldsymbol{k}\downarrow} + H.c. \right) , \tag{1.4}$$

with the electronic dispersion $\epsilon_{\boldsymbol{k}}$ and the fermionic annihilation (creation) operators $\hat{c}_{\boldsymbol{k}s}(\hat{c}^{\dagger}_{\boldsymbol{k}s})$ in the states of momentum $\boldsymbol{k}$ and spin $s = (\uparrow,\downarrow)$. The central object $\Delta \sim \sum_{\boldsymbol{k}} \langle \hat{c}_{\boldsymbol{k}\uparrow} \hat{c}_{-\boldsymbol{k}\downarrow} \rangle$ is the many-body formulation of a Cooper pair and in the language of a Ginzburg and Landau it is the superconducting order parameter, i.e. it acquires a non-zero expectation value in the superconducting state. As a two-electron wave-function the superconducting order parameter carries a charge $e^* = 2e$. The mean-field BCS Hamiltonian (1.4) can be diagonalized by a Bogoliubov transformation [41] leading to the quasi-particle energy spectrum $E_{\boldsymbol{k}} = \sqrt{\epsilon^2_{\boldsymbol{k}} + |\Delta|^2}$, and a self-consistency equation (or gap equation) which determines the value of Δ. Let us illustrate the spontaneous $U(1)$ symmetry breaking. The BCS ground state wave-function can be explicitly written as

$$|BCS\rangle_0 = \prod_{\boldsymbol{k}} \left(\beta^{+}_{\boldsymbol{k}} + \beta^{-}_{\boldsymbol{k}} \hat{c}^{\dagger}_{\boldsymbol{k}\uparrow} \hat{c}^{\dagger}_{-\boldsymbol{k}\downarrow} \right) |0\rangle , \tag{1.5}$$

with the notation $\beta^{\pm}_{\boldsymbol{k}} = \sqrt{1 \pm \epsilon_{\boldsymbol{k}}/E_{\boldsymbol{k}}}/\sqrt{2}$ and the vacuum state $|0\rangle$. The action of the $U(1)$ symmetry operation on the fermionic and bosonic fields in (1.4) is $\hat{c}_{\boldsymbol{k}s} \to e^{\mathrm{i}\varphi/2} \hat{c}_{\boldsymbol{k}s}$, $\hat{c}^{\dagger}_{\boldsymbol{k}s} \to e^{-\mathrm{i}\varphi/2} \hat{c}^{\dagger}_{\boldsymbol{k}s}$ and $\Delta \to e^{\mathrm{i}\varphi}\Delta$ and hence, the operation leaves the Hamiltonian (1.4) invariant. However, the ground state wave-function (1.5) is no longer invariant upon such a $U(1)$ operation as it changes according to

$$|BCS\rangle_0 \to \Pi_{\boldsymbol{k}} \left(\beta^{+}_{\boldsymbol{k}} + e^{-\mathrm{i}\varphi} \beta^{-}_{\boldsymbol{k}} \hat{c}^{\dagger}_{\boldsymbol{k}\uparrow} \hat{c}^{\dagger}_{-\boldsymbol{k}\downarrow} \right) |0\rangle \ \neq |BCS\rangle_0 .$$

The property of the Hamiltonian and its ground state not sharing the same symmetry anymore is known as spontaneous symmetry breaking.

Limits of the BCS theory The BCS theory of superconductivity has become one of the most successful theories in the second half of the 20th century. Despite its success, it does not account for effects that arise from e.g. the repulsive electron-electron interaction or the actual phonon spectrum. In certain materials such as lead or mercury, known for their strong electron-phonon coupling, experimental findings (e.g. the ratio $\Delta_0(T=0)/T_c$, or with the upper critical field) have deviated from the BCS predictions. In 1960 G.M. Eliashberg has been the first to formulate a theoretical framework

that rigorously included the electron-phonon coupling and thus, generalizes the BCS theory beyond the weak-coupling limit [42, 43]. His work has been supported by A.B. Migdals's insights [44]. The role of the repulsive Coulomb interaction has equally called for thorough investigations. It was realized that the emergence of superconductivity is more robust than initially expected. While a strong Coulomb repulsion is certainly bad for the Cooper pair formation, it was realized that the problem has to be approached through the different symmetry channels, dictated by the underlying lattice. Indeed, if the projection of the Coulomb interaction leads to at least one attractive channel, a corresponding Cooper pair will form, despite the fact that all the other channels are repulsive. Superconductivity that emerges from a non-trivial symmetry channel is commonly called unconventional superconductivity.

While many unconventional superconductors have been discovered during the last decades, the pairing states and in particular, the pairing mechanism are often not yet fully understood. Among the class of unconventional superconductors are the heavy-fermion compounds like $CeCu_2Si_2$ [45] or UPt_3 [46], organic materials like $(TMTSF)_2PF_6$ [47], or the high-temperature iron-based [7] and cuprate superconductors [5]. The feature all of them have in common is breaking of at least one additional symmetry other than the $U(1)$ symmetry. As will be shown in Sec.1.3, this requires then unconventional pairing state to transform according to a non-trivial irreducible representation. A particularly interesting superconductor for the present work is doped Bi_2Se_3 which is topic of chapter 2.

1.1.3 Electrical conductivity and superconducting phase rigidity

In this section we briefly discuss selected topics in the realm of superconductivity and condensed matter theory, which will be of direct relevance for the following thesis work. The first part is about the robustness of the superconducting phase coherence against fluctuations which is quantified by the so-called superfluid phase stiffness. Large values of the phase rigidity (stiffness) protect the superconductor from a collapse caused by phase fluctuations. Then, we will proceed with a brief discussion of collective excitations that exist beside the quasi-particle excitations and hence, they affect the response of a superconductor. Next, we review the electrical conductivity where we contrast the superconducting and the metallic behavior. Thereby, we demonstrate the intimate relation between the zero resistance characteristic of a superconductor and the strength of the phase stiffness. Finally, we will briefly analyze the optical response of superconductors by studying the f-sum rule.

Phase rigidity The role of the phase rigidity is best illustrated within a Ginzburg-Landau approach. To this end, we decompose the order parameter $\Delta(x) = |\Delta(x)|e^{i\varphi(x)}$ with both, amplitude and phase depending on space and imaginary time $x = \big(\boldsymbol{r}, \tau\big)$. The insertion into the Ginzburg-Landau expansion (1.1) and (1.2) yields

$$\mathcal{F}_\Delta\left[\Delta^*, \Delta\right] = \mathcal{F}_N + \underbrace{\frac{1}{2}\rho_s\left(\nabla_{\boldsymbol{r}}\varphi - e^*\boldsymbol{A}\right)^2}_{\text{phase sector}} + \underbrace{a(T)\,|\Delta|^2 + \frac{1}{2m}(\nabla_{\boldsymbol{r}}|\Delta|)^2 + b\,|\Delta|^4}_{\text{amplitude sector}} + \frac{\boldsymbol{B}^2}{2\mu_0}\,. \tag{1.6}$$

Here, the phase stiffness $\rho_s = |\Delta|^2/m \equiv n_s/m$ with the superfluid density n_s has been introduced as the parameter that energetically penalizes spatial variations in the phase. For brevity, the explicit x-dependencies are suppressed. We note that the expansion separates into a phase and an amplitude sector. The amplitude part describes the energy cost of fluctuations in $|\Delta|$ where the characteristic length scale is set by the correlation length $\xi(T) = 1/\sqrt{2m|a(T)|}$. On length scales larger than the

correlation length, amplitude fluctuations play a negligible role and the entire physics is dominated by the phase degrees of freedom. It is the large value of the phase stiffness that protects the superconductor from a collapse caused by strong phase fluctuations. Dictated by the *Leggett's theorem* [21], the superfluid phase stiffness acquires its maximum possible value $\rho_s = n/m$ in a Galilean invariant system at zero temperature where n denotes the entire electronic density. For many conventional superconductors Leggett's theorem is applicable. As a consequence, phase fluctuations play a negligible role in these compounds and the mean-field theory provides a sufficiently good description. We refer to chapter 4 for more details on the Leggett's theorem and its limitations.
Since the vector potential $\boldsymbol{A}$ in (1.6) only couples to the phase sector, the superconducting phase has to be responsible for the supercurrent—and with it, the phase stiffness becomes the defining quantity. From Eq. (1.6) we can directly compute the induced current $\boldsymbol{j} = e^*\rho_s(\nabla_{\boldsymbol{r}}\varphi - e^*\boldsymbol{A})/V$ and extract the relation between the phase stiffness and the penetration depth $\lambda_{\mathrm{L}} = \sqrt{1/\mu_0(e^*)^2\rho_s}$ in the London limit (1.3). Being directly related to the penetration depth, the phase stiffness is experimentally easily accessible. The derivative of the current with respect to the vector potential is also known as the *London response kernel* $Q = -\rho_s(e^*)^2$, see Eq. (1.7). The finite value of the response kernel, synonymous to a finite phase stiffness, is the decisive property that causes a vanishing resistivity in the superconducting state, as shown below.

Collective excitations Apart from the Bogoliubov quasi-particles the superconducting ground state can also be excited in the form of collective excitations. The two collective excitations in place are the phase- and the amplitude mode. If we express the free energy density (1.6) in Fourier space, the corresponding dispersion relations can be directly deduced for both sectors. The amplitude mode is 'massive' with a minimal excitation energy $|\Delta|$, i.e., the energy gap of the Bogoliubov quasi-particles. Consequently, the amplitude mode, often referred to as the Higgs mode, can always decay into quasi-particles and is therefore overdamped. The phase mode is a massless excitation that is a direct manifestation of the Goldstone theorem. According to the Goldstone theorem the spontaneous breaking of a continuous symmetry—such as the $U(1)$ symmetry—is always accompanied by a massless excitation, also named the Goldstone boson. In the condensed matter context, various Goldstone bosons are known, such as the acoustic phonons in the case of translational symmetry breaking, or the magnons for a broken spin-rotation symmetry. The amplitude- and the phase mode in a superconductor can be visually understood through the Mexican hat potential, see Fig.1.1(a). A uniform phase modifications evolves along the valley without any energy cost, while amplitude modifications have to go uphill which requires a finite energy.
Once an electromagnetic field is coupled to the superconductor, a gauge transformation can fully absorb the phase mode into the vector potential: A circumstance known as the Anderson-Higgs mechanism. This mechanism renders the electromagnetic field massive and accounts for the Meissner effect.

Electrical conductivity The electrical conductivity $\sigma(\nu, \boldsymbol{q})$ is the key response function in the presence of an electromagnetic field. It relates the electron current $\boldsymbol{j}(\nu, \boldsymbol{q})$ with the applied electrical field $\boldsymbol{E}(\nu, \boldsymbol{q})$ via $\boldsymbol{j}(\nu, \boldsymbol{q}) = \sigma(\nu, \boldsymbol{q})\boldsymbol{E}(\nu, \boldsymbol{q})$. Experimentally, the conductivity is typically accessed by means of optical measurements that involve photons with energies $\omega = c\,|\boldsymbol{q}|$. Since the speed of light c is large compared to the Fermi velocity of typical metals any reasonable photon energy ω essentially corresponds to a response at $\boldsymbol{q} = 0$. For that reason, the optical conductivity defined as $\sigma(\nu, \boldsymbol{q} = 0)$ is of particular interest. From the theoretical side, the conductivity can be extracted from the expectation value of the current operator $\langle\hat{\boldsymbol{j}}(\nu, \boldsymbol{q})\rangle_{\boldsymbol{A}}$ in an applied external vector potential $\boldsymbol{A}$. In a linear

response theory, one expands the current expectation value as a function of the vector potential such that $\boldsymbol{j}(\nu,\boldsymbol{q}) = \langle\hat{\boldsymbol{j}}(\nu,\boldsymbol{q})\rangle_{\boldsymbol{A}} = Q(\nu,\boldsymbol{q})\boldsymbol{A}(\nu,\boldsymbol{q})$ with the so-called London response kernel $Q(\nu,\boldsymbol{q})$ describing the current-current correlation function. Using the relation $\boldsymbol{A}(\nu,\boldsymbol{q}) = \boldsymbol{E}(\nu,\boldsymbol{q})/\mathrm{i}\nu$ one obtains the Kubo formula

$$\sigma(\nu,\boldsymbol{q}) = \frac{Q(\nu,\boldsymbol{q})}{\mathrm{i}\nu}\,.$$

Often, it is more convenient to work in the imaginary time representation with the Kubo formula

$$\sigma(\mathrm{i}\nu_m,\boldsymbol{q}) = -\frac{Q(\mathrm{i}\nu_m,\boldsymbol{q})}{\nu_m}\,.$$

The corresponding London response kernel can be computed from the free energy $F[\boldsymbol{A}]$ via

$$Q_{\alpha\beta}(q) = -\frac{1}{V}\frac{\delta^2 F[\boldsymbol{A}]}{\delta A^{\beta}_{q}\delta A^{\alpha}_{-q}}\bigg|_{\boldsymbol{A}=0} = \frac{V}{T}\langle j^{\alpha}_{q} j^{\beta}_{-q}\rangle - \frac{V}{T}\langle j^{\alpha}_{q}\rangle\langle j^{\beta}_{-q}\rangle\,, \tag{1.7}$$

with $q = (\mathrm{i}\nu_m,\boldsymbol{q})$. In the course of this approach, an analytical continuation has to be performed to arrive at the conductivity

$$\mathrm{Re}\,\sigma(\nu+\mathrm{i}0,\boldsymbol{q}) = \frac{\mathrm{Im}\,Q(\nu+\mathrm{i}0,\boldsymbol{q})}{\nu} - \pi\delta(\nu)\;\mathrm{Re}\,Q(\nu+\mathrm{i}0,\boldsymbol{q}). \tag{1.8}$$

One key difference between the optical responses of a superconductor and of a metal lies in the zero momentum and zero frequency limit where $\mathrm{Re}\,Q^{\mathrm{sc}}(0,0) = -\rho_s(e^*)^2$ and $\mathrm{Re}\,Q^{\mathrm{metal}}(0,0) = 0$, see also Eq.(1.10) below. Then, equation (1.8) shows that the superconductor has an infinite DC optical conductivity, that leads to the observed vanishing resistivity. The weight of the delta peak, and thus the strength of the corresponding superflow, is determined by the value of the phase stiffness ρ_s.

F-sum rule Under exploitation of the so-called f-sum rule, one can visualize the change in the optical conductivity during the transition from a metal into a superconductor. According to the f-sum rule the spectral weight of the optical conductivity is a conserved quantity which equals

$$\frac{2}{\pi}\int_0^{\infty} d\nu\;\mathrm{Re}\,\sigma_{\alpha\alpha}(\nu+\mathrm{i}0,0) = \frac{ne^2}{m}\,, \tag{1.9}$$

for a system with quadratic dispersion [48]. The optical conductivity of a metal is typically well-described by the Drude formula. In the Drude picture, any scattering effect that leads to a momentum relaxation inside the conductor is captured by a single transport scattering time τ_{tr}. Then, the dominant contribution to the London response kernel in the $\boldsymbol{q}=0$ limit becomes

$$Q^{\mathrm{Drude}}_{\alpha\beta}(\nu+\mathrm{i}0,0) = \frac{ne^2}{m}\,\frac{\mathrm{i}\tau_{\mathrm{tr}}^{-1}\nu - \nu^2}{\tau_{\mathrm{tr}}^{-2}+\nu^2}\,\delta_{\alpha\beta}\,, \tag{1.10}$$

Figure 1.2: (a) shows the Drude peak (1.11) of the optical conductivity of a metal. (b) illustrates the spectral weight transfer as the system becomes a superconductor. Due to the f-sum rule (1.9), the spectral weight is conserved, and the gapped part ($\omega < 2|\Delta|$) is transferred into the weight of the delta function which is responsible for the zero resistivity.

with the electron density n, the charge e and the mass m of an electron. The resulting Drude conductivity reads

$$\operatorname{Re}\sigma_{\alpha\beta}^{\text{Drude}}(\nu + \mathrm{i}0, 0) = \frac{ne^2}{m}\,\frac{\tau_{\text{tr}}^{-1}}{\tau_{\text{tr}}^{-2} + \nu^2}\,. \tag{1.11}$$

The involved relaxation time τ_{tr} can originate from various sources such as electrons scattering off impurities, phonons or other electrons. Despite its appealing simplicity, the formula (1.11) has a severe inconsistency. It causes a contradiction with the momentum conservation. Consider a gas of non-interacting electrons with a quadratic dispersion relation. Then, the total momentum is conserved, implying that it never decays and the momentum relaxation time τ_{tr} becomes infinite. As a consequence, the Drude conductivity (1.11) would diverge, which is an obviously unphysical result. It has to be evaded through the inclusion of the aforementioned momentum-relaxing scattering processes.

A consequence of the conserved spectral weight is illustrated in figure 1.2. As the metal transits into the superconducting state the spectral weight within the superconducting gap $0 < \nu < 2|\Delta|$ gets transferred into the weight of the delta function, i.e. into the phase stiffness. The implications of this issue will be further studied in chapter 4.

1.2 Saddle-point solutions and the key idea of a large-N theory

In condensed matter systems, many problems are approached within a functional field integral formalism. In this language the partition function $Z = \int \mathcal{D}\phi \exp(-\beta\mathcal{S}[\phi])$ becomes an integral over some bosonic (or fermionic) field variable ϕ. By setting k_B to unity, $\beta = 1/T$ is the inverse temperature and the energy and temperature are measured in the same units. The microscopic theory is encapsulated in the action $\mathcal{S}[\phi]$. The action can be expanded around a saddle-point value ϕ_0 (given the action is analytical and the value ϕ_0 exists) according to

$$\mathcal{S}\left[\phi\right] \approx \mathcal{S}\left[\phi_0\right] + \frac{\delta\mathcal{S}}{\delta\phi}\Big|_{\phi_0}\left(\phi - \phi_0\right) + \frac{1}{2}\frac{\delta^2\mathcal{S}}{\delta\phi^2}\Big|_{\phi_0}\left(\phi - \phi_0\right)^2 + \dots\,, \tag{1.12}$$

where the condition $\frac{\delta \mathcal{S}}{\delta \phi}\Big|_{\phi_0} = 0$ determines the value ϕ_0. If the expansion is truncated at the second order, the partition function becomes

$$Z \approx e^{-\beta \mathcal{S}[\phi_0]} \int \mathcal{D}\phi \exp\Big(-\beta \frac{1}{2} \frac{\delta^2 \mathcal{S}}{\delta \phi^2}\Big|_{\phi_0} (\phi - \phi_0)^2 \Big) . \tag{1.13}$$

For a large prefactor

$$\beta \frac{1}{2} \frac{\delta^2 \mathcal{S}}{\delta \phi^2}\Big|_{\phi_0} \phi_0^2 \gg 1 \,, \tag{1.14}$$

the exponential evolves into a delta function $\delta(\phi - \phi_0)$ that evaluates every correlation function at its mean-field value. In the limit set by (1.14) fluctuations of ϕ around the saddle-point value are negligible and the free energy (using $Z = \exp(-\beta F)$) coincides with the mean-field action $F\left[\phi_0\right] \approx \mathcal{S}\left[\phi_0\right]$. Due to its simplicity, the saddle-point approach has a certain appeal. Yet, its applicability depends crucially on the satisfaction of the condition (1.14). In numerous cases the action scales with the volume (it has the volume as a prefactor) such that the thermodynamic limit ($V \to \infty$) justifies the mean-field treatment. However, in the absence of such a naturally large prefactor, one has to become more inventive, and for example, turn towards a large-N approach.

The key idea of a large-N theory lies in the extension of a single field variable ϕ to a vector $\boldsymbol{\phi} = (\phi_1, \phi_2, \ldots, \phi_N)^T$ with a large number of components $N \gg 1$ [49]. For an action that scales with the value N, the parameter N becomes the large prefactor that validates the saddle-point condition (1.14). In such an approach, one has to consistently treat the number N as the largest 'scale' in the problem.

In the typical textbook example, the $(\boldsymbol{\phi}^2)^2$ theory, the large-N action reads

$$\mathcal{S}\left[\boldsymbol{\phi}\right] = r_0 \boldsymbol{\phi}^2 + \frac{u_0}{N} \left(\boldsymbol{\phi}^2\right)^2 . \tag{1.15}$$

Commonly, the action is decoupled by means of a Hubbard-Stratonovich transformation, see e.g. Eq.(3.6). This procedure introduces a new field λ, makes the action $\mathcal{S}[\boldsymbol{\phi}, \lambda]$ quadratic in $\boldsymbol{\phi}$ and allows for the subsequent integration,

$$\mathcal{S}\left[\boldsymbol{\phi}, \lambda\right] = \left(r_0 + \lambda\right) \boldsymbol{\phi}^2 - \frac{N}{u_0} \lambda^2 \,, \qquad \overset{\int \mathcal{D}\boldsymbol{\phi}}{\longrightarrow} \qquad \mathcal{S}'\left[\lambda\right] = N \Big(-\frac{1}{u_0} \lambda^2 + \frac{1}{2} \mathrm{tr} \log\left(r_0 + \lambda\right) \Big) . \tag{1.16}$$

The resulting effective action $\mathcal{S}'[\lambda]$ still contains the entire information of the problem, though it is represented in a different form. The integration in (1.16) has been carried out N times, which leads to the overall prefactor N and which would be used to justify an ensuing saddle-point analysis. This is one example of a large-N implementation and it will used in chapter 3.

While it is straightforward to construct a theory with innumerable components, the number of components of most realistic models is still close to one. Oftentimes, the large-N results have provided useful insights and made correct predictions. Yet, to actually demonstrate that the approach is applicable, i.e. to prove the condition (1.14) is difficult. The single tool to establish a justification is a numeric calculation. As an example, the large-N prediction for a classical $J_1 - J_2$ model on a square lattice is an Ising-nematic transition which has been directly observed in a Monte Carlo study [50, 51].

1.3 Symmetry constraints

Symmetries play a central role in the description of phase transitions. In this section, we introduce the symmetries that are relevant to solid state systems and derive a formalism on how they are implemented on the generalized BCS Hamiltonian, as well as on a Ginzburg-Landau expansion. For this, we have a picture in mind where a high-temperature phase has all the relevant symmetries intact, and at least one of the symmetries gets broken as the system transits into the ordered state. We specifically restrict the derivation to the temperature as the tuning parameter that causes the phase transition. One could equally formulate a similar theory with external tuning parameters like pressure, chemical doping or magnetic field that drive the transitions. The symmetries that play a role in condensed matter are the real space lattice symmetries, spin rotation symmetries, the $U(1)$ gauge symmetry and time-reversal symmetry. We comprise the unitary operations into the symmetry group $\mathcal{G} = \mathcal{G}_0 \times U(1)$, where $\mathcal{G}_0$ contains all the lattice symmetries including spin rotations. The time-reversal symmetry is described by an anti-unitary operator and will be treated separately. On a fundamental level, a system possesses a certain symmetry if the system Hamiltonian $\hat{\mathcal{H}}$ commutes with the corresponding symmetry operation $\hat{O}$, i.e.

$$\left[\hat{\mathcal{H}}, \hat{O}\right] = 0 \qquad \leftrightarrow \qquad \hat{\mathcal{H}} = \hat{O}\hat{\mathcal{H}}\hat{O}^\dagger \equiv \hat{\mathcal{H}}_O \,, \tag{1.17}$$

with the transformed Hamiltonian $\hat{\mathcal{H}}_O$. We have used $\hat{O}^{-1} = \hat{O}^\dagger$.[4] In the following, we provide an introduction into the theory of lattice and spin-space symmetries. For further reading we refer to the textbooks [52–54].

1.3.1 Rotations, inversion and translations

Point group elements Every physical lattice has a given set of symmetry operation that leaves a single lattice point and its environment invariant. We denote this set as $\mathcal{G}_p$, the set of point group symmetry elements, and we note that there is a total of 32 possible point groups. Point group symmetry elements comprise real-space rotations, the inversion operation, and combinations thereof. The framework of group theory has clear rules that dictate how the group elements can be arranged into classes and how a character table can be formed from those. In table 1.1 we show exemplary the character tables of the point groups $\mathsf{D_3}$, $\mathsf{C_3}$ and $\mathsf{D_{3d}}$. It is worth pointing out that every lattice rotation has its origin in the fully-rotational invariant $SO(3)$ representation which is characterized by the operator

$$R_{SO(3)}(\vartheta, \hat{\boldsymbol{n}}) = \exp\left(-\mathrm{i}\vartheta\, \boldsymbol{J}\cdot\hat{\boldsymbol{n}}\right) \,, \tag{1.18}$$

with the angle ϑ, the unit rotation axis $\hat{\boldsymbol{n}}$, and $\boldsymbol{J} = (J_1, J_2, J_3)$ being the $|\boldsymbol{J}| = 1$ angular momentum, where $(J_k)_{ij} = -\mathrm{i}\epsilon_{ijk}$. The rotation operator $R^*_{SO(3)}(\vartheta, \hat{\boldsymbol{n}}) = R_{SO(3)}(\vartheta, \hat{\boldsymbol{n}})$ is real. As an example, the point group $\mathsf{D_3}$ consists of a set of six distinct rotation. These six rotation elements arrange into three classes, and according to basic group theory rules, this leads to three so-called irreducible representations (IRs), namely $\{A_1, A_2, E\}$. The IRs play an essential role in the symmetry classification as they form a basis into which every function f in the space operated on by the group elements g can

[4] Only the particle-hole and the chiral symmetry are defined through an anti-commutation with the Hamiltonian, see section 2.1.

be decomposed,

$$f = \sum_{n} \sum_{\mu=1}^{\dim(n)} f^{n,\mu} \,. \tag{1.19}$$

Throughout this work we use the notation where n denotes an IR and $\mu = 1...\dim(n)$ counts the respective components. The basis (1.19) is a reasonable choice since different IRs, i.e. different symmetry channels, decouple from each other on a quadratic level, as shown in section (1.3.5). The transformation matrix for a group element $g \in \mathcal{G}$ of a certain IR n is denoted by $\mathcal{R}_n(g)$. (For one-dimensional IRs, the 'matrix' $\mathcal{R}_n(g)$ is simply a scalar and equal to the character of the element g.) The character $\chi_n(g)$ of a group element g within an IR n is defined as $\chi_n(g) = \mathrm{tr}\mathcal{R}_n(g)$ and appears as an entry in the character table. The dimension of an IR n is identical to $\chi_n(E)$ with E being the identity element. The vector representation in the last column of the character table denotes the IRs according to which the coordinates transform. The corresponding matrices read $\mathcal{R}_v(g)$.

Irreducible representations can be complex if the so-called Frobenius-Schur test yields zero.[5] In that case, they occur in conjugated pairs, n and $\bar{n}$, and the corresponding transformation matrices are complex conjugates of one another $\mathcal{R}_{\bar{n}}(g) = \mathcal{R}_n^*(g)$, see e.g. the $\mathsf{C_3}$ point group.[6]

Apart from the pure rotation elements, lattice symmetry elements also involve any combination of a rotation and the inversion operation. The inversion element is distinct because it commutes with every other point group element. Depending on whether a system possesses the inversion symmetry or not, the system is classified as centro- or non-centro-symmetric. A centro-symmetric point group can always be written as a direct product between the inversion group $\{E, I\}$ and the corresponding proper subgroup, e.g. $\mathsf{D_{3d}} = \mathsf{D_3} \times \{E, I\}$. Accordingly, the character table is doubled and the IRs are classified as even (g for 'gerade') and odd (u for 'ungerade') depending on their behavior upon inversion.

Spin rotations Let us consider symmetries related to spins, in particular to spin 1/2 systems suited for electrons. An isolated spin has a full rotational invariance that is described by the $SU(2)$ representation. The corresponding spin rotation operator reads

$$R_{SU(2)}(\vartheta, \hat{\boldsymbol{n}}) = \exp\left(-\mathrm{i}\frac{\vartheta}{2}\,\mathfrak{s}\cdot\hat{\boldsymbol{n}}\right) , \tag{1.20}$$

with the rotation angle ϑ and the unit rotation axis $\hat{\boldsymbol{n}}$. In a lattice systems one would expect that the spin rotational invariance has to be broken due to the interaction with neighboring atoms. While strictly speaking, the statement is always true, the magnitude of the effect crucially depends on the strength of the spin-orbit coupling (SOC). There are many materials where the role of the spin-orbit coupling is negligible such that there is effectively no communication between the 'spin world' and the 'real world' and the spin technically retains its full $SU(2)$ invariance. Such a system is then described within the symmetry group $\mathcal{G}_0 = \mathcal{G}_p \times SU(2)$. Spin-orbit coupling is a relativistic effect that originates from the motion of electrons. It can be viewed as a current loop that generates a magnetic field

[5] The Frobenius-Schur test evaluates $\sum_g \chi_n(g^2)$.

[6] There is a subtlety as to why the IRs are denoted by E—usually used for two-dimensional IRs—even though they transform according to a one-dimensional IR upon the point group symmetry operations. It is the time-reversal symmetry that transforms one into the other, and hence, lumps the two into a two-dimesional IR.

$\mathsf{D_3}$	E	$2C_{3z}$	$3C_{2x}$	$\boldsymbol{r}$
A_1	1	1	1	
A_2	1	1	-1	z
E	2	-1	0	(x, y)

$\mathsf{C_3}$	E	C_3	C_3^2	$\boldsymbol{r}$
A	1	1	1	z
E	1	ϵ	ϵ^*	$x + \mathrm{i}y$
$\bar{E}$	1	ϵ^*	ϵ	$x - \mathrm{i}y$

$\mathsf{D_{3d}}$	E	$2C_{3z}$	$3C_{2x}$	I	$2IC_{3z}$	$3IC_{2x}$	$\boldsymbol{r}$
A_{1g}	1	1	1	1	1	1	
A_{2g}	1	1	-1	1	1	-1	
E_g	2	-1	0	2	-1	0	
A_{1u}	1	1	1	-1	-1	-1	
A_{2u}	1	1	-1	-1	-1	1	z
E_u	2	-1	0	-2	1	0	(x, y)

Table 1.1: Character tables of the points groups $\mathsf{D_3}$, $\mathsf{C_3}$ and $\mathsf{D_{3d}}$, where $\epsilon = \exp\big(\mathrm{i}2\pi/3\big)$.

which interacts with the immanent magnetic moments of the electrons (the spins). Thus, there is a net coupling between the orbital motion in real space and the spin. The corresponding microscopic spin-orbit coupling Hamiltonian can be cast in the form

$$\mathcal{H}_{SOC} = \frac{e}{4m^2c^2}\boldsymbol{p}\cdot\left(\mathfrak{s}\times\boldsymbol{\nabla}V\right) ,$$

with mass m, charge e and momentum $\boldsymbol{p}$ of the electron, the electric potential V caused by the electrons, the speed of light c and the Pauli matrix vector $\mathfrak{s} = (\mathfrak{s}_x, \mathfrak{s}_y, \mathfrak{s}_z)$.
In a system where spin-orbit coupling is relevant, the spin is locked to the lattice degrees of freedom and they transform jointly. Then, the 4π periodicity of the spinor has to be accounted for in order to be implemented into the body of group theory. This leads to the so-called *double group* $\mathcal{G}_p'$ where rotations about the angle ϑ and $\vartheta + 2\pi$ are distinct. As a consequence, the amount of symmetry elements is doubled explaining its name-giving. As an example, let us generate the double group $\mathsf{D_3'}$ from the point group $\mathsf{D_3}$. Then, the six elements $\{\bar{E}, \bar{C}_{3z}, \bar{C}_{3z}^{-1}, \bar{C}_{2x}, \bar{C}_{2A}, \bar{C}_{2B}\}$[7] are added to the group $\mathsf{D_3}$ where the bar denotes that the rotation winds by the angle $\varphi + 2\pi$. To determine the new multiplication table one can use the spinor representation and express the elements as $C_{2x} = R_{SU(2)}(\pi, \hat{\boldsymbol{e}}_x)$, $\bar{C}_{2x} = R_{SU(2)}(3\pi, \hat{\boldsymbol{e}}_x)$, and so forth. Similar to the ordinary point group, the character table of the double group (see table 2.2) follows from the multiplication table. Double groups always contain the original point group, i.e. the original IRs with the trivial $\varphi + 2\pi$ rotations are always part of it (in the $\mathsf{D_3'}$ case A_1, A_2,E_1) [53]. Additionally, three IRs (E_2, $\bar{E}_2$ and E_3) have been added to the character table 2.2 where all of them transform odd upon the 2π rotation $\bar{E}$, i.e. they are qualified as possible electronic representations. Since the inversion operation also commutes with all the elements of $\mathsf{D_3'}$, the double group $\mathsf{D_{3d}'}$ can be directly constructed as the direct product $\mathsf{D_{3d}'} = \mathsf{D_3'} \times \{E, I\}$.

[7] The A and B axes read $\hat{\boldsymbol{n}}_{A,B} = (\pm 1, -\sqrt{3}, 0)/2$.

D_3'	E	$2C_{3z}$	$3C_{2x}$	$\bar{E}$	$2\bar{C}_{3z}$	$3\bar{C}_{2x}$	$\boldsymbol{r}$
A_1	1	1	1	1	1	1	
A_2	1	1	-1	1	1	-1	z
E_1	2	-1	0	2	-1	0	(x, y)
E_2	1	-1	i	-1	1	-i	
$\bar{E}_2$	1	-1	-i	-1	1	i	
E_3	2	1	0	-2	-1	0	

Table 1.2: Character table of the double group D_3'. The elements group into the classes like $2C_{3z} = \{C_{3z}, C_{3z}^{-1}\}$, $2\bar{C}_{3z} = \{\bar{C}_{3z}, \bar{C}_{3z}^{-1}\}$, $3C_{2x} = \{C_{2x}, \bar{C}_{2A}, \bar{C}_{2B}\}$ and $3\bar{C}_{2x} = \{\bar{C}_{2x}, C_{2A}, C_{2B}\}$.

Translations The lattice translation symmetry accounts for the equality of every lattice point. It is described by the set of translation vectors

$$\boldsymbol{T}_{\boldsymbol{l}} = l_1\boldsymbol{t}_1 + l_2\boldsymbol{t}_2 + l_3\boldsymbol{t}_3\,, \qquad \boldsymbol{l} = \big(l_1, l_2, l_3\big)\,, \qquad l_i \in \mathbb{Z}\,,$$

that cover every lattice point and form the group of translations $\mathbb{T}$. Here, $\boldsymbol{t}_1$,$\boldsymbol{t}_2$,$\boldsymbol{t}_3$ denote the primitive lattice vectors. Together, rotation and translation elements form the so-called *space group* $\mathcal{G}_s$ which contains the whole set of coordinate transformations that map the lattice onto itself. In three dimensions there is a total of 230 different space groups. Yet, for many application one does not need the entire space group information. For example, if one wants to study a quantity that is expected to be identical at every lattice point, the necessary symmetry information is already contained in the underlying point group. In the remaining work we deal with homogeneous mean-field solutions where the point group picture suffices.

Lastly, we mention the concept of *extended point groups*. The extended point group allows for a handy symmetry description of an inhomogeneous, but commensurate state. In such a state, e.g. an anti-ferromagnet, the actual unit cell is larger than the crystal unit cell. Moreover, the larger unit cell requires larger primitive vectors and the commensurate state identifies a set of translations, the group $\mathbb{T}_f$, which do not leave the state invariant. Then, this translational group $\mathbb{T}_f$ is incorporated into the point group $\mathcal{G}_p$ by means of an induced representation [53] leading to the extended point group. The resulting character table contains IRs according to which the commensurate state transforms.

1.3.2 Time-reversal symmetry

This section is devoted to a particular symmetry operation acting on time: The time-reversal operation $\hat{\mathcal{T}}$ reverses the arrow of time $t \to -t$, and the corresponding symmetry evaluates whether the evolution backwards in time mimics the forward evolution. Let us illustrate the meaning on the classical example of a dissipative system where a particle comes to rest due to friction. The evolution backwards in time accelerates the particle spontaneously from rest, a circumstance that clearly contradicts our physical intuition. Another example of a system without time-reversal symmetry is a charged particle that spirals around a fixed magnetic field. Upon a reversal of the direction of time, the particle still spirals around the magnetic field, but its orientation towards the magnetic field lines has changed. An important observation in this context is that magnetic fields break the time-reversal symmetry.

In the quantum mechanical world, it is the Hamiltonian $\hat{\mathcal{H}}$ that governs the time evolution from a state $|\psi_i\rangle$ to a state $|\psi_f\rangle = \exp(-\mathrm{i}\delta t\,\hat{\mathcal{H}})|\psi_i\rangle$. The application of the time-reversal operation leads to the time-reversed state $\hat{\mathcal{T}}|\psi_i\rangle = \exp(-\mathrm{i}\delta t\,\hat{\mathcal{H}}_{\mathcal{T}})\hat{\mathcal{T}}|\psi_f\rangle$ that evolves with the time-reversed Hamiltonian $\hat{\mathcal{H}}_{\mathcal{T}} = \hat{\mathcal{T}}\hat{\mathcal{H}}\hat{\mathcal{T}}^\dagger$ from state $\hat{\mathcal{T}}|\psi_f\rangle$ to $\hat{\mathcal{T}}|\psi_i\rangle$. The system is said to obey the time-reversal symmetry if the time-reversed and the original Hamiltonian $\hat{\mathcal{H}}_{\mathcal{T}} = \hat{\mathcal{H}}$ are identical, i.e. if the Hamiltonian commutes with the time-reversal operation $[\hat{\mathcal{H}}, \hat{\mathcal{T}}] = 0$. Formally, the time-reversal operator is an anti-unitary operator[8] $\hat{\mathcal{T}} = \hat{\mathcal{U}}_{\mathcal{T}}\,\mathcal{K}$ with $\hat{\mathcal{T}}^{-1} = \hat{\mathcal{T}}^\dagger$. An anti-unitary operator can always be written as a product of a unitary operation $\hat{\mathcal{U}}_{\mathcal{T}}$ and the complex conjugation operation $\mathcal{K}$. The time-reversal operation squares to $\hat{\mathcal{T}}^2 = \pm 1$, where the plus and minus sign applies to integer and half-integer spin particles, respectively. In the remainder of this work we will only deal with electronic theories such that the minus sign applies and the unitary matrix has to be anti-symmetric $\hat{\mathcal{U}}_{\mathcal{T}}^T = -\hat{\mathcal{U}}_{\mathcal{T}}$. Let us examine the action of the time-reversal operation on the eigenstate $|\boldsymbol{k}, s_\alpha\rangle$ of the system Hamiltonian with momentum $\boldsymbol{k}$ and spin $s \in \{\uparrow, \downarrow\}$. Here, the time-reversal operation inverses the momentum and flips the spin leading to the state $\hat{\mathcal{T}}|\boldsymbol{k}, s_\alpha\rangle = |-\boldsymbol{k}, \mathrm{i}\tau^y_{\alpha\beta} s_\beta\rangle$ where the relative minus sign ($\mathrm{i}\tau^y$) accounts for $\hat{\mathcal{T}}^2 = -1$. The action of the time-reversal operation can be conveniently generalized to $\mathcal{T} = \exp(-\mathrm{i}\pi S_y)\mathcal{K}$ with the S_y-component of the total spin $\boldsymbol{S}$ [55].

Kramer's theorem The role of the time-reversal symmetry in the context of superconductivity is immense. As introduced in Sec. 1.1.2, the two constituents of the Cooper pair are time-reversed partners, and their mutual existence at the Fermi energy is owed to the Kramer's degeneracy as a consequence of the time-reversal symmetry. The Kramer's theorem says that an energy level is at least two-fold degenerate in case of a time-reversal invariant Hamiltonian that describes an odd number of half-integer spin particles. The proof is simple and goes as follows: From the commutation relation $[\hat{\mathcal{H}}, \hat{\mathcal{T}}] = 0$ follows that $|\psi\rangle$ and $\hat{\mathcal{T}}|\psi\rangle$ are two eigenstates of the Hamiltonian with the same eigenvalue. The question is whether both states represent the same state or if they are linearly independent solutions. For $\hat{\mathcal{U}}_{\mathcal{T}}^T = -\hat{\mathcal{U}}_{\mathcal{T}}$ it is easily shown that it holds $\langle\psi|\hat{\mathcal{T}}\psi\rangle = -\langle\psi|\hat{\mathcal{T}}\psi\rangle = 0$. Thus, the two states are not only linearly independent but even orthogonal. The preceding condition only holds for a half-integer total spin $S = \sum N_i s_i$, i.e. for an odd number N_i of half-integer particles.

1.3.3 Constraints on the generalized mean-field Hamiltonian

In this section, we impose the $U(1)$, the time-reversal and the lattice symmetries on a generalized BCS Hamiltonian and we deduce the resultant constraints on its constituents: the single-particle Hamiltonian and the pairing field. The following formalism could similarly be imposed on any Hamiltonian but for the purpose of this work, it is most convenient to study the implications on the superconducting Hamiltonian. The generalized mean-field BCS Hamiltonian reads

$$\hat{\mathcal{H}} = \sum_{\boldsymbol{k}} \hat{c}^\dagger_{\boldsymbol{k},\alpha} h_{\alpha\beta}(\boldsymbol{k}) \hat{c}_{\boldsymbol{k},\beta} + \sum_{\boldsymbol{k},\boldsymbol{q}} \left(\hat{c}^\dagger_{\boldsymbol{k}+\frac{\boldsymbol{q}}{2},\alpha} \Delta_{\alpha\beta}(\boldsymbol{k},\boldsymbol{q}) \hat{c}^\dagger_{-\boldsymbol{k}+\frac{\boldsymbol{q}}{2},\beta} + H.c. \right), \tag{1.21}$$

where $\hat{c}_{\boldsymbol{k},\alpha}$ and $\hat{c}^\dagger_{\boldsymbol{k},\alpha}$ denote fermionic annihilation and creation operators for the quasi-particle state $(\boldsymbol{k}, \alpha)$. The Hamiltonian (1.21) generalizes the BCS Hamiltonian (1.4) in the sense, that the pairing field $\Delta_{\alpha\beta}(\boldsymbol{k}, \boldsymbol{q})$ is a matrix in the space of the microscopic degrees of freedom $\alpha, \beta = 1, .., N_0$ which comprise spin, orbitals, layers in stacked system and so forth. In comparison to the original BCS

[8] An operator $\hat{T}$ is anti-unitary if and only if it fulfils $\hat{T}^\dagger\hat{T} = \hat{T}\hat{T}^\dagger = \mathbb{1}$, and it is anti-linear, i.e. $\hat{T}c = c^*\hat{T}$ for any $c \in \mathbb{C}$.

theory where only singlet pairing—between a spin up and a spin down electron—was considered, the generalized pairing field $\Delta_{\alpha\beta}(\boldsymbol{k},\boldsymbol{q})$ allows for pairing between any of the above degrees of freedom. The dependence on the center-of-mass momentum $\boldsymbol{q}$ genuinely entails an inhomogeneous pairing state that varies in amplitude from unit cell to unit cell. In the present derivation, the momentum $\boldsymbol{q}$ is included to eventually study 'small' fluctuations on top of the homogeneous ground state. For that matter, it suffices to satisfy the point group symmetries instead of the entire space group. The function $h(\boldsymbol{k})$ is referred to as the single-particle Hamiltonian, as it contains all the band structure information of the non-interacting part.
In what follows it is important to properly distinguish between first and second quantized operators. We use hats to denote the latter, i.e. $\mathcal{T}$ and $\hat{\mathcal{T}}$ are the time-reversal operators acting in single-particle and in Fock space, respectively.

$U(1)$ symmetry Upon the action of the $U(1)$ gauge symmetry the fermionic operators transform as $\hat{c}^\dagger_{\boldsymbol{k},\alpha} \to \hat{c}^\dagger_{\boldsymbol{k},\alpha} e^{-\mathrm{i}\varphi/2}$ and $\hat{c}_{\boldsymbol{k},\alpha} \to \hat{c}_{\boldsymbol{k},\alpha} e^{\mathrm{i}\varphi/2}$. Therefore, the enforced invariance of the Hamiltonian (1.21) under this symmetry operation requires the pairing function to transforms as

$$\Delta_{\alpha\beta}(\boldsymbol{k},\boldsymbol{q}) \overset{U(1)}{\to} \Delta_{\alpha\beta}(\boldsymbol{k},\boldsymbol{q}) e^{\mathrm{i}\varphi} \,. \tag{1.22}$$

One arrives at the same conclusion arguing from the two-particle wave-function perspective $\Delta \sim \langle \hat{c}\hat{c} \rangle$.

Time-reversal symmetry In the present electronic theory, the particles have half-integer spins. Then, the time-reversal operator $\hat{\mathcal{T}} = \hat{\mathcal{U}}_{\mathcal{T}} \mathcal{K}$ with $\hat{\mathcal{T}}^{-1} = \hat{\mathcal{T}}^\dagger$ has to satisfy $\hat{\mathcal{T}}^2 = -1$ and as a consequence thereof, it holds $\hat{\mathcal{U}}^T_{\mathcal{T}} = -\hat{\mathcal{U}}_{\mathcal{T}}$. For the sake of generality, we leave the unitary matrix $\hat{\mathcal{U}}_{\mathcal{T}}$ unspecified. The action on the fermionic operators is defined by

$$\hat{\mathcal{T}} \hat{c}^\dagger_{\boldsymbol{k},\alpha} \hat{\mathcal{T}}^\dagger = \hat{c}^\dagger_{-\boldsymbol{k},\alpha'} \Big(\mathcal{U}_{\mathcal{T}}\Big)_{\alpha'\alpha} , \qquad \hat{\mathcal{T}} \hat{c}_{\boldsymbol{k},\alpha} \hat{\mathcal{T}}^\dagger = \Big(\mathcal{U}^\dagger_{\mathcal{T}}\Big)_{\alpha\alpha'} \hat{c}_{-\boldsymbol{k},\alpha'} \,, \tag{1.23}$$

with the inverted crystal momentum $\boldsymbol{k} \to -\boldsymbol{k}$. Note that the matrix $\mathcal{U}_{\mathcal{T}}$ does not act in Fock space. Time-reversal invariance implies $\hat{\mathcal{H}}_{\mathcal{T}} \equiv \hat{\mathcal{T}} \hat{\mathcal{H}} \hat{\mathcal{T}}^\dagger = \hat{\mathcal{H}}$ (cf. 1.17) and thus, we compute the time-reversed Hamiltonian[9]

$$\begin{aligned}
\hat{\mathcal{H}}_{\mathcal{T}} &= \sum_{\boldsymbol{k}} \underbrace{\hat{\mathcal{T}} \Big(\hat{\boldsymbol{c}}^\dagger_{\boldsymbol{k}}\Big)^T \hat{\mathcal{T}}^\dagger}_{(\hat{\boldsymbol{c}}^\dagger_{-\boldsymbol{k}})^T \mathcal{U}_{\mathcal{T}}} \mathcal{K} h(\boldsymbol{k}) \mathcal{K} \underbrace{\hat{\mathcal{T}} \hat{\boldsymbol{c}}_{\boldsymbol{k}} \hat{\mathcal{T}}^\dagger}_{\mathcal{U}^\dagger_{\mathcal{T}} \hat{\boldsymbol{c}}_{-\boldsymbol{k}}} + \sum_{\boldsymbol{k},\boldsymbol{q}} \Big(\underbrace{\hat{\mathcal{T}} \Big(\hat{\boldsymbol{c}}^\dagger_{\boldsymbol{k}+\frac{\boldsymbol{q}}{2}}\Big)^T \hat{\mathcal{T}}^\dagger}_{(\hat{\boldsymbol{c}}^\dagger_{-\boldsymbol{k}-\frac{\boldsymbol{q}}{2}})^T \mathcal{U}_{\mathcal{T}}} \mathcal{K} \Delta(\boldsymbol{k},\boldsymbol{q}) \mathcal{K} \underbrace{\hat{\mathcal{T}} \hat{\boldsymbol{c}}^\dagger_{-\boldsymbol{k}+\frac{\boldsymbol{q}}{2}} \hat{\mathcal{T}}^\dagger}_{\mathcal{U}^T_{\mathcal{T}} \hat{\boldsymbol{c}}^\dagger_{\boldsymbol{k}-\frac{\boldsymbol{q}}{2}}} + H.c. \Big) \\
&= \sum_{\boldsymbol{k}} \Big(\hat{\boldsymbol{c}}^\dagger_{\boldsymbol{k}}\Big)^T \, \mathcal{T} \, h(-\boldsymbol{k}) \, \mathcal{T}^\dagger \, \hat{\boldsymbol{c}}_{\boldsymbol{k}} + \sum_{\boldsymbol{k},\boldsymbol{q}} \Big(\Big(\hat{\boldsymbol{c}}^\dagger_{\boldsymbol{k}+\frac{\boldsymbol{q}}{2}}\Big)^T \mathcal{T} \, \Delta(-\boldsymbol{k},-\boldsymbol{q}) \, \mathcal{T}^T \, \hat{\boldsymbol{c}}^\dagger_{-\boldsymbol{k}+\frac{\boldsymbol{q}}{2}} + H.c. \Big) \,,
\end{aligned} \tag{1.24}$$

using the vector notation $(\hat{\boldsymbol{c}}^\dagger_{\boldsymbol{k}})^T = (\hat{c}^\dagger_{\boldsymbol{k},1}, \hat{c}^\dagger_{\boldsymbol{k},2}, \dots)$. From (1.24) we derive the constraints on the single-particle Hamiltonian $h(\boldsymbol{k})$ and the pairing function $\Delta(\boldsymbol{k},\boldsymbol{q})$ due to time-reversal invariance, reading

$$\mathcal{T} \, h(-\boldsymbol{k}) \, \mathcal{T}^\dagger = h(\boldsymbol{k}) \qquad \leftrightarrow \qquad \mathcal{U}_{\mathcal{T}} \, h^T(-\boldsymbol{k}) \, \mathcal{U}^\dagger_{\mathcal{T}} = h(\boldsymbol{k}) \,, \tag{1.25}$$

$$\mathcal{T} \, \Delta(-\boldsymbol{k},-\boldsymbol{q}) \, \mathcal{T}^T = \Delta(\boldsymbol{k},\boldsymbol{q}) \qquad \leftrightarrow \qquad \mathcal{U}_{\mathcal{T}} \, \Delta^*(-\boldsymbol{k},-\boldsymbol{q}) \, \mathcal{U}^T_{\mathcal{T}} = \Delta(\boldsymbol{k},\boldsymbol{q}) \,. \tag{1.26}$$

[9] Note that $\hat{\mathcal{U}}_{\mathcal{T}}$ acts in Fock space while $h(\boldsymbol{k})$ lives in the single-particle space, such that they commute. Moreover, it holds $\hat{\mathcal{U}}_{\mathcal{T}} \mathcal{K} = \mathcal{K} \hat{\mathcal{U}}^*_{\mathcal{T}}$ and $\mathcal{K} \hat{\mathcal{U}}^\dagger_{\mathcal{T}} = \hat{\mathcal{U}}^T_{\mathcal{T}} \mathcal{K}$

Lattice symmetries The language and concepts necessary to describe the lattice transformation behavior of spin 1/2 fermions were introduced in section (1.3.1). Concerning the role of spin-orbit coupling, we have clarified that the fermionic fields/operators either transform under the crystal double group $\mathcal{G}_0^{SOC} = \mathcal{G}_p'$ or the symmetry group $\mathcal{G}_0^{\cancel{SOC}} = \mathcal{G}_p \times SU(2)$ depending on whether SOC is relevant or not. In any case, the corresponding transformation can be cast by the unitary operation $\hat{\mathcal{U}}_g$ whose action on the fermionic operators is defined by

$$\hat{\mathcal{U}}_g \hat{c}^\dagger_{\boldsymbol{k},\alpha} \hat{\mathcal{U}}_g^\dagger = \hat{c}^\dagger_{\mathcal{R}_v(g)\boldsymbol{k},\alpha'} \left(\mathcal{U}_g\right)_{\alpha'\alpha} , \qquad \hat{\mathcal{U}}_g \hat{c}_{\boldsymbol{k},\alpha} \hat{\mathcal{U}}_g^\dagger = \left(\mathcal{U}_g^\dagger\right)_{\alpha\alpha'} \hat{c}_{\mathcal{R}_v(g)\boldsymbol{k},\alpha'} ,$$

with g being a group element from either $\mathcal{G}_0^{SOC}$ or $\mathcal{G}_0^{\cancel{SOC}}$. The coordinates transform as $\boldsymbol{k'} = \mathcal{R}_v(g)\boldsymbol{k}$ with the transformation matrix of the coordinates representation $\mathcal{R}_v(g)$. The invariance upon the lattice symmetries implies $\hat{\mathcal{H}}_{\mathcal{U}_g} \equiv \hat{\mathcal{U}}_g \hat{\mathcal{H}} \hat{\mathcal{U}}_g^\dagger = \hat{\mathcal{H}}$, see Eq. (1.17). Hence, we compute the transformed Hamiltonian

$$\hat{\mathcal{H}}_{\mathcal{U}_g} = \sum_{\boldsymbol{k}} \left(\hat{\boldsymbol{c}}^\dagger_{\boldsymbol{k}}\right) \mathcal{U}_g \, h(\mathcal{R}_v^\dagger(g)\boldsymbol{k}) \, \mathcal{U}_g^\dagger \hat{\boldsymbol{c}}_{\boldsymbol{k}} + \sum_{\boldsymbol{kq}} \left(\left(\hat{\boldsymbol{c}}^\dagger_{\boldsymbol{k}+\frac{\boldsymbol{q}}{2}}\right)^T \mathcal{U}_g \, \Delta(\mathcal{R}_v^\dagger(g)\boldsymbol{k}, \mathcal{R}_v^\dagger(g)\boldsymbol{q}) \, \mathcal{U}_g^T \, \hat{\boldsymbol{c}}^\dagger_{-\boldsymbol{k}+\frac{\boldsymbol{q}}{2}} + H.c. \right) , \tag{1.27}$$

and obtain the constraints on the single-particle Hamiltonian and the pairing function

$$\mathcal{U}_g \, h(\mathcal{R}_v^\dagger(g)\boldsymbol{k}) \, \mathcal{U}_g^\dagger = h(\boldsymbol{k}) , \qquad \forall g \in \{\mathcal{G}_0^{SOC} \text{ or } \mathcal{G}_0^{\cancel{SOC}}\} , \tag{1.28}$$

$$\mathcal{U}_g \, \Delta(\mathcal{R}_v^\dagger(g)\boldsymbol{k}, \mathcal{R}_v^\dagger(g)\boldsymbol{q}) \, \mathcal{U}_g^T = \Delta(\boldsymbol{k}, \boldsymbol{q}) , \qquad \forall g \in \{\mathcal{G}_0^{SOC} \text{ or } \mathcal{G}_0^{\cancel{SOC}}\} . \tag{1.29}$$

With the derived conditions for each type of symmetry class, the symmetry-allowed contributions to the generalized BCS Hamiltonian (1.21) are strongly constrained.

1.3.4 Pairing field and its symmetry constraints

Apart from the previously derived constraints (1.26) and (1.29), there is one more condition on the pairing function. By construction, it is a two-electron wave-function and hence, it has to be anti-symmetric upon an electron exchange. Using the fermionic anti-commutation relations in the Hamiltonian (1.21) therefore allows to impose the additional constraint

$$\Delta(-\boldsymbol{k}, \boldsymbol{q}) = -\Delta^T(\boldsymbol{k}, \boldsymbol{q}) . \tag{1.30}$$

In order to meet all the requirements it is convenient to express the pairing field in the basis of the IRs n according to (1.19),

$$\Delta_{\alpha\beta}(\boldsymbol{k}, \boldsymbol{q}) = \sum_{n,\mu} \Delta^{n,\mu}_{\boldsymbol{q}} \left(\chi^{n,\mu}_{\boldsymbol{k},\boldsymbol{q}} \lambda^{n,\mu}\right)^\dagger_{\alpha\beta} , \qquad \Delta^{n,\mu}_{\boldsymbol{q}}, \chi^{n,\mu}_{\boldsymbol{k},\boldsymbol{q}} \in \mathbb{C}, \qquad \lambda^{n,\mu}_{\alpha\beta} \in \mathbb{C}^{N_{dof} \times N_{dof}}, \tag{1.31}$$

with the components $\mu = 1 ... \dim(n)$. Here, the complex field $\Delta^{n,\mu}_{\boldsymbol{q}}$ represents the position-dependent order parameter in the Ginzburg-Landau theory. The function $\chi^{n,\mu}_{\boldsymbol{k},\boldsymbol{q}} \lambda^{n,\mu}_{\alpha\beta}$ is called the associated partner function, where we have detached the matrix part $\lambda^{n,\mu}_{\alpha\beta}$ from its overall spatial dependence $\chi^{n,\mu}_{\boldsymbol{k},\boldsymbol{q}}$. In the course of the mean-field decoupling of the BCS interaction term (see appendix A.1), the pairing function is identified as $\Delta^{n,\mu}_{\boldsymbol{q}} \sim \sum_{\boldsymbol{k}} \langle \hat{c}_{-\boldsymbol{k}+\frac{\boldsymbol{q}}{2},\alpha} \, \chi^{n,\mu}_{\boldsymbol{k},\boldsymbol{q}} \lambda^{n,\mu}_{\alpha\beta} \, \hat{c}_{\boldsymbol{k}+\frac{\boldsymbol{q}}{2},\beta} \rangle$, which is why it couples to the Hermitian

conjugated of the associated partner function in Eq. (1.31). The benefit that comes with the basis choice (1.31) lies in the transformation behavior upon the spatial symmetry operations, reading

$$\mathcal{U}_g \left(\chi^{n,\mu}_{\mathcal{R}_v^\dagger(g)\boldsymbol{k},\mathcal{R}_v^\dagger(g)\boldsymbol{q}} \lambda^{n,\mu} \right)^\dagger \mathcal{U}_g^T = \mathcal{R}_n^T(g)_{\mu\mu'} \left(\chi^{n,\mu'}_{\boldsymbol{k},\boldsymbol{q}} \lambda^{n,\mu'} \right)^\dagger , \qquad \forall g \in \{\mathcal{G}_0^{SOC} \text{ or } \mathcal{G}_0^{\cancel{SOC}}\} . \tag{1.32}$$

The IRs n according to which the pairing field transforms have to be part of the underlying point group $\mathcal{G}_p$. The reason is that the non-trivial 2π rotations caused by a single fermion cancel out for a two-fermion function like $\Delta(\boldsymbol{k},\boldsymbol{q})$. As before, we study the cases with and without SOC separately.

SOC is relevant The spin and lattice degrees of freedom transform jointly under the double group $\mathcal{G}_0^{SOC} = \mathcal{G}_p'$. By using Eq. (1.31) and exploiting Eq. (1.32), it is straightforward to check that the condition (1.29) can be recast in terms of the order parameter relation

$$\Delta^{n,\mu}_{\mathcal{R}_v^\dagger(g)\boldsymbol{q}} = \mathcal{R}_n^\dagger(g)_{\mu\mu'} \Delta^{n,\mu'}_{\boldsymbol{q}} , \qquad \forall g \in \mathcal{G}_p' . \tag{1.33}$$

This transformation rule is very convenient when implementing the symmetry on the free energy expansion.

SOC is irrelevant Without SOC, the spin transforms independently from the lattice, and it is useful to detach the spin degrees of freedom from the remainder $\lambda^{n,\mu} \to \lambda^{n,\mu}\tilde{\mathfrak{s}}^{\mathrm{j},\eta}$ with the spin Pauli matrices $\tilde{\mathfrak{s}}^{\mathrm{j},\eta}$. Here, we use the notation of the point group IR n and the $SU(2)$ IR j with their respective components $\mu = 1,..,\dim(n)$ and $\eta = 1,..,\dim(\mathrm{j})$. The corresponding symmetry elements factorize as $\mathcal{U}_g \to \mathcal{U}_g R_{SU(2)}(\vartheta,\hat{\boldsymbol{n}})$ where $g \in \mathcal{G}_p$ is a point group element. Accordingly, the pairing field expansion becomes

$$\Delta(\boldsymbol{k},\boldsymbol{q}) = \sum_{n,\mu} \sum_{\mathrm{j},\eta} \Delta_{\boldsymbol{q}}^{(n,\mathrm{j}),(\mu,\eta)} \left(\chi^{n,\mu}_{\boldsymbol{k},\boldsymbol{q}} \lambda^{n,\mu} \right)^\dagger \left(\tilde{\mathfrak{s}}^{\mathrm{j},\eta} \right)^\dagger , \qquad \Delta_{\boldsymbol{q}}^{(n,\mathrm{j}),(\mu,\eta)} \in \mathbb{C}. \tag{1.34}$$

For the spin degree of freedom the condition (1.29) becomes

$$R_{SU(2)}(\vartheta,\hat{\boldsymbol{n}}) \left(\tilde{\mathfrak{s}}^{\mathrm{j},\eta'} \right)^\dagger R_{SU(2)}^T(\vartheta,\hat{\boldsymbol{n}}) = \mathcal{R}_{\mathrm{j}}(\vartheta,\hat{\boldsymbol{n}})_{\eta'\eta} \left(\tilde{\mathfrak{s}}^{\mathrm{j},\eta} \right)^\dagger . \tag{1.35}$$

The evaluation of the equation (1.35) shows that the spin part decomposes into the two IRs $\mathrm{j} = \{\mathrm{s},\mathrm{t}\}$ for the singlet (s) and triplet (t) states. The singlet and triplet states are represented by the $SO(1)$ and $SO(3)$ groups, respectively, with the corresponding group elements reading $\mathcal{R}_{\mathrm{s}}(\vartheta,\hat{\boldsymbol{n}}) = R_{SO(1)}(\vartheta,\hat{\boldsymbol{n}}) = 1$ and $\mathcal{R}_{\mathrm{t}}(\vartheta,\hat{\boldsymbol{n}}) = R_{SO(3)}(\vartheta,\hat{\boldsymbol{n}})$. The associated matrices become

$$(\tilde{\mathfrak{s}}^{\mathrm{s}})^\dagger = \mathrm{i}\mathfrak{s}^y , \qquad (\tilde{\mathfrak{s}}^{\mathrm{t}})^\dagger = \left(\mathfrak{s}^x,\mathfrak{s}^y,\mathfrak{s}^z\right) \mathrm{i}\mathfrak{s}^y .$$

The implementation of the point group constraints leads to the very same relation (1.33) as in the SOC-free case. Thus, similarly to the previous case, the condition on the pairing function (1.29) can be recast in terms of the order parameter transformation rule

$$\Delta^{(n,\mathrm{j}),(\mu,\eta)}_{\mathcal{R}_v^\dagger(g)\boldsymbol{q}} = \mathcal{R}_n^\dagger(g)_{\mu\mu'} \mathcal{R}_{\mathrm{j}}(\vartheta,\hat{\boldsymbol{n}})_{\eta\eta'} \Delta_{\boldsymbol{q}}^{(n,\mathrm{j}),(\mu',\eta')} , \qquad \forall g \in \mathcal{G}_p , \forall \vartheta \in \mathbb{R} , \forall \hat{\boldsymbol{n}} \in \mathbb{R}^3, |\hat{\boldsymbol{n}}| = 1 . \tag{1.36}$$

In section (1.3.5) below we demonstrate from symmetry grounds that an order parameter will stabilize only a single IR n_0 at the transition temperature. For the present case this means that the order parameter in the spin space is either a singlet or a triplet,

$$\text{singlet:} \qquad \Delta(\boldsymbol{k},\boldsymbol{q}) = \left(\chi^{n_0,\mu}_{\boldsymbol{k},\boldsymbol{q}}\lambda^{n_0,\mu}\right)^\dagger \Delta^{n_0,\mu}_{\mathrm{s},\boldsymbol{q}}\,\mathrm{i}\mathfrak{s}^y\,, \tag{1.37}$$

$$\text{triplet:} \qquad \Delta(\boldsymbol{k},\boldsymbol{q}) = \left(\chi^{n_0,\mu}_{\boldsymbol{k},\boldsymbol{q}}\lambda^{n_0,\mu}\right)^\dagger \boldsymbol{\Delta}^{n_0,\mu}_{\mathrm{t},\boldsymbol{q}}\cdot\left(\mathfrak{s}^x,\mathfrak{s}^y,\mathfrak{s}^z\right)\mathrm{i}\mathfrak{s}^y\,, \tag{1.38}$$

with $\boldsymbol{\Delta}^{n_0,\mu}_{\mathrm{t},\boldsymbol{q}} = (\Delta^{n_0,\mu}_{\mathrm{t1},\boldsymbol{q}},\Delta^{n_0,\mu}_{\mathrm{t2},\boldsymbol{q}},\Delta^{n_0,\mu}_{\mathrm{t3},\boldsymbol{q}})$. Due to the anti-symmetry constraint (1.30), the corresponding spatial functions have to satisfy $\chi^{n_0,\mu}_{-\boldsymbol{k},\boldsymbol{q}}(\lambda^{n_0,\mu})^T = \pm\chi^{n_0,\mu}_{\boldsymbol{k},\boldsymbol{q}}\lambda^{n_0,\mu}$ for the singlet (+) and triplet (−) state.

Finally, we write the spin- and lattice IRs in (1.36) in a compact form using $\tilde{n} = \big(n,\mathrm{j}\big)$, $\tilde{\mu} = \big(\mu,\eta\big)$, $\tilde{g} = (g,\vartheta,\hat{\boldsymbol{n}})$ and $\mathcal{R}^\dagger_{\tilde{n}}(\tilde{g})_{\tilde{\mu}\tilde{\mu}'} = \mathcal{R}^\dagger_n(g)_{\mu\mu'}\mathcal{R}_{\mathrm{j}}(\vartheta,\hat{\boldsymbol{n}})_{\eta\eta'}$. Then, both cases, with and without SOC look formally identical and can be treated on equal footing. In the remainder of this chapter, we will therefore treat both cases as one.

Pairing field and centro-symmetry Following up on the discussion on singlet and triplet pairing, we want to shed some light on a closely related topic. Consider a spin-orbit coupled systems with spin 1/2 electrons and both, time-reversal and inversion symmetries intact. In these so-called time-reversal invariant and centro-symmetric systems every energy level is at least four-fold degenerate, with the states at a given momentum $\boldsymbol{k}$ being doubly degenerate. Moreover, it has been shown in Ref. [56–58] that regardless of the degree of entanglement between spin and orbit, it is always possible to construct a pseudo-spin basis $\{|\boldsymbol{k},+\rangle,|\boldsymbol{k},-\rangle\}$ within which the operations act as

$$\hat{\mathcal{U}}_I|\boldsymbol{k},\pm\rangle = |-\boldsymbol{k},\pm\rangle\,, \qquad\qquad \hat{\mathcal{T}}|\boldsymbol{k},\pm\rangle = \pm|-\boldsymbol{k},\mp\rangle\,.$$

Thus, the two degenerate states $|\boldsymbol{k},\pm\rangle$ transform just like common $SU(2)$ spinor under the time-reversal $\hat{\mathcal{T}}$ and the inversion $\hat{\mathcal{U}}_I$ operation. It should be noted that the pseudo-spin is not to be confounded with the actual spin in the sense that physical quantities such as magnetic fields still couple to the electron spin, not the pseudo-spin. The Pauli matrices in pseudo-spin space are denoted by $\tilde{\mathfrak{s}}^i$ and in this basis the pairing field can be expressed in the form

$$\Delta(\boldsymbol{k},\boldsymbol{q}) = d^0_{\boldsymbol{k},\boldsymbol{q}}\,\mathrm{i}\tilde{\mathfrak{s}}^y + \boldsymbol{d}_{\boldsymbol{k},\boldsymbol{q}}\cdot\left(\tilde{\mathfrak{s}}^x,\tilde{\mathfrak{s}}^y,\tilde{\mathfrak{s}}^z\right)\mathrm{i}\tilde{\mathfrak{s}}^y\,, \tag{1.39}$$

reminiscent of the singlet and triplet representation (1.37-1.38). Indeed, the terminology is adapted such that pairing states with $d^0_{\boldsymbol{k},\boldsymbol{q}}$ and $\boldsymbol{d}_{\boldsymbol{k},\boldsymbol{q}} = (d^{(x)}_{\boldsymbol{k},\boldsymbol{q}},d^{(y)}_{\boldsymbol{k},\boldsymbol{q}},d^{(z)}_{\boldsymbol{k},\boldsymbol{q}})$ are characterized as singlet and triplet states (in pseudo-spin space), respectively. The anti-symmetry constraint (1.30) requires the d-functions to be even $d^0_{-\boldsymbol{k},\boldsymbol{q}} = d^0_{\boldsymbol{k},\boldsymbol{q}}$ and odd $\boldsymbol{d}_{-\boldsymbol{k},\boldsymbol{q}} = -\boldsymbol{d}_{\boldsymbol{k},\boldsymbol{q}}$, respectively. In the case of zero external momentum $\boldsymbol{q} = \boldsymbol{0}$, a parity even (odd) pairing channel can only have a finite $d^0_{\boldsymbol{k},\boldsymbol{0}}$ ($\boldsymbol{d}_{\boldsymbol{k},\boldsymbol{0}}$) component while the other one has to vanish.

Note that the pseudo-spin basis (1.39) has only a single microscopic degree of freedom left (pseudo-spin). Here, it is commonly assumed that the other electronic bands are sufficiently well separated in energy such that there is essentially no coupling to them. Then, the d-representation (1.39) has the physical significance it is usually attributed to.

Time-reversal symmetry constraint To meet the time-reversal symmetry constraint (1.26) it is convenient to introduce the new matrix $\Lambda^{n,\mu} = \mathcal{U}_{\mathcal{T}}\lambda^{n,\mu}$. Then, it can be shown that the time-reversal invariance requires the associated partner functions to satisfy (see appendix A.1)

$$\left(\chi^{n,\mu}_{\boldsymbol{k},\boldsymbol{q}}\Lambda^{n,\mu}\right)^{\dagger} = \left(\chi^{\bar{n},\mu}_{\boldsymbol{k},-\boldsymbol{q}}\Lambda^{\bar{n},\mu}\right) , \tag{1.40}$$

where n and $\bar{n}$ denote a pair of complex conjugated IRs. According to the relation (1.40) a real IR ($\bar{n} = n$) has to be accompanied by a Hermitian matrix $\Lambda^{n,\mu}$, given it holds $\chi^{n,\mu}_{\boldsymbol{k},\boldsymbol{q}} = \chi^{n,\mu}_{\boldsymbol{k},-\boldsymbol{q}}$. For the case of a complex conjugated pair ($\bar{n} \neq n$), the condition (1.40) requires the two IRs to transform jointly. Note that the pure lattice and spin symmetries let them to transform independently. As a consequence of the time-reversal constraint, pairs of complex conjugated IRs are conventionally lumped together into a $2\dim(n)$ dimensional IR. As show in the appendix A.1, the time-reversal constraint (1.26) translates into the order parameter condition

$$\Delta^{n,\mu}_{\boldsymbol{q}} = \left(\Delta^{\bar{n},\mu}_{-\boldsymbol{q}}\right)^{*} , \tag{1.41}$$

which can be easily implemented in a free energy expansion. Before we proceed, let us examine what it needs for a superconductor to break TRS on the basis of three examples:

(i) The pairing state is homogeneous ($\boldsymbol{q} = 0$) and transforms according to a multi-dimensional real IR ($n = \bar{n} = n_0$) such that the condition (1.41) becomes

$$e^{\mathrm{i}\varphi_1}\left(\Delta_0^{n_0,1}, \Delta_0^{n_0,2}e^{\mathrm{i}\varphi_{21}}, \Delta_0^{n_0,3}e^{\mathrm{i}\varphi_{31}}, \dots\right) = e^{-\mathrm{i}\varphi_1}\left(\Delta_0^{n_0,1}, \Delta_0^{n_0,2}e^{-\mathrm{i}\varphi_{21}}, \Delta_0^{n_0,3}e^{-\mathrm{i}\varphi_{31}}, \dots\right) , \quad \Delta_0^{n_0,i} > 0 .$$

Owed to the $U(1)$ symmetry, the overall phase can always be gauged away and does not play a role. Thus, the condition can only be violated if the order parameter has multiple components and if the respective ground state symmetry is such that at least one relative phase is $\varphi_{ij} \neq \{0, \pi\}$. By implication, this excludes any time-reversal symmetry breaking in case of a uniform single-component order parameter.

(ii) For a homogeneous ($\boldsymbol{q} = 0$) pairing states that transforms according to a complex conjugated pair n_0,$\bar{n}_0$ where we assume $\dim(n_0) = 1$ for brevity. The condition (1.41) becomes

$$e^{\mathrm{i}\varphi_1}\left(\Delta_0^{n_0}, \Delta_0^{\bar{n}_0}e^{\mathrm{i}\varphi_{21}}\right) = e^{-\mathrm{i}\varphi_1}\left(\Delta_0^{\bar{n}_0}e^{-\mathrm{i}\varphi_{21}}, \Delta_0^{n_0}\right) , \qquad \Delta_0^{n_0}, \Delta_0^{\bar{n}_0} > 0 .$$

Here, the TRS is always spontaneously broken unless the ground state happens to be of the form $\varphi_{21} = 0$ and $\Delta_0^{n_0} = \Delta_0^{\bar{n}_0}$.

(iii) For a spatially inhomogeneous pairing state such as a pair density wave with a fixed ordering vector $\boldsymbol{Q}$. Here, the wave-function could either be single-$\boldsymbol{Q}$ dependent with $\Delta^{\boldsymbol{Q}}_{\boldsymbol{q}} = e^{\mathrm{i}\varphi_1}\Delta_0\delta(\boldsymbol{q} - \boldsymbol{Q})$, or double-$\boldsymbol{Q}$ dependent with $\Delta^{\boldsymbol{Q}}_{\boldsymbol{q}} = e^{\mathrm{i}\varphi_1}\Delta_0[\delta(\boldsymbol{q} - \boldsymbol{Q}) + \delta(\boldsymbol{q} + \boldsymbol{Q})]$. The single-$\boldsymbol{Q}$ state would necessarily break TRS as $\boldsymbol{q} \to -\boldsymbol{q}$ leads to a different state, while the double-$\boldsymbol{Q}$ solution would leave the TRS intact—at least in the given representation with zero phase difference and equal amplitudes for the oppositely propagating waves.

1.3.5 Constraints on the free energy expansion

In this section we want to transfer the previously implemented symmetries into constraints on a free energy expansion. Moreover, we discuss how symmetry-compliant contributions can be derived and demonstrate that the free energy expansion diagonalizes in terms of the IRs n. With the previously obtained transformation rules of the order parameter upon the $U(1)$ (1.22), the point group (1.33) and the time-reversal symmetry (1.41) operations, we can directly postulate the corresponding constraints on the free energy density, reading

$$U(1): \quad \mathcal{F}[(\Delta_{\boldsymbol{q}}^{n,\mu})^*, \Delta_{\boldsymbol{q}}^{n,\mu}, \boldsymbol{q}] = \mathcal{F}[(\Delta_{\boldsymbol{q}}^{n,\mu})^* e^{-\mathrm{i}\varphi}, \Delta_{\boldsymbol{q}}^{n,\mu} e^{\mathrm{i}\varphi}, \boldsymbol{q}] \qquad ,\forall \varphi \in \mathbb{R}\,, \tag{1.42}$$

$$\text{lattice}: \quad \mathcal{F}[(\Delta_{\boldsymbol{q}}^{n,\mu})^*, \Delta_{\boldsymbol{q}}^{n,\mu}, \boldsymbol{q}] = \mathcal{F}[(\Delta_{\boldsymbol{q}}^{n,\mu'})^* \mathcal{R}_n(g)_{\mu'\mu}, \mathcal{R}_n^\dagger(g)_{\mu\mu'} \Delta_{\boldsymbol{q}}^{n,\mu'}, \mathcal{R}_v^\dagger(g)\,\boldsymbol{q}] \qquad ,\forall g \in \mathcal{G}_p\,, \tag{1.43}$$

$$\text{TRS}: \quad \mathcal{F}[(\Delta_{\boldsymbol{q}}^{n,\mu})^*, \Delta_{\boldsymbol{q}}^{n,\mu}, \boldsymbol{q}] = \mathcal{F}[\Delta_{\boldsymbol{q}}^{\bar{n},\mu}, (\Delta_{\boldsymbol{q}}^{\bar{n},\mu})^*, -\boldsymbol{q}]\,. \tag{1.44}$$

Now, let us study how these constraints effect a free energy expansion, that can be written in the form

$$\mathcal{F}[(\Delta_{\boldsymbol{q}}^{n,\mu})^*, \Delta_{\boldsymbol{q}}^{n,\mu}, \boldsymbol{q}] \approx \mathcal{F}\left[0,0,\boldsymbol{0}\right] + \sum_{nn'} \sum_{\mu\mu'} (\Delta_{\boldsymbol{q}}^{n,\mu})^*\, M_{nn'}^{\mu\mu'}(T,\boldsymbol{q})\, \Delta_{\boldsymbol{q}}^{n',\mu'} + \mathcal{F}_{\text{int}}\left[(\Delta_{\boldsymbol{q}}^{n,\mu})^*, \Delta_{\boldsymbol{q}}^{n,\mu}, \boldsymbol{q}\right]\,. \tag{1.45}$$

Here, we have already employed the $U(1)$ condition (1.42) which prohibits any odd powers in $\Delta_{\boldsymbol{q}}^{n,\mu}$ such that the interaction contribution is at least of fourth-order in $\Delta_{\boldsymbol{q}}^{n,\mu}$. The zeroth-order term in (1.45) denotes the normal state contribution.

Quadratic part The point group symmetry constraints (1.43) impose the condition

$$M_{nn'}^{\mu\mu'}(T,\boldsymbol{q}) = \mathcal{R}_n(g)_{\mu\nu}\, M_{nn'}^{\nu\nu'}(T, \mathcal{R}_v^{-1}(g)\boldsymbol{q})\, \mathcal{R}_{n'}^\dagger(g)_{\nu'\mu'}\,, \qquad \forall g \in \mathcal{G}_p\,, \tag{1.46}$$

on the matrix $M_{nn'}^{\mu\mu'}(T,\boldsymbol{q})$. Let us assume that the pairing state is homogeneous such that it holds $\boldsymbol{q} = \boldsymbol{0}$ for the mean-field transition. This allows us to sum Eq.(1.46) over all group elements g, and to apply the *grand orthogonality theorem* of group theory [52]

$$\sum_{g\in\mathcal{G}_p} \mathcal{R}_n(g)_{\mu\nu} \mathcal{R}_{n'}^*(g)_{\mu'\nu'} = \frac{|\mathcal{G}_p|}{d_n}\, \delta_{nn'}\delta_{\mu\mu'}\delta_{\nu\nu'}\,. \tag{1.47}$$

Here, $|\mathcal{G}_p|$ denotes the order (i.e. the number of elements) of the group $\mathcal{G}_p$ and d_n the dimension of the IR n. This simplifies the quadratic terms to a matrix

$$M_{nn'}^{\mu\mu'}(T,\boldsymbol{0}) = M_{nn'}^{\nu\nu'}(T,\boldsymbol{0}) \frac{1}{d_n}\, \delta_{\nu\nu'}\delta_{nn'}\,\delta_{\mu\mu'} \equiv a_n(T)\,\delta_{nn'}\,\delta_{\mu\mu'}\,, \tag{1.48}$$

that is diagonal in terms of the IRs. Insertion of the matrix (4.21) into the free energy expansion (1.45) shows that the quadratic contribution turns into an independent sum over the IRs n,

$$\mathcal{F}_{\text{quad}}[(\Delta_{\boldsymbol{0}}^{n,\mu})^*, \Delta_{\boldsymbol{0}}^{n,\mu}, \boldsymbol{0}] = \sum_n a_n(T) \sum_\mu (\Delta_{\boldsymbol{0}}^{n,\mu})^*\, \Delta_{\boldsymbol{0}}^{n,\mu}\,. \tag{1.49}$$

Let us comment on the physical consequence of the diagonalized free energy contribution (1.49): Within the Ginzburg-Landau formalism, the second-order phase transition occurs when the quadratic coefficient vanishes, see section 1.1.1. In Eq. (1.49) we have many quadratic coefficients, all of which are symmetry-distinct. Consequently, all of them should vanish at a different temperature—disregarding accidental degeneracies. Following that line of reasoning, there has to be one symmetry channel, i.e. one IR n_0, whose coefficient $a_{n_0}(T)$ vanishes first. This first channel dictates the primary pairing state.

From here on, there could be different scenarios. In the simplest one all the remaining channels are still far from ordering and any kind of back-channeling can be safely neglected. A more subtle situation arises when various coefficients $a_n(T)$ become soft ($\hat{=}$approach zero) around the same temperature. This situation calls for a careful analysis of the interactions between the different channels, and falls into the subject of competing orders. Such a scenario arises as an accidental degeneracy that can be imposed by a fine-tuned choice of tuning parameters. In reverse, accidental degeneracies can be removed by small system perturbations such as stress or magnetic fields. Accidental degeneracies are not considered in the remainder of this work.

Lastly, we apply the time-reversal symmetry constraint (1.44) on (1.49) which leads to the expected condition $a_n(T) = a_{\bar{n}}(T)$, according to which complex pairs transform as an effective $2\dim(n)$ dimensional IR. In the following we treat complex IRs as multi-dimensional where we employ the notation $\tilde{n} \equiv n \oplus \bar{n}$.

Interaction part In line with the previous discussion the system is assumed to order uniformly in the single symmetry channel n_0. The most general form of the interaction term reads

$$\mathcal{F}_{\text{int}}\left[(\Delta_{\mathbf{0}}^{n_0,\mu})^*, \Delta_{\mathbf{0}}^{n_0,\mu}, \mathbf{0}\right] = u_{\mu_1\mu_2\mu_3\mu_4}(\Delta_{\mathbf{0}}^{n_0,\mu_1})^*(\Delta_{\mathbf{0}}^{n_0,\mu_2})^*\Delta_{\mathbf{0}}^{n_0,\mu_3}\Delta_{\mathbf{0}}^{n_0,\mu_4} + \mathcal{O}\left(\left(\Delta_{\mathbf{0}}^{n_0,\mu}\right)^6\right), \tag{1.50}$$

where the summation over doubly occurring indices is implied. Most of the parameters $u_{\mu_1\mu_2\mu_3\mu_4}$ are not independent. To demonstrate this, it is convenient to introduce the bilinear combination

$$\mathsf{B}^{n,i,l} = (\Delta_{\mathbf{0}}^{n_0,\mu})^*\, \lambda_{\mu\mu'}^{n,i,l}\, \Delta_{\mathbf{0}}^{n_0,\mu'}\,, \tag{1.51}$$

and classify the matrices $\lambda^{n,i,l}$ such that they satisfy the sesquilinear transformation condition

$$\mathcal{R}_{n_0}(g)_{\mu\nu}\, \lambda_{\nu\nu'}^{n,i,l}\, \mathcal{R}_{n_0}^{\dagger}(g)_{\nu'\mu'} = \mathcal{R}_n^{-1}(g)_{ll'}\, \lambda_{\mu\mu'}^{n,i,l'}\,. \tag{1.52}$$

Here, the bilinear transforms according to the IR n with its components $l = 1, .., \dim(n)$. The index i accounts for multiply occurring IRs, which will be referred to as the multiplicity in the following. For example, the bilinear transforms according to the product representation $\Gamma_{n_0}^* \otimes \Gamma_{n_0}$ that can be decomposed as

$$\Gamma_{n_0}^* \otimes \Gamma_{n_0} = \#_{n_a}\Gamma_{n_a} \oplus \#_{n_b}\Gamma_{n_b} \oplus \dots\,, \qquad\qquad \#_{n_a}, \#_{n_b} \in \mathbb{N}^+\,. \tag{1.53}$$

The IR n can be any of the IRs from the set $\{n_a, n_b, \dots\}$, and each IR n in (A.14) occurs $\#_n$ times which is accounted for by the multiplicity index $i = 1, .., \#_n$. With the classified matrices (A.12) it is evident that the bilinear transforms according to

$$\mathsf{B}^{n,i,l} = \mathcal{R}_n^{-1}(g)_{ll'}\mathsf{B}^{n,i,l'}\,. \tag{1.54}$$

Using this identity, the free energy contribution (A.10) can re-expressed in terms of bilinear combinations

$$\mathcal{F}_{int}\left[(\Delta_{\mathbf{0}}^{n_0,\mu})^*,\Delta_{\mathbf{0}}^{n_0,\mu},\mathbf{0}\right]=u_{n,i,l}^{n',i',l'}\,\mathsf{B}^{n,i,l}\,\mathsf{B}^{n',i',l'}+\mathcal{O}\left(\left(\Delta_{\mathbf{0}}^{n_0,\mu}\right)^6\right). \tag{1.55}$$

This form is reminiscent of the quadratic term (1.45), and with the same reasoning we can first simplify the condition (1.43) to

$$u_{n,i,l}^{n',i',l'}=\mathcal{R}_{\bar{n}}(g)_{l\ell}u_{n,i,\ell}^{n',i',\ell'}\,\mathcal{R}_{n'}^*(g)_{l'\ell'}\qquad\qquad\forall g\in\mathcal{G}_p\,, \tag{1.56}$$

where we have used $\mathcal{R}_n^*(g)=\mathcal{R}_{\bar{n}}(g)$. Remember that complex IRs are included via the substitution $n\to\tilde{n}=n\oplus\bar{n}$. After the summation over g and the application of the *grand orthogonality theorem* (1.47) one finds the interaction parameters

$$u_{n,i,l}^{n',i',l'}=\delta_{\bar{n}n'}\delta_{ll'}\delta_{\ell\ell'}\frac{1}{d_{n'}}\,u_{n,i,\ell}^{\bar{n},i',\ell'}\equiv\delta_{\bar{n}n'}\delta_{ll'}u_n^{i,i'}\,,$$

to be diagonal in terms of the IRs but it still depends on the multiplicity index i. Then, the quartic part of the free energy density becomes

$$\mathcal{F}_{int}\left[(\Delta_{\mathbf{0}}^{n_0,\mu})^*,\Delta_{\mathbf{0}}^{n_0,\mu},\mathbf{0}\right]=\sum_n\sum_{i,i'}u_n^{i,i'}\sum_l\mathsf{B}^{n,i,l}\,\mathsf{B}^{\bar{n},i',l}+\mathcal{O}\Big(\left(\Delta_{\mathbf{0}}^{n_0,\mu}\right)^6\Big), \tag{1.57}$$

where the interaction coefficients $u_n^{i,i'}$ satisfy $u_n^{i,i'}=u_n^{i',i}$ to guarantee the reality of the free energy. It should be noted that due to Fierz identities not all of the remaining parameters $u_n^{i,i'}$ are independent.

Bilinear examples We find it instructive to illustrate the classification of the bilinear combinations on two simple examples.

(i) Consider an order parameter that transforms according to the IR $n_0=E$ of the point group $\mathsf{D_3}$ (see Tab. 1.1). The corresponding bilinear decomposition (A.14) reads $\Gamma_E^*\otimes\Gamma_E=\Gamma_{A_1}\oplus\Gamma_{A_2}\oplus\Gamma_E$. With the set of transformation matrices $\mathcal{R}_E(g)$[10] one can determine the associated matrices $\lambda^{n,i,l}$ via (A.12). This tedious task can be significantly simplified by using appropriate numerical tools such as the Mathematica package provided by [53]. The classified matrices are listed in table 1.3, together with the behavior of the corresponding bilinear combination $\mathsf{B}^{n,i,l}$ upon the time-reversal operation (1.41).

(ii) Now, we consider an order parameter that transforms according to the complex IR $E\oplus\bar{E}$ of the point group $\mathsf{C_3}$ (see Tab. 1.1). The bilinear decomposition (A.14) yields $(E\oplus\bar{E})^*\otimes(E\oplus\bar{E})=2A\oplus(E\oplus\bar{E})$ with a multiplicity $\#_A=2$. Again, the classified results are listed in table 1.3.

[10] The motivated reader is welcome to check the condition him-/herself. The matrices of the IR E of the $\mathsf{D_3}$ point group read $C_{2x}=\sigma^z$, $C_{2\{A/B\}}=(-\sigma^z\mp\sqrt{3}\sigma^x)/2$, $C_{3z}^{\pm1}=(-\sigma^0\mp\mathrm{i}\sqrt{3}\sigma^y)/2$

D_3	matrix $\lambda^{n,i,l}$	TRS of $\mathsf{B}^{n,i,l}$
A_1	σ^0	$+$
A_2	σ^y	$-$
E	$(\sigma^z, -\sigma^x)$	$(+,+)$

C_3	matrix $\lambda^{n,i,l}$	TRS of $\mathsf{B}^{n,i,l}$
A	$\{\sigma^0, \sigma^z\}$	$\{+,-\}$
$E \oplus \bar{E}$	$(\sigma^x + i\sigma^y, \sigma^x - i\sigma^y)$	$(+,+)$

Table 1.3: Association of the IRs n occurring in the bilinear combinations $\mathsf{B}^{n,i,l}$ and their respective matrices $\lambda^{n,i,l}$ resulting from (A.12). We have considered the IR $n_0 = E$ of the D_3, and the IR $n_0 = E \oplus \bar{E}$ of the C_3 point group. The index $l = 1, .., \dim(n)$ couting the components of multi-dimensional IRs n is denoted by curved brackets, while the multiplicity index i is denoted by curly brackets. The respective transformation behavior of $\mathsf{B}^{n,i,l}$ upon the time-reversal symmetry (1.44) is attached.

Fluctuation part We close this chapter by discussing the symmetry-allowed free-energy terms accounting for long-wavelength fluctuations. To follow a similar approach as before, we expand the quadratic coefficient (1.45) in powers of momentum according to

$$M^{\mu\mu'}_{n_0 n_0}(T, \boldsymbol{q}) \approx a_{n_0}(T)\delta_{\mu\mu'} + \sum_n \sum_i \sum_l \lambda^{n,i,l}_{\mu\mu'} \left(d^{n,i,l}_{\alpha} \mathrm{i} q_\alpha + d^{n,i,l}_{\alpha\beta} q_\alpha q_\beta + \dots \right), \tag{1.58}$$

with n_0 denoting the stabilized IR. Upon the point group symmetries, the matrices $\lambda^{n,i,l}$ and the spatially-dependent parts in (1.58) transform independently. With the matrices transforming according to (A.12) the only way the condition (1.46) can be met is for the spatial coefficients to satisfy

$$d^{n,i,l'}_{\alpha'} \mathcal{R}^\dagger_v(g)_{\alpha'\alpha} = d^{n,i,l}_{\alpha} \mathcal{R}_n(g)_{ll'} , \tag{1.59}$$

$$d^{n,i,l'}_{\alpha'\beta'} \mathcal{R}^\dagger_v(g)_{\alpha'\alpha} \mathcal{R}^\dagger_v(g)_{\beta'\beta} = d^{n,i,l}_{\alpha\beta} \mathcal{R}_n(g)_{ll'} . \tag{1.60}$$

The allowed free energy contributions read $\lambda^{n,i,l} d^{n,i,l}$, i.e. they only exist for IRs n according to which a matrix $\lambda^{n,i,l}$ *and* a gradient coefficient $d^{n,i,l}$ transforms. Additionally, the contributions have to respect the time-reversal symmetry. As demonstrated in table 1.3, the bilinears transform either even or odd upon the time-reversal operation, and hence, they can only be paired with a spatial expansion term of even or odd power, respectively. In the appendix A.3 we show the derivation of a fully symmetry-compliant momentum-dependent function that is not limited to small momenta.

A system allowing for a linear gradient term is of particular interest as it would minimize the ground state energy for a finite momentum $\boldsymbol{q}$ and hence, cause an inhomogeneous ground state order. Such a contribution can only exist in systems without inversion symmetry, i.e. in non-centro-symmetric systems. The resulting ground state would be somewhat similar to an FFLO state [59, 60], and for example, in the point group O such a linear contribution is symmetry allowed for an order parameter transforming according to $n_0 = T$ [61].

Chapter 2

2 Undoped and doped Bi_2Se_3

This chapter serves as an introduction into the versatile physical properties of the topological insulator family Bi_2Se_3, Bi_2Te_3 and Sb_2Te_3, as well as on the superconducting state that emerges out of Bi_2Se_3 upon Cu, Nb or Sr doping. The compound Bi_2Se_3 is considered a prototypical topological insulator whose non-trivial properties originate from a strong spin-orbit coupling. The emergent superconducting state has consistently been reported to be a two-component odd-parity state that breaks the in-plane C_{3z} rotational symmetry and thereby, it causes a nematic distortion. The superconductor also shows indications to be topologically non-trivial. In this chapter, we outline and discuss the current experimental situation and we revisit the theoretically established two-states model.

First, we provide a brief introduction into the concept of topology. Then, we introduce the topological insulator Bi_2Se_3 where we present a derivation of the associated model Hamiltonian and we discuss the non-trivial topology. Third, the possible pairing states are classified and contrasted with the experiments. In agreement with previous works, we identify the E_u state as the most consistent pairing candidate. Lastly, we discuss the E_u ground state phases. Of particular interest are the two distinct nematic solutions—one fully-gapped and one nodal—which are discerned by a sixth-order parameter. A study of this parameter is attached in the last part.

2.1 Topology

Anti-unitary symmetries play a central role in the field of topology. While a Hamiltonian can be block-diagonalized with respect to the IRs related to the unitary symmetries, the anti-unitary symmetries can not be 'removed' from these blocks. Hence, the presence or the absence of an anti-unitary symmetry can be used to classify such an irreducible block [54]. The two anti-unitary symmetries relevant for condensed matter systems are the time-reversal $\hat{\mathcal{T}}$ and the particle-hole (or charge conjugation) $\hat{\mathcal{C}}$ symmetry which are defined by the commutation and anti-commutation relation with the Hamiltonian

$$\left[\hat{H}, \hat{\mathcal{T}}\right] = 0\,, \qquad \left\{\hat{H}, \hat{\mathcal{C}}\right\} = 0\,,$$

respectively. The two symmetries can either be present, and square to ± 1, or they can be absent [62]. This yields $3 \times 3 = 9$ classes which exhausts all but one of the symmetry classes developed by Altland and Zirnbauer [63–65], see table 2.1. In the case where both $\hat{\mathcal{T}}$ and $\hat{\mathcal{C}}$ are absent, the combined symmetry $\hat{\mathcal{T}}\hat{\mathcal{C}}$, also named the chiral symmetry, can either satisfy the chiral relation $\{\hat{H}, \hat{\mathcal{T}}\hat{\mathcal{C}}\} = 0$, or not, which completes the ten classes. The three last columns in the table denote the possible

Class	$\hat{\mathcal{T}}$	$\hat{\mathcal{C}}$	$\hat{\mathcal{T}}\hat{\mathcal{C}}$	$d=1$	$d=2$	$d=3$
A	0	0	0	0	$\mathbb{Z}$	0
AIII	0	0	1	$\mathbb{Z}$	0	$\mathbb{Z}$
AI	0	0	0	0	0	0
BDI	1	1	1	$\mathbb{Z}$	0	0
D	0	1	0	$\mathbb{Z}_2$	$\mathbb{Z}$	0
DIII	-1	1	1	$\mathbb{Z}_2$	$\mathbb{Z}_2$	$\mathbb{Z}$
AII	-1	0	0	0	$\mathbb{Z}_2$	$\mathbb{Z}_2$
CII	-1	-1	1	$2\mathbb{Z}$	0	$\mathbb{Z}_2$
C	0	-1	0	0	$2\mathbb{Z}$	0
CI	1	-1	1	0	0	$2\mathbb{Z}$

Table 2.1: Periodic table of topological matter. The classes can be grouped into the three standard Wigner-Dyson classes $\{\mathrm{A}, \mathrm{AI}, \mathrm{AII}\}$, the three chiral classes $\{\mathrm{AIII}, \mathrm{BDI}, \mathrm{CII}\}$ and the four BdG (superconductor) classes $\{\mathrm{D}, \mathrm{C}, \mathrm{DIII}, \mathrm{CI}\}$ [67].

existence of a system in the dimension d, with the associated topological index, either $\mathbb{Z}_2$ or $\mathbb{Z}$. These topological numbers distinguish a topological non-trivial ($\neq 0$) from a trivial ($= 0$) phase and are well-defined within the bulk of a fully-gapped systems.

In real material samples, the non-trivial bulk index reveals itself at the boundary. This is a direct consequence of the so-called bulk-boundary correspondence [55, 66]. A topological character can only be changed by means of a gap-closing, i.e. the gap has to close at the boundary between topologically non-identical systems which leads to a localized zero-energy state. Depending on whether the particle-hole symmetry is present or not, the edge state is a real Majorana mode, or a complex mode of Dirac type. In particular, in the four superconducting (BdG) classes $\{\mathrm{D}, \mathrm{C}, \mathrm{DIII}, \mathrm{CI}\}$ the particle-hole symmetry is naturally present and thus, topological superconductors host Majorana edge modes.

Topological insulator The field of topological states of matter has emerged with the detection of the integer quantum Hall effect in 1980 [11] in a system where the time-reversal symmetry has been broken by means of a magnetic field. The physics of the integer quantum Hall effect is captured by a Chern insulator whose characteristic is the broken TRS [68].

For more than 20 years, topological states were only known in combination with a broken time-reversal symmetry. It took until 2005, when Kane and Mele [69, 70] introduced a model that keeps the time-reversal symmetry intact, while it still hosts gapless edge states. Thus, they introduced a time-reversal invariant insulator, whose existence had been experimentally confirmed shortly after [71]. This discovery blew the field of topological insulators wide open [12, 66, 72]. The mechanism playing a key role in the formation of a topologically non-trivial insulator is the band inversion [73] which is also the mechanism at work for the Bi_2Se_3 family. The topological insulator Bi_2Se_3 falls into the symmetry class AII, where the electronic bands require $\hat{\mathcal{T}}^2 = -1$, and particle-hole symmetry is absent. As a

three-dimensional material it is described by a $\mathbb{Z}_2$ invariant[1] that is defined by

$$\nu_2 = \Pi_{i=1,..8} \frac{\sqrt{\det w(\boldsymbol{K}_i)}}{\mathrm{Pf}\, w(\boldsymbol{K}_i)} \,. \tag{2.1}$$

The product comprises the eight time-reversal invariant momenta $\boldsymbol{K}_i$ $(i = 1, \ldots, 8)$ of the Brioullin zone. A time-reversal invariant momentum is defined by $\boldsymbol{K}_i = -\boldsymbol{K}_i + \boldsymbol{G}$ with a reciprocal lattice vector $\boldsymbol{G}$. The sewing matrix $w_{ij}(\boldsymbol{k}) = \langle u_i(-\boldsymbol{k})|\hat{\mathcal{T}}|u_j(\boldsymbol{k})\rangle$ connects an occupied eigenstate $|u_i(\boldsymbol{k})\rangle$ of band i with the time-reversed counterpart of band j. In the presence of an additional inversion symmetry, i.e. in centro-symmetric systems like Bi_2Se_3, the expression (2.1) simplifies to

$$(-1)^{\nu_2} = \Pi_{i=1,..8} \left(\Pi_{j=1}^{N} \xi_{2j}(\boldsymbol{K}_i) \right) \,, \tag{2.2}$$

where $\xi_{2j}(\boldsymbol{K}_i) = \xi_{2j-1}(\boldsymbol{K}_i) = \pm 1$ denotes the parity eigenvalue of the $2j$th occupied energy band at the momentum $\boldsymbol{K}_i$. The product involves the $2N$ occupied bands.

Topological superconductor A topological superconductor naturally respects the particle-hole symmetry $\hat{\mathcal{C}}$ and it is classified according to one of the four Bogoliubov-de-Gennes (BdG) classes {D, C, DIII, CI}. Owed to the reality constraint posed by $\hat{\mathcal{C}}$, the topological edge states in superconductors are of Majorana type. Such edge states cause particular attraction for their potential applicability in quantum information technology. In a type-II superconductor these Majorana states also occur at the edges of vortices where the topological index changes analogously to the sample boundary [75–77]. One key experimental signature of Majorana modes is a zero-bias peak in the differential conductance.

Let us have a closer look on time-reversal invariant superconductors, i.e. members of the classes DIII—relevant for doped Bi_2Se_3—and CI. In three dimensions, the topological bulk index of both classes can be cast as a winding number that is computed via

$$\nu_w = \frac{1}{24\pi^2} \int d^3k\, \epsilon^{\mu\nu\rho} \mathrm{tr} \left[\left(q_{\boldsymbol{k}}^{-1} \partial_\mu q_{\boldsymbol{k}} \right) \left(q_{\boldsymbol{k}}^{-1} \partial_\nu q_{\boldsymbol{k}} \right) \left(q_{\boldsymbol{k}}^{-1} \partial_\rho q_{\boldsymbol{k}} \right) \right] \,, \tag{2.3}$$

with $\mu, \nu, \rho = k_x, k_y, k_z$ [67]. The integral extends over the entire Brioullin zone.[2] The matrix $q_{\boldsymbol{k}}$ is defined through the projector

$$Q_{\boldsymbol{k}} = 2P_{\boldsymbol{k}} - \mathbb{1} \quad \overset{\text{basis transf.}}{\longrightarrow} \quad \begin{pmatrix} 0 & q_{\boldsymbol{k}} \\ q_{\boldsymbol{k}}^\dagger & 0 \end{pmatrix} \,,$$

that can be brought, upon a basis transformation, into a block off-diagonal form. Hereby, the projection matrix $P_{\boldsymbol{k}}^{ij} = |u_i(\boldsymbol{k})\rangle\langle u_j(\boldsymbol{k})|$ projects into the occupied eigenstates of the Hamiltonian. Genuinely, the computation of topological indices like (2.3) is quite tedious. In the particular case of a centro-symmetric system where the pairing state has odd parity, it has been proven [16, 78] that the above winding number become non-zero if the two conditions are met: (i) the superconducting gap is fully established, and (ii) the Fermi surfaces enclose an odd number of time-reversal invariant momenta $\boldsymbol{K}_i$. In the reminder of this section we refer to these conditions as the Fu and Berg criterion.

[1] Actually, it is described by one strong $\mathbb{Z}_2$ invariant, and three weak $\mathbb{Z}_2$ invariants. For a discussion on the weak invariants, we refer to [74].

[2] In a continuum model, the integral can be carried out over the entire three-sphere [67].

While insulators characteristically have a large and full energy gap, superconductors may develop nodal gaps, i.e. gaps that vanish along certain directions in momentum space. Such nodal superconductors are not subject to the above classification that vitally depends on the existence of a full energy gap. Still, nodal superconductors can have non-zero topological numbers which are then defined as loops around the nodal structures [79]. These systems also host gapless edge modes which may exist along certain hinges or sample edges only [80]. For a comprehensive review on topological superconductivity we refer to Ref.[81] and references therein.

2.2 Topological insulator Bi_2Se_3

In this section, we introduce the Bi_2Se_3 material class including its structural and symmetry properties, as well as the established low-energy description. After having outlined the structural properties, we employ the framework developed in chapter 1.3.3 to deduce the model Hamiltonian. Lastly, we demonstrate the occurrence of topological helical edge states. In the pseudo-spin basis the topological $\mathbb{Z}_2$ index can be easily computed.

Crystal structure and symmetry elements The compound Bi_2Se_3 (and similarly Bi_2Te_3 and Sb_2Te_3) crystallizes into a trigonal structure that is characterized by the A, B, C stacking sketched in figure 2.1(a). The structure forms so-called quintuple layers between Se-Bi-Se-Bi-Se that are densely packed. Two adjacent outer Se layers are only weakly coupled through van-der-Waals interactions. The low energy physics are dominated by the properties within such a quintuple layer.
The primitive cell is constructed from the three lattice vectors $\boldsymbol{t}_1 = (0, -a/\sqrt{3}, c/3)$ and $\boldsymbol{t}_{2,3} = (\pm a/2, a/2\sqrt{3}, c/3)$ with the lattice constants $a = 4.1$ Å and $c = 28.6$ Å [82], and it is shown in figure 2.1(a,b), indicating the involved symmetry elements. The appropriate space group is $R\bar{3}m$ ($\mathsf{D}^5_{\mathsf{3d}}$) with the underlying point group $\mathsf{D_{3d}} = \{E, C_{2x}, C_{2\{A,B\}}, C_{3z}^{\pm 1}\} \times \{E, I\}$ consisting of twelve symmetry elements [83]. The in-plane axes read $\hat{\boldsymbol{n}}_{\{A,B\}} = (\pm 1, -\sqrt{3}, 0)/2$. Evidently, the x and y directions in these systems are not equivalent and have to be properly distinguished.[3] Using reciprocal lattice vectors $\boldsymbol{b}_1 = 2\pi(0, -2/a\sqrt{3}, 1/c)$ and $\boldsymbol{b}_{2,3} = 2\pi(\pm 1/a, 1/a\sqrt{3}, 1/c)$, the shape of the first Brillouin zone is shown in Fig.2.1(d). The eight time-reversal invariant (and inversion-invariant) momenta $\boldsymbol{K}_i$ read

$$\boldsymbol{\Gamma} = (0,0,0), \qquad \boldsymbol{L}_j = \frac{1}{2}\boldsymbol{b}_j, \qquad \boldsymbol{F}_j = \frac{1}{2}(\boldsymbol{b}_{1+j \bmod 3} + \boldsymbol{b}_{1+(j+1) \bmod 3}), \qquad \boldsymbol{Z} = \frac{1}{2}\sum_{j=1}^{3}\boldsymbol{b}_j, \tag{2.4}$$

with $j = \{1, 2, 3\}$.

2.2.1 Deduction of the model Hamiltonian

The well-established model Hamiltonian for the topological insulator family Bi_2Se_3, Bi_2Te_3 and Sb_2Te_3 has been proposed in [84, 85]. It is based on ab-initio calculations that exposed two bands which reside close to the Fermi surface at the Γ- point, in agreement with ARPES measurements [86]. Due to the presence of inversion and time-reversal symmetry, the two bands are doubly degenerate and they have been associated with hybridized P_z-orbitals from Bi and Se atoms within the quintuple layer. In their calculation the authors of Ref.[85] included an atomic spin-orbit coupling Hamiltonian $\mathcal{H}_{a-soc} = \lambda \boldsymbol{l} \cdot \boldsymbol{s}$

[3] It is also common to use the indications a and a^*, where it holds $a \hat{=} x$ and $a^* \hat{=} y$.

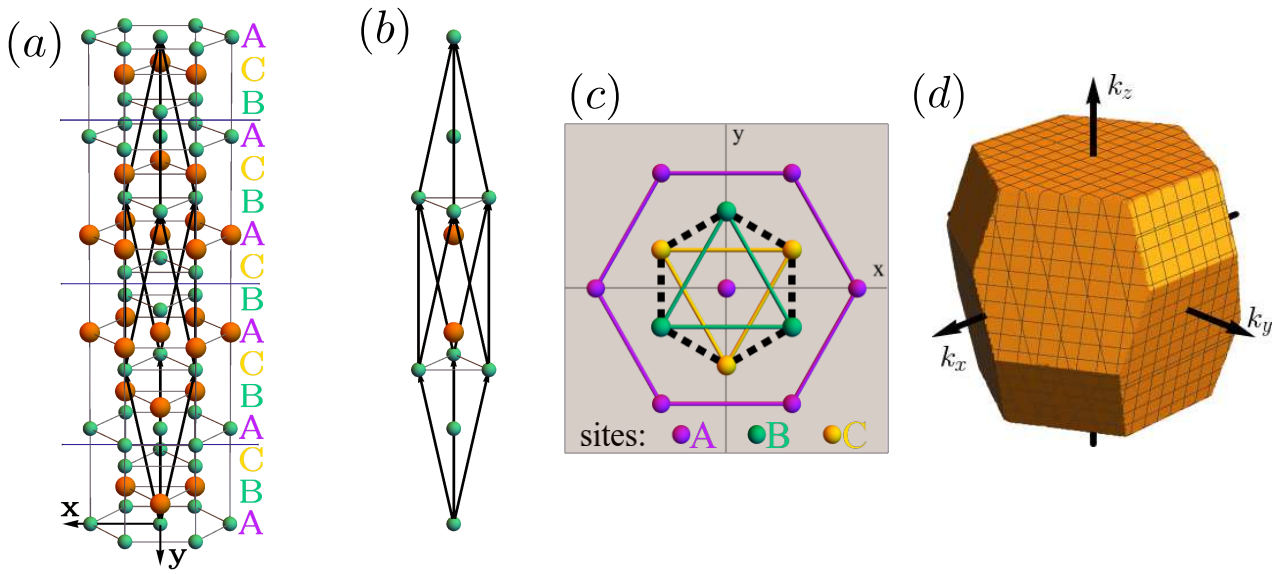

Figure 2.1: Figure (a) shows the unit cell of Bi_2Se_3 with the A,B,C stacking and the quintuple layers indicated. The orange and green spheres represent Bi and Se atoms, respectively. Figure (b) shows the primitive cell, while Figure (c) displays the top view on unit cell. Figure (d) depicts the first Brillouin cell.

with realistic values for the coupling constants, $\lambda(\mathrm{Bi}) = 1.25\,\mathrm{eV}$ and $\lambda(\mathrm{Se}) = 0.22\,\mathrm{eV}$ [87]. The energy levels have been found to cross at a certain momentum which is a prerequisite for the system to become topologically non-trivial. The two doublet states $(|P1_z^+,\uparrow\rangle, |P1_z^+,\downarrow\rangle)$ and $(|P2_z^-,\uparrow\rangle, |P2_z^-,\downarrow\rangle)$—with parity $\pm$ and spin $\uparrow,\downarrow$—transform according to the irreducible representations (IRs) E_{3g} and E_{3u} of the double group $\mathsf{D}'_{3\mathsf{d}}$ (cf. table 2.2), respectively.

In the following we derive the model Hamiltonian from [84, 85] with fully symmetry-compliant momentum dependencies apt for a lattice description. This part also serves as a pedagogical introduction into symmetry classifications based on a crystal double group.

Transformation matrices Regarding the upcoming classification it is convenient to first state the involved transformation matrices of the two-dimensional IRs, E_u,E_g, E_{3u} and E_{3g} of the double group $\mathsf{D}'_{3\mathsf{d}}$. The double group $\mathsf{D}'_{3\mathsf{d}}$ originates from the point group $\mathsf{D}_{3\mathsf{d}} = \mathsf{D}_3 \times \{E, I\}$ which itself is the product group consisting of the inversion and the D_3 groups. The D_3 group elements are denoted by $g_0 = \{E, C_{2x}, C_{2\{A,B\}}, C_{3z}^{\pm 1}\}$.

The IR E_u is the vector representation, i.e. it transforms like an (x, y)-vector. The IR E_g transforms like a pseudo-vector, i.e. it differs from E_u by a sign flip upon the inversion operation $\mathcal{R}_{E_{u/g}}(Ig_0) = \mp\mathcal{R}_{E_{u/g}}(g_0)$. For the elements g_0 the vector transformation matrices read

$$\mathcal{R}_{E_{u/g}}(C_{2x}) = \begin{pmatrix} 1 & 0 \\ 0 & -1 \end{pmatrix}, \quad \mathcal{R}_{E_{u/g}}(C_{2\{A,B\}}) = \frac{1}{2}\begin{pmatrix} -1 & \mp\sqrt{3} \\ \mp\sqrt{3} & 1 \end{pmatrix}, \quad \mathcal{R}_{E_{u/g}}(C_{3z}^{\pm 1}) = \frac{1}{2}\begin{pmatrix} -1 & \mp\sqrt{3} \\ \pm\sqrt{3} & -1 \end{pmatrix}. \tag{2.5}$$

The two IRs $E_{u/g}$ are real and thus, they transform trivially under 2π rotations, i.e. $\mathcal{R}_{E_{u/g}}(\bar{g}) =$

$\mathcal{R}_{E_{u/g}}(g)$ for $g \in \mathsf{D_{3d}}$ where $\bar{g}$ results from g by a rotation angle shift $\vartheta \to \vartheta + 2\pi$. This completes the matrix set for the real IRs $E_{u/g}$.

The spinor IR E_{3g} originates from an $SU(2)$ representation. The $SU(2)$ rotation matrix reads $R_{SU(2)}(\vartheta, \hat{\boldsymbol{n}}) = \exp\left(-\mathrm{i}\frac{\vartheta}{2}\,\mathfrak{s}\cdot\hat{\boldsymbol{n}}\right)$ which allows for a representation of the elements by, for example, $\mathcal{R}_{E_{3u}/E_{3g}}(C_{2x}) = R_{SU(2)}(\pi, \hat{\boldsymbol{e}}_x)$. Accordingly, the spinor matrices read

$$\mathcal{R}_{E_{3u/3g}}(C_{2x}) = -\begin{pmatrix} 0 & \mathrm{i} \\ \mathrm{i} & 0 \end{pmatrix}, \quad \mathcal{R}_{E_{3u/3g}}(C_{2\{A,B\}}) = \pm\begin{pmatrix} 0 & e^{\pm\mathrm{i}2\pi/3} \\ e^{\mp\mathrm{i}2\pi/3} & 0 \end{pmatrix}, \quad \mathcal{R}_{E_{3u/3g}}(C_{3z}^{\pm 1}) = -\begin{pmatrix} e^{\pm\mathrm{i}2\pi/3} & 0 \\ 0 & e^{\mp\mathrm{i}2\pi/3} \end{pmatrix}$$

with $\hat{\boldsymbol{n}}_{\{A,B\}} = (\pm 1, -\sqrt{3}, 0)/2$. Note that the two IRs only differ by the inversion symmetry $\mathcal{R}_{E_{3u/3g}}(Ig_0) = \mp\mathcal{R}_{E_{3u/3g}}(g_0)$. Since the two IRs originate from an $SU(2)$ representation they pick up a minus sign upon a 2π rotation, leading to the property $\mathcal{R}_{E_{3u/3g}}(\bar{g}) = -\mathcal{R}_{E_{3u/3g}}(g)$ which completes the matrix sets.

Symmetry constraints on Hamiltonian The Hamiltonian is derived in the basis of the two doublets $P1$ and $P2$ where we introduce the basis vector $\hat{\boldsymbol{c}} = (|P1_z^+,\uparrow\rangle, |P1_z^+,\downarrow\rangle, |P2_z^-,\uparrow\rangle, |P2_z^-,\downarrow\rangle)$ that transforms according to the representation $E_{3g} \oplus E_{3u}$. The authors in [84] have clarified that a C_{2x} rotation should create a relative minus sign between the two orbitals. This means the transformation matrices are not simply $\mathcal{R}_{E_{3g}}(g) \oplus \mathcal{R}_{E_{3u}}(g)$ but they have to be adjusted by the similarity transformation $S_{E_{3g}} = R_{SU(2)}(-\pi, \hat{\boldsymbol{e}}_z)$ leading to the unitary transformation matrices

$$\mathcal{U}_c(g) = \left(S_{E_{3g}}\mathcal{R}_{E_{3g}}(g)S_{E_{3g}}^\dagger \oplus \mathcal{R}_{E_{3u}}(g)\right). \tag{2.6}$$

To derive the Hamiltonian $\hat{\mathcal{H}} = \sum_{\boldsymbol{k}}(\hat{\boldsymbol{c}}_{\boldsymbol{k}}^\dagger)^T h(\boldsymbol{k})\hat{\boldsymbol{c}}_{\boldsymbol{k}}$, the single-particle Hamiltonian $h(\boldsymbol{k})$ has to fulfill the lattice (1.28) and the time-reversal (1.25) constraints, reading

$$\mathcal{U}_c(g)\, h(\mathcal{R}_v^\dagger(g)\boldsymbol{k})\, \mathcal{U}_c^\dagger(g) = h(\boldsymbol{k}), \qquad \mathcal{U}_\mathcal{T}\, h^T(-\boldsymbol{k})\, \mathcal{U}_\mathcal{T}^\dagger = h(\boldsymbol{k}). \tag{2.7}$$

The time-reversal operation $\mathcal{T} = \mathcal{U}_\mathcal{T}\,\mathcal{K}$ with the unitary part $\mathcal{U}_\mathcal{T} = \mathrm{i}\sigma^0\mathfrak{s}^y$ acts on the states $\hat{\boldsymbol{c}}$, where σ and $\mathfrak{s}$ denote the orbital and spin space Pauli matrices, respectively.

To account for the lattice constraint (2.7) we detach the orbital (spin, etc.) degrees of freedom from the spatial part of the single-particle Hamiltonian $h(\boldsymbol{k})_{\alpha\beta} = \omega^{n,i,\mu}(\boldsymbol{k})\lambda^{n,i,\mu}_{\alpha\beta}$ where the matrices $\lambda^{n,i,\mu}$ are chosen such that they satisfy the condition

$$\mathcal{U}_c(g)\,\lambda^{n,i,\mu}\,\mathcal{U}_c^\dagger(g) = \mathcal{R}_n^\dagger(g)_{\mu\mu'}\lambda^{n,i,\mu'}, \tag{2.8}$$

with the IR n, the corresponding components $\mu = 1, .., \dim(n)$ and the multiplicity index i. Doubly occurring indices are assumed to be summed over. The occurring IRs and their multiplicities can be read off from the decomposition of the bilinear form

$$\left(E_{3g} \oplus E_{3u}\right)^* \otimes \left(E_{3g} \oplus E_{3u}\right) = 2A_{1g} \oplus 2A_{1u} \oplus 2A_{2g} \oplus 2A_{2u} \oplus 2E_g \oplus 2E_u\,. \tag{2.9}$$

Here, each of the six IRs occurs twice ($i = 1, 2$). Since the bilinear combination of the IRs E_{3g} and E_{3u} transforms trivially upon 2π rotations, the decomposed IRs in (2.9) have to be part of the underlying point group $\mathsf{D_{3d}}$. We list the identified matrices $\lambda^{n,i,\mu}$ in table 2.3, together with their transformation behavior upon the time-reversal operation (2.7).

D'_{3d}	E	$2C_{3z}$	$3C_{2x}$	$\bar{E}$	$2\bar{C}_{3z}$	$3\bar{C}_{2x}$	IE	$2IC_{3z}$	$3IC_{2x}$	$I\bar{E}$	$2I\bar{C}_{3z}$	$3I\bar{C}_{2x}$	Reality
A_{1g}	1	1	1	1	1	1	1	1	1	1	1	1	pot. real
A_{2g}	1	1	-1	1	1	-1	1	1	-1	1	1	-1	pot. real
E_g	2	-1	0	2	-1	0	2	-1	0	2	-1	0	pot. real
E_{2g}	1	-1	i	-1	1	-i	1	-1	i	-1	1	-i	ess. complex
$\bar{E}_{2g}$	1	-1	-i	-1	1	i	1	-1	-i	-1	1	i	ess. complex
E_{3g}	2	1	0	-2	-1	0	2	1	0	-2	-1	0	pseudo-real
A_{1u}	1	1	1	1	1	1	-1	-1	-1	-1	-1	-1	pot. real
A_{2u}	1	1	-1	1	1	-1	-1	-1	1	-1	-1	1	pot. real
E_u	2	-1	0	2	-1	0	-2	1	0	-2	1	0	pot. real
E_{2u}	1	-1	i	-1	1	-i	-1	1	-i	1	-1	i	ess. complex
$\bar{E}_{2u}$	1	-1	-i	-1	1	i	-1	1	i	1	-1	-i	ess. complex
E_{3u}	2	1	0	-2	-1	0	-2	-1	0	2	1	0	pseudo-real

Table 2.2: Character table of the double group D'_{3d}. The elements group into the classes like $2C_{3z} = \{C_{3z}, C_{3z}^{-1}\}$, $2\bar{C}_{3z} = \{\bar{C}_{3z}, \bar{C}_{3z}^{-1}\}$, $3C_{2x} = \{C_{2x}, \bar{C}_{2A}, \bar{C}_{2B}\}$ and $3\bar{C}_{2x} = \{\bar{C}_{2x}, C_{2A}, C_{2B}\}$. A vector transforms according to $E_u \oplus A_{2u}$.

It is convenient to classify the spatial functions $\omega^{n,i,\mu}(\boldsymbol{k})$ such that they satisfy the transformation property.

$$\omega^{n,i,\mu}(\mathcal{R}_v^\dagger(g)\boldsymbol{k}) = \omega^{n,i,\mu'}(\boldsymbol{k})\mathcal{R}_n(g)_{\mu'\mu} \,. \tag{2.10}$$

By this means, the combination $\omega^{n,i,\mu}(\boldsymbol{k})\lambda^{n,i,\mu}_{\alpha\beta}$ transforms trivially and is an allowed contribution to the Hamiltonian. The simplest solutions to (2.10) are obtained from a power expansion around the Γ-point in terms of $\boldsymbol{k}$

$$\omega^{n,i,\mu}(\boldsymbol{k}) \approx \omega^{n,i,\mu}_{\alpha} k_\alpha + \omega^{n,i,\mu}_{\alpha\beta} k_\alpha k_\beta + \omega^{n,i,\mu}_{\alpha\beta\gamma} k_\alpha k_\beta k_\gamma + \mathcal{O}(k^4)\,.$$

Then, the polynomials have to satisfy the conditions

$$\omega^{n,i,\mu}_{\alpha'}\mathcal{R}_v^\dagger(g)_{\alpha'\alpha} = \omega^{n,i,\mu'}_{\alpha}\mathcal{R}_n(g)_{\mu'\mu}\,, \qquad \omega^{n,i,\mu}_{\alpha'\beta'}\mathcal{R}_v^\dagger(g)_{\alpha'\alpha}\mathcal{R}_v^\dagger(g)_{\beta'\beta} = \omega^{n,i,\mu'}_{\alpha\beta}\mathcal{R}_n(g)_{\mu'\mu}\,, \qquad \text{etc.},$$

$\mathsf{D}'_{3\mathsf{d}}$	matrix $\lambda^{n,1,\mu}$	TRS	matrix $\lambda^{n,2,\mu}$	TRS
A_{1g}	$\sigma^0\mathfrak{s}^0$	$+$	$\sigma^z\mathfrak{s}^0$	$+$
A_{2g}	$\sigma^0\mathfrak{s}^z$	$-$	$\sigma^z\mathfrak{s}^z$	$-$
E_g	$\sigma^0\left(\mathfrak{s}^x,\mathfrak{s}^y\right)$	$-$	$\sigma^z\left(\mathfrak{s}^x,\mathfrak{s}^y\right)$	$-$
A_{1u}	$\sigma^x\mathfrak{s}^z$	$-$	$\sigma^y\mathfrak{s}^z$	$+$
A_{2u}	$\sigma^x\mathfrak{s}^0$	$+$	$\sigma^y\mathfrak{s}^0$	$-$
E_u	$\sigma^x\left(\mathfrak{s}^y,-\mathfrak{s}^x\right)$	$-$	$\sigma^y\left(\mathfrak{s}^y,-\mathfrak{s}^x\right)$	$+$

Table 2.3: Association of the IRs n occurring in the bilinear form of the basis states (2.9) and their respective matrices $\lambda^{n,i,\mu}$ resulting from (2.8). Additionally, the respective transformation behavior upon the time-reversal symmetry operation (2.7) is added. The matrices highlighted in purple are the ones that can be paired with a spatial function to transform trivially, and thus, occur in the Hamiltonian (2.16).

and the resultant functions read

$$A_{1g}: \quad f_{\boldsymbol{k}}^{A_{1g}} = \mathsf{d}_1^{A_{1g}}\left(\tilde{k}_x^2+\tilde{k}_y^2\right)+\mathsf{d}_2^{A_{1g}}\tilde{k}_z^2 \tag{2.11}$$

$$A_{1u}: \quad f_{\boldsymbol{k}}^{C_3} = R_1\left(\tilde{k}_x^3-3\tilde{k}_x\tilde{k}_y^2\right) \tag{2.12}$$

$$A_{2u}: \quad f_{\tilde{\boldsymbol{k}}}^{z} = v_z\tilde{k}_z+R_2\left(\tilde{k}_y^3-3\tilde{k}_y\tilde{k}_x^2\right) \tag{2.13}$$

$$E_g: \quad \begin{pmatrix} f_{\boldsymbol{k}}^{E_g,1} \\ f_{\boldsymbol{k}}^{E_g,2} \end{pmatrix} = 2\mathsf{d}_1^{E_g}\begin{pmatrix} \tilde{k}_y\tilde{k}_z \\ -\tilde{k}_x\tilde{k}_z \end{pmatrix}+\mathsf{d}_2^{E_g}\begin{pmatrix} \tilde{k}_x^2-\tilde{k}_y^2 \\ -2\tilde{k}_x\tilde{k}_y \end{pmatrix} \tag{2.14}$$

$$E_u: \quad \begin{pmatrix} f_{\boldsymbol{k}}^{x} \\ f_{\boldsymbol{k}}^{y} \end{pmatrix} = v_0\begin{pmatrix} \tilde{k}_x \\ \tilde{k}_y \end{pmatrix}+\mathsf{d}_2^{E_u}\tilde{k}_z\begin{pmatrix} 2\tilde{k}_x\tilde{k}_y \\ \tilde{k}_x^2-\tilde{k}_y^2 \end{pmatrix}. \tag{2.15}$$

with the dimensionless momentum $\tilde{\boldsymbol{k}} = (k_x a, k_y a, k_z c)$. In the appendix A.3 we show the spatial functions in a lattice representation that is fully symmetry-compliant.

Altogether, the symmetry-allowed contributions can be added to reproduce the model Hamiltonian from Ref.[84]

$$h(\boldsymbol{k}) = \sigma^0\mathfrak{s}^0\left(-\mu+C_{\boldsymbol{k}}\right)+\sigma^z\mathfrak{s}^0M_{\boldsymbol{k}}+\sigma^x\left(\mathfrak{s}^y f_{\boldsymbol{k}}^x-\mathfrak{s}^x f_{\boldsymbol{k}}^y\right)-\sigma^y\mathfrak{s}^0 f_{\tilde{\boldsymbol{k}}}^z+\sigma^x\mathfrak{s}^z f_{\boldsymbol{k}}^{C_3}, \tag{2.16}$$

with the functions $M_{\boldsymbol{k}} = M_0 + M_2(\tilde{k}_x^2+\tilde{k}_y^2) + M_1 2(1-\cos(\tilde{k}_z))$ and $C_{\boldsymbol{k}} = C_0 + C_2(\tilde{k}_x^2+\tilde{k}_y^2) + C_1 2(1-\cos(\tilde{k}_z))$. The parameters have been derived from ab-initio calculations in Ref.[84]. Unless stated otherwise, we use their values for Bi_2Se_3 reading $M_0 = -0.28\,\mathrm{eV}$, $M_2 = 44.5\,\mathrm{eV\AA}^2/a^2$, $M_1 = 6.86\,\mathrm{eV\AA}^2/c^2$, $C_0 = -0.0083\,\mathrm{eV}$, $C_2 = 30.4\,\mathrm{eV\AA}^2/a^2$, $C_1 = 5.74\,\mathrm{eV\AA}^2/c^2$ $v_0 = 3.33\,\mathrm{eV\AA}/a$, $v_z = -2.26\,\mathrm{eV\AA}/c$, $R_1 = 50.6\,\mathrm{eV\AA}^3/a^3$, and $R_2 = 113.3\,\mathrm{eV\AA}^3/a^3$.

Pseudo-spin band basis In a system with both, time-reversal and inversion symmetry intact each energy level is at least fourfold degenerate, and more importantly, the existence of a pseudo-spin basis is guaranteed. In a pseudo-spin basis the basis components transform just like an ordinary $SU(2)$ spinor under the inversion and the time-reversal operation (cf. Sec.1.3.4). In the context of Bi_2Se_3 this basis has been introduced by the name *manifestly covariant Bloch basis (MCBB)* [57]. We label the corresponding band basis vector by $\hat{\boldsymbol{\psi}}_k = (|\psi^c_k,+\rangle, |\psi^c_k,-\rangle, |\psi^v_k,+\rangle, |\psi^v_k,-\rangle)$ with the conduction and the valence band doublets satisfying the $SU(2)$ transformation relations

$$\hat{\mathcal{T}}|\psi^{c,v}_k,\pm\rangle = \pm\mathrm{sign}(M_{\boldsymbol{k}})|\psi^{c,v}_{-k},\mp\rangle\,, \qquad \hat{\mathcal{U}}_I|\psi^{c,v}_k,\pm\rangle = (\pm1)^{c,v}\mathrm{sign}(M_{\boldsymbol{k}})|\psi^{c,v}_{-k},\pm\rangle\,. \tag{2.17}$$

The inversion operation $\hat{\mathcal{U}}_I$ eigenvalue $(\pm1)^{c,v}$ picks $+1$ for the conduction and -1 for the valence band. For the single-particle Hamiltonian (2.16) in the basis $\hat{\boldsymbol{c}}_{\boldsymbol{k}}$, the appropriate unitary transformation matrix $U_b(\boldsymbol{k})$ that diagonalizes the system into the pseudo-spin basis $\hat{\boldsymbol{\psi}}_k = U_b^\dagger(\boldsymbol{k})\hat{\boldsymbol{c}}_{\boldsymbol{k}}$ reads

$$\begin{aligned} U_b(\boldsymbol{k}) = \mathrm{sign}(M_{\boldsymbol{k}})\beta^+_{\boldsymbol{k}}\left(\alpha^+_{\boldsymbol{k}}\sigma^z\mathfrak{s}^0 + \alpha^-_{\boldsymbol{k}}\sigma^x\mathfrak{s}^z\right) - \tilde{f}^z_{\boldsymbol{k}}\beta^-_{\boldsymbol{k}}\left(\alpha^+_{\boldsymbol{k}}\sigma^y\mathfrak{s}^0 + \mathrm{i}\alpha^-_{\boldsymbol{k}}\sigma^0\mathfrak{s}^z\right) \\ + \tilde{f}^x_{\boldsymbol{k}}\beta^-_{\boldsymbol{k}}\left(-\alpha^+_{\boldsymbol{k}}\sigma^x\mathfrak{s}^y + i\alpha^-_{\boldsymbol{k}}\sigma^z\mathfrak{s}^x\right) + \tilde{f}^y_{\boldsymbol{k}}\beta^-_{\boldsymbol{k}}\left(\alpha^+_{\boldsymbol{k}}\sigma^x\mathfrak{s}^x + i\alpha^-_{\boldsymbol{k}}\sigma^z\mathfrak{s}^y\right)\,, \end{aligned} \tag{2.18}$$

with the functions being defined below.[4] The Hamiltonian in the band basis $\hat{\mathcal{H}} = \sum_{\boldsymbol{k}}(\hat{\boldsymbol{\psi}}^\dagger_{\boldsymbol{k}})^T h_b(\boldsymbol{k})\hat{\boldsymbol{\psi}}_{\boldsymbol{k}}$ is characterized through the single-particle Hamiltonian $h_b(\boldsymbol{k}) = U_b^\dagger(\boldsymbol{k})h(\boldsymbol{k})U_b(\boldsymbol{k}) = \mathrm{diag}(E^+_{\boldsymbol{k}}, E^+_{\boldsymbol{k}}, E^-_{\boldsymbol{k}}, E^-_{\boldsymbol{k}})$ with the eigenenergies $E^\pm_{\boldsymbol{k}} = -\mu + f^0_{\boldsymbol{k}} \pm \lambda_{\boldsymbol{k}}$. We have defined $\lambda_{\boldsymbol{k}} = \sqrt{M^2_{\boldsymbol{k}} + \boldsymbol{f}^2_{\boldsymbol{k}} + (f^{C_3}_{\boldsymbol{k}})^2}$, $\boldsymbol{f}_{\boldsymbol{k}} = (f^x_{\boldsymbol{k}}, f^y_{\boldsymbol{k}}, f^z_{\boldsymbol{k}})^T$, $\hat{M}_{\boldsymbol{k}} = M_{\boldsymbol{k}}/\sqrt{M^2_{\boldsymbol{k}} + \boldsymbol{f}^2_{\boldsymbol{k}}}$, $\beta^\pm_{\boldsymbol{k}} = \frac{1}{2}\sqrt{1 \pm |\hat{M}_{\boldsymbol{k}}|}$, $\hat{f}^{C_3}_{\boldsymbol{k}} = f^{C_3}_{\boldsymbol{k}}/\lambda_{\boldsymbol{k}}$, $\alpha^\pm_{\boldsymbol{k}} = \frac{1}{\sqrt{2}}\Big(\mathrm{sign}(M_{\boldsymbol{k}})\sqrt{1+\hat{f}^{C_3}_{\boldsymbol{k}}} \pm \sqrt{1-\hat{f}^{C_3}_{\boldsymbol{k}}}\Big)$ and $\tilde{f}^j_{\boldsymbol{k}} \equiv f^j_{\boldsymbol{k}}/|\boldsymbol{f}_{\boldsymbol{k}}|$, $\hat{f}^j_{\boldsymbol{k}} = f^j_{\boldsymbol{k}}/\sqrt{M^2_{\boldsymbol{k}} + \boldsymbol{f}^2_{\boldsymbol{k}}}$ with $j = \{x,y,z\}$.

Edge states The model Hamiltonian (2.16) involves a non-trivial topological index ν_2 characterized by the $\mathbb{Z}_2$ number (2.1). The pseudo-spin relation (2.17) directly leads to the sewing matrix $w(\boldsymbol{k}) = \mathrm{sign}(M_{\boldsymbol{k}})\mathrm{i}\tilde{\mathfrak{s}}^y$, and hence to the topological index

$$\nu_2 = \prod_{i=1}^{8}\mathrm{sign}(M_{\boldsymbol{K}_i}). \tag{2.19}$$

In a system stacked along the z-direction (infinite in the x and y directions) it is sufficient to consider $M_{\boldsymbol{\Gamma}} = M_0$ and $M_{\boldsymbol{Z}} = M_0 + 4M_1$. If the two values have opposite sign, the system is topologically non-trivial, as demonstrated in figure 2.2. The emerging gapless edge states are helical. To see this, we focus on the vicinity of the Γ-point, where the cubic momentum contributions can be neglected. Then, the Hamiltonian commutes with the helicity operator

$$\hat{h}_{\mathrm{helicity}} = \sigma^0\left(\mathfrak{s}\times\hat{\boldsymbol{k}}\right)_z = \sigma^0\left(\mathfrak{s}^x\tilde{k}_y - \mathfrak{s}^y\tilde{k}_x\right)/\sqrt{\tilde{k}^2_x + \tilde{k}^2_y}\,, \tag{2.20}$$

and consequently, they share an eigenbasis. In particular, the edge states are eigenstates of both, the Hamiltonian and the helicity operator. The helicity operator (2.20) coerces the states to have their

[4] It is easily checked that the new basis $\hat{\boldsymbol{\psi}}_k$ actually satisfies the conditions (2.17), by using the inversion and time-reversal operations in the original (momentum independent) basis states $\hat{\mathcal{U}}_c(I)\hat{\boldsymbol{c}} = \sigma^z\mathfrak{s}^0\hat{\boldsymbol{c}}$ and $\hat{\mathcal{T}}\hat{\boldsymbol{c}} = \mathrm{i}\sigma^0\mathfrak{s}^y\hat{\boldsymbol{c}}$.

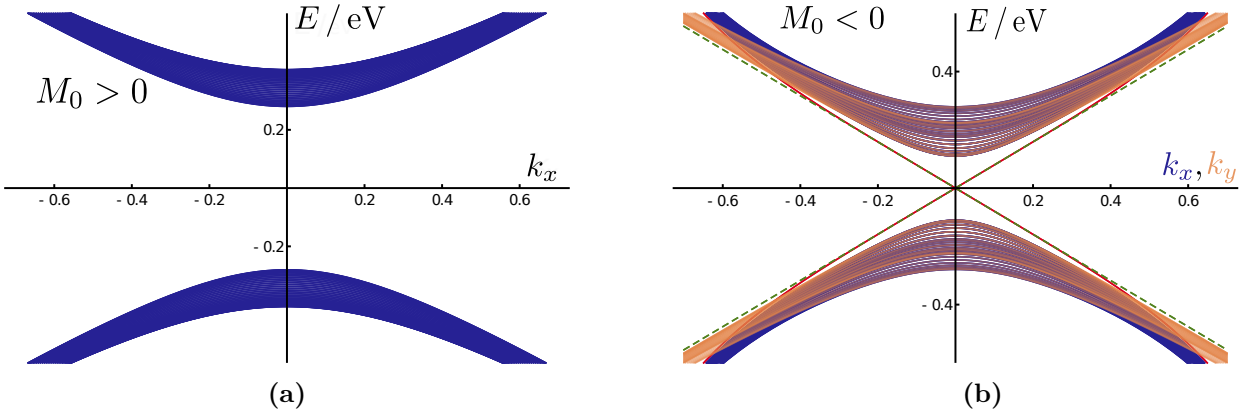

(a) **(b)**

Figure 2.2: Energy dispersions of the Hamiltonian (2.16) for a system stacked along the z-direction, and infinite in the x, y-directions. The left figure depicts a trivial state with $M_0 > 0$. The right figure shows the system in a topological state. The negative mass $M_0 < 0$ has caused a non-trivial ν_2 (2.19), which lead to gapless states living on the edges (top and bottom layer) of the sample. The crystalline inequivalence between the k_x and k_y direction is equally reflected by the bulk and the edge states, with $k_{F,x} < k_{F,y}$.

in-plane spin orthogonal to the momentum $\hat{\boldsymbol{k}}$, and hence, the spin winds around the Dirac cone. Due to inversion and time-reversal symmetry every state is fourfold degenerate with two respective states living on either side of the sample. The two edge states on one side have opposite helicity and they counter-propagate [84].

In figure 2.2(b), we illustrate the inequivalence between the k_x and k_y directions caused by the hexagonal warping terms R_1 and R_2 at finite momenta. The edge states reflect the same inequivalence with $k_{F,x} < k_{F,y}$, which has been extensively studied in [88, 89].

2.3 Doped Bi_2Se_3 and nematic superconductivity

In this section, we introduce the multi-faceted superconducting state which emerges out of the topological insulator Bi_2Se_3 upon Cu, Sr or Nb doping. We approach the issue from the theoretical side first, where we begin by classifying and analyzing the possible superconducting pairing states. Afterwards, the experimental achievements are outlined and contrasted with the pairing candidates. In the last part, we study the E_u ground state phases with an analysis of the discriminating parameter ν_- attached. The parameter ν_-discerns between the otherwise degenerate states $(1,0)$ and $(0,1)$.

2.3.1 Pairing state candidates

Using the developed formalism from section 1.3.4, we can directly classify the possible pairing states. We start from the generalized BCS mean-field Hamiltonian (1.21)

$$\hat{\mathcal{H}} = \sum_{\boldsymbol{k}} \left(\hat{\boldsymbol{c}}^\dagger_{\boldsymbol{k}}\right)^T h(\boldsymbol{k}) \hat{\boldsymbol{c}}_{\boldsymbol{k}} + \sum_{\boldsymbol{kq}} \left(\left(\hat{\boldsymbol{c}}^\dagger_{\boldsymbol{k}+\frac{\boldsymbol{q}}{2}}\right)^T \Delta(\boldsymbol{k},\boldsymbol{q}) \hat{\boldsymbol{c}}^\dagger_{-\boldsymbol{k}+\frac{\boldsymbol{q}}{2}} + H.c. \right), \tag{2.21}$$

written in the basis $\hat{\boldsymbol{c}} = (|P1^+_z,\uparrow\rangle, |P1^+_z,\downarrow\rangle, |P2^-_z,\uparrow\rangle, |P2^-_z,\downarrow\rangle)$.[5] Following the lines of Sec.1.3.4, we expand the pairing function in terms of the IRs n and their components $\mu = 1,..,\dim(n)$,

$$\Delta_{\alpha\beta}(\boldsymbol{k},\boldsymbol{q}) = \sum_{n,\mu} \Delta^{n,\mu}_{\boldsymbol{q}} \left(\chi^{n,\mu}_{\boldsymbol{k},\boldsymbol{q}} \lambda^{n,\mu}\right)^\dagger_{\alpha\beta} , \qquad \Delta^{n,\mu}_{\boldsymbol{q}} \in \mathbb{C} .$$

The microscopic degrees of freedom are denoted by $\alpha,\beta = 1,\ldots,N_0$. The associated partner functions $(\chi^{n,\mu}_{\boldsymbol{k},\boldsymbol{q}}\lambda^{n,\mu})$ account for spatial variations of the gap function. These functions have to satisfy the following constraints (see 1.3.4)

$$\text{lattice}: \quad \mathcal{U}_c(g)\left(\chi^{n,\mu}_{\mathcal{R}^\dagger_v(g)\boldsymbol{k},\mathcal{R}^\dagger_v(g)\boldsymbol{q}} \lambda^{n,\mu}\right)^\dagger \mathcal{U}_c^T(g) = \mathcal{R}^T_n(g)_{\mu\mu'} \left(\chi^{n,\mu'}_{\boldsymbol{k},\boldsymbol{q}} \lambda^{n,\mu'}\right)^\dagger \qquad \forall g \in \mathsf{D}'_{\mathsf{3d}} , \tag{2.22}$$

$$\text{anti-symmetry}: \quad \left(\chi^{n,\mu}_{\boldsymbol{k},\boldsymbol{q}}\right)^* \left(\lambda^{n,\mu}\right)^\dagger = -\left(\chi^{n,\mu}_{-\boldsymbol{k},\boldsymbol{q}}\right)^* \left(\left(\lambda^{n,\mu}\right)^\dagger\right)^T , \tag{2.23}$$

$$\text{time-reversal}: \quad \chi^{n,\mu}_{\boldsymbol{k},\boldsymbol{q}} \mathcal{U}_{\mathcal{T}} \left(\left(\lambda^{n,\mu}\right)^\dagger\right)^\dagger \mathcal{U}_{\mathcal{T}} = \left(\chi^{\bar{n},\mu}_{\boldsymbol{k},-\boldsymbol{q}}\right)^* \left(\lambda^{\bar{n},\mu}\right)^\dagger . \tag{2.24}$$

To make further progress, we assume the orbital basis to be roughly momentum independent.[6] Then, it is justified to expand the spatial function $\chi^{n,\mu}_{\boldsymbol{k},\boldsymbol{q}} \approx \chi^{n,\mu}_0 + \chi^{n,\mu}_{1,i}\tilde{k}_i + \ldots$ in powers of $\boldsymbol{k}$ and $\boldsymbol{q}$. The insertion of the expansion into the lattice constraint (2.22) leads to the simpler conditions

$$\mathcal{U}_c(g)(\chi^{n,\mu}_0)^* \left(\lambda^{n,\mu}\right)^\dagger \mathcal{U}_c^T(g) = \mathcal{R}^T_n(g)_{\mu\mu'} (\chi^{n,\mu}_0)^* \left(\lambda^{n,\mu'}\right)^\dagger \qquad \forall g \in \mathsf{D}'_{\mathsf{3d}} , \tag{2.25}$$

$$\mathcal{U}_c(g) (\chi^{n,\mu}_{1,i})^* \mathcal{R}^\dagger_v(g)_{i,i'} \tilde{k}_{i'} \left(\lambda^{n,\mu}\right)^\dagger \mathcal{U}_c^T(g) = \mathcal{R}^T_n(g)_{\mu\mu'} (\chi^{n,\mu'}_{1,i})^* \tilde{k}_i \left(\lambda^{n,\mu'}\right)^\dagger \qquad \forall g \in \mathsf{D}'_{\mathsf{3d}} , \tag{2.26}$$

[5] The pairing state candidates have been first identified in [16] where they have worked within a rotated basis $\exp(-\mathrm{i}\frac{\pi}{4}\sigma^y)\mathfrak{s}^0\,\hat{\boldsymbol{c}}$.

[6] This assumption is often applied. Certainly, the resulting pairing states give qualitative insights into the respective gap structures. Yet, the justifiability of the assumption can only be determined through a microscopic computation.

$\mathsf{D}'_{\mathsf{3d}}$	$\chi_0^{n,\mu}(\lambda^{n,1,\mu})^\dagger$	$\tilde{k}_i\chi_{1,i}^{n,\mu}\,(\lambda^{n,1,\mu})^\dagger$
A_{1g}	$\left\{\mathsf{i}\sigma^0\mathfrak{s}^y, \mathsf{i}\sigma^z\mathfrak{s}^y\right\}$	…
A_{2g}	—	$\left\{k_z\sigma^x\mathfrak{s}^x, \mathsf{i}\sigma^x\left(\mathsf{i}k_x\mathfrak{s}^z + k_y\mathfrak{s}^0\right)\right\}$
E_g	—	$\left\{\mathsf{i}k_z\sigma^x\begin{pmatrix}\mathsf{i}\mathfrak{s}^z\\ \mathfrak{s}^0\end{pmatrix}, \mathsf{i}\sigma^x\begin{pmatrix}k_x\mathfrak{s}^0+\mathsf{i}k_y\mathfrak{s}^z\\ \mathsf{i}k_x\mathfrak{s}^z-k_y\mathfrak{s}^0\end{pmatrix}, \mathsf{i}\sigma^y\mathfrak{s}^y\begin{pmatrix}k_y\\ -k_x\end{pmatrix}, \sigma^x\mathfrak{s}^x\begin{pmatrix}k_x\\ k_y\end{pmatrix}\right\}$
A_{1u}	$\sigma^y\mathfrak{s}^x$	…
A_{2u}	$\mathsf{i}\sigma^x\mathfrak{s}^y$	…
E_u	$\sigma^y\left(\mathsf{i}\mathfrak{s}^0, \mathfrak{s}^z\right)$	…

Table 2.4: Classified homogeneous pairing states. The first column shows the resulting pairing matrices $\lambda^{n,i,\mu}$ for on-site pairing (2.25). The second column depicts the leading-order contributions in the even-parity channels A_{2g} and E_g, resulting from (2.26).

with the unitary matrices (2.6).

We list the resulting, leading-order pairing terms for each irreducible representation in table 2.4. The on-site pairing states, shown in the first column, are only possible in the trivial or the odd-parity channels. Note that the bilinear decomposition of the pairing function, would naively generate twelve pairing channels, as shown in (2.9). Yet, many of the occurring matrices are not anti-symmetric, and hence, they violate the condition (2.23). This circumstance could, in principle, be fixed by pairing them with the trivially-transforming spatial function $\chi^{n,\mu}_{\boldsymbol{k},\boldsymbol{q}} = \chi_3^n\,\tilde{\boldsymbol{k}}\cdot\tilde{\boldsymbol{q}}$. However, the condensation of a pairing state with a finite center-of-mass momentum $\boldsymbol{q}$ is in general energetically more costly, and thus, such inhomogeneous pairing states are not listed in the table. The second column of the table shows the linear-in-momentum contributions for the even-parity channels A_{2g} and E_g. As a final touch, the expressions need to satisfy the time-reversal symmetry constraint (2.24) which is always possible, and which simply requires the right placement of the imaginary unit i, as done in the table 2.4.

Visualization of pairing states The pairing states and the corresponding gap structure can be best visualized in the band basis. In the pseudo-spin basis, the pairing function can be expressed in terms of the $\boldsymbol{d}$-vector representation (cf. (1.39))

$$\Delta(\boldsymbol{k},\boldsymbol{q}) = d^0_{\boldsymbol{k},\boldsymbol{q}}\,\mathsf{i}\tilde{\mathfrak{s}}^y + \boldsymbol{d}_{\boldsymbol{k},\boldsymbol{q}}\cdot\left(\tilde{\mathfrak{s}}^x,\tilde{\mathfrak{s}}^y,\tilde{\mathfrak{s}}^z\right)\mathsf{i}\tilde{\mathfrak{s}}^y\,, \tag{2.27}$$

where the entire gap function information is encapsulated in the d functions with $d^0_{-\boldsymbol{k},\boldsymbol{q}} = d^0_{\boldsymbol{k},\boldsymbol{q}}$ and $\boldsymbol{d}_{-\boldsymbol{k},\boldsymbol{q}} = -\boldsymbol{d}_{\boldsymbol{k},\boldsymbol{q}}$. To employ a $\boldsymbol{d}$-vector description, the generalized mean-field Hamiltonian (2.21) is 'rotated' into the band basis (2.18) where the resultant pairing function becomes

$$\Delta_b(\boldsymbol{k},\boldsymbol{q}) = U_b^\dagger(\boldsymbol{k}+\frac{\boldsymbol{q}}{2})\Delta(\boldsymbol{k},\boldsymbol{q})U_b^*(-\boldsymbol{k}+\frac{\boldsymbol{q}}{2})\,. \tag{2.28}$$

In the course of the unitary transformation one has to adjust the bookkeeping—in a 'one-by-one' correspondence, the former orbital and spin matrices $\left(\sigma,\mathfrak{s}\right)$ convert into the band and the pseudo-spin indices $\left(\tilde{\sigma},\tilde{\mathfrak{s}}\right)$. As pointed out in (1.39), the notation (2.27) is only applicable to centro-symmetric and time-

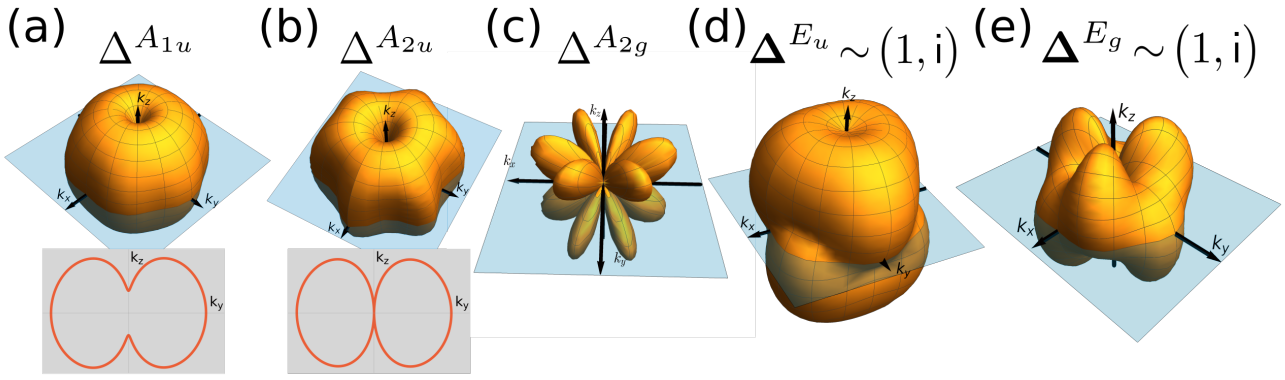

Figure 2.3: Bogoliubov gap structure for the five indicated pairing states, evaluated for a spherical Fermi surface. The three states $\Delta^{A_{1u}}$, $\Delta^{A_{2u}}$ and $\Delta^{A_{2g}}$ exhibit a six-fold symmetric gap structure, while the chiral states $\mathbf{\Delta}^{E_{u/g}} \sim (1, \mathrm{i})$ respect a three-fold symmetry. The $\Delta^{A_{2u}}$ and the $\mathbf{\Delta}^{E_g} \sim (1, \mathrm{i})$ gaps have a point node, and the $\Delta^{A_{2g}}$ state forms various line nodes.

reversal invariant systems.[7] Starting from a multi-orbital basis, the 2×2 pseudo-spin description makes only sense if the influence from the other bands can be neglected. In doped Bi_2Se_3 the chemical potential is moved into the conduction band, and following the outlined logic, we assume that their is no substantial coupling to the valence band states. Thus, we restrict the analysis on the conduction band subspace $\Delta_{cc}(\boldsymbol{k}, \boldsymbol{q})$ which is extracted from the pairing function via $\Delta_b(\boldsymbol{k}, \boldsymbol{q}) = \Delta_{cc}(\boldsymbol{k}, \boldsymbol{q})\mathrm{i}\tilde{\mathfrak{s}}^y \frac{\tilde{\sigma}^0+\tilde{\sigma}^z}{2} + \dots$. The explicit calculation is shown in the appendix B. For zero center-of-mass momentum $\boldsymbol{q}$ the BdG Hamiltonian (2.21) can be recast in Nambu space $\hat{\boldsymbol{\psi}}_{\boldsymbol{k}}^{\mathsf{Nam}} = ((|\psi_{\boldsymbol{k}}^c, +\rangle, |\psi_{\boldsymbol{k}}^c, -\rangle), \mathrm{i}\tilde{\mathfrak{s}}^y((|\psi_{-\boldsymbol{k}}^c, +\rangle, |\psi_{-\boldsymbol{k}}^c, -\rangle)^\dagger)^T)^T$,

$$\hat{\mathcal{H}} = \frac{1}{2}\sum_{\boldsymbol{k}} \left((\hat{\psi}_{\boldsymbol{k}}^{\mathsf{Nam}})^\dagger\right)^T \begin{pmatrix} h_b(\boldsymbol{k}) & 2\Delta_{cc}(\boldsymbol{k}, 0) \\ 2\Delta_{cc}^\dagger(\boldsymbol{k}, 0) & -h_b^T(-\boldsymbol{k}) \end{pmatrix} \hat{\psi}_{\boldsymbol{k}}^{\mathsf{Nam}} .$$

This Hamiltonian can be directly diagonalized to extract the Bogoliubov quasi-particle eigenenergies

$$\Lambda_{\boldsymbol{k}}^e = \pm\sqrt{(E_{\boldsymbol{k}}^+)^2 + |d_{\boldsymbol{k},\boldsymbol{0}}^0|^2}\,, \qquad \text{and} \qquad \Lambda_{\boldsymbol{k}}^u = \pm\sqrt{(E_{\boldsymbol{k}}^+)^2 + |\boldsymbol{d}_{\boldsymbol{k},\boldsymbol{0}}|^2 \pm |\boldsymbol{d}_{\boldsymbol{k},\boldsymbol{0}}^* \times \boldsymbol{d}_{\boldsymbol{k},\boldsymbol{0}}|}\,, \tag{2.29}$$

with e/u applicable to parity even or odd pairing states, respectively. The energy gaps in (2.29) directly allow for a visualization of the respective pairing states in momentum space.

The A_{1g} pairing state with $d_{\boldsymbol{k},\boldsymbol{0}}^{0,A_{1g}} = \Delta_{\boldsymbol{0}}^{A_{1g},1,1} + \Delta_{\boldsymbol{0}}^{A_{1g},2,1}\hat{M}_{\boldsymbol{k}}\sqrt{1-(\hat{f}_{\boldsymbol{k}}^{C_3})^2}$ will not be further examined as it is fully symmetry-compliant and can not be the cause for any symmetry breaking other than $U(1)$. For the five other pairing candidates the d-components read

$$\boldsymbol{d}_{\boldsymbol{k},\boldsymbol{0}}^{A_{1u}} = -\Delta_{\boldsymbol{0}}^{A_{1u}}\mathrm{sign}(\hat{M}_{\boldsymbol{k}})\sqrt{1-(\hat{f}_{\boldsymbol{k}}^{C_3})^2}\,\hat{\boldsymbol{f}}_{\boldsymbol{k}}\,, \tag{2.30}$$

$$\boldsymbol{d}_{\boldsymbol{k},\boldsymbol{0}}^{A_{2u}} = \Delta_{\boldsymbol{0}}^{A_{2u}}\left(-\hat{f}_{\boldsymbol{k}}^y, \hat{f}_{\boldsymbol{k}}^x, \hat{M}_{\boldsymbol{k}}\hat{f}_{\boldsymbol{k}}^{C_3}\right)^T + \Delta_{\boldsymbol{0}}^{A_{2u}}\frac{\mathrm{sign}(\hat{M}_{\boldsymbol{k}})\hat{f}_{\boldsymbol{k}}^{C_3}\hat{f}_{\boldsymbol{k}}^z}{1+|\hat{M}_{\boldsymbol{k}}|}\,\hat{\boldsymbol{f}}_{\boldsymbol{k}}\,, \tag{2.31}$$

[7] The description in terms of a $\boldsymbol{d}$-vector can be modified to also account for non-centro-symmetric systems, see e.g. [56].

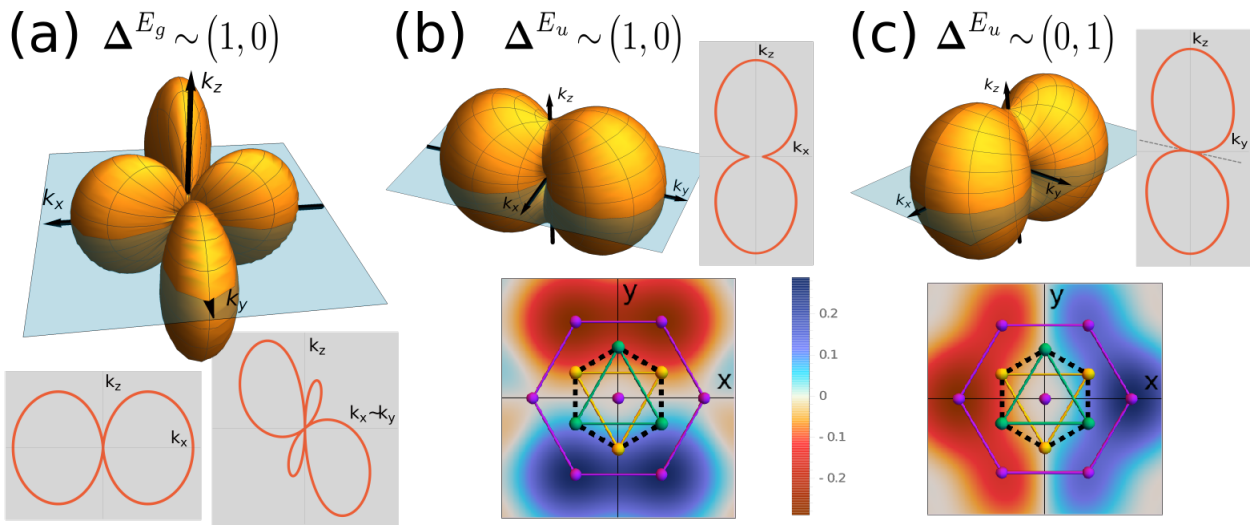

Figure 2.4: Bogoliubov gap structure for the three indicated pairing states, evaluated for a spherical Fermi surface. (a) shows the $\mathbf{\Delta}^{E_g} \sim (1,0)$ state whose gap exhibits some sort of a two- to four-fold symmetry. The gap leads to a point and a line node on the Fermi surface, as indicated in the panels below. (b) and (c) show the gap structure for the odd-parity states $\mathbf{\Delta}^{E_u} \sim (1,0)$ and $\mathbf{\Delta}^{E_u} \sim (0,1)$. The gap structures are clearly two-fold symmetric, with the $(1,0)$ state having a full gap, and $(0,1)$ state leading to a point node. In the panels below, the $d_z(x,y,0) = \sum_{\boldsymbol{k}\in 1.\mathrm{BZ}} e^{-\mathrm{i}(\tilde{x}\tilde{k}_x+\tilde{y}\tilde{k}_y)} (\boldsymbol{d}^{E_u}_{\boldsymbol{k},\mathbf{0}})_z$ component is plotted in real space color-coded underneath the lattice unit cell (cf. Fig.2.1).

$$d^{0,A_{2g}}_{\boldsymbol{k},\mathbf{0}} = \Delta^{A_{2g}}_{\mathbf{0}} \hat{f}^{C_3}_{\boldsymbol{k}} \hat{f}^{z}_{\boldsymbol{k}} \,\mathrm{sign}(\hat{M}_{\boldsymbol{k}}) / \sqrt{1-\hat{M}^2_{\boldsymbol{k}}}\,, \tag{2.32}$$

$$\boldsymbol{d}^{E_u}_{\boldsymbol{k},\mathbf{0}} = \begin{pmatrix} \hat{f}^{z}_{\boldsymbol{k}} \Delta^{E_u,2}_{\mathbf{0}} + \hat{M}_{\boldsymbol{k}} \hat{f}^{C_3}_{\boldsymbol{k}} \Delta^{E_u,1}_{\mathbf{0}} \\ -\hat{f}^{z}_{\boldsymbol{k}} \Delta^{E_u,1}_{\mathbf{0}} + \hat{M}_{\boldsymbol{k}} \hat{f}^{C_3}_{\boldsymbol{k}} \Delta^{E_u,2}_{\mathbf{0}} \\ \hat{f}^{y}_{\boldsymbol{k}} \Delta^{E_u,1}_{\mathbf{0}} - \hat{f}^{x}_{\boldsymbol{k}} \Delta^{E_u,2}_{\mathbf{0}} \end{pmatrix} + \mathrm{sign}(\hat{M}_{\boldsymbol{k}}) \frac{\hat{f}^{C_3}_{\boldsymbol{k}} (\hat{f}^{x}_{\boldsymbol{k}} \Delta^{E_u,1}_{\mathbf{0}} + \hat{f}^{y}_{\boldsymbol{k}} \Delta^{E_u,2}_{\mathbf{0}})}{1+|\hat{M}_{\boldsymbol{k}}|} \hat{\boldsymbol{f}}_{\boldsymbol{k}}\,, \tag{2.33}$$

$$\frac{d^{0,E_g}_{\boldsymbol{k},\mathbf{0}}}{\mathrm{sign}(\hat{M}_{\boldsymbol{k}})} = \frac{\sqrt{1-(\hat{f}^{C_3}_{\boldsymbol{k}})^2}}{\sqrt{1-\hat{M}^2_{\boldsymbol{k}}}} \left(\begin{pmatrix} \hat{f}^{z}_{\boldsymbol{k}} \hat{f}^{y}_{\boldsymbol{k}} \\ -\hat{f}^{z}_{\boldsymbol{k}} \hat{f}^{x}_{\boldsymbol{k}} \end{pmatrix} \cdot \mathbf{\Delta}^{E_g,1}_{\mathbf{0}} + \begin{pmatrix} (\hat{f}^{x}_{\boldsymbol{k}})^2 - (\hat{f}^{y}_{\boldsymbol{k}})^2 \\ -2\hat{f}^{x}_{\boldsymbol{k}} \hat{f}^{y}_{\boldsymbol{k}} \end{pmatrix} \cdot \mathbf{\Delta}^{E_g,2}_{\mathbf{0}} \right) + \frac{\hat{f}^{C_3}_{\boldsymbol{k}}}{\sqrt{1-\hat{M}^2_{\boldsymbol{k}}}} \begin{pmatrix} \hat{f}^{x}_{\boldsymbol{k}} \\ \hat{f}^{y}_{\boldsymbol{k}} \end{pmatrix} \cdot \mathbf{\Delta}^{E_g,3}_{\mathbf{0}}. \tag{2.34}$$

In the figures 2.3 and 2.4, we have visualized the respective quasi-particle gap structures (2.29) for an isotropic Fermi surface.

Figures 2.3 (a)-(c) display the gap structures of the three one-dimensional pairing states. All of them respect a six-fold in-plane rotational symmetry, and most notably, they differ in their nodal structures. The A_{1u} state has a full gap, the A_{2u} state has a point node along the k_z-direction, and the A_{2g} state establishes various line nodes. The two two-dimensional pairing channels $\mathbf{\Delta}^{E_{u/g}}$ can realize the three distinct ground state solutions: a time-reversal symmetry breaking chiral state $(1,\mathrm{i})$ and the two nematic states $(1,0)$ and $(0,1)$, cf. Sec.2.3.3. In the figures 2.3 (d)-(e), the E_u and E_g chiral quasi-particle gaps are visualized. Both gaps respect a three-fold in-plane rotational symmetry. The odd-parity state forms a full gap, while the even-parity state leads to a point node along the k_z-direction. In what follows in this and the next chapter, the two nematic states, $(1,0)$ and $(0,1)$, in

particular for the odd-parity channel E_u are most important. The corresponding gap structures are visualized in figure 2.4. The figure (a) shows the $\mathbf{\Delta}^{E_g} \sim (1,0)$ state. This state is certainly incompatible with the C_{3z} crystal symmetry. It replaces the symmetry by some sort of a two-fold symmetry that has a certain imprint of a four-fold symmetry. The state leads to a point node along the k_z-direction and a line node, as indicated in the panels below the main figure. Note that time-reversal symmetric even-parity states like A_{2g} or E_g necessarily establish line nodes on the Fermi surface, see Ref.[57]. The gap of the $\mathbf{\Delta}^{E_g} \sim (0,1)$ state is not depicted. It is essentially the $(1,0)$-gap rotated by 45° around the z-axis, and most importantly, both states share the same properties. The last figures, 2.4 (b)-(c), visualize the gap structure of the two odd-parity nematic states. These states show a pronounced two-fold symmetry with their axes aligned with the k_x- or k_y-direction, respectively. Moreover, they differ in their nodal structure. While the $(1,0)$ state establishes a full gap, the $(0,1)$ state has a symmetry-protected point node along the curve $(0, \tilde{k}_y, -R_2\tilde{k}_y^3/v_z)$. The the node is protected by the reflection symmetry $M_x : x \to -x$. The distinction between these two states is a pivotal issue in this thesis. Due to their relevance, the two pairing states are also plotted in real space together with the unit cell lattice positions (cf. Fig.2.1) in the respective panels below the main figures. Drawn is the z-component of the $\boldsymbol{d}$-vectors $d_z(x,y,0) = \sum_{\boldsymbol{k}\in 1.\mathrm{BZ}} e^{-\mathrm{i}(\tilde{x}\tilde{k}_x+\tilde{y}\tilde{k}_y)}(\boldsymbol{d}^{E_u}_{\boldsymbol{k},\mathbf{0}})_z$ color-coded on the ground.

Concerning the topological features, we know from the Fu and Berg criterion that the odd-parity states with a full gap are topologically non-trivial if their Fermi surfaces enclose an odd number of TRI momenta [16]. Consequently, the odd-parity fully-gapped states $\Delta^{A_{1u}}$, $\mathbf{\Delta}^{E_u} \sim (1,0)$ and $\mathbf{\Delta}^{E_u} \sim (1,\mathrm{i})$ are topologically non-trivial—given the Fermi surfaces behave as required. The corresponding topological invariant is the $\mathbb{Z}$ winding number (2.3). The odd-parity nodal states $\Delta^{A_{1u}}$ and $\mathbf{\Delta}^{E_u} \sim (0,1)$ can principally be classified as weak topological superconductors with a $\mathbb{Z}_2$ topological index defined around the nodal structures [79].

2.3.2 Discovery of nematic superconductivity

In a pioneering work in 2009, the doping of Bi_2Se_3 with Cu has been reported to generate a superconducting state with a T_c of around $3-4\,\mathrm{K}$ [14]. In the light of a possible topological state the observation of superconductivity has attracted a lot of attention and caused an intense follow-up research. Soon after, specific heat and magnetization measurements identified $Cu_xBi_2Se_3$ as a bulk superconductor [18, 19]. Later it was found, that doping with Sr and Nb drives Bi_2Se_3 into a superconducting state with a similar $T_c \approx 3-4\,\mathrm{K}$ [90, 91]. ARPES and quantum oscillation measurements in the normal state of $Cu_xBi_2Se_3$ have observed a Fermi surface evolution from ellipsoidal towards cylindrical with increasing carrier concentration [92]. The carrier concentration is as low as $n \sim 10^{20}\,\mathrm{cm}^{-3}$ [14, 19], and has been reported to be even lower for Sr doped systems $n \sim 2\times10^{19}\,\mathrm{cm}^{-3}$ [90, 91]. Additionally, the ARPES data has demonstrated that Cu doping—electron doping—pushes the chemical potential into the conduction band with $\mu \sim 0.2-0.5\,\mathrm{eV}$ above the Dirac point, while it leaves the band structure and the edge states essentially untouched [92, 93].

A major advancement towards the identification of the superconducting pairing state has been reported in 2015 [15]. A spin-rotational symmetry breaking within the basal plane has been detected in an NMR Knight shift measurement that was directly linked to the superconducting state, see Fig.2.5(a). In particular, a two-fold symmetry within the basal plane was observed whereas the crystal structure is three-fold symmetric. This contradiction has been consistently confirmed in various subsequent experiments for each of the three compounds with probes ranging from angular-dependent specific heat, resistivity, magnetization, the upper critical field, even to direct visualization via STM imaging [15, 17, 94–103], see e.g. Fig.2.5(b). The most viable explanation for the emergent two-fold symmetry

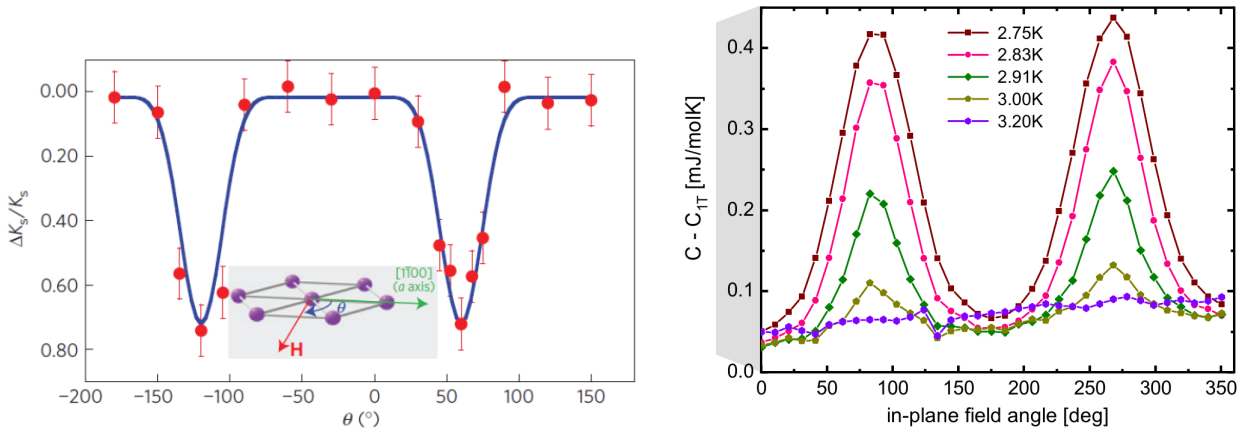

(a) **(b)**

Figure 2.5: (a) NMR Knight shift measurement that demonstrates a clear two-fold symmetry within the basal plane of Cu doped Bi_2Se_3 that occurs alongside the superconducting transition [15]. Adapted by permission from Springer Nature, copyright 2016. (b) Two-fold symmetry observed in the angular-dependent specific heat measurement of Sr doped Bi_2Se_3 [99]. Adapted by permission from the American Physical Society, copyright 2018.

is a spontaneous C_{3z} rotational symmetry breaking caused by the superconducting state.

With regards to the possible pairing states that have been analyzed in the preceding section, only the four nematic states $\mathbf{\Delta}^{E_{u/g}} \sim (1,0)$ and $\mathbf{\Delta}^{E_{u/g}} \sim (0,1)$ do not respect the C_{3z} rotational symmetry. In particular, the pronounced two-fold symmetric signals seen in Fig. 2.5 point towards the odd-parity pairing states $\mathbf{\Delta}^{E_u}$, cf. Fig. 2.4. Moreover, the even-parity $\mathbf{\Delta}^{E_g}$ states have line nodes and the expected heat capacity behavior $C \sim T^2$ is inconsistent with measurements [101]. Consequently, the odd-parity $\mathbf{\Delta}^{E_u}$ states are the most-likely pairing candidates for doped Bi_2Se_3. The final discrimination on which of the two possible states is realized has yet to be delivered. Experiments yield ambiguous findings on this issue. As an example, one penetration depth measurement detects characteristics of a nodal structure [103]—favoring $\mathbf{\Delta}^{E_u} \sim (0,1)$—while another favors the fully-gapped state $\mathbf{\Delta}^{E_u} \sim (1,0)$. Specific heat data [101] also indicates a fully-gapped state. See Ref.[104] for a thorough comparison.

The question about the topological character of the pairing state has just the same not been completely resolved. While some early STM measurements observed a zero-bias peak in the differential conductivity, others did not [17, 104, 105].

Conclusively, it seems justified to attribute the pairing state to the E_u symmetry channel while the question about the realized state is still under debate.

2.3.3 Ginzburg-Landau expansion of E_u superconductivity

For the reasons discussed above it is worth shedding some light on the symmetry properties of the two-dimensional pairing state $\boldsymbol{\Delta}^{E_u} = (\Delta^{E_u,1}, \Delta^{E_u,2})$. In this section, we derive the corresponding Ginzburg-Landau expansion from symmetry principles and study the mean-field ground states. The occurring Ginzburg-Landau parameters are computed in the appendix B.1. In particular, we present the sixth-order parameter which discriminates between the two otherwise degenerate states $(1,0)$ and $(0,1)$. The computation suggests that the fully-gapped state $(1,0)$ is realized on a mean-field level.

Symmetry-based derivation of free energy expansion The constraints imposed by the $U(1)$, time-reversal and lattice symmetries on a free energy expansion are derived in section 1.3.5. For later convenience, we work with the action instead of the free energy. Both quantities satisfy the same constraints. First, we identify the transformation behavior of the bilinear combinations (1.51) in position space $x = (\boldsymbol{r}, \tau)$

$$\mathsf{B}^{n,l}(x) = \left(\boldsymbol{\Delta}^{E_u}(x)\right)^\dagger \tau^{n,l}\, \boldsymbol{\Delta}^{E_u}(x)\,, \tag{2.35}$$

with the matrices $\tau^{n,l}$ being classified via the condition (A.12) and listed in table 2.5. The involved transformation matrices $R_{E_u}(g)$ are explicitly stated in (2.5). Since the decomposition of the product representation $\Gamma^*_{E_u} \otimes \Gamma_{E_u} = \Gamma_{A_{1g}} \oplus \Gamma_{A_{2g}} \oplus \Gamma_{E_g}$ only contains singly-occurring IRs, the multiplicity index is omitted in the following. The table 2.5 also displays the time-reversal behavior according to (1.44). Hence, the expanded mean-field action becomes

$$\mathcal{S}_{\mathrm{mf}} = r_0 T \int_x \mathsf{B}^{A_{1g}} + uT \int_x \left(\mathsf{B}^{A_{1g}}\right)^2 + vT \int_x \left(\mathsf{B}^{A_{2g}}\right)^2 + \mathcal{S}^{(6)}_{\mathrm{int}}\,, \tag{2.36}$$

where we have exploited Eq.(A.17) and introduced the two independent parameters u and v. The x-dependence is implicitly assumed. The fourth-order contribution has a redundancy owed to the Fierz identity $(\mathbf{B}^{E_g})^2 = (\mathsf{B}^{A_{1g}})^2 - (\mathsf{B}^{A_{2g}})^2$ which has reduced the number of interaction parameters by one as compared to Eq.(A.17). The full set of ground state phases (see below) can only be attained by inclusion of sixth-order contributions. The corresponding symmetry deduction is shown in appendix A.2, and yields

$$\mathcal{S}^{(6)}_{\mathrm{int}} = T\nu_- \int_x \mathsf{B}^{E_g,1}\Big((\mathsf{B}^{E_g,1})^2 - 3(\mathsf{B}^{E_g,2})^2\Big) + T\nu_+ \int_x \mathsf{B}^{A_{1g}}\Big((\mathsf{B}^{A_{1g}})^2 + 3(\mathsf{B}^{A_{2g}})^2\Big) + T\nu_{E_u} \int_x \mathsf{B}^{A_{1g}} (\mathbf{B}^{E_g})^2, \tag{2.37}$$

with the three sixth-order interaction parameters ν_-, ν_+ and ν_{E_u}.

Before we study the mean-field phases in the next paragraph, we want to close this symmetry discussion with the introduction of two additional contribution that are relevant for chapter 3: the allowed gradient terms $\mathcal{S}_{\mathrm{grad}}$ and the magnetic field coupling $\mathcal{S}_{B_z}$. The spatial functions are classified according to the condition (2.10) and attached to the table 2.5. Evidently, only the combinations $f^{n,l}_{\boldsymbol{k}} \mathsf{B}^{n,l}$ transform trivially. Thus, the leading-order fluctuation contribution to the action reads

$$\mathcal{S}_{\mathrm{grad}} = T \int_x \left(\boldsymbol{\Delta}^{E_u}\right)^\dagger \left(f^{A_{1g}}_{-\mathrm{i}\boldsymbol{\nabla}} \tau^0 + \boldsymbol{f}^{E_g}_{-\mathrm{i}\boldsymbol{\nabla}} \cdot \boldsymbol{\tau}^{E_g}\right) \boldsymbol{\Delta}^{E_u}\,, \tag{2.38}$$

$\mathsf{D}_{3\mathsf{d}}$	matrix $\tau^{n,l}$	TRS of $\mathsf{B}^{n,l}$	spatial functions	magnetic field $\boldsymbol{B}$
A_{1g}	τ^0	$+$	$f_{\boldsymbol{k}}^{A_{1g}}$	
A_{2g}	τ^y	$-$		B_z
E_g	$\boldsymbol{\tau}^{E_g} = \left(\tau^z, \text{-}\tau^x\right)$	$(+,+)$	$\boldsymbol{f}_{\boldsymbol{k}}^{E_g} = \left(f_{\boldsymbol{k}}^{E_g,1}, f_{\boldsymbol{k}}^{E_g,2}\right)$	$\left(B_x, B_y\right)$

Table 2.5: Association of the bilinear combinations $\mathsf{B}^{n,l} = (\boldsymbol{\Delta}^{E_u})^\dagger \, \tau^{n,l} \, \boldsymbol{\Delta}^{E_u}$ (2.35) with the respective IR n according to the transformation condition (A.12). Additionally, the table shows the transformation behavior of the bilinear upon the time-reversal symmetry operation (1.44). The last two columns show the classification of the contemplable spatial functions and the magnetic field in terms of the IRs n.

with the functions

$$f_{\boldsymbol{k}}^{A_{1g}} \approx \mathsf{d}_0 \left(\tilde{k}_x^2 + \tilde{k}_y^2\right) + \mathsf{d}_z \tilde{k}_z^2 \,, \qquad \begin{pmatrix} f_{\boldsymbol{k}}^{E_g,1} \\ f_{\boldsymbol{k}}^{E_g,2} \end{pmatrix} \approx 2\tilde{\mathsf{d}} \begin{pmatrix} \tilde{k}_y \tilde{k}_z \\ \text{-}\tilde{k}_x \tilde{k}_z \end{pmatrix} + \mathsf{d}' \begin{pmatrix} \tilde{k}_x^2 - \tilde{k}_y^2 \\ \text{-}2\tilde{k}_x \tilde{k}_y \end{pmatrix} . \tag{2.39}$$

Lastly, we apply a magnetic field $\boldsymbol{B}$ to the superconductor. A magnetic field transforms according to the pseudo-vector IR $(E_g \oplus A_{2g})$, and it is odd upon the time-reversal operation, see table 2.5. Apart from the typical orbital coupling, the two-dimensional E_u order parameter allows for a direct linear coupling of the form

$$\mathcal{S}_{B_z} = \alpha' T \int_x B_z \mathsf{B}^{A_{2g}}(x) \,, \tag{2.40}$$

that is fully symmetry-compliant. We study the implications of this magnetic term in section 3.5.

Mean-field ground state phases A multi-component order parameter can possess a manifold of distinct uniform ground state phases. We derive the E_u ground state phase diagram where we find the three phases shown in figure 2.6(a), in agreement with previous studies [57, 106].

For the explicit calculation, the order parameter is decomposed according to $(\Delta^{E_u,1}, \Delta^{E_u,2}) = \Delta_0 e^{\mathrm{i}\varphi_1} (\sin\!\big(\theta\big), \cos\!\big(\theta\big) e^{\mathrm{i}\delta\varphi})$ with $\Delta_0 > 0$, $\varphi_1, \delta\varphi, \theta \in [0, 2\pi)$. The relative phase $\delta\varphi$ is fixed by the minimization of the non-trivial fourth-order contribution $v(\mathsf{B}^{A_{2g}}) = v\Delta_0^4 \sin^2(2\theta) \sin^2(\delta\varphi)$, and it depends on the sign of the parameter v. The corresponding angle θ and the magnitude Δ_0 are determined from the fourth-order mean-field equations

$$0 = r_0 + 2u\Delta_0^2 + 4v\Delta_0^2 \sin^2(\theta) \sin^2(\delta\varphi) \,, \qquad 0 = \Delta_0^2 \sin\!\big(\delta\varphi\big) \Big(\cos\!\big(\delta\varphi\big) - \mathrm{i} \cos\!\big(2\theta\big) \sin\!\big(\delta\varphi\big)\Big) \,. \tag{2.41}$$

Thereafter, the solutions are adjusted as to comply with the sixth-order contribution

$$\mathcal{S}_{\mathrm{int}}^{(6)} = \Delta_0^6 \left[v_+ + v_{E_u} - v_- \cos\left(6\theta\right) + \sin^2\left(\delta\varphi\right) \sin^2\left(2\theta\right) \Big(3v_+ - v_{E_u} - 3v_- \cos\left(2\theta\right)\Big)\right] . \tag{2.42}$$

For $v < 0$ it holds $\delta\varphi = \big\{\pi, 3\pi\big\}/2$, and the equations (2.41) are solved for the four angles $\theta = \big\{1, 3, 5, 7\big\}\,\pi/4$ and $\Delta_0 = \sqrt{-r_0/2(u+v)}$. The sixth-order term (2.42) does not substantially influence

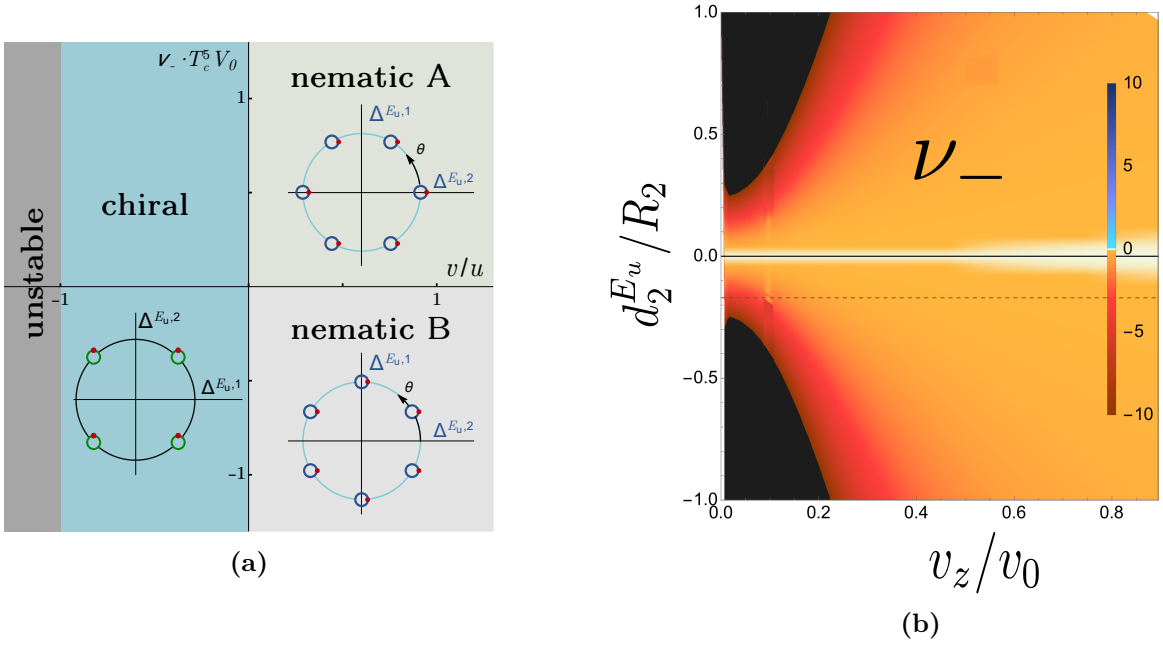

Figure 2.6: Figure (a) depicts the mean-field phase diagram of an E_u order parameter. The six-(four-)fold degenerate ground states are indicated (blue and green circles) together with their respective relative phases (red dot). Figure (b) shows the sixth-order interaction parameter ν_- (2.45) evaluated for $R_1 = 0$.

this so-called chiral configuration. As a consequence of the complex nature $(\mathbf{\Delta}^{E_u})^* \neq \mathbf{\Delta}^{E_u}$, the solution breaks the time-reversal symmetry. A representative state is $\mathbf{\Delta}^{E_u} = \Delta_0(1, \mathrm{i})$.

For positive $v > 0$ and $\delta\varphi = \{0, \pi\}$, the mean-field equations yield $\Delta_0 = \sqrt{-r_0/2u}$ but leave the angle θ degenerate. In this case, the $\cos(6\theta)$ term in the sixth-order contribution (2.42) lifts the θ degeneracy and breaks these nematic states into two distinct phases, labeled as nematic A and nematic B. The nematic solutions read

$$\text{sc. nematic A}: \quad \nu_- > 0\,, \quad \theta = \{0, 2, 4, 6, 8, 10\}\,\frac{\pi}{6}\,, \quad \text{repr.state: } \mathbf{\Delta}^{E_u} = \Delta_0(0, 1) \tag{2.43}$$

$$\text{sc. nematic B}: \quad \nu_- < 0\,, \quad \theta = \{1, 3, 5, 7, 9, 11\}\,\frac{\pi}{6}\,, \quad \text{repr.state: } \mathbf{\Delta}^{E_u} = \Delta_0(1, 0)\,, \tag{2.44}$$

where we have added a corresponding representative state, for convenience.

The complete mean-field phase diagram is shown in figure 2.6(a). We have chosen a representation where the θ orientation is displayed by the large circle and the red dot on the respective small circle indicates the corresponding relative phases $\delta\varphi$.

Sixth-order interaction parameter ν_- Among the Ginzburg-Landau parameters, the sixth-order parameter ν_- is particularly important as it discriminates between the nematic phases A and B. We have derived this parameter from the underlying microscopic Hamiltonian (2.21) (see appendix B), with the final expression reading

$$\nu_- = -\frac{1}{12VT^5}\sum_{\boldsymbol{k}} \eta^e_{\boldsymbol{k}} \left(\left(\hat{f}^{C_3}_{\boldsymbol{k}}\right)^2 - 1\right)^3 \left(\left(\hat{f}^{x}_{\boldsymbol{k}}\right)^2 - \left(\hat{f}^{y}_{\boldsymbol{k}}\right)^2\right)^3 . \tag{2.45}$$

In this notation it holds $\eta^e_{\boldsymbol{k}} = 32T^6 \sum_{\omega_n} \mathrm{g}^3_k \mathrm{g}^3_{-k}$, $\mathrm{g}_k = (\mathrm{i}\omega_n - E^+_{\boldsymbol{k}})^{-1}$, $k = \left(\omega_n, \boldsymbol{k}\right)$ with the fermionic Matsubara frequency ω_n. The gradient functions are defined in section 2.2.1.

The above parameter (2.45) is only non-zero in the presence of the hexagonal warping term $\hat{f}^{C_3}_{\boldsymbol{k}}$ with $R_1 \neq 0$, or if there is a finite coupling between the basal plane and the z-direction with $\mathsf{d}_2^{E_u} \neq 0$. In figure 2.6(b) we show the computed value of (2.45) as a function of the z-anisotropy v_z/v_0 and the (unknown) parameter $\mathsf{d}_2^{E_u}/R_2$. Regardless of its value, we only find $\nu_- < 0$. Indeed, if we employ the continuum limit (see appendix B.32 for details) the leading contributions to the parameter ν_- are of the form $\nu_- = -c_1(\mathsf{d}_2^{E_u})^2 - c_2 R_1^2 < 0$ with $c_{1,2} > 0$. As a result, we find the microscopic model to favor a negative parameter ν_-, and hence, the suggested mean-field solution is the fully-gapped state $\boldsymbol{\Delta}^{E_u} = \Delta_0 e^{\mathrm{i}\varphi_1}\left(1, 0\right)$. The discussion on the realized ground state is postponed to the next chapter 3, where the effect of fluctuations is included.

Chapter 3
3 Vestigial superconductivity

This work has been inspired by the superconducting state that emerged in doped Bi_2Se_3. In this material class, the superconducting transition has consistently been reported to be accompanied by a nematic distortion. This phenomenon is most consistent with a superconducting order parameter that transforms according to the two-dimensional odd-parity IR E_u. Additionally, doped Bi_2Se_3 tends to exhibit a low carrier density and a small ratio of coherence length over Fermi wave length ξ_0/λ_F such that fluctuations of the order parameter may not be negligible. Based on these observations, we perform a large-N analysis where the superconducting fluctuations are consistently accounted for. We find that the system can stabilize a vestigial nematic phase at a temperature T_{nem} above the superconducting transition temperature T_{c}. Moreover, we demonstrate that the vestigial nematic phase leads to an in-plane crystal anisotropy that manifests itself in observables such as the conductivity σ, the susceptibility χ or the upper critical field H_{c2}. Additionally, we visualize the corresponding unit cell distortion and we determine the direction of the sound velocity. Lastly, we study the role of a magnetic field in z-direction with the focus on the possible phases and the associated spatial structures of a single vortex. While the core work was reported in a recent publication, see Ref.~[107], special topics (susceptibility, lattice deformation, upper critical field) were treated in a collaboration with the experimental group of Rolf Lortz [20]. The experimental collaborators have found good evidence for the existence of a vestigial nematic phase in Nb and Cu doped samples. The discussion of the magnetic field effect was conducted in collaboration with Erez Berg.

3.1 Introduction to vestigial physics

The word 'vestigial' can be paraphrased by 'forming a very small remnant of something that was once greater or more noticeable'. The word has been transported into the context of condensed matter physics to identify the field of fluctuation induced preformed phases, so-called vestigial phases. Suppose a system is in an ordered phase, characterized by various broken symmetries, say for concreteness O_1 and O_2. In a vestigial scenario these symmetries are restored sequentially with increasing temperature. At the lowest temperature both O_1 and O_2 are broken, but above that exists a phase where only the symmetry O_1 is restored while O_2 remains broken. This preceding phase forms a residue of the fully-broken state. However, not every preceding phase is a vestigial phase in the original sense. For example, the liquid phase of water is a preceding phase to the ice (the solid phase), but it is not a vestigial phase of the latter. The discrimination between vestigial and non-vestigial preceding phases results through the identification of the driving mechanism. In the context of vestigial phases it is fluctuations,

more precisely, fluctuations of the primary order parameter (magnetization, superconducting order parameter, etc.) that lead to a preformed stabilized phase. In that sense, the two phases are intimately connected and are expected to respond jointly to system perturbations such as stress, doping or magnetic fields. Moreover, a vestigial phase can only exists in proximity to its primary phase where fluctuations are still substantial. To become more formal, let us denote the primary order parameter as ϕ and assume its appearance $\langle\phi\rangle \neq 0$ breaks the symmetry O_1. It is known that the primary order parameter causes a finite expectation value of the correlation function $\langle\phi\phi\rangle$ already above the phase transition. For example, in the context of superconductivity this correlation function renormalizes the conductivity or the susceptibility [108–110]. In its nature the correlation function $\langle\phi\phi\rangle$ is a measure for the strength of fluctuations and it is central for the study of vestigial physics. However, as $\langle\phi\phi\rangle$ belongs to the trivial irreducible representation, it can not break a symmetry on its own and it requires some extension. The idea of vestigial nematicity was inspired by the orthorhombic distortion discovered in the phase diagram of the iron-based superconductors [111]. For a comprehensive review article on vestigial phases the reader is directed to the recent article [112]. The key element of such a vestigial theory is the multi-dimensionality of the primary order parameter $\boldsymbol{\phi}$. Only if $\boldsymbol{\phi} = (\phi^1, \phi^2, \dots)$ transforms according to a higher dimensional IR, say n_0, the bilinear $\boldsymbol{\phi}\lambda^n\boldsymbol{\phi}$ can potentially transform according to a non-trivial IR n and thus, break additional symmetries. The statement is easily verified from a group theoretical perspective where the decomposition of the bilinear $\Gamma_{n_0} \otimes \Gamma_{n_0} = \Gamma_0 \oplus \Gamma_1 \oplus \dots$ can only contain a non-trivial IR if it holds $\dim(n_0) > 1$. Still, the trivially transforming correlation function $\langle\boldsymbol{\phi}\boldsymbol{\phi}\rangle$ does not break a symmetry and can not induce a phase transition. Only non-trivially transforming correlation functions $\langle\boldsymbol{\phi}\lambda^n\boldsymbol{\phi}\rangle$ are potential order parameters that may stabilize at a temperature above the primary transition and hence define a vestigial phase.

It has been demonstrated [111] that the geometry and the dimensionality of the system play a central role in the formation of vestigial orders. Specifically, only anisotropic systems where the order parameter fluctuates in $d < 3$ space-time dimensions are prone to stabilize vestigial phases (see section 3.2.6 for more details). From the more quantitative approach, the range of the vestigial phase sensitively depends on the extent of fluctuations: Only a system with a wide critical range can open an experimentally accessible vestigial phase.

Ginzburg regime The Ginzburg-Landau description of phase transitions retains its validity as long as all the order parameters and their fluctuations are small. In close proximity to the phase transition the correlation length diverges and hence, order parameter fluctuations are inevitably strong such that the Ginzburg-Landau description breaks down, see illustration below. The quantity that determines the

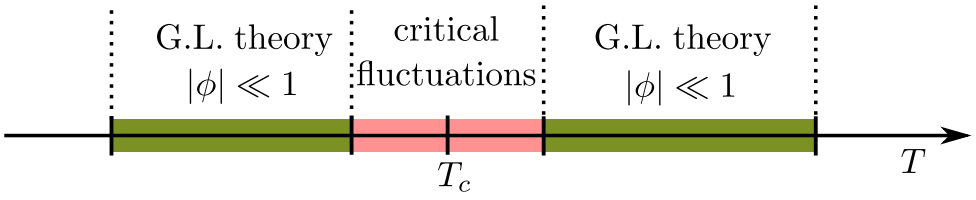

extent of this critical region is called the Ginzburg parameter Gi [48, 113, 114]. The corresponding statement, originally proposed to validate the mean-field treatment, says that fluctuations in the system can be neglected if the relative distance δT from the transition temperature T_c is larger than

the Ginzburg parameter, $\delta T/T_c \gg \mathrm{Gi}'$.[1] For the purpose of a vestigial study we rather read the statement in reverse: fluctuation effects are significant within the relative temperature range

$$\frac{\delta T}{T_c} \lesssim \mathrm{Gi}'$$

that is of the order of the Ginzburg parameter $\mathrm{Gi}' = \left(S_G/k_B\right)^{-2(4-d)}$ with the dimension d, the Boltzmann constant k_B and the 'entropy reduction per coherence volume' $S_G = \Delta C_v\, \xi_0^d$ associated with the formation of an ordered state. Here, ΔC_v is the heat capacity jump and ξ_0 the coherence length. The Ginzburg criterion can be cast in terms of the coherence length ξ_0 as $\left(\xi/\xi_0\right)^{4-d} \ll S_G/k_B$. It directly tells that a large coherence length ξ_0 stabilizes the mean-field solution and suppresses the fluctuation regime. Let us examine the value of the Ginzburg parameter Gi' on the basis of two examples where we compare the coherence length with the typical length scale. (i) In a typical superconductor the entropy of condensation per unit cell is of the order $S_G \sim k_B\Delta/E_F$ while it holds for the coherence length $\xi_0 \sim v_F/\Delta$ with the Fermi velocity v_F. Thus, the Ginzburg parameter in three dimensions can be estimated by $\mathrm{Gi}' \sim \left(\Delta/E_F\right)^4 \sim 10^{-16}$ for typical values of $\Delta \sim 10\,\mathrm{K}$ and $E_F \sim 10^5\,\mathrm{K}$. (ii) For an insulating magnet such as an anti-ferromagnetic Mott insulator one obtains a coherence length as short as the lattice spacing. A Mott insulator typically only has a single energy scale (e.g. the Hubbard U) such that the 'transition entropy' is of order unity, and consequently, the Ginzburg parameter can reach values as high as $\mathrm{Gi}' \sim 1$. In light of this comparably large number, the emergence of a vestigial nematicity above the anti-ferromagnetic Mott insulator in the iron-based materials becomes an almost natural consequence [111].

As illustrated by the first example, a typical superconductor is perfectly well described by a mean-field theory and fluctuations can be genuinely neglected. This situation may change for unconventional superconductors where many members exhibit a small carrier concentration. Of particular interest in the following is doped Bi_2Se_3, introduced in chapter 2. In this material class, the ratio of the coherence length over the Fermi wavelength has been reported to be as small as $\xi_0/\lambda_F \sim 2..4$ [14, 18, 19] which according to the prior arguments enhances the significance of fluctuation physics.

Vestigial scenarios In systems that stabilize a multi-component order parameter $\boldsymbol{\phi}$ the primary phase will always be accompanied by at least one composite order. [2]Out of the multiple scenarios where one or more composite order parameters can be stabilized, we focus on the case where exactly one composite order forms. This composite appears either as a vestigial phase or simultaneously with the primary order. For bilinear composites, there is a total of seven possible ways the primary order parameter $\boldsymbol{\phi}$ can engage with its composite companion $\langle\boldsymbol{\phi}\lambda^n\boldsymbol{\phi}\rangle$, as sketched in figure 3.1. It is clear that the correlation function $\langle\boldsymbol{\phi}\lambda^n\boldsymbol{\phi}\rangle$ has to be finite as soon as $\boldsymbol{\phi}$ acquires a finite expectation value such that the primary phase can never precede. In the situation where fluctuations are weak, or the system's geometry is unfavorable for a preformed phase, both order parameters undergo a joint transition, tagged by J_{ij} with i, j denoting the order of the composite and primary transition, respectively. The most likely scenario involves the joint first-order transition J_{11}. While the cases J_{12} and J_{22} can in principle exist, they turn out to be highly unlikely as will be demonstrated in section

[1]The actual Ginzburg parameter satisfies the inequality $\mathrm{Gi} \ll 1$, yet we find that the introduced parameter Gi' as the temperature deviation gives a more feasible picture.

[2]A clarification to the usage of the terminology. We use the term composite order parameter for the non-trivially transforming expectation value $\langle\boldsymbol{\phi}\lambda\boldsymbol{\phi}\rangle$, and as soon as it precedes its primary phase, it becomes a vestigial order parameter.

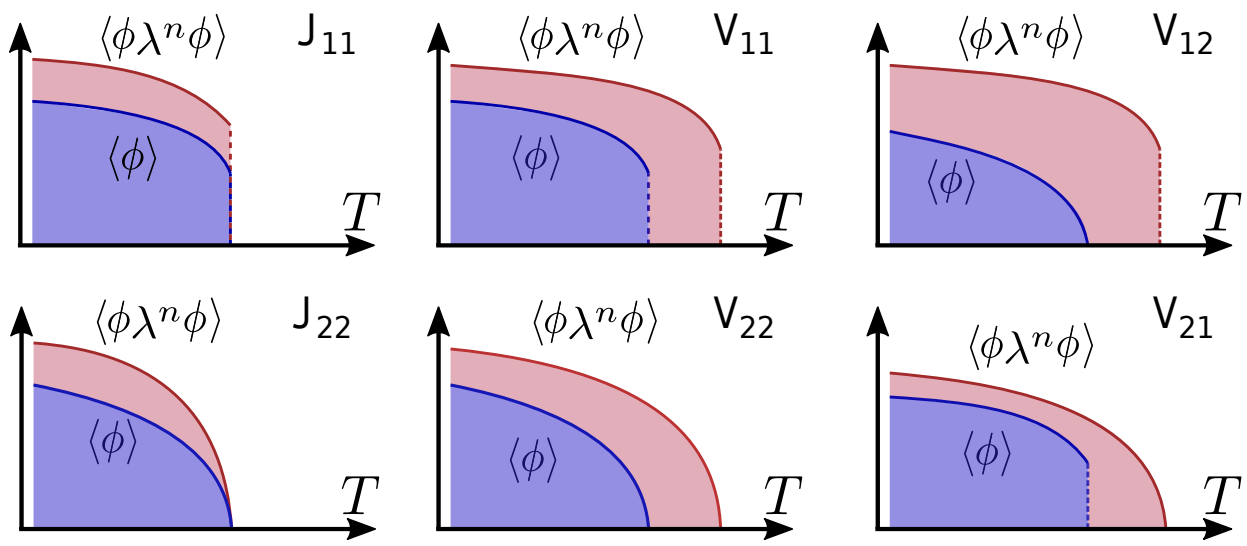

Figure 3.1: Six possible scenarios a multi-dimensional primary order parameter $\boldsymbol{\phi}$ can be accompanied by a single composite order parameter $\langle \boldsymbol{\phi}\lambda^n\boldsymbol{\phi}\rangle$. The scenarios are labeled by V_{ij} and J_{ij} for vestigial and joint with the indices i and j denoting the order of the composite and the primary transition, respectively.

(3.2.6.1). In figure 3.1, the four panels on the right illustrate all possible vestigial scenarios V_{ij} , where the individual transitions can be either first- or second-order.

3.2 Large-N analysis of superconducting fluctuations

In line with the reports on doped Bi_2Se_3 we assume that the superconducting order parameter $\boldsymbol{\Delta}^{E_u} = (\Delta^{E_u,1}, \Delta^{E_u,2})$ transforms according to the two-dimensional IR E_u of the crystal point group $\mathsf{D}_{3\mathsf{d}}$. We start from the corresponding Ginzburg-Landau theory, and decouple the interaction terms by introduction of the composite fields $\mathsf{C}^{A_{1g}}$, $\mathsf{C}^{A_{2g}}$ and $\boldsymbol{\mathsf{C}}^{E_g}$ through a Hubbard-Stratonovich transformation . In terms of symmetry properties the composite fields transform according to the indicated IRs which occur in the product decomposition $\Gamma^*_{E_u} \otimes \Gamma_{E_u} = \Gamma_{A_{1g}} \oplus \Gamma_{A_{2g}} \oplus \Gamma_{E_g}$. The composite fields are the central objects that play the role of the composite/vestigial order parameters. Note that only $\mathsf{C}^{A_{2g}}$ and $\boldsymbol{\mathsf{C}}^{E_g}$ qualify as legitimate composite order parameters as they transform non-trivially. With regards to the implementation, the composite fields embody bilinear combinations of the primary order parameter such that the expectation values of C represent exactly the correlation functions $\sim \langle (\boldsymbol{\Delta}^{E_u})^\dagger \lambda^{n,l} \boldsymbol{\Delta}^{E_u}\rangle$. The goal of this study is to determine whether superconducting fluctuations can drive these objects into separate phases above T_c. To this end, the superconducting fluctuations are integrated out, and the resultant effective action is studied through a large-N based saddle-point analysis.
In the scope of a large-N theory, the large number N of field components $\boldsymbol{\phi} = (\phi_1, \phi_2, \ldots, \phi_N)^T$ typically justifies the saddle-point treatment, cf. Sec. 1.2. In the present case we deal with $N = 2$ components, the real and imaginary parts of the order parameter field.

The Ginzburg-Landau expansion was derived on symmetry grounds in section 2.3.3 with the parameters computed from the microscopic Hamiltonian. This Ginzburg-Landau action $\mathcal{S} = \mathcal{S}_0 + \mathcal{S}_{\text{int}} + \mathcal{S}_A$ decomposes into three contributions: the kinetic, non-interacting $\mathcal{S}_0$, the interacting $\mathcal{S}_{\text{int}}$, and the cou-

pling term to an external magnetic field $\mathcal{S}_A$. Employing the notation from chapter 2.3, we write the kinetic part as

$$\mathcal{S}_0 = V \sum_q \left(\boldsymbol{\Delta}_q^{E_u}\right)^\dagger \underbrace{\left(\left(r_0 + \gamma_0|\nu_m| + f_{\boldsymbol{q}}^{A_{1g}}\right)\tau^0 + \boldsymbol{f}_{\boldsymbol{q}}^{E_g}\cdot\boldsymbol{\tau}^{E_g}\right)}_{\equiv(\mathcal{G}_p^0)^{-1}} \boldsymbol{\Delta}_q^{E_u}\,, \tag{3.1}$$

with the Pauli matrix vector $\boldsymbol{\tau}^{E_g} = \left(\tau^z, -\tau^x\right)$ and the gradient terms in the continuum limit

$$f_{\boldsymbol{q}}^{A_{1g}} = \mathsf{d}_0\left(\tilde{q}_x^2 + \tilde{q}_y^2\right) + \mathsf{d}_z\tilde{q}_z^2\,, \qquad \begin{pmatrix} f_{\boldsymbol{q}}^{E_g,1} \\ f_{\boldsymbol{q}}^{E_g,2}\end{pmatrix} = 2\tilde{\mathsf{d}}\begin{pmatrix}\tilde{q}_y\tilde{q}_z \\ -\tilde{q}_x\tilde{q}_z\end{pmatrix} + \mathsf{d}'\begin{pmatrix}\tilde{q}_x^2 - \tilde{q}_y^2 \\ -2\tilde{q}_x\tilde{q}_y\end{pmatrix}. \tag{3.2}$$

We use the dimensionless momentum $\tilde{\boldsymbol{q}} = (q_x a, q_y a, q_z c)^T$, as well as the notation $q = (\boldsymbol{q}, \nu_m)$, $p = (\boldsymbol{p}, \nu_n)$ with the bosonic Matsubara frequencies $\nu_m = 2\pi m T$. The dynamics of the superconductor are governed by the term $\gamma_0|\nu_m|$, as derived in the appendix B.28. The interaction contribution reads

$$\mathcal{S}_{\text{int}} = V\sum_q\left(\frac{\left(u+\zeta v\right)}{N} V\sum_q \mathsf{B}_q^{A_{1g}}\mathsf{B}_{-q}^{A_{1g}} + \left(1-\zeta\right)\frac{v}{N}\mathsf{B}_q^{A_{2g}}\mathsf{B}_{-q}^{A_{2g}} - \zeta\frac{v}{N}\mathbf{B}_q^{E_g}\mathbf{B}_{-q}^{E_g}\right), \tag{3.3}$$

where we have used the notation of the bilinear combinations $\mathsf{B}_q^{n,l} = \sum_p(\boldsymbol{\Delta}_p^{E_u})^\dagger\tau^{n,l}\boldsymbol{\Delta}_{p+q}^{E_u}$ with the matrices $\tau^{n,l}$ listed in table 2.5. The fourth-order interaction term has a certain degree of redundancy due to the Fierz identity $(\mathsf{B}^{A_{1g}})^2 = (\mathsf{B}^{A_{2g}}) + (\mathbf{B}^{E_g})^2$ which has been accounted for by means of the (redundancy) parameter $\zeta \in [0,1]$. Note that any value of $\zeta \in [0,1]$ is a valid representation of the interaction and leads to the same mean-field ground state. However, for the study of vestigial phases the chosen value of ζ matters. This topic will be discussed in more detail in section 3.2.3. In line with a large-N theory, the interaction parameters have been rescaled $\left\{u, v\right\} \to \left\{u, v\right\}/N$. Furthermore, we are neglecting the sixth-order interaction terms that discriminate between the (otherwise degenerate) superconducting nematic ground states A and B, see Eq. 2.43.[3] While the first part of this chapter will be studied in absence of an external field, we study the role of the magnetic field in the second part. The contribution to the action due to the magnetic field coupling reads

$$\mathcal{S}_A = V\sum_{q,q'}\left(\boldsymbol{\Delta}_q^{E_u}\right)^\dagger \underbrace{\left(\alpha' B_z\tau^y\delta_{qq'} - e\hat{V}^\alpha_{\frac{\boldsymbol{q}}{2}+\frac{\boldsymbol{q}'}{2}}A^\alpha_{q\text{-}q'} + \frac{e^2}{2}\hat{O}^{\alpha\beta}_{\frac{\boldsymbol{q}}{2}+\frac{\boldsymbol{q}'}{2}}\sum_{q_1}A^\alpha_{q_1}\cdot A^\beta_{q\text{-}q'\text{-}q_1}\right)}_{\equiv\left(\mathcal{G}^A\right)^{-1}_{q,q'}} \boldsymbol{\Delta}_{q'}^{E_u}\,, \tag{3.4}$$

where the first term $\alpha' B_z\mathsf{B}^{A_{2g}}$ has been identified in Sec. 2.3.3 to be fully symmetry-compliant. Microscopically, the parameter α' originates from both, the Zeeman and the orbital coupling, see appendix B.1.2. The remaining contributions in (3.4) result from the orbital coupling of the superconducting field to the vector potential $\boldsymbol{A}$, which has formally been carried out by means of a *Peierls substitution*

[3] Those terms could be treated by introducing, instead of a Hubbard-Stratonovich transformation, two new fields λ and σ. The first to replace x by means of a delta-function $\int D\lambda\,\delta(\lambda - x)\ldots$, and the second by re-expressing the delta-function according to $\delta(\lambda - x) = \int D\sigma\exp(\mathrm{i}\sigma(\lambda - x))$.

to be lattice-compliant. The involved derivatives read

$$\hat{V}^{\alpha}_{\boldsymbol{q}} = \frac{\partial\left(\mathcal{G}^{0}_{p}\right)^{-1}}{\partial p_{\alpha}}\bigg|_{p=q}, \qquad \hat{O}^{\alpha\beta}_{\boldsymbol{q}} = \frac{\partial^{2}\left(\mathcal{G}^{0}_{p}\right)^{-1}}{\partial p_{\alpha}\partial p_{\beta}}\bigg|_{p=q}, \tag{3.5}$$

and we note that the charge $e\hat{=}2e$ has to be interpreted as the charge of a Cooper pair.

3.2.1 Derivation of effective action and saddle-point equations

In this section, we decouple the interaction terms, derive the effective action by integrating out the superconducting fluctuations, and compute the corresponding saddle-point equations. For the first step, a *Hubbard-Stratonovich transformation* removes the interaction terms at the expense of an additional field integration. On a technical level, the partition function is multiplied by unity which is expressed as

$$1 = \int \mathcal{D}\left[\mathsf{C}^{n,l}\right] \exp\!\left(\beta V \frac{1}{4u_n}\sum_{q}\left(\mathsf{C}^{n,l}_{q} - 2u_n\mathsf{B}^{n,l}_{q}\right)\left(\mathsf{C}^{n,l}_{-q} - 2u_n\mathsf{B}^{n,l}_{-q}\right)\right), \tag{3.6}$$

where $u_{A_{1g}} = (u+\zeta v)/N$, $u_{A_{2g}} = v/N$ and $u_{E_g} = -v/N$. The four new composite fields $\mathsf{C}^{n,l}_{q}$ can be interpreted as $\mathsf{C}^{n,l}_{q} = 2u_n\langle\mathsf{B}^{n,l}_{q}\rangle$, and correspondingly, they are real fields in position space which obey the condition $(\mathsf{C}^{n,l}_{q})^{*} = \mathsf{C}^{n,l}_{-q}$. After the transformation, the action becomes

$$\mathcal{S}_2 = N\mathcal{S}_{\mathsf{C}} + V\sum_{q,q'}\left(\boldsymbol{\Delta}^{E_u}_{q}\right)^{\dagger}\left(\mathcal{G}^{\mathrm{tot}}\right)^{-1}_{q,q'}\boldsymbol{\Delta}^{E_u}_{q'}, \tag{3.7}$$

where we have introduced $(\mathcal{G}^{\mathrm{tot}})^{-1} = (\mathcal{G}^{\mathsf{C}})^{-1} + (\mathcal{G}^{A})^{-1}$ and defined

$$\mathcal{S}_{\mathsf{C}} = -\frac{1}{4(u+\zeta v)}V\sum_{q}\mathsf{C}^{A_{1g}}_{q}\mathsf{C}^{A_{1g}}_{-q} - \frac{(1-\zeta)}{4v}V\sum_{q}\mathsf{C}^{A_{2g}}_{q}\mathsf{C}^{A_{2g}}_{-q} + \frac{\zeta}{4v}V\sum_{q}\mathbf{C}^{E_g}_{q}\mathbf{C}^{E_g}_{-q}$$

$$\left(\mathcal{G}^{\mathsf{C}}\right)^{-1}_{q,q'} = \left((r_0+\gamma_0|\nu_m| + f^{A_{1g}}_{\boldsymbol{q}})\delta_{qq'} + \mathsf{C}^{A_{1g}}_{q-q'}\right)\tau^0 + \left(\boldsymbol{f}^{E_g}_{\boldsymbol{q}}\delta_{qq'} + \zeta\mathbf{C}^{E_g}_{q-q'}\right)\cdot\boldsymbol{\tau}^{E_g} + \left(1-\zeta\right)\mathsf{C}^{A_{2g}}_{q-q'}\tau^{y}.$$

Since the action (3.7) is now quadratic in the superconducting order parameter field, the functional integration in $\boldsymbol{\Delta}^{E_u}$ can be carried out directly. From a physical point of view, the integration imposes renormalization effects on the remaining fields associated with superconducting fluctuations. This is the adequate approach for the description above the superconducting phase transition. However, if the superconducting field is stabilized, its expectation value becomes an observable that should not be integrated out. Before proceeding let us discuss this issue:

While it is technically rather simple to derive the effective action comprising both, fluctuation and interaction effects in the regime above the superconducting transition, it is more subtle to deduce the analogous description inside the superconducting state. The difficulty arises from the fact that only the non-condensed part of the pairing field can be integrated out. We present two possible methods how this can be established. While both lead to the same outcome (at zero external field) they conceptually differ.

(i) Following the textbook [49] approach for the description of the primarily ordered state within a large-N theory, one decomposes the vector $\boldsymbol{\phi} = \phi_L + \boldsymbol{\pi}$ into one longitudinal ϕ_L, and $N-1$ transverse

components $\boldsymbol{\pi}$. In the ordered state, we let the longitudinal component condense while the transverse components remain purely fluctuating. They form $N-1$ copies of the same Gaussian integral $\int D\pi_j \exp(-\Lambda\pi_j^2/2)$ leading to an action contribution of the form $(N-1)\log\Lambda$ after the integration. In the large-N limit it holds $N-1\approx N$ and the omitted component is compensated for. In the spirit of the large-N theory, the residual longitudinal mode $\phi_L \to \phi_L\sqrt{N}$ needs to be rescaled to acquire 'weight' as it is compared to terms of order $\mathcal{O}(N)$. Translated into the present superconducting setup, the superconducting field is decomposed $\boldsymbol{\Delta}^{E_u} = \boldsymbol{\Delta}_L^{E_u} + \mathsf{i}\boldsymbol{\Delta}_T^{E_u}$ into the longitudinal and transverse components which both are two-dimensional themselves. Following the logic from above, there must not be any mixing between the longitudinal and the transverse component which puts stringent constraints on the form of the Green's function matrix in (3.7). For more details on the approach we refer to the appendix C.1 where we show that the decoupling only works for zero magnetic field ($\boldsymbol{A}=0$) and for the two specific values $\zeta=\{0,1\}$. Then, the corresponding longitudinal and transverse components can be expressed as

$$\boldsymbol{\Delta}_{L,q}^{E_u} = \begin{pmatrix} \operatorname{Re}\Delta_q^{E_u,1} \\ \zeta\operatorname{Re}\Delta_q^{E_u,2} + \mathsf{i}\left(1-\zeta\right)\operatorname{Im}\Delta_q^{E_u,2} \end{pmatrix}, \qquad \boldsymbol{\Delta}_{T,q}^{E_u} = \begin{pmatrix} \operatorname{Im}\Delta_q^{E_u,1} \\ \zeta\operatorname{Im}\Delta_q^{E_u,2} - \mathsf{i}\left(1-\zeta\right)\operatorname{Re}\Delta_q^{E_u,2} \end{pmatrix}.$$

(ii) The bottleneck of the first approach lies in the fixing of the condensation direction, which enforces constraints. Let us now define the condensed direction $\boldsymbol{\Delta}^{\circ,E_u}$ as the solution of the equation

$$\left.\frac{\delta\mathcal{S}_2}{\delta\bar{\boldsymbol{\Delta}}_q^{E_u}}\right|_{\boldsymbol{\Delta}_q^{E_u}=\boldsymbol{\Delta}_q^{\circ,E_u}} = 0\,. \tag{3.8}$$

Then, we decompose the superconducting field $\boldsymbol{\Delta}^{E_u} = \boldsymbol{\Delta}^{\circ,E_u} + \delta\boldsymbol{\Delta}^{E_u}$ into the condensed saddle-point component $\boldsymbol{\Delta}^{\circ,E_u}$ and fluctuations $\delta\boldsymbol{\Delta}^{E_u}$ around it (in all N directions). By construction, the condensed and the fluctuation parts in (3.7) decouple such that the corresponding integration over $\delta\boldsymbol{\Delta}^{E_u}$ can be carried out. The resulting action looks similar to that obtained in method (i). The key differences lie in the absence of constraints on the coupling matrix, and that the condensation direction did not have to be fixed a priori. A more detailed discussion is provided in appendix C.1. Owed to the appeal that comes with the postponed choice of the condensation direction of the superconducting ground state, we will employ the second method (ii) in the following.

In line with the second method, the superconducting field is decomposed according to $\boldsymbol{\Delta}^{E_u} = \boldsymbol{\Delta}^{\circ,E_u} + \delta\boldsymbol{\Delta}^{E_u}$ with the condensed component defined by (3.8). After integration of the fluctuations $\delta\boldsymbol{\Delta}^{E_u}$ the effective action valid above and below the superconducting transition reads

$$\mathcal{S}^{eff} = N\Big\{\mathcal{S}_{\mathsf{C}} + V\sum_{q,q'}\left(\boldsymbol{\Delta}_q^{\circ,E_u}\right)^\dagger\left(\mathcal{G}^{\mathrm{tot}}\right)^{-1}_{q,q'}\boldsymbol{\Delta}_{q'}^{\circ,E_u} + \frac{T}{2}\operatorname{tr}\log\left(2VT\left(\mathcal{G}^{\mathrm{tot}}\right)^{-1}\right)\Big\}. \tag{3.9}$$

In the spirit of the large-N approach, the condensed field has been rescaled $\boldsymbol{\Delta}_q^{\circ,E_u} \to \sqrt{N}\boldsymbol{\Delta}_q^{\circ,E_u}$ such that it matches in order $\mathcal{O}(N)$ with the other terms. The large prefactor N justifies the upcoming saddle-point solution.

The effective action (3.9) is a function of six fields with respect to which it shall be minimized. Technically, the action (3.9) is varied with respect to the four composite fields $\mathsf{C}_q^{n,l}$, while the condensed superconducting components impose the two additional constraints (3.8). Searching for uniform solutions, $\mathsf{C}_q^{n,l} = \mathsf{C}_0^{n,l}\delta_{q,0}$ and $\boldsymbol{\Delta}_q^{\circ,E_u} = \boldsymbol{\Delta}_0^{\circ,E_u}\delta_{q,0}$, in the absence of external fields, the six saddle-point

equations become

$$0 = -\frac{1}{2\left(u+\zeta v\right)}\left(R_0 - r_0\right) + \left(\mathbf{\Delta}_0^{\mathsf{o},E_u}\right)^\dagger \tau^0 \mathbf{\Delta}_0^{\mathsf{o},E_u} + \frac{T}{2V}\sum_q \mathrm{tr}_\tau\left(\mathcal{G}_q^{\mathsf{C}}\tau^0\right) \tag{3.10}$$

$$0 = \left(1-\zeta\right)\left\{ -\frac{1}{2v}\mathsf{C}_0^{A_{2g}} + \left(\mathbf{\Delta}_0^{\mathsf{o},E_u}\right)^\dagger \tau^y \mathbf{\Delta}_0^{\mathsf{o},E_u} + \frac{T}{2V}\sum_q \mathrm{tr}_\tau\left(\mathcal{G}_q^{\mathsf{C}}\tau^y\right)\right\} \tag{3.11}$$

$$0 = \zeta\left\{ \frac{1}{2v}\mathsf{C}_0^{E_g,l} + \left(\mathbf{\Delta}_0^{\mathsf{o},E_u}\right)^\dagger \tau^{E_g,l} \mathbf{\Delta}_0^{\mathsf{o},E_u} + \frac{T}{2V}\sum_q \mathrm{tr}_\tau\left(\mathcal{G}_q^{\mathsf{C}}\tau^{E_g,l}\right)\right\} \tag{3.12}$$

$$0 = \left(\mathcal{G}_0^{\mathsf{C}}\right)^{-1} \mathbf{\Delta}_0^{\mathsf{o},E_u}\,. \tag{3.13}$$

We identify the combination $R_0 = r_0 + \mathsf{C}_0^{A_{1g}}$ which characterizes the fluctuation induced mass renormalization. For brevity, we write $f_q^{(0)} = f_{\boldsymbol{q}}^{A_{1g}} + \gamma_0|\nu_m|$ and $(\mathcal{G}^{\mathsf{C}})^{-1}_{q,q} \to (\mathcal{G}_q^{\mathsf{C}})^{-1}$ in the following. The traces tr_τ act on the space of the superconducting components denoted by the Pauli matrices τ.

The above saddle-point equations contain all the information about the renormalization effects caused by fluctuations. As we shall see in the following, these effects will allow us to predict a vestigial nematic phase for doped Bi_2Se_3.

With parameters chosen to be compatible with the microscopic description of doped Bi_2Se_3 we present the corresponding self-consistent saddle-point solutions, i.e. the temperature behavior of the respective order parameters, in section 3.2.6.2. In the sections preceding this result, we discuss various aspects of the problem which help us simplify the eventual solution finding process. In particular, we aim to keep the framework applicable to both possible vestigial phases, a vestigial chiral ($|\mathsf{C}_0^{A_{2g}}| \neq 0$) and a vestigial nematic ($|\mathbf{C}_0^{E_g}| \neq 0$). First, in section 3.2.2 the ground state symmetry of the two-dimensional E_g composite field $\mathbf{C}^{E_g}$ is discussed and the ground state phases are computed. Second, in section 3.2.3, we address the role played by the (redundancy) parameter ζ and show that the parameter has to assume one of the extremes $\zeta = 0$ or $\zeta = 1$. Third, in section 3.2.4 we elaborate on the intimate relation between the primary and the composite order parameter and derive a direct constraint on the superconducting state. In section 3.2.5—after implementing the previously derived properties into the saddle-point equations—we confront the two vestigial scenarios: chiral and nematic. We further show that the number of saddle-point equations reduces to two in each temperature regime. Before turning to the full (numeric) solution of the saddle-point equations, we evaluate analytic solutions in section 3.2.6.1 for a simplified model where the order parameter fluctuates classically and in the A_{1g} channel only. To this end, we introduce a graphical presentation that conveniently illustrates the vestigial scenario. Finally, in section 3.2.6.2 we solve the full equations numerically, and display the results in the same representation.

3.2.2 Symmetry properties of an E_g order parameter

The composite field $\mathbf{C}^{E_g}$ transforms according to a two-dimensional IR such that it can exhibit various ground states similar to the superconducting order parameter $\mathbf{\Delta}^{E_u}$, see section 2.3.3. Following the scheme of section 1.3, we can study the transformation rules the composite order parameter has to satisfy. We need to ensure that the coupling term $\mathsf{C}^{E_g,l}_{q-q'}(\mathbf{\Delta}^{E_u}_q)^\dagger \tau^{E_g,l}\mathbf{\Delta}^{E_u}_{q'}$ transforms trivially upon the symmetry operations. Since the bilinear transforms trivially upon the $U(1)$ symmetry the composite field does the same. For the point group (1.33) and time-reversal (1.41) operations, the composite field $\mathbf{C}^{E_g}$ has to compensate for the $\mathbf{\Delta}^{E_u}$ transformation, leading to

$$\mathsf{C}^{E_g,l}_{q-q'} \overset{(1.43)}{\to} \mathsf{C}^{E_g,l'}_{\mathcal{R}_v^\dagger(g)(q-q')}\mathcal{R}^\dagger_{E_g}(g)_{l'l}\,, \qquad\qquad \mathsf{C}^{E_g,l}_{q-q'} \overset{(1.44)}{\to} \mathsf{C}^{E_g,l}_{-(q-q')}\,. \tag{3.14}$$

The resulting free energy constraints can be cast in a similar fashion as in (1.42)-(1.44), namely

$$\text{lattice sym.}: \qquad \mathcal{F}[\mathsf{C}^{E_g,l}_{\boldsymbol{q}},\boldsymbol{q}] = \mathcal{F}[\mathsf{C}^{E_g,l'}_{\boldsymbol{q}}\mathcal{R}^\dagger_{E_g}(g)_{l'l},\mathcal{R}_v(g)\,\boldsymbol{q}] \qquad ,\forall g\in\mathcal{G}_p\,, \tag{3.15}$$

$$\text{time}-\text{reversal sym.}: \qquad \mathcal{F}[\mathsf{C}^{E_g,l}_{\boldsymbol{q}},\boldsymbol{q}] = \mathcal{F}[\mathsf{C}^{E_g,l}_{\boldsymbol{q}},-\boldsymbol{q}]\,. \tag{3.16}$$

From here, the route to classify the symmetry-allowed Ginzburg-Landau terms is similar to section 2.3.3. In fact, with $\mathcal{R}_{E_g}(g)$ and $\mathcal{R}_{E_u}(g)$ only differing by a minus sign (which cancels for even Ginzburg-Landau contributions), the classification of the bilinear combinations is identical to the results in table 2.5. The differences to the superconducting E_u case are two-fold:
(i) The field $\mathbf{C}^{E_g} = (\mathbf{C}^{E_g})^*$ is real (in position space) such that the bilinear combination $\mathbf{C}^{E_g}_0\tau^y\mathbf{C}^{E_g}_0$ vanishes, and the number of fourth-order interaction parameters naturally reduces to one.
(ii) The composite field $\mathbf{C}^{E_g}$ is no subject to the $U(1)$ symmetry constraint such a cubic term is not prohibited a priori. Indeed, the decomposition $\Gamma_{E_g}\otimes\Gamma_{E_g}\otimes\Gamma_{E_g} = \Gamma_{A_{1g}}\oplus\dots$ reveals that such a term is explicitly symmetry-allowed. The corresponding identification from symmetry grounds is conducted in the appendix A.2.
The resulting free energy expansion in terms of the uniform $\mathbf{C}^{E_g}_0$ order parameter becomes

$$\mathcal{S}_{E_g} = NV\left\{r_{\mathsf{c}}\left(\mathbf{C}^{E_g}_0\right)^2 + g_{\mathsf{c}}\left(\left(\mathsf{C}^{E_g,1}_0\right)^3 - 3\mathsf{C}^{E_g,1}_0\left(\mathsf{C}^{E_g,2}_0\right)^2\right) + u_{\mathsf{c}}\left(\left(\mathbf{C}^{E_g}_0\right)^2\right)^2\right\}, \tag{3.17}$$

with the cubic g_{c} and quartic u_{c} interaction parameters. In the literature this action is similar to the well-known Landau expansion of the Z_3-Potts model [115].

Owed to the cubic contribution $g_{\mathsf{c}}|\mathbf{C}^{E_g}_0|^3\cos\left(3\theta_{\mathsf{c}}\right)$ in the action (3.17), the resulting ground state depends on the relative angle θ_{c} between the two field components $\mathbf{C}^{E_g}_0 = |\mathbf{C}^{E_g}_0|(\cos\theta_{\mathsf{c}},\sin\theta_{\mathsf{c}})$. The angle θ_{c} adjusts according to the sign of g_{c} in order to minimize the free energy which leads to the two distinct three-fold degenerate ground states

$$\text{vestigial nematic A}: \qquad g_{\mathsf{c}}<0\,, \qquad \theta_{\mathsf{c}} = \left\{0,2,4\right\}\frac{\pi}{3}\,, \tag{3.18}$$

$$\text{vestigial nematic B}: \qquad g_{\mathsf{c}}>0\,, \qquad \theta_{\mathsf{c}} = \left\{1,3,5\right\}\frac{\pi}{3}\,. \tag{3.19}$$

The absolute value of the order parameter is identical in both phases and reads

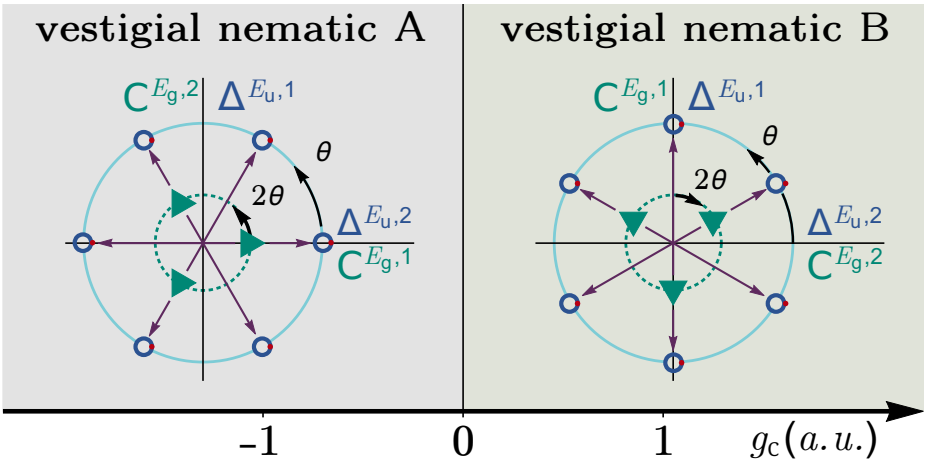

Figure 3.2: Ground state phase diagram of the composite order parameter $\mathbf{C}_0^{E_g}$ falling into the IR E_g. The green triangles denote the three-fold degenerate ground states in the $(\mathsf{C}_0^{E_g,1}, \mathsf{C}_0^{E_g,2})$ plane. The purple arrows indicated the respective association with two distinct superconducting ground states according to (3.29) and (3.30).

$$|\mathbf{C}_0^{E_g}| = \frac{3|g_c|}{8u_c}\left(1 + \sqrt{1 - \frac{32 r_c u_c}{9 g_c^2}}\right). \tag{3.20}$$

The two ground state phases are visualized as green triangles in figure 3.2 in the $(\mathsf{C}_0^{E_g,1}, \mathsf{C}_0^{E_g,2})$ plane. A finite value of the cubic parameter g_c causes the composite order parameter to jump at a temperature $0 < r_c < \frac{9g_c^2}{32u_c} \equiv r_c^{\max}$. As illustrated in figure 1.1(b), at the temperature $r_c^{\max}$ the free energy has an additional real saddle-point. Only at a lower temperature $r_c < r_c^{\max}$ this new solution turns into the global minimum. Yet, it happens above the critical temperature $r_c = 0$ where the quadratic coefficient vanishes. As a consequence, dictated by symmetry the transition into the $|\mathbf{C}_0^{E_g}| \neq 0$ phase is of first-order. The parameter g_c discriminates between the two possible phases and it quantifies the extent of the first-order jump.[4]

Derivation of the E_g expansion parameters The Ginzburg-Landau parameters for the composite field $\mathbf{C}^{E_g}$ can be derived explicitly from an expansion of the effective action (3.9) above T_c for small $\mathbf{C}^{E_g}$, see appendix C.2. The expressions for the quadratic r_c and cubic g_c coefficients become

$$r_c = \frac{1}{4v} - \frac{1}{2}\frac{T}{V}\sum_q \frac{\left(R_0^p + f_q^{(0)}\right)^2}{\left(\det\left(\mathcal{G}_q^{\mathsf{C}}[R_0^p, \mathsf{C}_0^{E_g,l} = \mathsf{C}_0^{A_{2g}} = 0]\right)^{-1}\right)^2}, \tag{3.21}$$

[4] As has been outlined in 1.1.1 first-order phase transitions can be lifted to second-order if the higher order terms push the extra minimum above zero. The present statement is restricted to the description of weak first-order phase transitions.

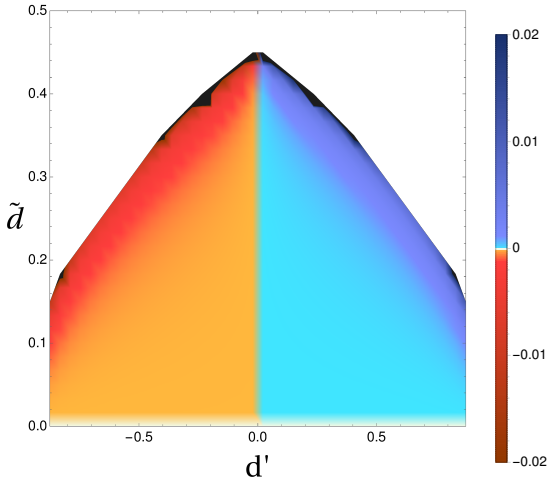

Figure 3.3: Evaluation of the cubic parameter g_{c} as it results from the equation (3.22) as a function of d' and $\tilde{\mathsf{d}}$. The value g_{c} is largest at the edges of stability. The chosen parameters were $R_0^p/\mathsf{d}_0 = 1, \mathsf{d}_z/\mathsf{d}_0 = 0.2$.

$$g_{\mathsf{c}} = -\frac{1}{3}\frac{T}{V}\sum_q \frac{\left(f_{\boldsymbol{q}}^{E_g,1}\right)^3 - 3f_{\boldsymbol{q}}^{E_g,1}\left(f_{\boldsymbol{q}}^{E_g,2}\right)^2}{\left(\det\left(\mathcal{G}_q^{\mathsf{c}}[R_0^p, \mathsf{C}_0^{E_g,l} = \mathsf{C}_0^{A_{2g}} = 0]\right)^{-1}\right)^3}\,, \tag{3.22}$$

with R_0^p being the R_0-solution in the para-nematic regime, i.e. the solution of equation (3.10) above T_c with $\boldsymbol{\Delta}_0^{\circ,E_u} = \mathsf{C}_0^{E_g,l} = \mathsf{C}_0^{A_{2g}} = 0$.
The cubic parameter is particularly interesting as its sign decides on the chosen $\mathbf{C}^{E_g}$ ground state, A or B. With regards to the spatial functions (3.2), or their lattice counterparts (2.14), we note that the cubic parameter $g_{\mathsf{c}} = 0$ vanishes if the fluctuations in the E_g symmetry channel disappear, i.e. for $\mathsf{d}' = \tilde{\mathsf{d}} = 0$. Moreover, it holds that a simultaneous sign flip of d' and $\tilde{\mathsf{d}}$, also switches the sign of g_{c}, leading to $g_{\mathsf{c}} \propto \mathrm{sign}(\mathsf{d}'\tilde{\mathsf{d}})$. Now, we assume that the integrand in (3.22) falls off rapidly in the q_x, q_y plane such that the integration boundaries do not substantially contribute. Then, the sign flip of the parameter $\tilde{\mathsf{d}} \to -\tilde{\mathsf{d}}$ can be compensated for by simultaneous flipping $q_z \to -q_z$[5] and thus, the cubic parameter has to be an even function in $\tilde{\mathsf{d}}$. Accordingly, the cubic parameter $g_{\mathsf{c}} \propto \mathrm{sign}(\mathsf{d}')$ is an odd function in d', which means that the sign of g_{c} and consequently the chosen nematic ground state solely depends on the sign of d'. In Fig. 3.3 we show the obtained value of g_{c} as a function of d' and $\tilde{\mathsf{d}}$. The value of d' that was computed for doped Bi_2Se_3 (B.23) is positive, such that the corresponding value of g_{c} is positive, and B (3.19) is the expected vestigial nematic ground state.

[5]Tihs only holds for negligible contributions from the Brioullin zone boundary in Fig.2.1

3.2.3 Determination of the (redundancy) parameter ζ

The (redundancy) parameter ζ—directly linked to the Fierz identity—ensures the degenerate representations of the fourth-order interaction term. By exploiting the ground state symmetry of the E_g composite field $\mathsf{C}_0^{E_g} = |\mathsf{C}_0^{E_g}|(\cos\theta_\mathsf{c}, \sin\theta_\mathsf{c})$ with the particular angles θ_c, above T_c the three saddle-point equations (3.11),(3.12) can be reduced to

$$0 = \big(1-\zeta\big)\,\mathsf{C}_0^{A_{2g}}\left\{\frac{1}{2v} + \frac{T}{V}\sum_q \frac{(1-\zeta)}{\det\left(\mathcal{G}_q^\mathsf{C}\right)^{-1}}\right\}, \quad 0 = \zeta\left\{\frac{|\mathsf{C}_0^{E_g}|}{2v} - \frac{T}{V}\sum_q \frac{\zeta|\mathsf{C}_0^{E_g}| + \boldsymbol{f}_\boldsymbol{q}^{E_g}\cdot\frac{\mathsf{C}_0^{E_g}}{|\mathsf{C}_0^{E_g}|}}{\det\left(\mathcal{G}_q^\mathsf{C}\right)^{-1}}\right\}, \quad (3.23)$$

where the second equation results from the addition of the two original equations (3.12) for $\mathsf{C}_0^{E_g}$.[6]

If we assume that both composite order parameters $|\mathsf{C}_0^{E_g}|$ and $\mathsf{C}_0^{A_{2g}}$ are finite above T_c, then both curly brackets in the Eqs. (3.23) have to vanish simultaneously. However, a numeric evaluation of the two occurring integrals has shown that both integrals are strictly positive, and zero is only acquired for $|\mathsf{C}_0^{E_g}| = \mathsf{C}_0^{A_{2g}} = 0$.[7] Hence, the two curly brackets can not simultaneously yield zero, and in particular, the sign of the parameter v decides on which bracket may disappear. For positive (negative) v, the composite field $|\mathsf{C}_0^{E_g}|$ ($\mathsf{C}_0^{A_{2g}}$) is allowed to become finite while it must hold that $\mathsf{C}_0^{A_{2g}} = 0$ ($|\mathsf{C}_0^{E_g}| = 0$). The association between v and the composite fields is in line with the superconducting mean-field analysis from section 2.3.3. To see this, we use the relations for the composite fields

$$\mathsf{C}_0^{E_g,l} = -2v\langle\left(\boldsymbol{\Delta}_0^{E_u}\right)^\dagger \tau^{E_g,l}\boldsymbol{\Delta}_0^{E_u}\rangle\,, \qquad \mathsf{C}_0^{A_{2g}} = 2v\langle\left(\boldsymbol{\Delta}_0^{E_u}\right)^\dagger \tau^{y}\boldsymbol{\Delta}_0^{E_u}\rangle\,. \quad (3.24)$$

and insert the superconducting mean-field ground states (2.43)-(2.44). This leads to the same association as above,

$$v > 0: \qquad |\mathsf{C}_0^{E_g}| \neq 0\,, \qquad \mathsf{C}_0^{A_{2g}} = 0\,, \quad (3.25)$$

$$v < 0: \qquad |\mathsf{C}_0^{E_g}| = 0\,, \qquad \mathsf{C}_0^{A_{2g}} \neq 0\,. \quad (3.26)$$

As a conclusion, the present system can only stabilize one composite field, either $|\mathsf{C}_0^{E_g}|$ for $v > 0$, or $\mathsf{C}_0^{A_{2g}}$ for $v < 0$. Note that the mutual exclusion of the composite fields is not a generic feature but depended on the details of the saddle-point equations. For the two cases where one of the composite fields vanishes, we may minimize the energy with respect to the (still free) parameter ζ. A simple computation then yields that the parameter ζ assumes one of two extreme values, i.e. $\zeta = 0$ or $\zeta = 1$ for $v < 0$ or $v > 0$, respectively.

3.2.4 Relation between the superconducting and the composite order parameters

A peculiar phenomenon in the field of vestigial phases is the preselection of the primary ground state at the onset temperature T_{vest} of the vestigial phase. This intimate connection manifests itself in

[6] The subtraction of the two equations vanishes, as the integral $\sum_q \left(f_\boldsymbol{q}^{E_g,1}\sin(2\theta) - f_\boldsymbol{q}^{E_g,2}\cos(2\theta)\right)/\det\mathcal{G}[0]_{q,q} = 0$ yields zero for the possible C^{E_g} ground states. The integral can be shown to be odd upon application of the remaining two-fold rotation elements C_{2x}, C_{2A} or C_{2B}, depending on the realized ground state.

[7] In the case $\boldsymbol{f}_\boldsymbol{q}^{E_g} = 0$, the integrals become identical, and the mutual exclusion in (3.23) is plainly visible.

the saddle-point equation (3.13), reading $0 = (\mathcal{G}_0^{\mathsf{C}})^{-1}\boldsymbol{\Delta}_0^{\circ,E_u}$. We discuss the resulting relations for the nematic ($\zeta = 1$) and the chiral ($\zeta = 0$) cases separately. The diagonalization of the saddle-point equation leads to a condition which the two $\boldsymbol{\Delta}_0^{\circ,E_u}$ components have to satisfy. We note that the renormalized mass $R_0 > 0$ has to be positive.[8]

In the nematic case ($\zeta = 1$), the saddle-point equation (3.13) takes on the diagonalized form

$$0 = \begin{pmatrix} R_0 - |\mathsf{C}_0^{E_g}| & 0 \\ 0 & R_0 + |\mathsf{C}_0^{E_g}| \end{pmatrix} \frac{1}{|\mathsf{C}_0^{E_g}|} \begin{pmatrix} \mathsf{C}_0^{E_g,2}\Delta_0^{\circ,E_u,1} + \left(|\mathsf{C}_0^{E_g}| + \mathsf{C}_0^{E_g,1}\right)\Delta_0^{\circ,E_u,2} \\ -\mathsf{C}_0^{E_g,2}\Delta_0^{\circ,E_u,1} + \left(|\mathsf{C}_0^{E_g}| - \mathsf{C}_0^{E_g,1}\right)\Delta_0^{\circ,E_u,2} \end{pmatrix}, \tag{3.27}$$

which only allows for a superconducting solution when $R_0 = |\mathsf{C}_0^{E_g}|$. Additionally, the second entry in the vector in (3.27) must vanish. Using $\mathsf{C}_0^{E_g} = |\mathsf{C}_0^{E_g}|(\cos(\theta_{\mathsf{c}}), \sin(\theta_{\mathsf{c}}))$ and introducing the angle $\theta = \theta_{\mathsf{c}}/2 \in [0, \pi]$, [it holds $(|\mathsf{C}_0^{E_g}| - \mathsf{C}_0^{E_g,1})/\mathsf{C}_0^{E_g,2} = \sin\theta/\cos\theta$] the constraint is fulfilled for

$$\boldsymbol{\Delta}_0^{\circ,E_u} = |\boldsymbol{\Delta}_0^{E_u}| e^{\mathsf{i}\varphi_0} \begin{pmatrix} \sin\theta \\ \cos\theta \end{pmatrix}, \tag{3.28}$$

in agreement with Sec. 2.3.3. Thus, depending on the nematic angle θ_{c}, a particular superconducting angle $\theta = \theta_{\mathsf{c}}/2$ is selected. The corresponding association

$$\text{vestigial nematic A}: \quad g_{\mathsf{c}} < 0\,, \quad \theta_{\mathsf{c}} = \{0,2,4\}\frac{\pi}{3}\,, \quad \rightarrow \quad \text{sc. nematic A}: \quad \theta = \{0,2,4\}\frac{\pi}{6}\,, \tag{3.29}$$

$$\text{vestigial nematic B}: \quad g_{\mathsf{c}} > 0\,, \quad \theta_{\mathsf{c}} = \{1,3,5\}\frac{\pi}{3}\,, \quad \rightarrow \quad \text{sc. nematic B}: \quad \theta = \{1,3,5\}\frac{\pi}{6}\,, \tag{3.30}$$

is also illustrated in figure 3.2 by means of the purple arrows.

In the chiral case ($\zeta = 0$), the diagonalized saddle-point equation (3.13) reads

$$0 = \begin{pmatrix} R_0 - \mathsf{C}_0^{A_{2g}} & 0 \\ 0 & R_0 + \mathsf{C}_0^{A_{2g}} \end{pmatrix} \frac{1}{\sqrt{2}} \begin{pmatrix} -\mathsf{i}\Delta_0^{\circ,E_u,1} + \Delta_0^{\circ,E_u,2} \\ \mathsf{i}\Delta_0^{\circ,E_u,1} + \Delta_0^{\circ,E_u,2} \end{pmatrix}, \tag{3.31}$$

which leads to the conditions $R_0 = |\mathsf{C}_0^{A_{2g}}|$ and $\Delta_0^{\circ,E_u,1} = \mathsf{i}\,\mathrm{sign}(\mathsf{C}_0^{A_{2g}})\,\Delta_0^{\circ,E_u,2}$ in the superconducting regime. The corresponding ground state thus becomes

$$\boldsymbol{\Delta}_0^{\circ,E_u} = |\boldsymbol{\Delta}_0^{E_u}| e^{\mathsf{i}\varphi_0} \frac{1}{\sqrt{2}} \begin{pmatrix} 1 \\ -\mathsf{i}\,\mathrm{sign}\left(\mathsf{C}_0^{A_{2g}}\right) \end{pmatrix}, \tag{3.32}$$

in agreement with the ground state obtained from the mean-field analysis of section 2.3.3.

[8] At $R_0 = 0$, the superconducting pairing susceptibility would diverge if there was no additional composite order parameter. With a composite order parameter present, the susceptibility already diverges at $R_0 = |\mathsf{C}^{n,l}| > 0$.

3.2.5 Contrasting the nematic and chiral scenario

In the preceding three sections, we have accumulated properties and conditions that help to simplify the saddle-point equations. After the implementation, the former six coupled saddle-point equations reduce to two in the respective temperature regimes. We contrast the respective equations for the nematic and the chiral cases in the boxes below, followed by a discussion on the respective symmetry reduction.

In the **nematic case** ($v > 0 \quad \& \quad \zeta = 1$) the connection between the real composite and the superconducting order parameter is established via $\mathsf{C}_0^{E_g} = |\mathsf{C}_0^{E_g}|(\cos(\theta_\mathsf{c}), \sin(\theta_\mathsf{c}))$ and $\boldsymbol{\Delta}_0^{\circ,E_u} = |\boldsymbol{\Delta}_0^{E_u}| e^{\mathrm{i}\varphi_0}(\sin\theta, \cos\theta)$, and the saddle-point equations read for $T > T_c$

$$0 = \frac{(R_0 - r_0)}{2u'} - \frac{T}{V}\sum_q \frac{R_0 + f_q^{(0)}}{\det\left(\mathcal{G}_q^\mathsf{C}\right)^{-1}}, \tag{3.33}$$

$$0 = \frac{|\mathsf{C}_0^{E_g}|}{2v} - \frac{T}{V}\sum_q \frac{|\mathsf{C}_0^{E_g}| + \boldsymbol{f}_\boldsymbol{q}^{E_g}\cdot\frac{\mathsf{C}_0^{E_g}}{|\mathsf{C}_0^{E_g}|}}{\det\left(\mathcal{G}_q^\mathsf{C}\right)^{-1}}. \tag{3.34}$$

For $T < T_c$ it holds $R_0 = |\mathsf{C}_0^{E_g}|$ and the equations read

$$\frac{v - u'}{v}|\mathsf{C}_0^{E_g}| = r_0 + 2u'\frac{T}{V}\sum_q \frac{f_q^{(0)} - \boldsymbol{f}_\boldsymbol{q}^{E_g}\cdot\frac{\mathsf{C}_0^{E_g}}{|\mathsf{C}_0^{E_g}|}}{\det\left(\mathcal{G}_q^\mathsf{C}\right)^{-1}}, \tag{3.35}$$

$$|\boldsymbol{\Delta}_0^{E_u}|^2 = \frac{|\mathsf{C}_0^{E_g}|}{2v} - \frac{T}{V}\sum_q \frac{|\mathsf{C}_0^{E_g}| + \boldsymbol{f}_\boldsymbol{q}^{E_g}\cdot\frac{\mathsf{C}_0^{E_g}}{|\mathsf{C}_0^{E_g}|}}{\det\left(\mathcal{G}_q^\mathsf{C}\right)^{-1}}, \tag{3.36}$$

where we defined $u' = u + v$.

In the **chiral case** ($v < 0 \quad \& \quad \zeta = 0$) the connection between the real composite $\mathsf{C}_0^{A_{2g}}$ and the superconducting order parameter is established via $\boldsymbol{\Delta}_0^{\circ,E_u} = |\boldsymbol{\Delta}_0^{E_u}| e^{\mathrm{i}\varphi_0}(1, -\mathrm{i}\,\mathrm{sign}(\mathsf{C}_0^{A_{2g}}))/\sqrt{2}$, and the saddle-point equations read for $T > T_c$

$$0 = \frac{(R_0 - r_0)}{2u} - \frac{T}{V}\sum_q \frac{R_0 + f_q^{(0)}}{\det\left(\mathcal{G}_q^\mathsf{C}\right)^{-1}}, \tag{3.37}$$

$$0 = \frac{\mathsf{C}_0^{A_{2g}}}{2|v|} - \frac{T}{V}\sum_q \frac{\mathsf{C}_0^{A_{2g}}}{\det\left(\mathcal{G}_q^\mathsf{C}\right)^{-1}}, \tag{3.38}$$

and for $T < T_c$ it holds $R_0 = |\mathsf{C}_0^{A_{2g}}|$ and the equations read

$$\frac{|v| - u}{|v|}|\mathsf{C}_0^{A_{2g}}| = r_0 + 2u\frac{T}{V}\sum_q \frac{f_q^{(0)}}{\det\left(\mathcal{G}_q^\mathsf{C}\right)^{-1}}, \tag{3.39}$$

$$|\boldsymbol{\Delta}_0^{E_u}|^2 = \frac{|\mathsf{C}_0^{A_{2g}}|}{2|v|} - \frac{T}{V}\sum_q \frac{|\mathsf{C}_0^{A_{2g}}|}{\det\left(\mathcal{G}_q^\mathsf{C}\right)^{-1}}. \tag{3.40}$$

The above boxes display the summary of the results from the preceding sections. The contrast shows that on a technical level the two scenarios are described by almost similar equations, and technically, the vestigial phase can equally be realized in each of the two channels. However, we want to point out the physical differences related to the two outcomes.

The nematic composite field $\mathsf{C}_0^{E_g}$ is a Z_3-Potts variable (cf. Sec.3.2.2), and as such it always causes a first-order transition. In terms of symmetries, it leaves the time-reversal symmetry $\mathcal{T}$ intact but it breaks almost all of the point group symmetries. In fact, a given ground state configuration only retains one of the two-fold rotations, together with inversion, which reduces the point group from $\mathsf{D}_{3\mathsf{d}}$

to $\mathsf{C_{2h}}$. For example, the ground state $\theta_\mathsf{c} = \pi$ retains the four elements $\{E, I, C_{2x}, IC_{2x}\}$[9] constituting a $\mathsf{C_{2h}}$ group. Accordingly, the symmetry group in the vestigial nematic phase is reduced to $\mathcal{G}^{\text{vest. nem.}} = \mathsf{C_{2h}} \times \mathcal{T} \times U(1)$. Once the system undergoes the superconducting phase transition into the E_u state with odd parity, the symmetry group is further reduced by the inversion and the $U(1)$ operation, yielding the reduction scheme

$$\mathsf{D_{3d}} \times \mathcal{T} \times U(1) \quad \overset{\text{vest.nem.}}{\longrightarrow} \quad \mathcal{G}^{\text{vest. nem.}} = \mathsf{C_{2h}} \times \mathcal{T} \times U(1) \quad \overset{\text{sc.}}{\longrightarrow} \quad \mathcal{G}^{\text{sc. nem.}} = \mathsf{C_2} \times \mathcal{T}\,. \tag{3.41}$$

The chiral order parameter $\mathsf{C}_0^{A_{2g}}$ on the other hand, is a time-reversal symmetry breaking Ising variable, which is not symmetry constrained to a certain order of phase transition. In terms of point group symmetries, it transforms according to the IR A_{2g} and consequently, it breaks the three two-fold rotation symmetries and the three mirror symmetries. The remaining point group elements constitute the point group $\mathsf{S_6} = \{E, C_{3z}, C_{3z}^{-1}, I, IC_{3z}, IC_{3z}^{-1}\}$ and hence, the unitary symmetry group in the vestigial chiral phase reads $\mathcal{G}_U^{\text{vest. chiral}} = \mathsf{S_6} \times U(1)$. The corresponding superconducting state only transforms trivially upon the element E such that the residual unitary symmetry group becomes $\mathcal{G}_U^{\text{sc. chiral}} = \mathsf{C_1}$, and the reduction scheme reads

$$\mathsf{D_{3d}} \times \mathcal{T} \times U(1) \quad \overset{\text{vest.chiral}}{\longrightarrow} \quad \mathcal{G}_U^{\text{vest. chiral}} = \mathsf{S_6} \times U(1) \quad \overset{\text{sc.}}{\longrightarrow} \quad \mathcal{G}_U^{\text{sc. chiral}} = \mathsf{C_1}\,. \tag{3.42}$$

3.2.6 Solution of the saddle-point equations for doped Bi_2Se_3

Contrary to the preceding sections, where the formalism was kept as generic as possible, we now focus on the description of doped Bi_2Se_3 where the parameter $v > 0$ (see Fig.B.1(b)) is positive, and accordingly, it holds $\mathsf{C}_0^{A_{2g}} = 0$ and $\zeta = 1$. Moreover, in line with our microscopic derivation we assume that $\mathsf{d}' > 0$ (see (B.23)) such that $g_\mathsf{c} > 0$, and the nematic ground state angle becomes $\theta_\mathsf{c} = \{1, 3, 5\}\,\pi/3$, with $\mathbf{C}_0^{E_g} = |\mathbf{C}_0^{E_g}|(-1, 0)$ being one representative state. The corresponding superconducting ground state angle reads $\theta = \{1, 3, 5\}\,\pi/6$ with $\mathbf{\Delta}^{E_u} = \Delta_0 e^{\mathrm{i}\varphi_0}(1, 0)$ being the representative—fully-gapped—state, see Fig. 2.4. The mean-field ground state analysis has shown that the sixth-order interaction parameter ν_- lifts the degeneracy between the two nematic phases (A and B). Here, the microscopic calculation suggests $\nu_- < 0$ for doped Bi_2Se_3 which similarly points to the fully-gapped state. As a first result, we note that both the mean-field (neglecting fluctuations) and the fluctuation-induced analysis (neglecting sixth-order interactions) seem to be favoring the fully-gapped state in doped Bi_2Se_3.

The goal of this section is to study qualitatively whether a vestigial nematic scenario is possible for doped Bi_2Se_3 and to derive the temperature behavior of the nematic and the superconducting order parameters. In section 3.2.6.1 we address the simplified situation where only fluctuations within the A_{1g} symmetry channel are allowed. This model can be solved analytically and serves as a starting point to interpret the possible solutions. In section 3.2.6.2 the saddle-point solutions are solved numerically with fluctuations allowed in all the symmetry channels. Depending on the degree of z-anisotropy, we find either joint transition or a vestigial nematic solution.

As stated above, the following analysis is done in the classical limit where quantum fluctuations are neglected. Quantum fluctuations effectively increase the dimension into which the superconducting field can fluctuate. This has an unfavorable effect on the likelihood of a vestigial scenario, see Ref. [111]. From a technical point of view, the classical limit amounts to the high temperature regime where it holds $T\gamma_0 \gg r_0$, and the Matsubara summations can be restricted to the leading contributions with

[9] The other symmetry elements do not leave the integrals in (3.33)-(3.36) invariant.

$\nu_m = 0$.

A few words about the critical temperature T_c are in order. From the action (3.9) one can infer that the superconducting pairing susceptibility reads $\chi_{\text{pair}} = R_0/(R_0^2 - |\mathsf{C}_0^{E_g}|^2)$ which diverges for $R_0 = |\mathsf{C}_0^{E_g}|$. With a decrease in temperature ($\hat{=}$ decrease in $r_0 = a_0(T - T_c^0)$) the renormalized mass R_0 decreases. In the absence of any composite order parameter, the superconducting pairing susceptibility would diverge for $R_0 = 0$ at a critical temperature defined through (cf. Eq. (3.33))

$$r_0^c = -2(u+v)\frac{T}{V}\sum_q \frac{f_q^{(0)}}{\det\left(\mathcal{G}_q^{\mathsf{C}}\right)^{-1}}\bigg|_{R_0=|\mathsf{C}_0^{E_g}|=0} < 0\,. \tag{3.43}$$

In this case the superconducting order parameter undergoes a second-order phase transition (cf. Eq. (3.10))

$$|\mathbf{\Delta}_0^{E_u}|^2 = \frac{-\delta r_0}{2\,(u+v)}\,, \tag{3.44}$$

with the defined effective temperature parameter $\delta r_0 = r_0 - r_0^c$. The negative sign of the critical temperature value r_0^c (3.43) leads us to conclude that superconducting fluctuations would always lower the transition temperature as a leading order effect. Indeed, by inserting $r_0 = a_0(T - T_c^0)$ into $\delta r_0 = r_0 - r_0^c = a_0\left(T - T_c\right)$ we identify the fluctuation renormalized transition temperature $T_c = T_c^0 + r_0^c/a_0 < T_c^0$.

The aforementioned situation has to be contrasted to the case where a composite order parameter is present: In that case the primary phase becomes critical for $R_0 = |\mathsf{C}_0^{E_g}|$, which (using $R_0 = r_0 + \mathsf{C}_0^{A_{1g}}$) translates into the new transition temperature $T_c = T_c^0 + (|\mathsf{C}_0^{E_g}| - \mathsf{C}_0^{A_{1g}})/a_0$. This corresponds to a relative enhancement of the transition temperature through the stabilized vestigial order parameter $|\mathsf{C}_0^{E_g}|$. In simple terms, fluctuations suppress T_c but the effect is reduced if they lead to the condensation of a vestigial phase.

3.2.6.1 Model with A_{1g} fluctuations in the classical regime

The purpose of studying a simplified model is two-fold. On the one hand, we introduce a convenient approach on how the solutions can be derived and interpreted. On the other hand, the model can be investigated analytically allowing for a discussion of the entire phase space. In the absence of E_g fluctuations, i.e. $\mathsf{d}' = \tilde{\mathsf{d}} = 0$, it is clear that $g_{\mathsf{c}} = 0$, and the nematic transition looses its Z_3-Potts character—the transition is not bound to be of first-order anymore. Within the present simplified model, the only gradient term reads $f_{\boldsymbol{q}}^{A_{1g}} = \mathsf{d}_0(\tilde{q}_x^2 + \tilde{q}_y^2) + \mathsf{d}_z\tilde{q}_z^2$. The system is assumed to extent infinitely in the q_x, q_y-plane while it is subject to a momentum cutoff Λ in the q_z direction. The cutoff is assumed to be the largest scale in the problem; in particular $\Lambda^2 \gg \{r_0, |\mathsf{C}_0^{E_g}|\}$, and the exercise becomes identical to a model considered in Ref. [111]. With a partial fraction decomposition, the two

integrals in (3.33)-(3.36) can be evaluated analytically, yielding

$$I_1\left(R_0,|\mathsf{C}_0^{E_g}|\right) = -\frac{8\pi \mathsf{d}_0 V_0}{\Lambda V}\sum_{\boldsymbol{q}}\left(\frac{R_0+f_{\boldsymbol{q}}^{A_{1g}}}{\det\left(\mathcal{G}_{\boldsymbol{q}}^{\mathsf{C}}\right)^{-1}}-\frac{1}{f_{\boldsymbol{q}}^{A_{1g}}}\right) \approx \sqrt{\tilde{R}_0+|\tilde{\mathsf{C}}_0^{E_g}|}+\sqrt{\tilde{R}_0-|\tilde{\mathsf{C}}_0^{E_g}|}-\frac{2}{\pi}\tilde{R}_0, \tag{3.45}$$

$$I_2\left(R_0,|\mathsf{C}_0^{E_g}|\right) = \frac{8\pi \mathsf{d}_0 V_0}{\Lambda V}\sum_{\boldsymbol{q}}\frac{|\mathsf{C}_0^{E_g}|}{\det\left(\mathcal{G}_{\boldsymbol{q}}^{\mathsf{C}}\right)^{-1}} \approx \sqrt{\tilde{R}_0+|\tilde{\mathsf{C}}_0^{E_g}|}-\sqrt{\tilde{R}_0-|\tilde{\mathsf{C}}_0^{E_g}|}-\frac{2}{\pi}|\tilde{\mathsf{C}}_0^{E_g}|. \tag{3.46}$$

Here, we have expanded the results for large $\Lambda^2 \gg \{R_0,|\mathsf{C}_0^{E_g}|\}/\mathsf{d}_0\tilde{v}$, kept the terms up to the second order and introduced the following dimensionless quantities: the coupling constants $\{\tilde{u},\tilde{v}\} = \{u',v\}T/\pi\mathsf{d}_0^2 V_0$, the fields $\{\tilde{R}_0,|\tilde{\mathsf{C}}_0^{E_g}|\} = \{R_0,|\mathsf{C}_0^{E_g}|\}/\Lambda^2\mathsf{d}_z$, and the anisotropy parameter $\Lambda_z = \Lambda\mathsf{d}_z/\mathsf{d}_0\tilde{v}$ where $V_0 = a^2c$. A reduction of Λ_z increases the system's anisotropy. Using the integral notation (3.45) and (3.46), the saddle-point equations can be expressed as

$$T>T_c: \quad \delta\tilde{r}_0 = \tilde{R}_0+\frac{\hat{u}}{4\Lambda_z}I_1\left(R_0,|\mathsf{C}_0^{E_g}|\right), \qquad 0=\left\{\frac{1}{2}|\tilde{\mathsf{C}}_0^{E_g}|-\frac{1}{8\Lambda_z}I_2\left(R_0,|\mathsf{C}_0^{E_g}|\right)\right\} \tag{3.47}$$

$$T<T_c: \quad \delta\tilde{r}_0 = \left(1\text{-}\hat{u}\right)\tilde{R}_0+\frac{\hat{u}}{2\Lambda_z}I_1\left(R_0,R_0\right), \quad |\tilde{\boldsymbol{\Delta}}_0^{E_u}|^2=\left\{\frac{1}{2}\tilde{R}_0-\frac{1}{8\Lambda_z}I_2\left(R_0,R_0\right)\right\} \tag{3.48}$$

with $\tilde{\boldsymbol{\Delta}}_0^{E_u} = \boldsymbol{\Delta}_0^{E_u}\sqrt{\pi\mathsf{d}_0V_0/T\Lambda_z^2}$, $\hat{u}=u'/v$ and the effective temperature parameter $\delta\tilde{r}_0 = (r_0-r_0^c)/\Lambda^2\mathsf{d}_z$, see (3.43). Conveniently, after all the rescaling procedures, the model only has two independent parameters left, $\hat{u}$ and Λ_z.

Let us now present the solution in a scheme that, we believe, is quite instructive. The idea is to solve the saddle-point equations in the respective regimes as a function of the renormalized mass parameter $\tilde{R}_0$, with the solutions being $\delta\tilde{r}_0(\tilde{R}_0)$. Thus, we consider the functions which assign to every value $\tilde{R}_0$ the corresponding system temperature $\delta\tilde{r}_0$. Within the three regimes, superconducting, vestigial nematic, and para-nematic ($\hat{=}$ above T_{nem}), the functions read explicitly

$$\delta\tilde{r}_0^{\mathrm{nem}}\left(\tilde{R}_0\right) = \tilde{R}_0+\frac{\hat{u}}{4\Lambda_z}I_1\left(R_0,|\mathsf{C}_0^{E_g}|\left(R_0\right)\right), \qquad \delta\tilde{r}_0^{\mathrm{paranem}}\left(\tilde{R}_0\right) = \tilde{R}_0+\frac{\hat{u}}{4\Lambda_z}I_1\left(R_0,0\right), \tag{3.49}$$

$$\delta\tilde{r}_0^{\mathrm{sc}}\left(\tilde{R}_0\right) = \left(1-\hat{u}\right)\tilde{R}_0+\frac{\hat{u}}{2\Lambda_z}I_1\left(R_0,R_0\right), \tag{3.50}$$

where $|\mathsf{C}_0^{E_g}|\left(R_0\right)$ is the solution of the second equation in (3.47). As illustrated in the figure 3.4, the nematic (red curve) and the superconducting (solid light blue curve) solutions are restricted to certain intervals. The nematic solution $\delta\tilde{r}_0^{\mathrm{nem}}$ only exists within the interval $\tilde{R}_{nem}^{(2\mathrm{nd})} < \tilde{R}_0 < \tilde{R}_{sc}^{(2\mathrm{nd})}$, where $\tilde{R}_{nem}^{(2\mathrm{nd})}$ denotes the critical nematic value where the nematic order parameter $|\mathsf{C}_0^{E_g}|$ emerges, and $\tilde{R}_{sc}^{(2\mathrm{nd})}$ denotes the critical superconducting value where it holds $\tilde{R}_0 = |\mathsf{C}_0^{E_g}|$, and the superconducting order parameter $|\tilde{\boldsymbol{\Delta}}_0^{E_u}|$ emerges. The superconducting solution $\delta\tilde{r}_0^{\mathrm{sc}}$ only exists for either $\tilde{R}_0 = 0$, or for $\tilde{R}_0 > \tilde{R}_{sc}^{(2\mathrm{nd})}$. In Fig.3.4, we plot the three solutions (3.49),(3.50) for a given parameter set. One can then track the system's ground state as the temperature is lowered, i.e. as $\delta\tilde{r}_0$ is reduced. At high temperatures the system is in the para-nematic state (light green curve), where neither a nematic nor a superconducting order parameter is present. As the temperature decreases, the first time an order can be established, the ground state switches onto the respective nematic or superconducting curve.

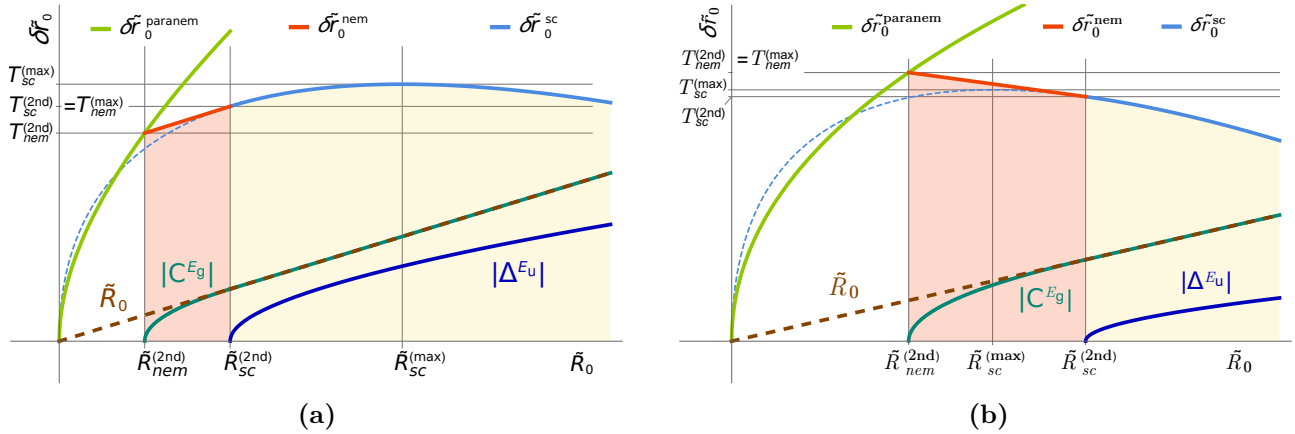

Figure 3.4: (a) and (b) depict a joint first-order (J_{11}) and a vestigial situation (V_{22}) with consecutive second-order phase transitions, respectively. The chosen parameters are $\Lambda_z = 1$, $u'/v = 2$ and $\Lambda_z = 0.2$, $u'/v = 2$ for the left and right, respectively.

We disregard first-order transitions for a moment. For concreteness, let us focus on Fig.3.4(b), where the ground state switches onto the red curve. Upon further cooling, the ground state follows the red curve until it becomes superconducting and evolves on the light blue line. This situation represents a V_{22} scenario, where a vestigial nematic phase preempts the superconductor, and both transitions are of second order. For a first-order transition, the ground state has to 'jump' onto another curve, such that the respective order parameter does not emerge continuously. This is the case in Fig.3.4(a) where the system undergoes a joint first-order phase transition into the superconducting state (J_{11}). The temperature where the transition happens is not right at the peak of the blue curve, but slightly below, see e.g. discussion in Sec 3.2.2. In this situation the vestigial nematic solution does not become the system's ground state at any temperature. It is quite convenient to note that, the figures also depict the order parameters as functions of $\tilde{R}_0$, such that their temperature behavior can indirectly be inferred. The two demonstrated examples represent two possible realizations resulting from the saddle-point equations (3.49) and (3.50).

We shall in the following take a more general view and try to understand if the system can establish other scenarios as well, and in particular what criteria it depends on. A vestigial scenario with a single composite order parameter has four characteristic temperatures: the two critical temperatures $T^{(2\text{nd})}_{\{sc,nem\}}$ where the corresponding susceptibilities diverge, and the two maximum temperatures $T^{(\max)}_{\{sc,nem\}}$ denoting the highest possible temperature for which the respective solution exists. We denote the corresponding renormalized mass value accordingly, $\tilde{R}^{(2\text{nd})}_{\{sc,nem\}}$ and $\tilde{R}^{(\max)}_{\{sc,nem\}}$. The respective relations of the points $(\tilde{R}, T)$ determine the realized scenario as summarized in table 3.1. In the present

joint J_{11}:	$T_{sc}^{(\max)} > T_{nem}^{(\max)}$			
vestigial $\begin{pmatrix}\mathsf{V}_{22}\\ \mathsf{V}_{21}\end{pmatrix}$:	$T_{sc}^{(\max)} < T_{nem}^{(\max)}$	& $T_{nem}^{(2nd)} = T_{nem}^{(\max)}$	& $\begin{pmatrix}\tilde{R}_{sc}^{(2nd)} > \tilde{R}_{sc}^{(\max)}\\ \tilde{R}_{sc}^{(2nd)} < \tilde{R}_{sc}^{(\max)}\end{pmatrix}$
vestigial $\begin{pmatrix}\mathsf{V}_{12}\\ \mathsf{V}_{11}\end{pmatrix}$:	$T_{sc}^{(\max)} < T_{nem}^{(\max)}$	& $T_{nem}^{(2nd)} < T_{nem}^{(\max)}$	& $\begin{pmatrix}\tilde{R}_{sc}^{(2nd)} > \tilde{R}_{sc}^{(\max)}\\ \tilde{R}_{sc}^{(2nd)} < \tilde{R}_{sc}^{(\max)}\end{pmatrix}$
joint $\begin{pmatrix}\mathsf{J}_{12}\\ \mathsf{J}_{22}\end{pmatrix}$:	$T_{sc}^{(\max)} = T_{nem}^{(\max)}$		& $\begin{pmatrix}\tilde{R}_{sc}^{(2nd)} < \tilde{R}_{nem}^{(2nd)}\\ \tilde{R}_{sc}^{(2nd)} = \tilde{R}_{nem}^{(2nd)}\end{pmatrix}$

Table 3.1: Comparison of the characteristic temperatures and their renormalized mass values, associated with the respective vestigial or joint scenario. The notation is V_{ij}, J_{ij} with i and j denoting the order of the composite and the primary transition, respectively (see Fig.3.1).

model, we can analytically extract the characteristic points,[10] yielding

$$\tilde{R}_{nem}^{(\mathrm{2nd})} = \frac{\pi^2}{4b_z^2}\,, \qquad T_{nem}^{(\mathrm{2nd})} = \frac{\pi}{8\Lambda_z b_z^2}\left(\hat{u} + 2\pi\Lambda_z(2\hat{u}+1)\right)\,, \tag{3.51}$$

$$\tilde{R}_{sc}^{(\mathrm{2nd})} = \frac{\pi^2}{2b_z^2}\,, \qquad T_{sc}^{(\mathrm{2nd})} = \frac{\pi^2(1+\hat{u})}{2b_z^2}\,, \tag{3.52}$$

$$\tilde{R}_{sc}^{(\max)} = \frac{\pi^2\hat{u}^2}{8(\hat{u}+\pi\Lambda_z(\hat{u}-1))}\,, \qquad T_{sc}^{(\max)} = \frac{\pi\hat{u}^2}{8\Lambda_z(\hat{u}+\pi\Lambda_z(\hat{u}-1))}\,, \tag{3.53}$$

where $b_z = 1 + 2\pi\Lambda_z$. Within the nematic regime, the solution reads

$$\delta\tilde{r}_0^{\mathrm{nem}}\left(\tilde{R}_0\right) = \frac{2\pi\Lambda_z - \hat{u}}{2\pi\Lambda_z}\,\tilde{R}_0 + \frac{\hat{u}\pi}{4\Lambda_z b_z}\,, \tag{3.54}$$

which is a straight line with either a positive or a negative slope, depending on $2\pi\Lambda_z \lessgtr \hat{u}$. As a consequence, the maximum value is always at the interval boundary, namely

$$2\pi\Lambda_z > \hat{u}: \qquad \tilde{R}_{nem}^{(\max)} = \tilde{R}_{sc}^{(\mathrm{2nd})} \qquad \& \qquad T_{nem}^{(\max)} = T_{sc}^{(\mathrm{2nd})}\,, \tag{3.55}$$

$$2\pi\Lambda_z < \hat{u}: \qquad \tilde{R}_{nem}^{(\max)} = \tilde{R}_{nem}^{(\mathrm{2nd})} \qquad \& \qquad T_{nem}^{(\max)} = T_{nem}^{(\mathrm{2nd})}\,. \tag{3.56}$$

In the case (3.55) with $2\pi\Lambda_z > \hat{u}$, the maximum nematic temperature equals $T_{nem}^{(\max)} = T_{sc}^{(\mathrm{2nd})}$ the critical superconducting temperature which by definition, is smaller (or equal) than its maximum. In this model it truly holds $T_{sc}^{(\mathrm{2nd})} < T_{sc}^{(\max)}$, such that the system will always undergo a joint (J_{11}) first-order phase transition. In particular, the statement is true for a three-dimensional isotropic system, restored by $\Lambda_z \to \infty$. No vestigial phase is to be expected for as long as the system is not (sufficiently) anisotropic. In the opposite case (3.56), when $2\pi\Lambda_z < \hat{u}$, the system can establish a vestigial nematic phase. Because it then holds $T_{nem}^{(\max)} = T_{nem}^{(\mathrm{2nd})}$ the phase transition is of second order. The possible

[10] The characteristic values $\tilde{R}_{nem}^{(\mathrm{2nd})}$ and $\tilde{R}_{sc}^{(\mathrm{2nd})}$ are the solutions of (3.47) and (3.48) evaluated at zero $|\mathbf{C}_0^{E_g}|$ and $|\tilde{\boldsymbol{\Delta}}_0^{E_u}|$, respectively. Alternatively, $\tilde{R}_{nem}^{(\mathrm{2nd})}$ is also the value where the quadratic Ginzburg-Landau coefficient r_{c} (3.21) vanishes.

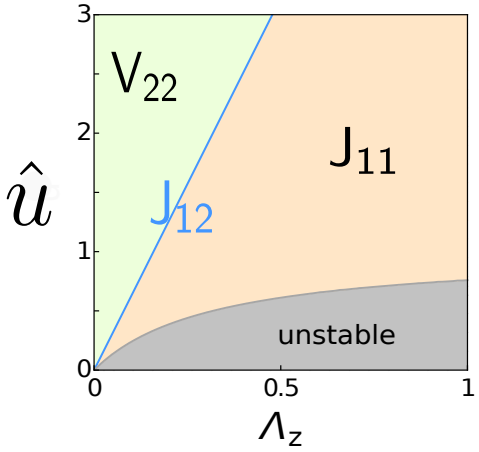

Figure 3.5: Phase diagram indicating which scenario is realized in the system. The condition $\hat{u} + \pi\Lambda_z(\hat{u} - 1) > 0$ guarantees the stability of the solution.

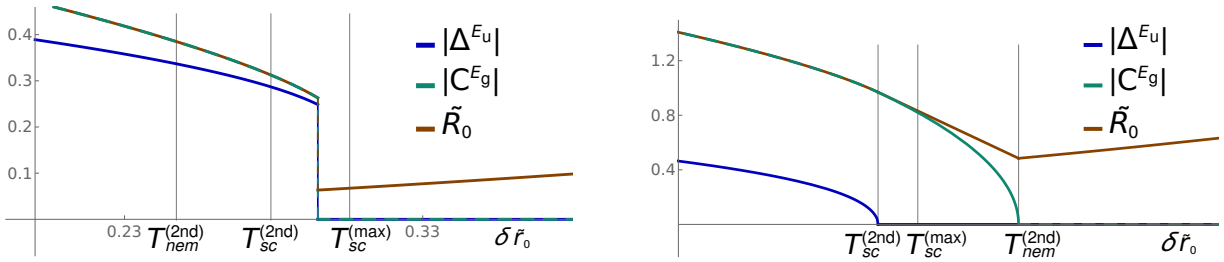

(a) (b)

Figure 3.6: Temperature behavior of the respective order parameters as they result from the scenarios depicted in Fig.3.4. The left and right depict a joint first-order (J_{11}) and a vestigial situation (V_{22}) with consecutive second order phase transition, respectively.

realizations are easily deduced by comparison of the characteristic values (3.51)-(3.56) with regards to the conditions in table 3.1.

The resultant phase diagram is depicted in Fig.3.5, showing that only three scenarios can be realized in this model. For a small degree of anisotropy (large Λ_z) the system always undergoes a joint first-order transition. At the fine-tuned points $2\pi\Lambda_z = \hat{u}$, the system realizes joint transitions with the superconducting transition being of second order. With respect to the representations in Fig.3.4 this amounts to a horizontal red line where $T_{nem}^{(\mathrm{max})} = T_{nem}^{(\mathrm{2nd})}$. For that reason, the joint transitions J_{12}, J_{22} are an artefact of a fine-tuned system and generically, they are not to be expected. For a large degree of anisotropy the system realizes the vestigial V_{22} scenario that is depicted in Fig.3.4(b).

Finally, we plot the order parameter behavior as a function of temperature in figure 3.6, corresponding to the system settings of Fig. 3.4. The figures reflect the qualitative conclusions already drawn. The single distinctive feature results from the first-order transition temperature in case (a). The transition temperature needs to be determined by means of the global free energy minimum which in the large-N limit, is identical to the saddle-point action (3.9). It is convenient to plot $F^{sc}(\delta\tilde{r}_0) - F^{paranem}(\delta\tilde{r}_0)$ such that its zero marks the transition temperature, see also Fig. 3.7(b) in the next section.

3.2.6.2 Full model in the classical regime

In this section, we include the E_g fluctuations which generate a finite cubic parameter g_{c}. As a consequence, the nematic order parameter $\mathbf{C}_0^{E_g}$ regains its Z_3-Potts character and has to undergo a first-order phase transition. Similarly to the previous case (3.2.6.1), we employ a momentum cutoff Λ in the q_z direction while the in-plane integration is free.[11]The saddle-point equations

$$T > T_c: \qquad \delta\hat{r}_0 = \hat{R}_0 + 2\hat{u}I_1(R_0, |\mathbf{C}_0^{E_g}|)\,, \qquad 0 = \frac{|\hat{\mathbf{C}}_0^{E_g}|}{2} - I_2(R_0, |\mathbf{C}_0^{E_g}|)\,, \tag{3.57}$$

$$T < T_c: \qquad \delta\hat{r}_0 = (1-\hat{u})|\hat{\mathbf{C}}_0^{E_g}| + 2\hat{u}I_3(R_0, R_0)\,, \qquad |\hat{\mathbf{\Delta}}_0^{E_u}|^2 = \frac{|\hat{\mathbf{C}}_0^{E_g}|}{2} - I_2(R_0, R_0)\,, \tag{3.58}$$

can be expressed in terms of the dimensionless quantities $\{\tilde{u}, \tilde{v}\} = \{u', v\}T/\pi \mathsf{d}_0^2 V_0$, $\hat{u} = u'/v$, as well as the dimensionless fields $\{\hat{R}_0, |\hat{\mathbf{C}}_0^{E_g}|, \delta\hat{r}_0\} = \{R_0, |\mathbf{C}_0^{E_g}|, \delta r_0\}/\mathsf{d}_0\tilde{v}$, and $\hat{\mathbf{\Delta}}_0^{E_u} = \mathbf{\Delta}_0^{E_u}\sqrt{\mathsf{d}_0\pi V_0/T}$. The two integrals read

$$I_1(R_0, |\mathbf{C}_0^{E_g}|) = -\frac{\pi \mathsf{d}_0 V_0}{V}\sum_{\boldsymbol{q}}\left(\frac{R_0 + f_{\boldsymbol{q}}^{A_{1g}}}{\det\left(\mathcal{G}_{\boldsymbol{q}}^{\mathsf{C}}\right)^{-1}} - \frac{f_{\boldsymbol{q}}^{A_{1g}}}{\det\left(\mathcal{G}_{\boldsymbol{q}}^{\mathsf{C}}\right)^{-1}}\bigg|_{R_0=|\mathbf{C}_0^{E_g}|=0}\right), \tag{3.59}$$

$$I_2(R_0, |\mathbf{C}_0^{E_g}|) = \frac{\pi \mathsf{d}_0 V_0}{V}\sum_{\boldsymbol{q}}\frac{|\mathbf{C}_0^{E_g}| + \boldsymbol{f}_{\boldsymbol{q}}^{E_g}\cdot\frac{\mathbf{C}_0^{E_g}}{|\mathbf{C}_0^{E_g}|}}{\det\left(\mathcal{G}_{\boldsymbol{q}}^{\mathsf{C}}\right)^{-1}}\,, \tag{3.60}$$

and $I_3(R_0, |\mathbf{C}_0^{E_g}|) = I_1(R_0, |\mathbf{C}_0^{E_g}|) + I_2(R_0, |\mathbf{C}_0^{E_g}|)$. When introducing the rescaled fields in (3.59) and (3.60), the prefactors cancel and the gradient parameter need to be rescaled according to $\mathsf{d}_0 \to 1$, $\mathsf{d}' \to \mathsf{d}'/\mathsf{d}_0$, $\tilde{\mathsf{d}} \to \tilde{\mathsf{d}}/\mathsf{d}_0\sqrt{\tilde{v}}$ and $\mathsf{d}_z \to \mathsf{d}_z/\mathsf{d}_0\tilde{v}$. Eventually, the model depends on the three gradient ratios, the interaction ratio $\hat{u}$, and the momentum cutoff $\Lambda_c = \Lambda c$.

To capture the essential physics in doped Bi_2Se_3, we choose $\hat{u} = 3$ and $\mathsf{d}'/\mathsf{d}_0 = 0.4$. The value of $\tilde{\mathsf{d}}/\mathsf{d}_0\sqrt{\tilde{v}} = 0.20$ is chosen such that it entails a rather large first-order jump (cf. Fig. 3.3). The parameter d_z can be understood as a proxy for the doping level, as the Fermi surface in $Cu_xBi_2Se_3$ has been reported to evolve from ellipsoidal towards cylindrical with increasing doping level [92]. For a comparably large d_z value, i.e. for a Fermi surfaces with a small anisotropy, the system undergoes joint first-order transitions, similar to Fig.3.4(a). Upon doping the z-anisotropy becomes larger and the value of d_z becomes smaller. A small value $\mathsf{d}_z/\mathsf{d}_0\tilde{v} = 0.07$ captures the vestigial nematic scenario shown in figure 3.7. In figure (a), the pronounced peak in $\delta\tilde{r}_0^{\mathrm{nem}}$ indicates a first-order transition. Upon further cooling, superconductivity emerges in a second-order transition when the susceptibility $\chi_{\mathrm{pair}} = R_0/(R_0^2 - |\mathbf{C}_0^{E_g}|^2)$ diverges. To determine T_{nem} we plot the free energy differences $F^{\{nem,sc\}}(\delta\tilde{r}_0) - F^{paranem}(\delta\tilde{r}_0)$ resulting from (3.9) and associate the zero with the transition temperature, see Fig.3.7(b) lower panel. In agreement with the symmetry constraint, the nematic order parameter undergoes a first-order transition at a temperature $T_{nem} > T_c$. The top panel of figure Fig.3.7(b) shows the temperature dependence of the nematic and the superconducting order parameters, together with their respective susceptibilities. The nematic susceptibility χ_{nem}, studied in Sec.3.2.7, is enhanced but—owed to the first-order nature of the transition—does not diverge.

[11]In Ref. [107], we employed a lattice version with natural cutoffs. However, for the present purpose, in particular to demonstrate a pronounced peak of $\delta\tilde{r}^{\mathrm{nem}}$ in Fig. 3.7(a) it is more convenient to work with the continuum model.

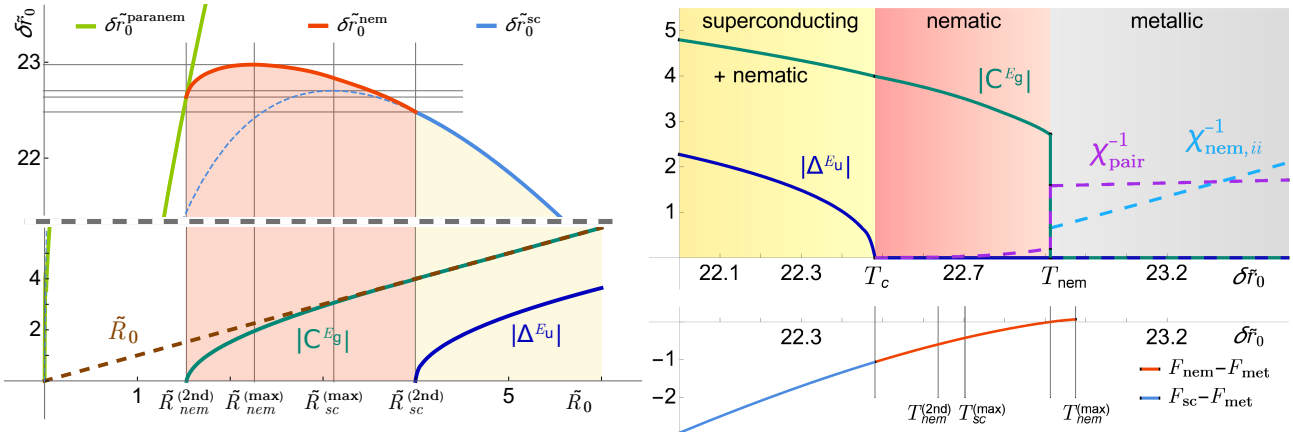

(a) (b)

Figure 3.7: The figures depict the expected vestigial nematic scenario for doped Bi_2Se_3. The system undergoes a first-order transition at the temperature determined from the free energy in the lower panel of (b). At the lower temperature it becomes superconducting where the pairing susceptibility diverges. The nematic susceptibility does not diverge due to the first-order vestigial nematic transition. The parameters were chosen as $u'/v = 3$, $\mathsf{d}'/\mathsf{d}_0 = 0.40$, $\mathsf{d}_z/\mathsf{d}_0\tilde{v} = 0.07$, $\tilde{\mathsf{d}}/\mathsf{d}_0\sqrt{\tilde{v}} = 0.20$ and the cutoff in z-direction $\Lambda_z c = 10$.

The above result demonstrates that a vestigial nematic scenario with $T_{\text{nem}} > T_c$ is possible in doped Bi_2Se_3; at least in a certain doping range. Additionally, our theory reveals that superconducting fluctuations experience a sudden enhancement at the vestigial nematic phase transition. This effect is reflected in an enhanced observable signal, e.g. in the magnetization is shown in Fig. 3.14. Furthermore, the nematic distortion triggers a distinct in-plane anisotropy which is studied next. The present theory can not reliably predict the extent of the nematic transition temperature $T_{\text{nem}} - T_c$ due to the uncertainties in the parameters. In the next section (3.2.7), we compute the nematic susceptibility. In section (3.3), we discuss how an in-plane anisotropy is imposed on the conductivity and the magnetic susceptibility, and the response of the atomic lattice is discussed in section (3.4). The nematic order causes a lattice distortion that is preceded by the softening of certain elastic constants due to the nematic fluctuations above T_{nem}.

3.2.7 Nematic susceptibility

By construction, the nematic susceptibility is the quantity that signals how far the system is away from the nematic critical temperature. As such it is directly related to the quadratic coefficient r_{c} in the corresponding Ginzburg-Landau expansion. Formally, the nematic susceptibility is defined as the correlation function

$$\chi_{\text{nem},ij}(q) = \langle \mathsf{B}_q^{E_g,i} \mathsf{B}_{-q}^{E_g,j} \rangle - \langle \mathsf{B}_q^{E_g,i} \rangle \langle \mathsf{B}_{-q}^{E_g,j} \rangle \,, \tag{3.61}$$

where $\mathbf{B}^{E_g}$ is the superconducting bilinear combination in the nematic E_g symmetry channel, see Eq. (3.3). Within the field integral approach it is common to introduce a conjugated field in order to compute a correlation function. The conjugated field $\mathbf{h}$ couples linearly to $\mathbf{B}^{E_g}$ generating the action contribution $\mathcal{S}_{\mathsf{h}} = -\sum_q \mathbf{h}_q \cdot \mathbf{B}^{E_g}_{-q}$. Consequently, the partition function $Z\left[\mathbf{h}\right]$ depends on the external

field, and the expectation value of $\mathbf{B}^{E_g}$ and the correlation function (3.61) can be derived as

$$\langle \mathsf{B}_q^{E_g,j}\rangle_{\mathsf{h}} = T\frac{\delta \log Z\left[\mathbf{h}\right]}{\delta \mathsf{h}_{j,-q}}, \qquad \chi_{\mathrm{nem},ij}(q) = T\frac{\delta^2 \log Z\left[\mathbf{h}\right]}{\delta \mathsf{h}_{i,q}\delta \mathsf{h}_{j,-q}}\bigg|_{\mathbf{h}=0} = \frac{\delta\langle \mathsf{B}_q^{E_g,j}\rangle_{\mathsf{h}}}{\delta \mathsf{h}_{i,q}}\bigg|_{\mathbf{h}=0}. \tag{3.62}$$

Hence, the partition function $Z\left[\mathbf{h}\right]$ needs to be evaluated. The addition of $\mathcal{S}_{\mathsf{h}}$ to the action (3.9) effectively amounts to the replacement $(\mathcal{G}^{\mathsf{C}})^{-1}_{q,q'} \to (\mathcal{G}^{\mathsf{C}}[\mathbf{h}])^{-1}_{q,q'} = (\mathcal{G}^{\mathsf{C}})^{-1}_{q,q'} - \mathbf{h}_{q-q'}\cdot\boldsymbol{\tau}^{E_g}$ in the action (3.7). If we then shift the composite field to $\tilde{\mathsf{C}}_q^{E_g,j} = \mathsf{C}_q^{E_g,j} - \mathsf{h}_{j,q}$ the external field dependence is moved into the kinetic term

$$\mathcal{S}_{\mathsf{C}} = \frac{1}{4v}V\sum_q (\tilde{\boldsymbol{C}}_q^{E_g} + \mathbf{h}_q)(\tilde{\boldsymbol{C}}_{-q}^{E_g} + \mathbf{h}_{-q}),$$

and the above derivations change to

$$T\frac{\delta \log Z\left[\mathbf{h}\right]}{\delta \mathsf{h}_{j,-q}} = -\frac{1}{2v}\left(\langle \tilde{\mathsf{C}}_q^{E_g,j}\rangle_{\mathsf{h}} + \mathsf{h}_{j,q}\right), \qquad \chi_{\mathrm{nem},ij}(q) = -\frac{1}{2v}\left(\frac{\delta\langle \tilde{\mathsf{C}}_q^{E_g,j}\rangle_{\mathsf{h}}}{\delta \mathsf{h}_{i,q}}\bigg|_{\mathbf{h}=0} + \delta_{ij}\right). \tag{3.63}$$

We use the relation (3.63) to derive the nematic susceptibility from the saddle-point equation instead of actually evaluating $Z\left[\mathbf{h}\right]$. In the presence of a finite field $\mathbf{h}$, the expectation value $\langle \mathsf{C}_q^{E_g,j}\rangle_{\mathsf{h}}$ [and equally $\langle \tilde{\mathsf{C}}_q^{E_g,j}\rangle_{\mathsf{h}}$] can already be finite above the nematic phase. The saddle-point equations related to $\tilde{\mathsf{C}}_q^{E_g,j}(\mathbf{h})$ above the nematic transition (using $\tilde{\mathsf{C}}_q^{E_g,j}(\boldsymbol{h}) = \tilde{\mathsf{C}}_0^{E_g,j}(\boldsymbol{h})\delta_{q,0}$) reads

$$0 = \frac{1}{2v}\left(\tilde{\mathsf{C}}_0^{E_g,j}(\boldsymbol{h}) + \mathsf{h}_{j,0}\right) + \frac{T}{2V}\sum_q \mathrm{tr}_\tau\left(\mathcal{G}^{\tilde{\mathsf{C}}}_{q,q}[\mathbf{h}]\tau^{E_g,j}\right). \tag{3.64}$$

We vary the equation (3.64) with respect to $\mathsf{h}_{i,0}$, evaluate it at zero field $\mathbf{h} = 0$, and insert the definition of the nematic susceptibility (3.63). We find

$$\chi_{\mathrm{nem}}(0) = \chi^{(0)}_{\mathrm{nem}}(0)\left(\mathbb{1} - 2v\chi^{(0)}_{\mathrm{nem}}(0)\right)^{-1},$$

where we have used that $\mathsf{C}_0^{A_{1g}} \neq \mathsf{C}_0^{A_{1g}}[\mathbf{h}]$, see appendix C.4.1 for details. Moreover, the bare susceptibility $\chi^{(0)}_{\mathrm{nem},lj}(0) = \frac{T}{2V}\sum_q \mathrm{tr}_\tau(\mathcal{G}_q^{\mathsf{C}}\tau^{E_g,l}\mathcal{G}_q^{\mathsf{C}}\tau^{E_g,j})|_{\mathbf{h}=0}$ is found to be proportional to the unity matrix $\chi^{(0)}_{\mathrm{nem},lj}(0) = \frac{1}{2}\tilde{\Pi}_{z,z}\delta_{l,j}$. Therefore, the nematic susceptibility is proportional to the unity matrix

$$\chi_{\mathrm{nem}}(0) = \frac{\frac{1}{2}\tilde{\Pi}_{z,z}}{1 - v\tilde{\Pi}_{z,z}}\mathbb{1} = \frac{\tilde{\Pi}_{z,z}}{8vr_{\mathsf{c}}}\mathbb{1}. \tag{3.65}$$

With its elements inversely proportional to the quadratic coefficient r_{c}, the diagonal element $\chi_{\mathrm{nem}}(0)_{ii}$ shows a Curie-Weiss behavior, as shown in figure 3.7(b). However, due to the first-order nature of the phase transition, the nematic susceptibility does not diverge: it rather reaches $\chi^{-1}_{\mathrm{nem}}(0) \sim g_{\mathsf{c}}^2$ at the T_{nem}. Experimentally, the enhancement of the nematic susceptibility should be directly observable via electronic Raman scattering in the E_g symmetry channel [116, 117].

3.3 In-plane anisotropy of the resistivity and magnetic susceptibility

In the following we analyze how the superconducting fluctuations renormalize the resistivity and the magnetic susceptibility above T_c. In particular, we discuss how the nematic order parameter imposes an anisotropy between two orthogonal in-plane directions. For simplicity, we disregard the normal state quasi-particle contributions. The following calculations are based on earlier works [108–110] and generalize them by including the effects of the nematic order parameter. In the following sections, we derive the general relations between the partition function and two observables (susceptibility and conductivity). We then present the key steps in evaluating the respective observables with the main results summarized in Fig. 3.8. More details on the derivations can be found in the appendix C.3.

3.3.1 London response kernel

The *London response kernel* $Q_{\alpha\beta}(q)$ with $\alpha, \beta = \{1, 2, 3\}$ and $q = (\nu_m, \boldsymbol{q})$ is also known as the current-current correlation function. As the vector potential $\boldsymbol{A}$ is the conjugated field to the current $\boldsymbol{j}$ they couple via $\mathcal{S}_A = V \sum_q \boldsymbol{j}_{-q} \cdot \boldsymbol{A}_q$ and both, the expectation value of the current and the London response kernel can be extracted via

$$\langle j_q^\alpha \rangle = \frac{T}{V} \frac{\delta \log Z[\boldsymbol{A}]}{\delta A_{-q}^\alpha}\bigg|_{\boldsymbol{A}=0}, \qquad Q_{\alpha\beta}(q) = \frac{T}{V} \frac{\delta^2 \log Z[\boldsymbol{A}]}{\delta A_q^\beta \delta A_{-q}^\alpha}\bigg|_{\boldsymbol{A}=0} = \frac{V}{T}\langle j_q^\alpha j_{-q}^\beta \rangle - \frac{V}{T}\langle j_q^\alpha \rangle \langle j_{-q}^\beta \rangle . \tag{3.66}$$

The response kernel presents the key quantity for determining the conductivity and susceptibility of the system. Indeed, as discussed in section 1.1.3 the London kernel is directly related to the conductivity via

$$\operatorname{Re}\sigma(\nu + \mathrm{i}0, \boldsymbol{q}) = \frac{\operatorname{Im} Q(\nu + \mathrm{i}0, \boldsymbol{q})}{\nu} - \pi\delta(\nu)\, \operatorname{Re} Q(\nu + \mathrm{i}0, \boldsymbol{q}). \tag{3.67}$$

The second (diverging) term is zero above T_c and finite below. The magnetization and the magnetic susceptibility on the other hand are defined as the derivatives of the free energy with respect to the magnetic field $\boldsymbol{H}$,

$$M_q^\alpha \left[\boldsymbol{H}\right] = -\frac{1}{\mu_0 V} \frac{\partial F\left[\boldsymbol{H}\right]}{\partial H_{-q}^\alpha}, \qquad \chi_{\alpha\beta}(q) = \frac{\partial M_q^\alpha \left[\boldsymbol{H}\right]}{\partial H_q^\beta}\bigg|_{\boldsymbol{H}=0}. \tag{3.68}$$

In the present model, the free energy depends explicitly on $\boldsymbol{H}$ due to the term $\alpha' B_z \mathsf{B}^{A_{2g}}$ and implicitly via the vector potential $\boldsymbol{A}$. Hence, it is convenient to view the free energy $F\left[\boldsymbol{H}, \boldsymbol{A}\right] = -T \log Z\left[\boldsymbol{H}, \boldsymbol{A}\right]$ as a function of both, the vector potential and the magnetic field, and expand it accordingly

$$F\left[\boldsymbol{H}, \boldsymbol{A}\right] \approx -T \log Z\left[\boldsymbol{0}, \boldsymbol{0}\right] - V\mu_0 \sum_q M_{-q}^\alpha[\boldsymbol{0}] H_q^\alpha - \frac{V\mu_0^2}{2} \sum_q Q_{\alpha\beta}^H(q) H_{-q}^\alpha H_q^\beta - \frac{V}{2} \sum_q Q_{\alpha\beta}^A(q) A_{-q}^\alpha A_q^\beta , \tag{3.69}$$

where we defined

$$Q^H_{\alpha\beta}(q) = \frac{T}{V\mu_0^2}\frac{\delta^2 \log Z\left[\boldsymbol{H},\boldsymbol{A}\right]}{\delta H^\beta_{-q}\delta H^\alpha_q}\Big|_{\boldsymbol{A}=\text{const}}\Big|_{\boldsymbol{A}=\boldsymbol{H}=0}, \qquad Q^A_{\alpha\beta}(q) = \frac{T}{V}\frac{\delta^2 \log Z[\boldsymbol{H},\boldsymbol{A}]}{\delta A^\beta_q \delta A^\alpha_{-q}}\Big|_{\boldsymbol{H}=\text{const}}\Big|_{\boldsymbol{A}=\boldsymbol{H}=0}. \tag{3.70}$$

As is shown in the appendix, the omitted expansion terms vanish due to the inversion symmetry. The quadratic terms in (3.69) need to be expressed in terms of $\boldsymbol{A}$ to identify the London response kernel Q, and in terms of $\boldsymbol{H}$ to compute the magnetic susceptibility χ. In Fourier space the magnetic flux density is related to the vector potential via $\boldsymbol{B}_q = \mathrm{i}\boldsymbol{q}\times\boldsymbol{A}_q$. Upon application of the Coulomb gauge $\boldsymbol{q}\cdot\boldsymbol{A}_q = 0$ the relation can be inverted to $A^\alpha_q = \mathrm{i}\epsilon_{\alpha\beta\gamma}q_\beta B^\gamma_q/|\boldsymbol{q}|^2$.[12] Assuming there is no finite magnetization above T_c it holds $\boldsymbol{H}_q = \boldsymbol{B}_q/\mu_0$ with the permeability constant μ_0. Then, the free energy (3.69) can be expressed in terms of $\boldsymbol{A}$ and $\boldsymbol{H}$, and we derive the London kernel and the magnetic susceptibility $\chi_{\alpha\beta}(q) = \mu_0\tilde{Q}_{\alpha\beta}(q)$ with

$$\text{London kernel:} \qquad Q_{\alpha\beta}(q) = Q^A_{\alpha\beta}(q) - Q^H_{\alpha'\beta'}(q)\epsilon_{\alpha\alpha'\gamma}\epsilon_{\beta\beta'\gamma'}q_\gamma q_{\gamma'}\,, \tag{3.71}$$

$$\text{magn. susceptibility:} \qquad \tilde{Q}_{\alpha\beta}(q) = Q^H_{\alpha\beta}(q) + Q^A_{\alpha'\beta'}(q)\epsilon_{\alpha\alpha'\gamma}\epsilon_{\beta\beta'\gamma'}\frac{q_\gamma q_{\gamma'}}{|\boldsymbol{q}|^4}\,. \tag{3.72}$$

3.3.2 Anisotropic response of physical observables

Let us compute the correlation functions for the action (3.9) in the presence of a magnetic field. Remember that a magnetic field couples through the Green's function matrix $(\mathcal{G}\left[\boldsymbol{A}\right])^{-1}_{q,q'} = (\mathcal{G}^{\mathsf{C}})^{-1}_{q,q'} + (\mathcal{G}^A\left[\boldsymbol{A}\right])^{-1}_{q,q'}$ with the second term reading

$$\left(\mathcal{G}^A\left[\boldsymbol{A}\right]\right)^{-1}_{q,q'} = \alpha' B_z\tau^y - e\hat{V}^\alpha_{\frac{q}{2}+\frac{q'}{2}}A^\alpha_{q-q'} + \frac{e^2}{2}\hat{O}^{\alpha\beta}_{\frac{q}{2}+\frac{q'}{2}}\sum_{q_1}A^\alpha_{q_1}\cdot A^\beta_{q-q'-q_1}\,,$$

and $\hat{V}^\alpha_{\boldsymbol{q}}$, $\hat{O}^{\alpha\beta}_{\boldsymbol{q}}$ defined in (3.5). To proceed we evaluate the partition function $Z\left[\boldsymbol{H},\boldsymbol{A}\right]$ at the saddle-point solution. Then, the correlation functions become quite handy: It holds $Q^A_{\alpha\beta}(q) = K_{\alpha\beta}(q) - K_{\alpha\beta}(0)$ and

$$K_{\alpha\beta}(q) = \frac{Te^2}{V}\sum_p \mathrm{tr}_\tau\left(\mathcal{G}^{\mathsf{C}}_{p+\frac{q}{2}}\hat{V}^\beta_{\boldsymbol{p}}\mathcal{G}^{\mathsf{C}}_{p-\frac{q}{2}}\hat{V}^\alpha_{\boldsymbol{p}}\right), \qquad Q^H_{\alpha\beta}(q) = \frac{T(\alpha')^2}{V}\delta_{q,0}\delta_{\alpha,z}\delta_{\beta,z}\sum_p \mathrm{tr}_\tau\left(\mathcal{G}^{\mathsf{C}}_p\tau^y\mathcal{G}^{\mathsf{C}}_p\tau^y\right), \tag{3.73}$$

where the function $K_{\alpha\beta}(q)$ is even $[K_{\alpha\beta}(-q) = K_{\alpha\beta}(q)]$ and symmetric $[K_{\beta\alpha}(q) = K_{\alpha\beta}(q)]$. From a diagrammatic point of view both summations in (3.73) represent a one-loop diagram with $\hat{V}$ or τ^y at the vertices. Since the nematic order parameter does not break the time-reversal symmetry, we find the zero-field magnetization $M^\alpha_q[0] = -\frac{T\delta_{q,0}}{\mu_0 V}\sum_p \mathrm{tr}_\tau(\mathcal{G}^{\mathsf{C}}_p\tau^y) = 0$ to vanish. We note however, that a vestigial chiral order parameter $\mathsf{C}_0^{A_{2g}}$ (which couples with τ^y) would induce a finite magnetization.

For the optical conductivity we explicitly derive the formula (3.67) in the appendix. After the

[12] To see this explicitly, one considers the term $\boldsymbol{q}\times\boldsymbol{B}_q$, inserts $\boldsymbol{B}_q$ and applies the Coulomb gauge.

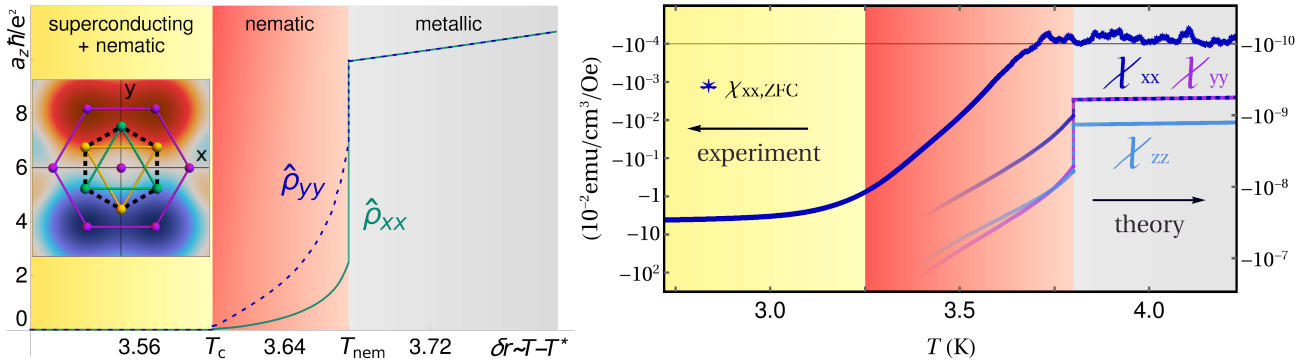

Figure 3.8: (a) shows the in-plane resistivity (3.74) and (b) the diamagnetic susceptibility (3.76) alongside the measurement by [20]. Both observables display an enhanced signal with the transition onset and a pronounced anisotropy in the nematic state. For the indicated ground state ($\theta_c = \pi$) we find $\rho_{yy} > \rho_{xx}$ and $\chi_{yy} < \chi_{xx}$ while it would be the opposite for $\theta_c = 0$. For a discussion of the experiment, see Sec.3.6. The plotted data originates from [107].

analytical continuation it becomes

$$\mathrm{Re}\,\sigma_{\alpha\beta}(\nu + \mathrm{i}0, \mathbf{0}) = \frac{Te^2}{\pi V} \sum_{\boldsymbol{p}} \int_{-\infty}^{\infty} d\epsilon\, \mathrm{tr}_\tau \left(\frac{\mathrm{Im}[\mathcal{G}^{\mathsf{C}}_{\boldsymbol{p}}(\epsilon + \nu + \mathrm{i}0)]}{\epsilon + \nu} \hat{V}^{\beta}_{\boldsymbol{p}} \frac{\mathrm{Im}[\mathcal{G}^{\mathsf{C}}_{\boldsymbol{p}}(\epsilon + \mathrm{i}0)]}{\epsilon} \hat{V}^{\alpha}_{\boldsymbol{p}} \right), \tag{3.74}$$

where the ϵ integration can be carried out analytically. Note that Q^H does not contribute to the London kernel (3.71) in the zero-momentum limit. The conductivity is evaluated numerically and the corresponding ρ_{xx} and ρ_{yy} resistivity components are plotted as a function of the temperature in figure 3.8(a). For the nematic ground state $\mathbf{C}_0^{E_g} = |\mathbf{C}_0^{E_g}|(-1, 0)$, we find $\rho_{yy} > \rho_{xx}$ inside the vestigial nematic phase. The relation $\rho_{yy} > \rho_{xx}$ holds for all three degenerate states $\theta_c = \{1, 3, 5\}\,\pi/3$. For the members of the second ground state set with $\theta_c = \{0, 2, 4\}\,\pi/3$ one finds the opposite order $\rho_{yy} < \rho_{xx}$.

To compute the DC magnetic susceptibility $\chi_{\alpha\beta}(\nu_m = 0, \boldsymbol{q} = 0)$ the zero-momentum limit can only be taken after the kernel $Q^A_{\alpha\beta}(q)$ is expanded according to

$$Q^A_{\alpha\beta}(q) \approx \frac{1}{2}\, \Gamma^{\gamma\delta}_{\alpha\beta}\, q_\gamma q_\delta\,, \qquad \text{with} \qquad \Gamma^{\gamma\delta}_{\alpha\beta} = \left. \frac{\partial^2 Q^A_{\alpha\beta}(q)}{\partial q_\gamma \partial q_\delta} \right|_{q=0}. \tag{3.75}$$

The zeroth-order term vanishes by construction and a linear term is forbidden since $Q^A_{\alpha\beta}(-q) = Q^A_{\alpha\beta}(q)$. The elements of the quadratic expansion tensor are subject to the constraints $\Gamma^{\gamma\delta}_{\alpha\beta} = \Gamma^{\gamma\delta}_{\beta\alpha} = \Gamma^{\delta\gamma}_{\alpha\beta} = \Gamma^{\alpha\beta}_{\gamma\delta}$. With this, the DC susceptibility in Eq. (3.72) becomes

$$\chi_{\alpha\beta}(\nu_m = 0, \boldsymbol{q} = 0) = \mu_0 Q^H_{\alpha\beta}(0) + \frac{1}{2}\mu_0 \Gamma^{\delta\delta'}_{\alpha'\beta'}\, \epsilon_{\alpha\alpha'\gamma}\epsilon_{\beta\beta'\gamma'}\hat{q}_\delta \hat{q}_{\delta'} \hat{q}_\gamma \hat{q}_{\gamma'}\,.$$

While this expression seems to depend on the momentum direction $\hat{q}_\gamma = q_\gamma/|\boldsymbol{q}|$, a careful study reveals that the expression is isotropic in momentum space. Due to the relation $\boldsymbol{H}_q = \mu_0 \mathrm{i}\boldsymbol{q} \times \boldsymbol{A}_q$, the

orthogonality between the momentum $\boldsymbol{q}$ and the magnetic field $\boldsymbol{H}$ has to be considered. In fact, for the respective susceptibility components in the relation $M_\alpha(\mathbf{0}) = \chi_{\alpha\beta}(\boldsymbol{q}_\perp)|_{|\boldsymbol{q}|\to 0} H^\beta(\mathbf{0})$, the transverse momentum $\boldsymbol{q}_\perp$ has to be chosen such that $\boldsymbol{q}_\perp \perp \boldsymbol{H}$. For example, for $\boldsymbol{H} = |\boldsymbol{H}|e_x$ it must hold $\boldsymbol{q}_\perp = |\boldsymbol{q}|\big(\cos\varphi, \sin\varphi, 0\big)$. After some algebra the diagonal components can be simplified to

$$\chi_{xx}(0,0) \overset{(*)}{=} \frac{\chi_0}{2}\frac{c^2}{a^2}\tilde{\Gamma}^{zz}_{yy}\,, \qquad \chi_{yy}(0,0) \overset{(*)}{=} \frac{\chi_0}{2}\frac{c^2}{a^2}\tilde{\Gamma}^{zz}_{xx}\,, \qquad \chi_{zz}(0,0) \overset{(*)}{=} \frac{\chi_0}{2}\left(2\tilde{Q}^H_{zz}(0) + \tilde{\Gamma}^{yy}_{xx}\right), \tag{3.76}$$

where the value of the susceptibilities scales with the number $\chi_0 = \mu_0 T e^2 a^4/V_0\hbar^2$. The Planck's constant $\hbar$ has been reinstalled.[13] The rescaled quantities $\tilde{Q}^H$ and $\tilde{\Gamma}^{\gamma\delta}_{\alpha\beta}$ are defined in the appendix C.3. The value $\tilde{Q}^H_{zz}(0) > 0$ is a purely para-magnetic contribution to the susceptibility $\chi_{zz}(0,0)$. The numerical evaluation of the formulae (3.76) is done in the high-temperature limit, i.e. for the leading Matsubara term with $\nu_n = 0$, with the results displayed in figure 3.8(b). Similar to the conductivity, the susceptibility displays an enhanced signal with the onset of the fluctuation-induced phase, and it develops an in-plane anisotropy where, for the chosen ground state ($\theta_\mathsf{c} = \pi$), it holds $\chi_{yy} < \chi_{xx}$. Note that for both quantities, conductivity and susceptibility, the inequalities between the xx and yy components flip as the ground state becomes $\theta_\mathsf{c} \to 0$.

3.4 Lattice deformation due to vestigial nematicity

Here, we investigate the interplay between the lattice degrees of freedom and the vestigial nematic order parameter. To this end, we introduce the language of elasticity theory and classify the occurring tensor with respect to their lattice transformation properties in Sec. 3.4.1. In section 3.4.2 we study how the vestigial nematic order parameter induces certain strain components and thereby, causes a lattice distortion. Also, the implications of nematic fluctuations above T_nem with respect to the renormalization of elastic constants and the sound velocity are analyzed.

3.4.1 Elasticity- and strain tensor, and their symmetry

In crystal elasticity theory infinitesimal strain is measured with the strain tensor

$$\epsilon_{\alpha\beta} = \frac{1}{2}\left(\frac{\partial u_\alpha}{\partial r_\beta} + \frac{\partial u_\beta}{\partial r_\alpha}\right), \tag{3.77}$$

which consists of the symmetrized differential of the lattice displacement field $u_\alpha(\boldsymbol{r})$ with $\alpha, \beta = \{1, 2, 3\}$. A structural phase transition is directly reflected by the strain tensor, and hence, certain strain components play the role of an order parameter in a Ginzburg-Landau sense. Let us briefly develop a theoretical framework suited for a proper description of lattice energetics. For this purpose, we follow the work by [54]: The energy of a solid must not depend on arbitrary rigid displacements $\boldsymbol{r} \to \boldsymbol{r} + \boldsymbol{t}_D$ and thus, the potential energy should only depend on position differences $\boldsymbol{r}_1 - \boldsymbol{r}_2$. By assuming that this difference is small compared to typical measurement length scales, the coordinate transformation $\boldsymbol{r} \to \boldsymbol{r}'(\boldsymbol{r})$ can be expanded and higher order terms may be neglected. Then, the

[13] We have marked the identities in (3.76) with an asterisk to annotate that the underlying relations have only been verified numerically, not analytically.

potential energy $V = \int_r \mathcal{V}(\boldsymbol{r})$ is characterized by a potential per unit undeformed volume

$$\mathcal{V}(\boldsymbol{r}) = \mathcal{V}\left(\frac{\partial r'_\alpha(\boldsymbol{r})}{\partial r_\gamma}\right), \tag{3.78}$$

which is a function of first-order derivatives only. The constant argument disappears due to the invariance under constant displacements. If one further imposes the invariance of the description under proper rotations of the crystal, the potential $\mathcal{V} \to \mathcal{V}\left(S_{\alpha\beta}\right)$ becomes a function of the six scalar products $S_{\alpha\beta} = \nabla_r r'_\alpha(\boldsymbol{r}) \cdot \nabla_r r'_\beta(\boldsymbol{r})$. The potential density can equally well be expressed in terms of the shifted variable $\hat{S}_{\alpha\beta} = (S_{\alpha\beta} - \delta_{\alpha\beta})/2$ which is directly related to the strain tensor (3.77). This becomes explicit when introducing the lattice displacement $u_\alpha(\boldsymbol{r}) = r'_\alpha(\boldsymbol{r}) - r_\alpha$, such that it holds $\hat{S}_{\alpha\beta} = \epsilon_{\alpha\beta} + \frac{1}{2}\nabla_r u(\boldsymbol{r}) \cdot \nabla_r u(\boldsymbol{r})$. In accordance with the assumption of the derivative expansion the second term can be neglected and one finds in the limit of infinitesimal strain

$$V = \frac{1}{2}\int_{\boldsymbol{r}} \epsilon_{\alpha\beta} C_{\alpha\beta\gamma\delta} \epsilon_{\gamma\delta}\,. \tag{3.79}$$

The absence of a linear term in ϵ is based on the assumption that the system has originally (e.g. at a high temperature) been in an equilibrium configuration [118]. As key observations of this brief introduction into the energetics of lattices, we keep in mind that the strain tensor $\epsilon_{\alpha\beta}$ is the defining field variable, and that the corresponding 'mass' is represented by the elastic stiffness tensor, or briefly the elastic tensor $C_{\alpha\beta\gamma\delta}$.

In terms of transformation properties we deduce from the definition $S_{\alpha\beta} = \nabla_r r'_\alpha(\boldsymbol{r}) \cdot \nabla_r r'_\beta(\boldsymbol{r})$ that $S_{\alpha\beta}$ (and similarly the strain tensor $\epsilon_{\alpha\beta}$) transforms according to the product representation of two vectors. More precisely, it transforms according to the symmetric part of the product representation, which makes the strain tensor $\epsilon_{\alpha\beta}$ a symmetric second-ranked tensor with six independent components, owed to $\epsilon_{\alpha\beta} = \epsilon_{\beta\alpha}$. Accordingly, the elastic stiffness tensor $C_{\alpha\beta\gamma\delta}$ becomes a symmetric fourth-ranked tensor, whose number of independent components is reduced to 21 owed to the symmetry constraint and the exchange of indices $C_{\gamma\delta\alpha\beta} = C_{\alpha\beta\gamma\delta}$.[14] The number of components further reduces in the presence of non-trivial crystal symmetry operations like rotations, reflections or inversion. Let us also note that the volume change associated with the lattice transformation implemented in (3.78) is given by the corresponding Jacobian

$$\frac{V'}{V} = \det\left(\frac{\partial r'_\alpha(\boldsymbol{r})}{\partial r_\gamma}\right) = \det\left(\delta_{\alpha\gamma} + \frac{\partial u_\alpha(\boldsymbol{r})}{\partial r_\gamma}\right) \approx 1 + \operatorname{div}\boldsymbol{u} = 1 + \operatorname{tr}\epsilon\,, \tag{3.80}$$

which has been expanded for small derivatives. Accordingly, only trivial strain, i.e. $\operatorname{tr}\epsilon \neq 0$, can cause a volume change. The conjugated field to the strain tensor $\epsilon_{\alpha\beta}$ is called the stress tensor $\sigma^{(s)}_{\alpha\beta}$ and it describes externally exerted stresses in the various symmetry channels. The quantity $\sigma^{(s)}_{\alpha\beta}$ is again a symmetric second-ranked tensor[15]and in linear response theory the important relation between stress-

[14] If we had not imposed rotational invariance, there would be 45 components, see [54] for a discussion.

[15] We have added the superindex (s) to distinguish the stress tensor from the electrical conductivity used in the previous section.

and the strain tensor reads

$$\sigma^{(s)}_{\alpha\beta} = C_{\alpha\beta\gamma\delta}\epsilon_{\gamma\delta}\,. \tag{3.81}$$

It is common practice in elasticity theory to introduce a contracted representation that maps the tensor equations (3.79) and (3.81) to regular matrix multiplications. To this end, the six elements of the second ranked tensors are compressed into the vectors

$$\begin{aligned}\boldsymbol{\epsilon} &= \big(\epsilon_1,\epsilon_2,\epsilon_3,\epsilon_4,\epsilon_5,\epsilon_6\big)^T &&= \Big(\epsilon_{xx},\epsilon_{yy},\epsilon_{zz},2\epsilon_{yz},2\epsilon_{zx},2\epsilon_{xy}\Big)^T\,,\\ \boldsymbol{\sigma}^{(s)} &= \Big(\sigma^{(s)}_1,\sigma^{(s)}_2,\sigma^{(s)}_3,\sigma^{(s)}_4,\sigma^{(s)}_5,\sigma^{(s)}_6\Big)^T &&= \Big(\sigma^{(s)}_{xx},\sigma^{(s)}_{yy},\sigma^{(s)}_{zz},\frac{\sigma^{(s)}_{yz}+\sigma^{(s)}_{zy}}{2},\frac{\sigma^{(s)}_{xz}+\sigma^{(s)}_{zx}}{2},\frac{\sigma^{(s)}_{xy}+\sigma^{(s)}_{yx}}{2}\Big)^T\,,\end{aligned}$$

and the elastic stiffness tensor turns into a matrix

$$\mathcal{C} = \begin{pmatrix} c_{11} & c_{12} & c_{13} & c_{14} & c_{15} & c_{16}\\ & c_{22} & c_{23} & c_{24} & c_{25} & c_{26}\\ & & c_{33} & c_{34} & c_{35} & c_{36}\\ & & & c_{44} & c_{45} & c_{46}\\ & & & & c_{55} & c_{56}\\ & & & & & c_{66}\end{pmatrix}.$$

The stress relation (3.81) now becomes the matrix equation of the form $\boldsymbol{\sigma}^{(s)} = \mathcal{C}\boldsymbol{\epsilon}$ and the potential energy reads

$$V = \frac{1}{2}\int_{\boldsymbol{r}} \boldsymbol{\epsilon}^T\mathcal{C}\boldsymbol{\epsilon}\,. \tag{3.82}$$

Symmetry properties in $SO(3)$ As mentioned earlier, the strain tensor transforms as the symmetric product representation of two vectors. To develop an intuitive understanding, let us first assume that the system has a full rotational symmetry, i.e. its symmetry group is $SO(3)$. The corresponding IRs read Γ_J with J denoting the angular momentum. A vector in this group transforms like (1.18) and falls into the $\Gamma_{J=1}$ IR. Its product representation becomes

$$\Gamma_{J=1}\otimes\Gamma_{J=1} = \big(\Gamma_{J=0}\oplus\Gamma_{J=2}\big)_s \oplus \big(\Gamma_{J=1}\big)_a\,,$$

where we have highlighted the symmetric and the asymmetric IRs. The strain tensor—transforming according to the symmetric part—decomposes into a singlet and a quintuplet representation. In order to classify the strain components in the sectors $\Gamma_{J=0}$ and $\Gamma_{J=2}$, we study the transformation property of a generic strain component $\epsilon^{n,l} = \lambda^{n,l}_{\alpha\beta}\partial_\alpha u_\beta$ where $\lambda^{n,l}$ is a matrix characterized by an IR n and its component $l = 1,\dots,\dim(n)$ and where both, ∂_α and u_β transform like vectors. The matrices $\lambda^{n,l}$ are chosen such that they satisfy the condition

$$\mathcal{R}_v(g)_{\alpha'\alpha}\mathcal{R}_v(g)_{\beta'\beta}\lambda^{n,l}_{\alpha'\beta'} = \mathcal{R}_n(g)_{ll'}\,\lambda^{n,l'}_{\alpha\beta}\,, \tag{3.83}$$

$\mathsf{D_{3d}}$	$\lambda^{n,l}_{\alpha\beta}\partial_\alpha u_\beta$	strain tensor component
A_{1g}	$\partial_x u_x + \partial_y u_y$ $\partial_z u_z$	$\epsilon^{A_{1g},1} = \frac{1}{\sqrt{2}}\left(\epsilon_{xx}+\epsilon_{yy}\right)$ $\epsilon^{A_{1g},2} = \frac{1}{\sqrt{2}}\epsilon_{zz}$
A_{2g}	$\partial_x u_y - \partial_y u_x$	0
E_g	$\left(\partial_x u_x - \partial_y u_y, -\partial_x u_y - \partial_y u_x\right)$ $\left(\partial_y u_z + \partial_z u_y, -\partial_x u_z - \partial_z u_x\right)$ $\left(\partial_y u_z - \partial_z u_y, -\partial_x u_z + \partial_z u_x\right)$	$\boldsymbol{\epsilon}^{E_g,1} = \frac{1}{\sqrt{2}}\left(\epsilon_{xx}-\epsilon_{yy}, -2\epsilon_{xy}\right)$ $\boldsymbol{\epsilon}^{E_g,2} = \sqrt{2}\left(2\epsilon_{yz}, -2\epsilon_{zx}\right)$ $(0,0)$

Table 3.2: The matrices $\lambda^{n,l}$ are determined from the condition (3.83), and they are related to the six strain tensor by $\epsilon^{n,l} = \lambda^{n,l}_{\alpha\beta}\partial_\alpha u_\beta$.

and hence, they determine the transformation property for the corresponding strain component $\epsilon^{n,l}$. Using the transformation matrices of $SO(3)$, the singlet and quintuplet strain components become

$$\Gamma_{J=0} : \left(\epsilon_{xx}+\epsilon_{yy}+\epsilon_{zz}\right) \tag{3.84}$$

$$\Gamma_{J=2} : \left(\epsilon_{xx}-\epsilon_{yy}+2\mathrm{i}\epsilon_{xy}, 2\epsilon_{zx}+2\mathrm{i}\epsilon_{yz}, \epsilon_{zz}-\frac{\epsilon_{xx}+\epsilon_{yy}}{2}, 2\epsilon_{zx}-2\mathrm{i}\epsilon_{yz}, \epsilon_{xx}-\epsilon_{yy}-2\mathrm{i}\epsilon_{xy}\right) . \tag{3.85}$$

The singlet corresponds to the trace of the elasticity tensor and it is thus, the only component that leads a volume change, see Eq. (3.80). The other five components do not cause a volume change and are termed as shear strain. The number of independent elastic tensor components $C_{\alpha\beta\gamma\delta}$ is determined by the number of trivially transforming bilinear combinations of the symmetric strain tensor. Specifically, one computes the product representation of the symmetric strain tensor

$$\left(\Gamma_{J=0}\oplus\Gamma_{J=2}\right)\otimes\left(\Gamma_{J=0}\oplus\Gamma_{J=2}\right) = \left(2\Gamma_{J=0}\oplus 2\Gamma_{J=2}\oplus\Gamma_{J=4}\right)_s \oplus \left(\Gamma_{J=1}\oplus\Gamma_{J=2}\oplus\Gamma_{J=3}\right)_a , \tag{3.86}$$

and counts how often the trivial (here $\Gamma_{J=0}$) IR appears (here twice). Thus, the fully rotational invariant system only allows for two independent elastic tensor components which are associated to a transverse and a longitudinal mode. From the decomposition (3.86), one notes that the bilinear separates into a 21-dimensional symmetric and a 15-dimensional asymmetric block, in agreement with the maximal number of 21 independent components.

Symmetry properties in $\mathsf{D_{3d}}$ The situation changes in a lattice where a point group reduces the symmetry operations. Let us consider here the point group $\mathsf{D_{3d}}$ (cf. table 1.1) which is the relevant symmetry group for doped Bi_2Se_3. In this group, the vector representation reads $E_u \oplus A_{2u}$ and the strain tensor decomposes into

$$\left(E_u\oplus A_{2u}\right)\otimes\left(E_u\oplus A_{2u}\right) = \left(2A_{1g}\oplus 2E_g\right)_s \oplus \left(A_{2g}\oplus E_g\right)_a ,$$

with four IRs constituting the symmetric part. Using the transformation matrices (2.5), the matrices $\lambda^{n,l}$ of the strain components $\epsilon^{n,l} = \lambda^{n,l}_{\alpha\beta}\partial_\alpha u_\beta$ can be directly determined via (3.83), see table 3.2. It is

convenient to work within the symmetry basis spanned by the IRs, where the strain- and stress tensors are expressed by

$$\boldsymbol{\epsilon}^{\mathsf{D_{3d}}} = \begin{pmatrix} \boldsymbol{\epsilon}^{A_{1g}} \\ \boldsymbol{\epsilon}^{E_g} \end{pmatrix}, \quad \text{with} \quad \boldsymbol{\epsilon}^{A_{1g}} = \begin{pmatrix} \epsilon^{A_{1g},1} \\ \epsilon^{A_{1g},2} \end{pmatrix}, \quad \boldsymbol{\epsilon}^{E_g} = \left(\epsilon^{E_g,1,1}, \epsilon^{E_g,1,2}, \epsilon^{E_g,2,1}, \epsilon^{E_g,2,2}\right)^T, \tag{3.87}$$

$$\boldsymbol{\sigma}^{\mathsf{D_{3d}}} = \begin{pmatrix} \boldsymbol{\sigma}^{A_{1g}} \\ \boldsymbol{\sigma}^{E_g} \end{pmatrix}, \quad \text{with} \quad \boldsymbol{\sigma}^{A_{1g}} = \begin{pmatrix} \sigma^{A_{1g},1} \\ \sigma^{A_{1g},2} \end{pmatrix}, \quad \boldsymbol{\sigma}^{E_g} = \left(\sigma^{E_g,1,1}, \sigma^{E_g,1,2}, \sigma^{E_g,2,1}, \sigma^{E_g,2,2}\right)^T. \tag{3.88}$$

The mapping between the original and the symmetry basis $\boldsymbol{\epsilon} = \mathcal{R}_0^{-1}\boldsymbol{\epsilon}^{\mathsf{D_{3d}}}$ is established via the non-orthogonal matrix

$$\mathcal{R}_0 = \frac{1}{\sqrt{2}} \begin{pmatrix} 1 & 1 & 0 & 0 & 0 & 0 \\ 0 & 0 & 1 & 0 & 0 & 0 \\ 1 & -1 & 0 & 0 & 0 & 0 \\ 0 & 0 & 0 & 0 & 0 & -1 \\ 0 & 0 & 0 & 2 & 0 & 0 \\ 0 & 0 & 0 & 0 & -2 & 0 \end{pmatrix},$$

with $\det \mathcal{R}_0 = 1$. In the symmetry basis, the strain tensor $\boldsymbol{\epsilon}^{\mathsf{D_{3d}}}$ transforms according to $\boldsymbol{\epsilon}^{\mathsf{D_{3d}}} \to \mathcal{R}_\epsilon(g)\boldsymbol{\epsilon}^{\mathsf{D_{3d}}}$ upon the point group symmetry operations g, where $\mathcal{R}_\epsilon(g) = (\mathcal{R}_{A_{1g}}(g) \oplus \mathcal{R}_{A_{1g}}(g) \oplus \mathcal{R}_{E_g}(g) \oplus \mathcal{R}_{E_g}(g))$. This allows for a direct determination of the symmetry-allowed components of the stiffness tensor in the potential energy

$$V = \frac{1}{2}\int_{\boldsymbol{r}} \left(\boldsymbol{\epsilon}^{\mathsf{D_{3d}}}\right)^T \mathcal{C}^{\mathsf{D_{3d}}}\boldsymbol{\epsilon}^{\mathsf{D_{3d}}}. \tag{3.89}$$

The constraint that the potential energy has to transform trivially under the point group operations g imposes the condition $\mathcal{R}_\epsilon^T(g)\mathcal{C}^{\mathsf{D_{3d}}}\mathcal{R}_\epsilon(g) = \mathcal{C}^{\mathsf{D_{3d}}}$. We derive the stiffness tensor[16]

$$\mathcal{C}^{\mathsf{D_{3d}}} = \begin{pmatrix} \mathcal{C}^{A_{1g}} & 0 \\ 0 & \mathcal{C}^{E_g} \end{pmatrix}, \quad \text{with} \quad \mathcal{C}^{\mathsf{A_{1g}}} = \begin{pmatrix} c_{A_{1g},1} & c_{A_{1g},3} \\ c_{A_{1g},3} & c_{A_{1g},2} \end{pmatrix}, \quad \mathcal{C}^{E_g} = \begin{pmatrix} c_{E_g,1} & c_{E_g,3} \\ c_{E_g,3} & c_{E_g,2} \end{pmatrix} \otimes \mathbb{1}_2. \tag{3.90}$$

In the $\mathsf{D_{3d}}$ point group the stiffness tensor has the six independent components $\{c_{A_{1g},i}, c_{E_g,i}\}$ with $i = 1, 2, 3$. For practical purposes, we also relate them to the components in the original basis which can be deduced from

$$\mathcal{C} = \mathcal{R}_0^T\mathcal{C}^{\mathsf{D_{3d}}}\mathcal{R}_0 = \begin{pmatrix} c_{11} & c_{12} & c_{13} & c_{14} & 0 & 0 \\ c_{12} & c_{11} & c_{13} & -c_{14} & 0 & 0 \\ c_{13} & c_{13} & c_{33} & 0 & 0 & 0 \\ c_{14} & -c_{14} & 0 & c_{44} & 0 & 0 \\ 0 & 0 & 0 & 0 & c_{44} & c_{14} \\ 0 & 0 & 0 & 0 & c_{14} & \frac{1}{2}(c_{11}-c_{12}) \end{pmatrix},$$

leading to the identification $c_{11} = \frac{1}{2}c_{A_{1g},1} + \frac{1}{2}c_{E_g,1}$,$c_{12} = \frac{1}{2}c_{A_{1g},1} - \frac{1}{2}c_{E_g,1}$, $c_{33} = \frac{1}{2}c_{A_{1g},2}$, $c_{44} = 2c_{E_g,2}$, $c_{13} = \frac{1}{2}c_{A_{1g},3}$, $c_{14} = c_{E_g,3}$.

Finally, let us provide quantitative values for the elastic components: In Ref. [119] first principle calculations were performed to determine these elastic constants for Bi_2Se_3 as a function of isotropic pressure. At ambient pressure the authors have obtained the values $c_{11} = 103.2\,\mathrm{GPa}$, $c_{12} = 27.9\,\mathrm{GPa}$, $c_{33} = 78.9\,\mathrm{GPa}$, $c_{44} = 37.7\,\mathrm{GPa}$, $c_{13} = 35.4\,\mathrm{GPa}$, $c_{14} = -26.5\,\mathrm{GPa}$. With increasing pressure the magnitudes of these constants grow more or less uniformly.

[16] For clarity, the matrix structure of $\mathcal{C}^{E_g}$ involes sub-diagonals; it is not block diagonal.

3.4.2 Interplay between nematicity and elasticity

After the introductory considerations on elasticity theory, we are now ready to study the impact of the vestigial nematicity on the underlying lattice degrees of freedom. The interplay between the electronic and lattice degrees of freedom with respect to phase transitions is often considered as a 'chicken or egg' causality dilemma. In our theory for Bi_2Se_3 with no intrinsic incorporation of a lattice softening, the answer is unambiguous: the electronic degrees of freedom drive the vestigial nematic phase transition and cause the impact on the structural order via the symmetry-allowed nemato-elastic coupling term

$$\mathcal{S}_{\mathrm{nem-el}} = V \sum_q \mathsf{B}_q^{E_g} \cdot \left(\kappa_{\mathsf{c}1} \boldsymbol{\epsilon}_{-q}^{E_g,1} + \kappa_{\mathsf{c}2} \boldsymbol{\epsilon}_{-q}^{E_g,2} \right) + V \sum_q \mathsf{B}_q^{A_{1g}} \left(\kappa_{A1} \boldsymbol{\epsilon}_{-q}^{A_{1g},1} + \kappa_{A2} \boldsymbol{\epsilon}_{-q}^{A_{1g},2} \right) . \tag{3.91}$$

Here, four coupling constants $\kappa_{\mathsf{c}\{1,2\}}$ and $\kappa_{A\{1,2\}}$ are allowed. Note the absence (to leading order) of a direct coupling between the strain tensor and the corresponding bilinear combination $\mathsf{B}^{A_{2g}}$. This implies that the chiral state qualitatively differs from the nematic state in that it does not trigger a lattice distortion. In the following, we study the effect of the coupling (3.91) in two steps: First we discuss the lattice deformations caused in the vestigial phase, see section 3.4.2.1, and thereafter, in section 3.4.2.2 we analyze the role of nematic fluctuations above T_{nem}. Details on the derivation are laid out in the appendix C.4.

3.4.2.1 Lattice deformation caused by vestigial nematicity

Let us describe the elasto-nematic coupling in the vicinity of the vestigial nematic phase transition where the Ginzburg-Landau formalism is applicable. Starting from the original superconducting basis, the relevant ingredients involve the inclusion of Eq. (3.91) to the original action (3.7), integrating out the superconducting fluctuations, and a Ginzburg-Landau expansion in terms of $\mathbf{C}^{E_g}$, see appendix C.2 for details. The resulting elasto-nematic problem $\mathcal{S} = \mathcal{S}_{E_g} + \mathcal{S}_{\mathrm{el}} + \mathcal{S}_{\mathrm{nem-el}}$ can be cast by the effective actions

$$\begin{aligned}
\mathcal{S}_{E_g} &= NT \int_{\boldsymbol{r},\tau} \left\{ r_{\mathsf{c}} |\mathbf{C}^{E_g}|^2 + g_{\mathsf{c}} \Big(\left(\mathsf{C}^{E_g,1} \right)^3 - 3\mathsf{C}^{E_g,1} \left(\mathsf{C}^{E_g,2} \right)^2 \Big) + u_{\mathsf{c}} |\mathbf{C}^{E_g}|^4 \right\} \\
\mathcal{S}_{\mathrm{el}} &= NT \int_{\boldsymbol{r},\tau} \left\{ \frac{1}{2} \left(\boldsymbol{\epsilon}^{\mathsf{D}_{3\mathsf{d}}} \right)^T \mathcal{C}^{\mathsf{D}_{3\mathsf{d}}} \boldsymbol{\epsilon}^{\mathsf{D}_{3\mathsf{d}}} - \boldsymbol{\sigma}^{\mathsf{D}_{3\mathsf{d}}} \cdot \boldsymbol{\epsilon}^{\mathsf{D}_{3\mathsf{d}}} - \mathbf{C}^{E_g} \cdot \left(\kappa'_{\mathsf{c}1} \boldsymbol{\epsilon}^{E_g,1} + \kappa'_{\mathsf{c}2} \boldsymbol{\epsilon}^{E_g,2} \right) \right\} ,
\end{aligned}$$

in position space $x = (\boldsymbol{r}, \tau)$. Additionally, the system may be subject to an external stress $\boldsymbol{\sigma}^{\mathsf{D}_{3\mathsf{d}}}$. The nematic part of the system already fulfills the saddle-point solution with the order parameter $\mathbf{C}_0^{E_g} = |\mathbf{C}_0^{E_g}|(\cos(\theta_{\mathsf{c}}), \sin(\theta_{\mathsf{c}}))$ characterized by the two three-fold degenerate solutions (3.18),(3.19). Minimization of the action with respect to the strain components yields the saddle-point equations

$$\boldsymbol{\epsilon}^{A_{1g}} = \left(\mathcal{C}^{A_{1g}} \right)^{-1} \boldsymbol{\sigma}^{A_{1g}} , \qquad \boldsymbol{\epsilon}^{E_g} = \left(\mathcal{C}^{E_g} \right)^{-1} \left(\boldsymbol{\sigma}^{E_g} + \begin{pmatrix} \kappa'_{\mathsf{c}1} \mathbf{C}_0^{E_g} \\ \kappa'_{\mathsf{c}2} \mathbf{C}_0^{E_g} \end{pmatrix} \right) , \tag{3.92}$$

with the inverse elastic matrix

$$\left(\mathcal{C}^{E_g} \right)^{-1} = \begin{pmatrix} \hat{c}_{E_g,2} & -\hat{c}_{E_g,3} \\ -\hat{c}_{E_g,3} & \hat{c}_{E_g,1} \end{pmatrix} \otimes \mathbb{1}_2 ,$$

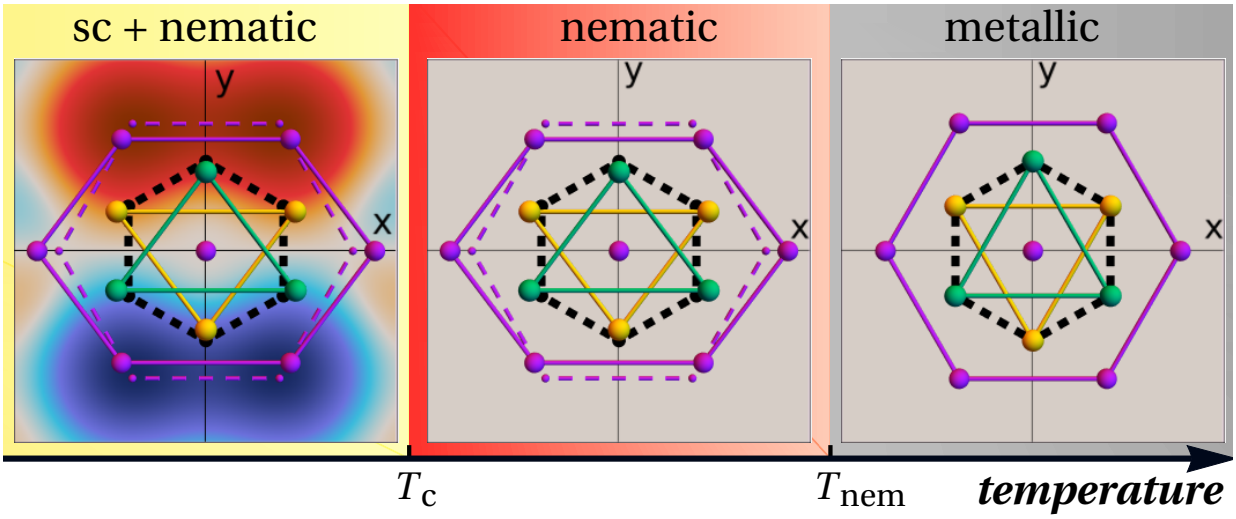

Figure 3.9: Vestigial nematic scenario from the viewpoint of the unit cell deformation. We have chosen an exaggerated distortion $\eta = 0.1$. The plotted superconducting state is the $\mathbf{\Delta}^{E_u} = (1, 0)$ shown in Fig.2.4. For more information on the crystal properties see section 2.2.

and $\hat{c}_{E_g,i} = c_{E_g,i}/(c_{E_g,1}c_{E_g,2} - (c_{E_g,3})^2)$. Contemplating the saddle-point equations we note first that there is no coupling between the nematic order parameter and the A_{1g} components of the strain tensor. Consequently, nematicity does not cause any dilatation. Second, the nematic order parameter acts as a new 'stress field' and hence, it induces all of the $\boldsymbol{\epsilon}^{E_g}$ components including the out-of-plane components $\boldsymbol{\epsilon}^{E_g,2}$. These strain components naturally entail a deformation of the unit cell. For a simplified visualization of the in-plane deformation, we assume that the out-of-plane strain components $\boldsymbol{\epsilon}^{E_g,2}$ are small. The in-plane doublet $\boldsymbol{\epsilon}^{E_g,1} = \left(\epsilon_{xx} - \epsilon_{yy}, -2\epsilon_{xy}\right)/\sqrt{2}$ then transforms (similar to $\mathbf{C}^{E_g}$) like a real E_g order parameter, and thus $\boldsymbol{\epsilon}^{E_g,1}$ realizes the very same ground state phases. Two such representative states are $\boldsymbol{\epsilon}^{E_g,1} = (\pm 1, 0)$. These states are characterized by a compression along x, and an extension along y (or vice-versa). The conservation of the unit cell volume (or the area $A_0 = 3ab$) imposes a constraint on the lattice parameter variations, as

$$a' = a(1 + \eta)\,, \qquad\qquad b' = b/(1 + \eta) \tag{3.93}$$

with $\eta \in \mathbb{R}$ and $|\eta| \ll 1$. We sketch the lattice distortions within a vestigial nematic scenario in figure 3.9 where we also illustrate one possible unit cell deformation, according to Eq. (3.93). Third, we note that the saddle-point equation (3.92) can also be read in reverse, i.e. any finite E_g strain component $\boldsymbol{\epsilon}^{E_g}$ can induce a nematic order parameter $\mathbf{C}^{E_g}$. This is particularly interesting in the context of doped Bi_2Se_3 as a puzzling observation has been reported: While the nematic ground state is three-fold degenerate, experiments report a sample-dependent (yet fixed) nematic direction. This axis is robust against many thermal cycles which is counter-intuitive if one assumes the degeneracy to hold [97, 99]. A viable explanation for this circumstance involves random internal strain fields which do not average out and therefore generate a small but finite E_g strain. The coupling of this strain field to the nematic order parameter breaks the threefold degeneracy and defines a preferred condensation direction. This hypothesis would imply that the nematic order parameter is finite above T_{nem} but owed to its Z_3-Potts nature, the first-order phase transition at T_{nem} would still be well-defined, see Ref.[20]. Let us

conclude by highlighting a promising experimental route to test these ideas. Due to recent advances in measuring samples under controlled external stress, experiments are currently conducted which aim to switch between the nematic phases A and B upon the application of external stress [120].

3.4.2.2 Renormalization due to nematic fluctuations above T_{nem}

Above the nematic transition T_{nem} the order parameter $\mathbf{C}^{E_g}$ is zero but as the system approaches the phase transition, nematic fluctuations get enhanced. In section 3.2.7 we have computed the corresponding susceptibility and determined its Curie-Weiss temperature behavior. We now want to discuss how the nematic fluctuations affect the underlying lattice. The enhanced fluctuations leave an imprint on the lattice degrees of freedom and the approaching phase transition is signaled by a so-called *lattice softening*, where certain elastic constants and the sound velocity of the corresponding acoustic phonon modes decrease simultaneously. In this part, we first study renormalization of the elastic constants before we determine the directions of the vanishing sound velocity. The elastic constants can experimentally be accessed by means of resonant ultra sound experiments [121], or bending experiments to determine the shear modulus [122]. Inelastic neutron scattering measurements can directly detect the directions of the decreasing acoustic phonon branches [123].

Owed to the linear coupling between the nematic bilinear combination $\mathbf{B}^{E_g}$ and the strain tensor $\boldsymbol{\epsilon}^{E_g}$, the respective response functions are related through the identity (a rigorous derivation is provided in the appendix C.4)

$$\left(\mathcal{C}_q^{r,E_g}\right)^{-1} = \left(\mathcal{C}^{E_g}\right)^{-1} + \left(\mathcal{C}^{E_g}\right)^{-1} \hat{\kappa}_{\mathsf{c}} \hat{\chi}_{\mathrm{nem}}(q) \hat{\kappa}_{\mathsf{c}} \left(\mathcal{C}^{E_g}\right)^{-1} ,$$

that relates the nematic susceptibility

$$\hat{\chi}_{\mathrm{nem}}(q) = \begin{pmatrix} 1 & 1 \\ 1 & 1 \end{pmatrix} \otimes \chi_{\mathrm{nem}}(q) , \qquad \text{with} \qquad \hat{\kappa}_{\mathsf{c}} = \begin{pmatrix} \kappa_{\mathsf{c}1} & 0 \\ 0 & \kappa_{\mathsf{c}2} \end{pmatrix} \otimes \mathbb{1}_2 ,$$

with the renormalized elastic tensor $\mathcal{C}_q^{r,E_g}$. In the long wavelength limit ($q = 0$) we use the identity $\hat{\chi}_{\mathrm{nem}}(0) = \chi^{\mathrm{val}}_{\mathrm{nem}}(0)\mathbb{1}_2$ with $\chi^{\mathrm{val}}_{\mathrm{nem}}(0) = \tilde{\Pi}_{z,z}/8vr_{\mathsf{c}}$ (cf. Eq.3.65) and compute the renormalized elastic tensor

$$\mathcal{C}_q^{r,E_g} = \frac{1}{1 + \frac{\chi^{\mathrm{val}}_{\mathrm{nem}}(0)}{c_{E_g,1}c_{E_g,2} - c^2_{E_g,3}} \left(\kappa_{\mathsf{c}2}\zeta_{13} + \kappa_{\mathsf{c}1}\zeta_{23}\right)} \begin{pmatrix} c_{E_g,1} + \frac{\chi^{\mathrm{val}}_{\mathrm{nem}}(0)\zeta_{13}^2}{c_{E_g,1}c_{E_g,2} - c^2_{E_g,3}} & c_{E_g,3} - \frac{\chi^{\mathrm{val}}_{\mathrm{nem}}(0)\zeta_{13}\zeta_{23}}{c_{E_g,1}c_{E_g,2} - c^2_{E_g,3}} \\ c_{E_g,3} - \frac{\chi^{\mathrm{val}}_{\mathrm{nem}}(0)\zeta_{13}\zeta_{23}}{c_{E_g,1}c_{E_g,2} - c^2_{E_g,3}} & c_{E_g,2} + \frac{\chi^{\mathrm{val}}_{\mathrm{nem}}(0)\zeta_{23}^2}{c_{E_g,1}c_{E_g,2} - c^2_{E_g,3}} \end{pmatrix} \otimes \mathbb{1}_2 .$$

Here, we have introduced $\zeta_{13} = \kappa_{\mathsf{c}2}c_{E_g,1} - \kappa_{\mathsf{c}1}c_{E_g,3}$ and $\zeta_{23} = \kappa_{\mathsf{c}1}c_{E_g,2} - \kappa_{\mathsf{c}2}c_{E_g,3}$. In the critical limit where $\chi^{\mathrm{val}}_{\mathrm{nem}}(0) \to \infty$, the determinant of the matrix vanishes and hence, at least two eigenvalues vanish accordingly.

The acoustic phonon spectrum is defined as the eigenvalue spectrum of the dynamic matrix $D(\boldsymbol{q})$, where the modes are computed from $\det(\rho\omega^2 - D(\boldsymbol{q})) = 0$. In order to derive the dynamic matrix, we exploit the stress tensor $\sigma^{(s)}$ as being a measure for the applied force per unit volume defined by $F_\alpha(\boldsymbol{r}) = \sum_\beta \frac{\partial \sigma^{(s)}_{\alpha\beta}(\boldsymbol{r})}{\partial r_\beta}$. This allows us to establish a classical equation of motion for the displacement

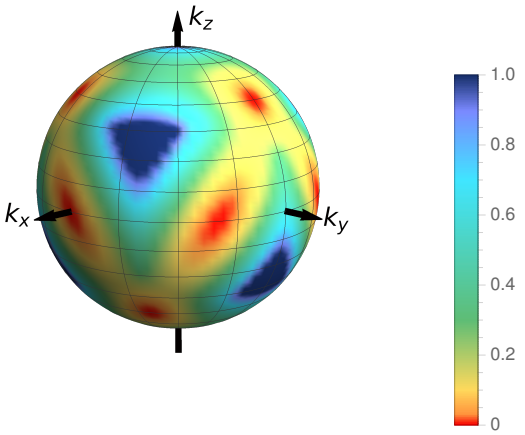

Figure 3.10: Plotted sound velocity on a unit sphere. The sound velocity vanishes along the directions of the 12 red spots.

field $u_\alpha(\boldsymbol{r})$ reading

$$\rho \frac{\partial^2 u_\alpha(\boldsymbol{r})}{\partial t^2} = \sum_\beta \frac{\partial \sigma^{(s)}_{\alpha\beta}(\boldsymbol{r})}{\partial r_\beta} \,,$$

with ρ denoting the mass density. T insertion of the linear relationship between stress and strain (3.81) leads to the wave equation

$$\rho \frac{\partial^2 u_\alpha(\boldsymbol{r})}{\partial t^2} = \sum_{\beta,\gamma,\delta} C_{\alpha\beta\gamma\delta} \frac{\partial^2 u_\gamma(\boldsymbol{r})}{\partial r_\beta \partial r_\delta} \,,$$

which by means of the wave ansatz $u_\alpha(\boldsymbol{r}) = u^{(0)}_\alpha \, e^{\mathrm{i}(\omega t - \boldsymbol{q}\cdot\boldsymbol{r})}$, directly converts into the eigenvalue problem $\rho\omega^2 u^{(0)}_\alpha = \sum_\gamma D_{\alpha\gamma}(\boldsymbol{q}) u^{(0)}_\gamma$. Thu, we define the dynamic matrix as

$$D_{\alpha\gamma}(\boldsymbol{q}) = \sum_{\beta,\delta} C_{\alpha\beta\gamma\delta} q_\beta q_\delta \,.$$

The eigenspectrum of the dynamic matrix contains a phonon mode with vanishing sound velocity $c_s(\hat{q})$ as soon as $\chi^{\mathrm{val}}_{\mathrm{nem}}(0)$ grows large. This mode is found along one of the twelve directions characterized by (using $\hat{q} = (\cos\varphi_s \sin\theta_s, \sin\varphi_s \sin\theta_s, \cos\theta_s)$)

$$\theta_s = \frac{\pi}{2} \;\&\; \varphi_s = \{0,1,2,3,4,5\}\frac{\pi}{3} \,, \quad \theta_s = \frac{\pi}{4} \;\&\; \varphi_s = \{1,5,9\}\frac{\pi}{6} \,, \quad \theta_s = \frac{3\pi}{4} \;\&\; \varphi_s = \{3,7,11\}\frac{\pi}{6} \,, \quad (3.94)$$

and indicated in figure 3.10. Along these directions the acoustic spectrum evolves quadratically and as mentioned above, inelastic neutron scattering experiments should be able to detect the decreasing sound velocity [123].

3.5 Implications of an external magnetic field

In this section we discuss the effect of an applied magnetic field on the properties of the superconducting state—in the presence and in the absence of a vestigial nematic phase. A particular interest arises from the direct coupling $\alpha' B_z \mathsf{B}^{A_{2g}}$ between the magnetic field component B_z and the bilinear combination $\mathsf{B}^{A_{2g}}$ which is symmetry-allowed due to the multi-dimensional nature of the order parameter. In section 3.5.1 we consider a magnetic field applied in the z-direction where we investigate the interplay between the α'-term and the orbital contributions with respect to the possible ground state phases, as well as the structure of the vortex state. Later, in section (3.5.2) we study the magnetic field in the basal plane and revisit the angle-dependence of the upper critical field from the viewpoint of a vestigial scenario.

Doped Bi_2Se_3 is a type-II superconductor with a rather large Ginzburg-Landau parameter $\kappa = \lambda_L/\xi$. Consequently, the Shubnikov state appears at a small magnetic field and occupies most of the phase diagram. In this state, the order parameter is inhomogeneous since the system is penetrated by quantized magnetic flux lines, so-called vortices, that form a superlattice. The description of a vortex lattice state goes back to Abrikosov [124]. It has been shown that the energetically most favorable vortex configuration is that of a close-packed triangular lattice [125]. For multi-component superconductors possible vortex lattices have been subject to intense studies in the context of UPt_3 and Sr_2RuO_4 [126–130]. Most noticeably, it has been found that the multi-component pairing states can favor a square or a rectangular lattice over a triangular one and that the vortex shape can become elongated. The situation in doped Bi_2Se_3 is quite comparable with elongated vortices already reported by STM imaging [17].

In order to address the above questions we consider a system close to the upper critical field, where we can solve the linearized Ginzburg-Landau equations: Starting from the Ginzburg-Landau expansion (3.7) in the presence of a magnetic field the real-space action reads

$$\mathcal{S} = NS_{\mathsf{C}} + N\int_{\boldsymbol{r}} \left(\boldsymbol{\Delta}^{E_u}\right)^\dagger \left(\left(R_0 + f^{A_{1g}}_{-\mathsf{i}\boldsymbol{\nabla}_{\boldsymbol{r}}-e\boldsymbol{A}}\right)\tau^0 + \left(\boldsymbol{f}^{E_g}_{-\mathsf{i}\boldsymbol{\nabla}_{\boldsymbol{r}}-e\boldsymbol{A}} + \mathsf{C}^{E_g}\right)\cdot\boldsymbol{\tau}^{E_g} + \alpha' B_z \tau^y\right)\boldsymbol{\Delta}^{E_u}. \quad (3.95)$$

We have restricted ourselves to static solutions and assumed that the magnetic field is uniform $\boldsymbol{B} = |\boldsymbol{B}|(\cos\varphi_B \sin\theta_B, \sin\varphi_B \sin\theta_B, \cos\theta_B)$ with the vector potential being $\boldsymbol{A}(\boldsymbol{r}) = -\boldsymbol{r}\times\boldsymbol{B}/2$. Note that this choice of magnetic field leaves the inversion symmetry intact such that the solution will decompose into party even and odd sectors. Next, we introduce the covariant derivatives $D_j = -\mathsf{i}\partial_j - eA_j(\boldsymbol{r})$. Similar to the Landau quantization for a fermionic theory, the magnetic field triggers a quantum harmonic oscillator algebra with $[D_x, D_y] = \mathsf{i}eB_z$, $[D_y, D_z] = \mathsf{i}eB_x$, and $[D_z, D_x] = \mathsf{i}eB_y$. We derive the linearized Ginzburg-Landau equations by varying the action (3.95) with respect to $\boldsymbol{\Delta}^{E_u}$ and for later convenience, we represent the equations in the basis $\Delta^{E_u,\pm} = \Delta^{E_u,1} \pm \mathsf{i}\Delta^{E_u,2}$,

$$0 = \left(R_0 - \alpha' B_z + \mathsf{d}_0(D_x^2 + D_y^2) + \mathsf{d}_z D_z^2\right)\Delta^{E_u,+} + \left(\mathsf{d}' D_+^2 + \mathsf{i}\tilde{\mathsf{d}}\left\{D_z, D_-\right\}_+ + \mathsf{C}^{E_g,-}\right)\Delta^{E_u,-} \quad (3.96)$$

$$0 = \left(R_0 + \alpha' B_z + \mathsf{d}_0(D_x^2 + D_y^2) + \mathsf{d}_z D_z^2\right)\Delta^{E_u,-} + \left(\mathsf{d}' D_-^2 - \mathsf{i}\tilde{\mathsf{d}}\left\{D_z, D_+\right\}_+ + \mathsf{C}^{E_g,+}\right)\Delta^{E_u,+}, \quad (3.97)$$

with $\mathsf{C}^{E_g,\pm} = \mathsf{C}^{E_g,1} \pm \mathsf{i}\mathsf{C}^{E_g,2}$ and $D_\pm = D_x \pm \mathsf{i}D_y$.[17] The above equations are analyzed separately for the two cases of an out-of-plane $\boldsymbol{B} = B_z e_z$ and an in-plane $\boldsymbol{B} = |\boldsymbol{B}|(\cos\varphi_B e_x + \sin\varphi_B e_y)$ magnetic field.

[17] Additionally, the lattice constants have been absorbed into the parameter according to $(\mathsf{d}_0, \mathsf{d}')a^2 \to (\mathsf{d}_0, \mathsf{d}')$, $\mathsf{d}_z c^2 \to \mathsf{d}_z$ and $\tilde{\mathsf{d}}ac \to \tilde{\mathsf{d}}$.

3.5.1 Magnetic field in the z-direction

With the magnetic field pointing into the z-direction $\boldsymbol{B} = B_z e_z$ the harmonic quantization will occur in the x, y plane since $[D_x, D_y] = \mathrm{i}eB_z$. Moreover, we neglect modulations along the vortex axis as they commonly increase the vortex energy [32]. Thus, we require $D_z \Delta^{E_u,\pm} = 0$. With the annihilation and creation operators $a, a^\dagger = (D_x \pm i\mathrm{sign}(B_z) D_y)/\sqrt{2e|\boldsymbol{B}|}$ it holds $[a, a^\dagger] = 1$, and the gap equations become

$$0 = \Big(\hat{R}_0 - \hat{\alpha}\ \mathrm{sign}(B_z) + (a^\dagger a + \frac{1}{2})\Big)\Delta^{E_u,+} + \Big(\hat{\mathsf{d}}'\left(\theta(B_z)a^2 + \theta(-B_z)(a^\dagger)^2\right) + \hat{\mathsf{C}}^{E_g,-}\Big)\Delta^{E_u,-} \tag{3.98}$$

$$0 = \Big(\hat{R}_0 + \hat{\alpha}\ \mathrm{sign}(B_z) + (a^\dagger a + \frac{1}{2})\Big)\Delta^{E_u,-} + \Big(\hat{\mathsf{d}}'\left(\theta(B_z)(a^\dagger)^2 + \theta(-B_z)a^2\right) + \hat{\mathsf{C}}^{E_g,+}\Big)\Delta^{E_u,+}, \tag{3.99}$$

with the notation $\hat{R}_0 = R_0/2e|\boldsymbol{B}|\mathsf{d}_0$, $\hat{\alpha} = \alpha'/2e\mathsf{d}_0$, $\hat{\mathsf{C}}^{E_g,+} = \mathsf{C}^{E_g,+}/2e|\boldsymbol{B}|\mathsf{d}_0$, $\hat{\mathsf{d}}' = \mathsf{d}'/\mathsf{d}_0$. For clarity, we choose $B_z > 0$ in the following. The case $B_z < 0$ is immediately covered by interchanging $\Delta^{E_u,+} \leftrightarrow \Delta^{E_u,-}$ and $\mathsf{C}^{E_g,+} \leftrightarrow \mathsf{C}^{E_g,-}$. Following the approach in [128, 131] we expand the superconducting order parameter in the basis of the unperturbed harmonic oscillator

$$\Delta^{E_u,+} = \sum_{n_+=0}^{\infty} a_{n_+} |n_+\rangle\ , \qquad\qquad \Delta^{E_u,-} = \sum_{n_-=0}^{\infty} b_{n_-} |n_-\rangle\ , \tag{3.100}$$

where importantly, the two bases $\{|n_+\rangle\}$ and $\{|n_-\rangle\}$ are part of the same Hilbert space. It holds that $a|n_\pm\rangle = \sqrt{n_\pm}\,|n_\pm - 1\rangle$ and $a^\dagger|n_\pm\rangle = \sqrt{n_\pm + 1}\,|n_\pm + 1\rangle$. Inserting these expressions into (3.98),(3.99) yields a recursion formula for the expansion coefficients

$$\hat{R}_0 a_n = a_n\Big(\hat{\alpha} - n - \frac{1}{2}\Big) - \hat{\mathsf{d}}'\, b_{n+2}\sqrt{(n+2)\,(n+1)} - \hat{\mathsf{C}}^{E_g,-} b_n \tag{3.101}$$

$$\hat{R}_0 b_n = b_n\Big(-\hat{\alpha} - n - \frac{1}{2}\Big) - \hat{\mathsf{d}}'\, a_{n-2}\sqrt{n(n-1)} - \hat{\mathsf{C}}^{E_g,+}\, a_n\,, \tag{3.102}$$

where $n = 0, 1, 2, \ldots$. As a consequence of the inversion symmetry, the two subspaces of even and odd n are uncoupled. In a one-to-one correspondence even and odd identify the parity eigenvalues. With the lowest lying eigenstate being parity even, the ground state should also be parity even. We introduce the vector $\boldsymbol{\zeta} = (b_0, a_0, b_2, a_2, b_4, a_4, \ldots)^T$ for the even coefficients, and recast the recursion formula as the eigenvalue problem $\hat{R}_0\boldsymbol{\zeta} = M\boldsymbol{\zeta}$ with the matrix

$$M = \begin{pmatrix}
-\hat{\alpha}-\frac{1}{2} & -\hat{\mathsf{C}}^{E_g,+} & 0 & 0 & 0 & 0 & \ldots \\
-\hat{\mathsf{C}}^{E_g,-} & \hat{\alpha}-\frac{1}{2} & -\hat{\mathsf{d}}'\sqrt{2} & 0 & 0 & 0 & \\
0 & -\hat{\mathsf{d}}'\sqrt{2} & -\hat{\alpha}-\frac{5}{2} & -\hat{\mathsf{C}}^{E_g,+} & 0 & 0 & \\
0 & 0 & -\hat{\mathsf{C}}^{E_g,-} & \hat{\alpha}-\frac{5}{2} & -\hat{\mathsf{d}}'\sqrt{12} & 0 & \\
0 & 0 & 0 & -\hat{\mathsf{d}}'\sqrt{12} & -\hat{\alpha}-\frac{9}{2} & -\hat{\mathsf{C}}^{E_g,+} & \\
0 & 0 & 0 & 0 & -\hat{\mathsf{C}}^{E_g,-} & \hat{\alpha}-\frac{9}{2} & \ldots \\
\ldots & & & & \ldots & \ldots &
\end{pmatrix}. \tag{3.103}$$

The interpretation of the eigenwert problem is the following. Let us assume that $\lambda^{(j)}$ and $\boldsymbol{u}^{(j)}$ ($j = 1, 2, \ldots$) are the eigenvalues and -vectors of the matrix M. Then, the matrix equation is solved for $\boldsymbol{\zeta} = \boldsymbol{u}^{(j)}$ when $\hat{R}_0 = \lambda^{(j)}$ for any of the eigenvalues. Using $R_0 = a_0(T - T_c^0) + \mathsf{C}^{A_{1g}}$, the equation can

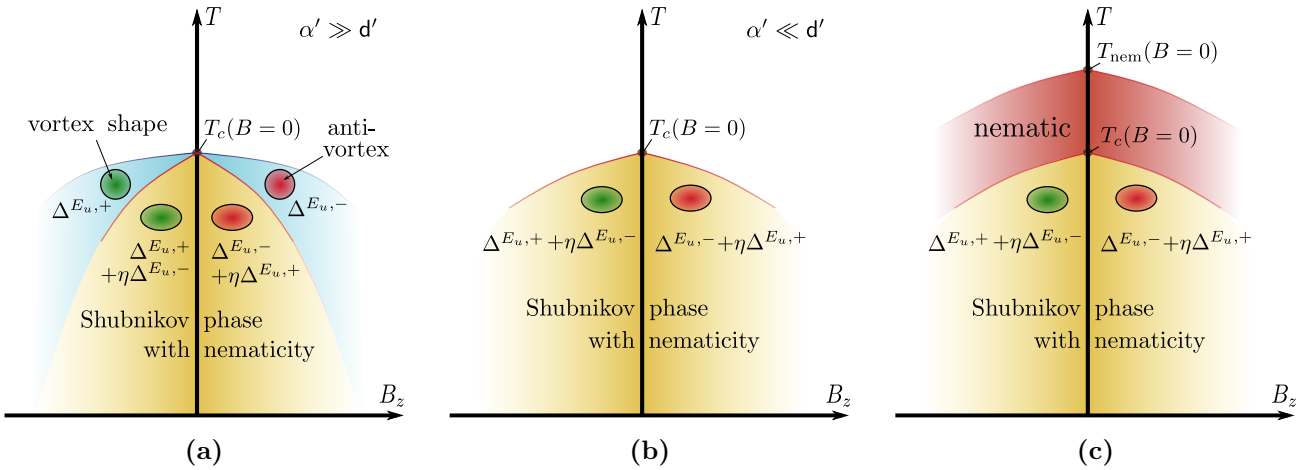

Figure 3.11: Three possible phase diagrams for a magnetic field along the z-direction. In case (a) the system undergoes split transitions where it first enters a chiral phase. In cases (b) and (c) the finite nematic order parameter is present right at T_c, and the systems are nematically distorted. The shapes of a single vortex in the respective phases are indicated.

be re-expressed as

$$0 = a_0\left(T - \left(T_c^0 + \frac{2e|\boldsymbol{B}|\mathsf{d}_0\lambda^{(j)} - \mathsf{C}^{A_{1g}}}{a_0}\right)\right),$$

and it is first satisfied when $\hat{R}_0$ reaches the largest eigenvalue $\lambda_{\max} = \max(\boldsymbol{\lambda})$. Thus, the highest possible $T_c(\boldsymbol{B})$ is achieved for $\lambda = \lambda_{\max}$. The diagonal elements of the matrix M become increasingly smaller such that the maximum eigenvalue should be dominated by the first few matrix entries. We study the maximum eigenvalue of M in two steps. First, we consider the simpler case without vestigial nematic order where we show that for a certain parameter range, the system can undergo split transitions where the precursor phase is non-nematic. Second, we discuss the vestigial nematic case.

In the absence of a nematic order, it is straightforward to determine the largest eigenvalue of the matrix M. In agreement with Ref. [131] we find two distinct possible ground state arrangements with the maximum eigenvalue

$$\lambda_{\max} = \begin{cases} \lambda^{(\mathrm{I})} = -\frac{1}{2} - \hat{\alpha} & , \hat{\alpha} < -(\hat{\mathsf{d}}')^2/2 \\ \lambda^{(\mathrm{II})} = -\frac{3}{2} + \sqrt{\left(1+\hat{\alpha}\right)^2 + 2(\hat{\mathsf{d}}')^2} & , \hat{\alpha} > -(\hat{\mathsf{d}}')^2/2 \end{cases}. \tag{3.104}$$

The corresponding eigenvectors read $\boldsymbol{u}^{(1)} = \left(1,0,0,0,\dots\right)^T$ and $\boldsymbol{u}^{(2)} = (0,\eta_+,-\mathrm{sign}(\hat{\mathsf{d}}')\eta_-,0,\dots)^T$ with $\eta_\pm = \frac{1}{\sqrt{2}}\left(1 \pm (1+\hat{\alpha})/\sqrt{\left(1+\hat{\alpha}\right)^2 + 2(\hat{\mathsf{d}}')^2}\right)^{1/2}$. Let us reassess the previous assumption of an absent nematic order parameter. For this, we explicitly state the corresponding superconducting order parameters (3.100) reading

$$(\mathrm{I}): \begin{pmatrix} \Delta^{E_u,+} \\ \Delta^{E_u,-} \end{pmatrix} = |\boldsymbol{\Delta}_0^{E_u}| \begin{pmatrix} 0 \\ \varphi_0(\boldsymbol{r}) \end{pmatrix}, \qquad (\mathrm{II}): \begin{pmatrix} \Delta^{E_u,+} \\ \Delta^{E_u,-} \end{pmatrix} = |\boldsymbol{\Delta}_0^{E_u}| \begin{pmatrix} \eta\lambda_+\varphi_0(\boldsymbol{r}) \\ -\mathrm{sign}(\hat{\mathsf{d}}')\eta_-\varphi_2(\boldsymbol{r}) \end{pmatrix}, \tag{3.105}$$

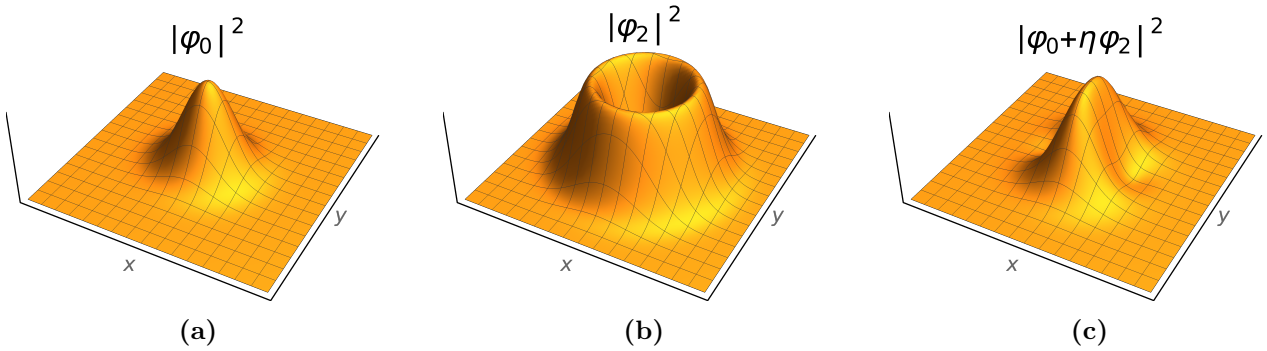

Figure 3.12: Spatial structure of the harmonic oscillator eigenfunction $\varphi_0(\boldsymbol{r})$ and $\varphi_2(\boldsymbol{r})$, and their addition with $\eta = 0.6$.

with the lowest lying harmonic oscillator eigenfunctions

$$\varphi_0(\boldsymbol{r}) = \sqrt{\frac{e|\boldsymbol{B}|}{2\pi}}\, e^{-\frac{e|\boldsymbol{B}|}{4}(x^2+y^2)}\,, \qquad \varphi_2(\boldsymbol{r}) = \frac{(e|\boldsymbol{B}|)^{\frac{3}{2}}}{4\sqrt{\pi}}\,(x-\mathrm{i}y)^2\, e^{-\frac{e|\boldsymbol{B}|}{4}(x^2+y^2)}\,. \tag{3.106}$$

The insertion of the states (3.105) into the nematic correlation function $\mathsf{C}_0^{E_g,l} = -2v\langle(\boldsymbol{\Delta}_0^{E_u})^\dagger \tau^{E_g,l}\boldsymbol{\Delta}_0^{E_u}\rangle$ shows that the second state (II) yields a finite value $|\mathbf{C}_0^{E_g}|$ and thus, it violates the initial assumption. The second state is to be discarded. The first state (I) on the other hand, is in line with the assumption ($|\mathbf{C}_0^{E_g}| = 0$) and deserves further attention.

The realization of the first case (I) is subject to the condition $|\hat{\alpha}| > (\hat{\mathsf{d}}')^2/2$. To start with a simple expression, let us assume that all gradient terms can be neglected. In this limit, the action becomes diagonal

$$\mathcal{S} = TNV\left(|\Delta^{E_u,+}|^2\left(r_0 - \alpha' B_z\right) + |\Delta^{E_u,-}|^2\left(r_0 + \alpha' B_z\right)\right)\,,$$

with the magnetic field lifting the $(\Delta^{E_u,1}, \Delta^{E_u,2})$-degeneracy. This causes the system to undergo a split transition where it first enters a purely chiral phase at $T_c^{(1)} = T_c^0 + |\alpha' B_z|/a_0$ before it undergoes a second phase transition at $T_c^{(2)} = T_c^0 - |\alpha' B_z|/a_0$ where the state develops a nematic character and breaks the in-plane rotational symmetry. In the discussed case (I), the gradients are not completely negligible but the situation is conceptually the same. The key difference is that the upper transition temperature $T_c = T_c^0 - \mathsf{C}^{A_{1g}}/a_0 + B_z(|\alpha'| - e\mathsf{d}_0)/a_0$ experiences a net decrease with B_z due to the trivial fluctuations d_0. In fact, the microscopic analysis (see Fig. B.1(a)) shows that the slope $|\alpha'| - e\mathsf{d}_0$ is negative. The solution (I) is rotationally invariant and the basis functions employed to construct the vortex solution inherit this invariance. We have sketched the resulting phase diagram in figure 3.11(a).

In the presence of a finite nematic order parameter $\mathbf{C}_0^{E_g}$ all matrix elements in M are coupled. Nonetheless, since the diagonal entries decrease with growing n, the first few entries dominantly contribute to $\lambda_{\max}$. As long as $\mathbf{C}_0^{E_g}$ is not too large, it is reasonable to study the leading 3×3 matrix. In

this case, the maximum eigenvalue and its eigenvector take the analytic form

$$\lambda^{(3)} = -\frac{3}{2} + \frac{1-\hat{\alpha}}{3}\left(1 + 4\eta_{(3)}\cos\left(\frac{1}{3}\arccos\left(\frac{4(1-\hat{\alpha})^2 + 27|\mathsf{C}_0^{E_g}|^2}{(1-\hat{\alpha})^2(2\eta_{(3)})^3} - \frac{3}{2\eta_{(3)}}\right)\right)\right), \tag{3.107}$$

$$\boldsymbol{u}^{(3)} = \frac{1}{|\boldsymbol{u}^{(3)}|}\Big(2(\hat{\mathsf{d}}')^2 + (1+\hat{\alpha})^2 - (\lambda^{(3)} + \frac{3}{2})^2, \hat{\mathsf{C}}^{E_g,-}\Big(\lambda^{(3)} + \frac{3}{2} + 1 + \hat{\alpha}\Big), -\sqrt{2}\hat{\mathsf{d}}'\hat{\mathsf{C}}^{E_g,-}, 0, 0, \dots\Big)^T, \tag{3.108}$$

with $\eta_{(3)} = \sqrt{1 + 3(\hat{\alpha} + (\hat{\mathsf{d}}')^2/2 + |\mathsf{C}_0^{E_g}|^2/4)/(1-\hat{\alpha})^2}$.[18] While the above expressions appear quite unhandy, the solution becomes more comprehensible if it is translated into the superconducting order parameter eigenstate

$$\begin{pmatrix} \Delta^{E_u,+} \\ \Delta^{E_u,-} \end{pmatrix} = |\boldsymbol{\Delta}_0^{E_u}|\; u_1^{(3)} \begin{pmatrix} \hat{u}_2^{(3)}\varphi_0(\boldsymbol{r}) \\ \varphi_0(\boldsymbol{r}) + \hat{u}_3^{(3)}\varphi_2(\boldsymbol{r}) \end{pmatrix}, \tag{3.109}$$

with $\hat{u}_{2,3}^{(3)} = u_{2,3}^{(3)}/u_1^{(3)}$. Since $\hat{u}_3^{(3)} \sim \hat{\mathsf{d}}'\hat{\mathsf{C}}^{E_g,-}$ the nematic order parameter couples the two oscillator eigenfunctions leading to the distinct two-fold rotational symmetry as illustrated in figure 3.12. The axis of elongation (either x or y) depends on the sign of $\hat{u}_3^{(3)} \sim \hat{\mathsf{d}}'\hat{\mathsf{C}}^{E_g,-}$ which is a fixed combination, see discussion below. Note that the solutions (3.109) form the basis for the construction of the vortex lattice. As such, the vortex solution will inherit the distortion from (3.109) [32, 130]. Figure 3.11 shows the complete phase diagram with the cases where a nematic order parameter is present, either via joint transition (b), or by means of a vestigial nematic phase (c).

[18] To recover the two uncoupled cases, the two identities are useful $\cos(3\alpha) = 4\cos^3(\alpha) - 3\cos(\alpha)$, and $\arccos(\cos(3\arccos(1/2\eta))) = 3\arccos(1/2\eta)\theta(1-\eta)\theta(\eta+\frac{1}{2}) + (2\pi - 3\arccos(1/2\eta))\theta(\eta-1)$.

3.5.2 Magnetic field in the basal plane

With the magnetic field being applied in the basal plane $\boldsymbol{B} = |\boldsymbol{B}|(\cos\varphi_B e_x + \sin\varphi_B e_y)$ the angular dependence of the upper critical field $H_{c2}(\varphi_B)$ can be determined. In Ref. [132] this problem has been addressed in relation to doped Bi_2Se_3. The key result is that a two-fold symmetric angle-dependence of the upper critical field emerges as soon as an E_g 'symmetry breaking field' is present. While the authors had to apply an external stress $\boldsymbol{\sigma}^{E_g,1}$ (3.88), in our case this 'symmetry breaking field' emerges naturally as the order parameter C^{E_g} in the vestigial nematic phase.

Since the mathematical treatment is similar to that of the out-of-plane field, the derivation has been moved into the appendix C.5. We focus on the resulting upper critical field, which—in absence and presence of nematic order—is shown in figure 3.13. In agreement with previous studies we find a two-fold angle dependence as soon as the nematic order parameter is finite. The orientation of the ellipse however, is unconditionally fixed within our theory. Specifically, the elongated axis has to align with the crystal x-axis. To demonstrate this, we use the result from Ref.[132] where the upper critical field has been analytically derived in the limit of small $\tilde{\mathsf{d}}$, reading

$$H_{c2}(\varphi_B) = H_{c2}^{(0)}\left(1 - \frac{\mathsf{d}'}{2\mathsf{d}_0}\mathrm{sign}(\mathsf{C}^{E_g,1})\cos\big(2\varphi_B\big)\right). \tag{3.110}$$

Here, the long axis is determined from the $\mathrm{sign}(\mathsf{d}'\mathsf{C}^{E_g,1})$. Having that in mind we recall that the $\mathrm{sign}(\mathsf{d}')$ implies a specific $\mathrm{sign}(\mathsf{C}^{E_g,1})$, see derivation in section 3.2.2. In fact, regardless of the actual $\mathrm{sign}(\mathsf{d}')$ (our analysis suggests $\mathsf{d}' > 0$), the product $\mathsf{d}'\mathsf{C}^{E_g,1} < 0$ is always negative and thus, the long H_{c2} axis has to be aligned with the crystal x-axis. This observation is particularly interesting in light of the discrepancy of the H_{c2} orientations in different experiments [104].

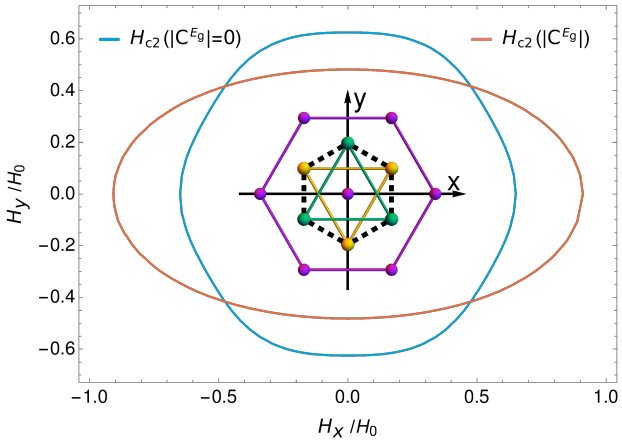

Figure 3.13: In-plane upper critical field H_{c2} as it results from (C.42) plotted for both, a nematic order parameter present and absent. The vestigial nematic theory confines the long axis to align with the crystal x-axis.

3.6 Conclusion of chapter 3 and discussion

Based on the observation of a two-dimensional superconducting pairing state in doped Bi_2Se_3 and the increased role of fluctuations due to a low carrier density, we have predicted the existence of a fluctuation-induced nematic phase that precedes superconductivity. As a consequence of this vestigial nematicity, the rotational C_{3z} and the $U(1)$ symmetry are separately broken at temperatures T_{nem} and $T_c < T_{\mathrm{nem}}$. The vestigial nematic state is characterized by strong anisotropic fluctuations that cause an anisotropy in various quantities, among them the electrical conductivity and the diamagnetic susceptibility. The nematic phase transition is of first order owed to the Z_3-Potts character of the nematic order parameter. Within this universality class the ground state is three-fold degenerate and thus, it gives rise to three distinct nematic domains. The nematic order parameter couples to both, in-plane $(\epsilon_{xx}-\epsilon_{yy}, \epsilon_{xy})$ and out-of-plane $(\epsilon_{yz}, \epsilon_{zx})$ strain components which makes the degenerate nematic ground especially vulnerable to intrinsic strain or external stress fields in the E_g symmetry channels. Focusing on the in-plane strain, we have evaluated the corresponding unit cell deformation. The nematic fluctuations reflect themselves in an enhanced nematic susceptibility that should be directly measurable by Raman scattering in the E_g symmetry channel. Moreover, we study the corresponding softening of the lattice in terms of decreasing E_g elastic constants and an accompanied vanishing of the sound velocity. The in-plane rotational symmetry breaking is also reflected in the upper critical field H_{c2}, and while there is discrepancy in experiments on the large H_{c2} axis, we demonstrate that the vestigial nematic scenario is only compatible with the large axis being aligned with the crystal x-axis (or the a direction). We also indicate a similar restriction for the nematically distorted vortices.

Strong experimental support for the existence of a vestigial nematic phase in Nb and Cu doped Bi_2Se_3 has been provided by Rolf Lortz and collaborators [20] with the main results shown in figure 3.14(b). The measured data agrees well with all the outlined vestigial nematic predictions. In particular, in the thermal expansion data an onset of in-plane anisotropy is observed at $T_{\mathrm{nem}} = 3.8\,\mathrm{K}$ significantly above the superconducting transition temperature $T_c = 3.25\,\mathrm{K}$. The latter is determined from the specific heat data. The step-like transition in the thermal expansion is characteristic for a first-order phase transition. Additionally, an enhanced response is detected in the susceptibility and in the resistivity near T_{nem}.

The sketch in figure 3.14(a) depicts the phase diagram for a doped Bi_2Se_3 compound. The vestigial nematic phase is expected to merge with superconductivity and to undergo joint first-order transitions as T_c decreases and quantum fluctuations become more important and additionally, the z-anisotropy gets less pronounced.

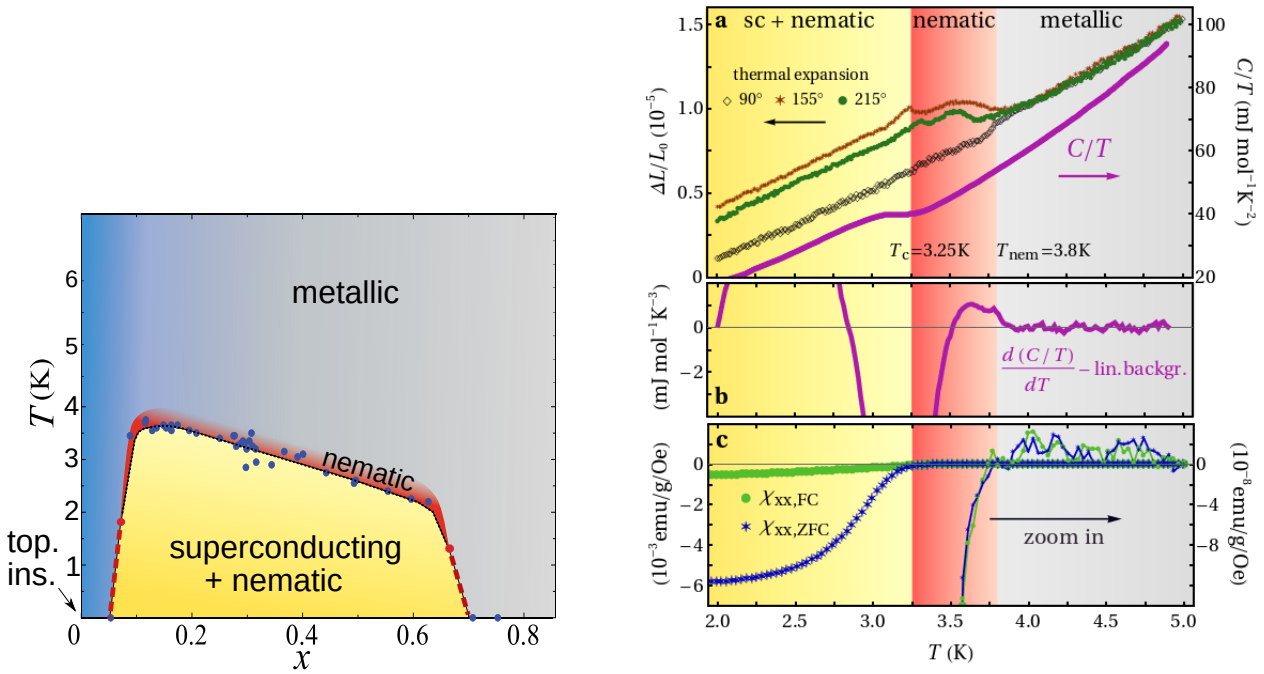

(a) (b)

Figure 3.14: (a) illustrates the expected phase diagram for doped Bi_2Se_3 as a function of doping, see [107]. As T_c decreases quantum fluctuations drive the system towards joint transitions. The red dots mark the corresponding tricritical point. (b) displays thermal expansion, specific heat, and magnetization measurements on a $Nb_{0.25}Bi_2Se_3$ sample [20]. The thermal expansion $\Delta L(T)/L_0$ is measured along three directions in the basal plane, showing a step-like onset of anisotropy at $\sim 3.8\,\mathrm{K}$. Also at $\sim 3.8\,\mathrm{K}$ the magnetization gets strongly enhanced. The data supports a vestigial nematic scenario with $T_{\mathrm{nem}} = 3.8\,\mathrm{K}$ above $T_c = 3.25\,\mathrm{K}$.

Chapter 4

4 Phase stiffness suppression due to umklapp scattering

In section 1.1.3 we have given a short introduction on the phase stiffness with an emphasis on its physical significance. In this chapter we will elaborate in more detail on its properties, and we will draw some attention on mechanisms that tend to overcome the so-called Leggett's theorem: At zero temperature and in a Galilean invariant system every single electron contributes to the superfluid density, and hence to the phase stiffness (4.1). In particular, we study the suppressive influence that the periodic lattice has on the phase stiffness. We show that this suppression is mediated by superconducting fluctuations, and that the suppression increases with increasing BCS coupling strength g as illustrated in figure 4.1. The suppression is most pronounced at a van-Hove point where the density of electronic states at the Fermi surface diverges. This work has been done in collaboration with Jörg Schmalian.

4.1 Introductory remarks

The superfluid stiffness is a measure for classical and quantum fluctuations of the superconducting phase. It has been introduced in section 1.1.3 as $\rho_s = n_s/m$ with the superfluid density n_s, i.e. as the fraction of electrons that in the picture of a two-fluid model $n = n_n + n_s$ are responsible for the superflow. In a clean conventional superconductor the superfluid stiffness is sufficiently large such that phase fluctuations play a negligible role in the determination of the critical temperature T_c. Instead, the critical temperature is dominated by the amplitude value $2|\Delta|$, which is the energy it needs to break a Cooper pair. Finite temperature fluctuations arise in the form of Bogoliubov quasi-particles that dominate the entropy, and set the scale for T_c. The reason why phase fluctuations have no significant impact on T_c has to do with the confinement by Leggett's theorem, which sets the energy scale $\rho_s = n/m \sim k_F^{d-2} E_F$ of phase fluctuations much higher than the counterpart of amplitude fluctuation $k_F^{2-d}|\Delta|$.

Leggett's theorem and its limits The Leggett's theorem says that in a Galilean invariant system, it is the entire electronic density n that contributes to the superfluid density n_s at zero temperature [21, 133, 134]. This statement remarkably holds regardless of the strength of the BCS interaction. Meaning that even if only a small fraction of the electronic system around the Fermi surface actually 'feels' the superconducting pairing, the supercurrent is carried by the entire electronic system. The only

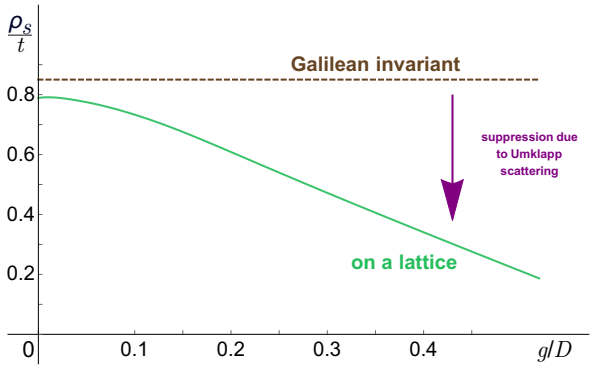

Figure 4.1: Phase stiffness ρ_s as a function of the BCS coupling strength g at zero temperature. In a Galilean invariant system (brown dashed) ρ_s is constant (4.1) (The value is chosen by hand.). The phase stiffness ρ_s as calculated in the present lattice model (solid green) clearly shows a significant suppression due to scattering processes off the periodic potential. Plotted are the dimensionless quantities ρ_s/t and g/D with $D = 4t$.

requirement is that the quasi-particle spectrum is parabolic $\epsilon_{\boldsymbol{k}} \sim \boldsymbol{k}^2$ such that the Galilean invariance is intact. The mathematical formulation of the theorem reads

$$\rho_s = \frac{n}{m}\,, \tag{4.1}$$

and has been rigorously proven in [21]. We want to illustrate the theorem from a different perspective, the optical conductivity. The f-sum rule introduced in section 1.1.3 says that the spectral weight of the optical conductivity is a conserved quantity. This means that upon the transition from a metallic into a superconducting state no spectral weight from the Drude peak can get lost, and in particular the weight within the frequency window $0 < \nu < 2|\Delta|$ gets transferred into the weight of the superconducting delta-function (1.8). The weight of the delta-function $\pi\rho_s(e^*)^2$ is a direct indicator of the phase stiffness. To demonstrate the Leggett's theorem, we have to treat the metal as a Galilean invariant system. In a Galilean invariant system the momentum is conserved such that the momentum relaxation scattering time $\tau_{\mathrm{tr}} \to \infty$ is by far the largest scale in the problem. In this limit $|\Delta| \gg \tau_{\mathrm{tr}}^{-1}$, the entire Drude weight is below $2|\Delta|$, and the total spectral weight gets transferred into the delta function, cf. Fig.4.2(a). The resultant phase stiffness $\rho_s = n/m$, where we have absorbed a factor of 4π into its definition, indeed confirms the theorem by Leggett. Also, the approach from the optical conductivity directly reveals how the phase stiffness is reduced once a system is not Galilean invariant anymore. If for example, the momentum relaxation time is large but not infinite, the phase stiffness reduces according to

$$\rho_s = \frac{n}{m}\left(1 - \frac{1}{\pi|\Delta|\tau_{\mathrm{tr}}}\right) \tag{4.2}$$

where parts of the former spectral weight reside above $2|\Delta|$ as illustrated in the figure. With this simple but powerful picture in mind, we understand that any source of momentum relaxing scattering would decrease the phase stiffness. The most frequently discussed suppression results from randomly placed impurities, see e.g. Ref.[135]. Apart from impurity scattering, momentum relaxing scattering events

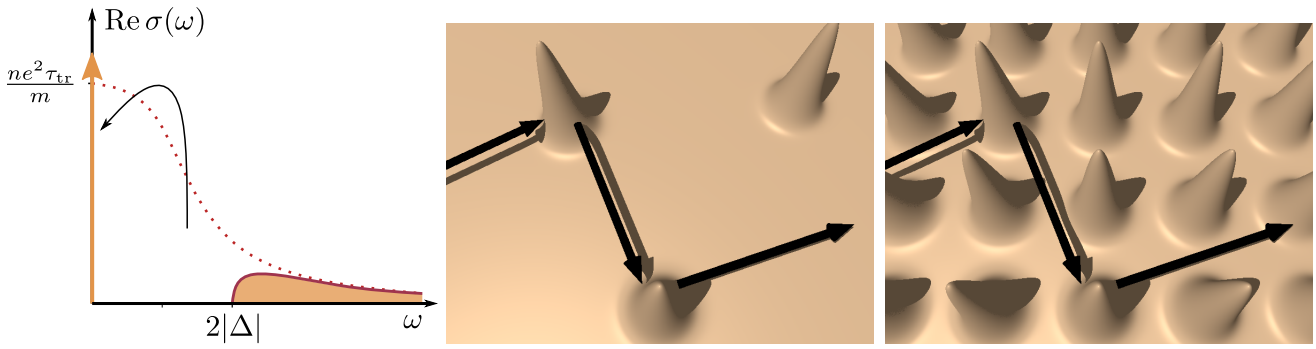

Figure 4.2: (a) demonstrates how the Drude spectral weight gets shifted into the weight of the superconducting delta-function, which is proportional to the phase stiffness ρ_s. (b) and (c) visualize the conceptual similarity with regards to scattering processes between randomly placed disorder and the lattice potential.

are naturally caused by the underlying lattice itself, in the form of umklapp scattering events. Thus, a periodic potential acts in a similar fashion as a disorder potential which is illustrated in Fig.4.2(b) and (c). In both cases the phase stiffness suppression can be cast by equation (4.2) with the origin of the transport scattering time differing. In one case, it results $\tau_{\rm tr}^{-1} \sim c|U|^2\nu_F$ from randomly placed impurity scatterers with amplitude U and concentration c, and in the other case it is determined by the scattering strength U_G of lattice vibrations $\tau_{\rm tr}^{-1} \sim |U_G|^2\nu_F$. This begs the question about the magnitude of the phase stiffness suppression caused by umklapp scattering events.
Besides this rather general motivation, there are a number of interesting open questions in several classes of superconductors.

Motivation Having discussed the conventional superconductors where phase fluctuations are negligible, there are materials that are believed to be described within the opposite limit. In the under-doped cuprate superconductors, the properties are assumed to be governed by the vicinity to the Mott insulating state [136–144]. This regime is characterized by a low carrier density and the expectation that the phase stiffness $\rho_s \sim x$ is proportional to the doping level. In its nature, the Mott state is a lattice-caused phenomenon where Galilean invariance is necessarily broken such that equation (4.1) is not applicable. In this regime there is strong experimental evidence that the phase fluctuations destroy the superconducting state and hence, determine T_c, while amplitude fluctuations play an inferior role. In fact, there is an observed large energy gap that even extends into the normal state [8–10].

Materials that fall into the intermediate regime between the clean conventional limit of e.g. In or Al on the one hand, and the under-doped cuprates like $YBa_2Cu_3O_{6+\delta}$ or $La_{2-x}Sr_xCuO_4$ on the other hand, should display both, strong electronic correlations and reasonably well-defined quasiparticles at an intermediate amount of carrier concentration. Examples thereof would be the iron-based superconductors, Sr_2RuO_4, or the over-doped side of the cuprates. In all three systems it is not appropriate, for different reasons, to apply an approximate parabolic or single-band dispersion, i.e. to employ effectively Galilean invariance. Strained Sr_2RuO_4 [145–148] and the over-doped cuprates [149–155] on the one hand, draw their physical properties from flat bands and the influence of the van-Hove singularity in the electronic dispersion which resides close to the Fermi energy, while most of the properties of iron-based superconductors [156] crucially depend on their multiple electronic bands. A

particularly interesting observation in the over-doped cuprates $TI_2Ba_2CuO_{6+\delta}$, $Y_{1-x}Ca_xBa_2Cu_3O_{7-\delta}$ and $La_{2-x}Sr_xCuO_4$ is the suppression of the phase stiffness as a function of doping in a wide regime from optical doping all the way to the point where superconductivity disappears [22, 23, 157–160]. A viable explanation that accounts for this effect has been provided by the theory of a dirty d-wave BCS superconductor [161, 162]. However, it seems worthwhile to investigate the effect caused by alternative Galilean invariance breaking sources that could suppress the phase stiffness even in the clean limit. This notion is supported by evidence that the phase stiffness suppression in these systems is probably not exclusively due to disorder [23, 159, 160, 163]. Even in systems where the phase stiffness suppression can be likely attributed to a dirty d-wave scenario [161, 162] or in a more general sense to emergent disorder as discussed in Ref.[164], the effect might still be facilitated by a reduction of the phase stiffness due to scattering events that are already present in the perfectly clean system.

Outline In this work, we determine the zero-temperature phase stiffness for a clean s- and d-wave superconductor with a flat electronic dispersion in the vicinity of a van-Hove singularity. We include Gaussian fluctuations beyond the mean-field theory, where we can separately study the renormalization effects of the lattice on the fermionic and the bosonic contributions to the phase stiffness. We find that the former changes the stiffness only little while the bosonic degrees of freedom already cause a significant phase stiffness reduction at a moderate dimensionless pairing interaction strength, cf. Fig.4.1. The calculation was done for a two-dimensional electronic dispersion on a square lattice with an attractive d-wave BCS interaction at a filling that puts the system close to the van-Hove point. Our results might be of relevance for the over-doped cuprates, and in particular, in vicinity of the quantum critical point the discussed effects should be of quantitative importance.

4.2 Theoretical approach to the phase stiffness

The superfluid stiffness ρ_s is a measure for the rigidity of the superconducting state against quantum or classical fluctuations in the phase of the condensate. In the sense of Eq. (1.6) $F \sim \frac{1}{2}\rho_s(\nabla\varphi + e^*\boldsymbol{A})^2$, it penalizes the corresponding fluctuations, while it determines the increase in kinetic energy in the presence of an external field. In order to define the stiffness ρ_s we follow Refs. [165–169] and impose a phase twist Φ onto the system. The phase twist induces a superfluid velocity $v_s \sim \Phi/L$ (see Eq.(4.6) below) and consequently, it enhances the kinetic energy according to $\sim L^d v_s^2 \sim L^{d-2}\Phi^2$ with the system length L and the sample dimension d. The associated proportionality factor is exactly the phase stiffness which can thus, be defined

$$\rho_s = \lim_{\Phi\to 0} \frac{\partial^2}{\partial \Phi^2} \lim_{L\to\infty} L^{2-d} F(\Phi) \,, \tag{4.3}$$

as the second derivative of the free energy with respect to the phase twist Φ. For a discussion of the order of limits we refer to [170]. In the following we will unfold the involved steps and derive the above relation a bit more carefully.

Twisted boundary conditions We find it instructive to outline the origin of the twisted boundary conditions. An easy way to understand the whereabouts of such a phase twist can be seen by considering a single-particle Schrödinger equation in a constant magnetic field

$$\frac{1}{2m}\left(-\mathrm{i}\boldsymbol{\nabla} - e\boldsymbol{A}\right)^2\psi + V(\boldsymbol{r})\psi = E\psi\,.$$

The magnetic field can be completely removed from the above equation upon application of the gauge transformation

$$\psi(x) \to \tilde{\psi}(x)e^{-\mathrm{i}e\int_0^x \boldsymbol{A}\cdot d\boldsymbol{\ell}}$$

where we have defined x as the dimension that winds around the magnetic field axis. The expense of such an operation lies in the enforcement of twisted boundary conditions on the new fermionic fields

$$\tilde{\psi}(x+L) = e^{i\Phi}\tilde{\psi}(x)\,, \tag{4.4}$$

with the introduced phase twist $\Phi = e\Phi_B$, the magnetic flux $\Phi_B = \mathrm{i}\oint_0^L \boldsymbol{A}\cdot d\boldsymbol{\ell}$. In general, it is more appropriate to invert the above logic and to assume that there is an imposed phase twist Φ to begin with. Its origin could e.g. be an Aharonov-Bohm flux. Without loss of generality, we apply the phase twist only along the x-direction. As a result of (4.4), the momentum quantization in x-direction becomes $k_n^x = \frac{2\pi}{L}n + \frac{\Phi}{L}$, and it is convenient to apply the gauge transformation

$$\tilde{\psi}(x) = e^{i\frac{\Phi}{L}x}\psi(x)\,, \tag{4.5}$$

such that the new fermionic fields $\psi(x) = \psi(x+L)$ satisfy periodic boundary conditions. From the superconducting order parameter $\Delta \propto \langle\tilde{\psi}\tilde{\psi}\rangle$, we can identify the superfluid velocity associated with the phase twist as

$$v_s = \frac{2\Phi}{ML}\,, \tag{4.6}$$

where $M = 2m$ is the mass of a Cooper pair. Altogether, the increase in kinetic energy can be computed by an expansion of the free energy in terms of a small phase twist Φ

$$\Delta F(\Phi) = F(\Phi) - F(0) \approx \frac{\Phi^2}{2}\left.\frac{\partial^2 F(\Phi)}{\partial\Phi^2}\right|_{\Phi\to 0} \equiv \frac{1}{2}\rho_s v_s^2 L^d\,, \tag{4.7}$$

where the superfluid number density n_s, or the phase stiffness $\rho_s = n_s/m$ have been defined by (4.3).

Full phase stiffness expression For the later treatment it proves useful to unpack the phase stiffness (4.3) similarly to the work in [166]. It is convenient to express the free energy $F(N) = \Omega(\mu(N)) + N\mu(N)$ in terms of the grand canonical potential $\Omega(\mu)$ where the chemical potential $\mu(N)$ is defined via $N = -\frac{\partial\Omega(\mu)}{\partial\mu}$. Our system is assumed to be inside the superconducting state such that the superconducting gap Δ can be treated like a thermodynamic quantity itself. Then, the free energy can be interpreted as $F(N) \to F(N, \Delta)$, similar to the magnetization M inside a magnetically order state. Additionally, we impose the phase twist Φ such that the explicit dependencies of the Legendre transform read

$$F\left(N, \Delta\left(\mu(N,\Phi),\Phi\right),\Phi\right) = \Omega\left(\mu(N,\Phi), \Delta\left(\mu(N,\Phi),\Phi\right),\Phi\right) - N\mu(N,\Phi)\,, \tag{4.8}$$

where we define the superconducting gap $\Delta\left(\mu,\Phi\right)$ by $0 = \frac{\partial\Omega(\mu,\Delta,\Phi)}{\partial\Delta}|_\mu$. Actually, in the course of the upcoming derivation we will decompose the grand canonical potential $\Omega = \Omega_F + \Omega_B$ into a mean-field part Ω_F and a fluctuation driven part Ω_B, where the gap will only be defined as the minimum value of the former part $0 = \frac{\partial\Omega_F}{\partial\Delta}|_\mu$. In other words, the superconducting gap that occurs in the thermodynamic relations is the mean-field gap. As we show in the appendix D.2, both the chemical potential and the mean-field gap evolve quadratically with the imposed phase twist such that the first-order derivatives vanish $\frac{\partial\Delta}{\partial\Phi}|_\mu|_{\Phi\to0} = \frac{\partial\mu}{\partial\Phi}|_{\Phi\to0} = 0$. This allows us to unpack the phase stiffness (4.3) according to

$$\begin{aligned}
\rho_s =& \frac{\partial^2\Omega}{\partial\Phi^2} + N\,\frac{\partial^2\mu}{\partial\Phi^2} \\
=& \frac{\partial^2\Omega}{\partial\Phi^2}\bigg|_{\Delta,\mu} + \left(\frac{\partial\Omega}{\partial\Delta}\bigg|_\mu\left(\frac{\partial^2\Delta}{\partial\Phi^2}\bigg|_\mu + \frac{\partial\Delta}{\partial\mu}\frac{\partial^2\mu}{\partial\Phi^2}\right) + \frac{\partial\Omega}{\partial\mu}\bigg|_\Delta\frac{\partial^2\mu}{\partial\Phi^2}\right) + N\,\frac{\partial^2\mu}{\partial\Phi^2} && (4.9)\\
=& \underbrace{\frac{\partial^2\Omega_F}{\partial\Phi^2}\bigg|_{\Delta,\mu}}_{\rho_s^{(F)}} + \underbrace{\frac{\partial^2\Omega_B}{\partial\Phi^2}\bigg|_{\Delta,\mu} + \frac{\partial\Omega_B}{\partial\Delta}\bigg|_\mu\frac{\partial^2\Delta}{\partial\Phi^2}\bigg|_\mu}_{\rho_s^{(B)}}\,, && (4.10)
\end{aligned}$$

where we implicitly assume the evaluation at zero phase twist $\Phi \to 0$. We have introduced the fermionic (F) and bosonic (B) contributions to the phase stiffness which will be at the core of the study in sections 4.4 and 4.5. In the last line (4.10) we have inserted the number equation

$$\begin{aligned}
N =& -\frac{\partial\Omega(\Delta(\mu),\mu)}{\partial\mu} = -\frac{\partial\Omega}{\partial\mu}\bigg|_\Delta - \frac{\partial\Omega}{\partial\Delta}\bigg|_\mu\frac{\partial\Delta}{\partial\mu} && (4.11)\\
=& \underbrace{-\frac{\partial\Omega_F}{\partial\mu}\bigg|_\Delta}_{N_F} + \underbrace{(-1)\frac{\partial\Omega_B}{\partial\mu}\bigg|_\Delta - \frac{\partial\Omega_B}{\partial\Delta}\bigg|_\mu\frac{\partial\Delta}{\partial\mu}}_{N_B}\,, && (4.12)
\end{aligned}$$

which has to hold for any value of the phase twist, in particular also for $\Phi = 0$. In the next section we implement our microscopic model and we derive the particular grand canonical potential. Finally we evaluate the formulae (4.10).

4.3 Microscopic model and thermodynamic potential

The aim of this section is to find an expression for the thermodynamic potential $\Omega(\Phi)$ as a function of the externally applied phase twist Φ. The grand canonical potential $\Omega(\Phi) = -T \ln Z(\Phi)$ can be derived microscopically via the partition function

$$Z(\Phi) = \int \mathcal{D}[\psi, \bar{\psi}]\, e^{-\mathcal{S}[\psi,\bar{\psi},\Phi]}\,,$$

which is expressed as a functional integral over the fermionic Graßmann fields ψ and $\bar{\psi}$ [169]. For brevity, we set the lattice constant $a = 1$ throughout this chapter. The present study is designed to capture the physics of the over-doped region of the cuprate high-temperature superconductors. These systems fall into the point group $\mathsf{C_{4v}}$ where most of the member states seem to be realizing a d-wave pairing state that transforms according to the IR B_1. This state is a singlet, and it transforms even upon the C_{2z} and odd upon the $C_{4z}^{\pm}$ operations, giving it a x^2-y^2 character. The corresponding action in position and imaginary time space reads (see Ref. [168])

$$\mathcal{S} = \int_{\tau,\boldsymbol{r},\boldsymbol{r}'} \bar{\tilde{\psi}}_\sigma(\boldsymbol{r},\tau)\Big[(\partial_\tau - \mu)\,\delta_{\boldsymbol{r},\boldsymbol{r}'} - t\delta^{nn}_{\boldsymbol{r},\boldsymbol{r}'} - t'\delta^{nnn}_{\boldsymbol{r},\boldsymbol{r}'}\Big]\tilde{\psi}_\sigma(\boldsymbol{r}',\tau) - \frac{g}{4}\int_{\tau,\boldsymbol{r},\boldsymbol{r}'} \mathsf{B}^\dagger(\boldsymbol{r},\boldsymbol{r}',\tau)\,\mathsf{B}(\boldsymbol{r},\boldsymbol{r}',\tau)\;\delta^{nn}_{\boldsymbol{r},\boldsymbol{r}'} \quad (4.13)$$

with the nearest (t) and next-to-nearest (t') neighbor hopping parameter, the BCS interaction constant g and the shorthand notations , $\delta^{nn}_{\boldsymbol{r},\boldsymbol{r}'} = \delta(\boldsymbol{r}-\boldsymbol{r}'\pm\boldsymbol{e}_x) + \delta(\boldsymbol{r}-\boldsymbol{r}'\pm\boldsymbol{e}_y)$, $\delta^{nnn}_{\boldsymbol{r},\boldsymbol{r}'} = \delta(\boldsymbol{r}-\boldsymbol{r}'\pm(\boldsymbol{e}_x+\boldsymbol{e}_y)) + \delta(\boldsymbol{r}-\boldsymbol{r}'\pm(\boldsymbol{e}_x-\boldsymbol{e}_y))$ that lead to the electronic dispersion relation. The dispersion comprises a two-dimensional square lattice with nearest (t) and next-to-nearest (t') neighbor hopping,

$$\epsilon_{\boldsymbol{k}} = -2t\,[\cos(k_x) + \cos(k_y)] - 4t'\cos(k_x)\cos(k_y) - \mu\,. \quad (4.14)$$

The bilinear combinations

$$\mathsf{B}(\boldsymbol{r},\boldsymbol{r}',\tau) = \tilde{\psi}_\downarrow(\boldsymbol{r}',\tau)\tilde{\psi}_\uparrow(\boldsymbol{r},\tau) - \tilde{\psi}_\uparrow(\boldsymbol{r}',\tau)\tilde{\psi}_\downarrow(\boldsymbol{r},\tau)$$

lead to the commonly known d-wave attraction $\mathsf{B}_q = \sum_k \gamma_{\boldsymbol{k}}\psi_{\downarrow -k+\frac{q}{2}}\psi_{\uparrow k+\frac{q}{2}}$ with $\gamma_{\boldsymbol{k}} = \cos(k_x) - \cos(k_y)$. The interaction term in (4.13) also contains an extended s-wave part that will be dropped once we switch into momentum space. The reason why we introduced the action in position space lies in the simpler treatment of the phase twist Φ. We want to impose twisted boundary conditions (4.4) onto our system. As a first step, we apply the fermionic gauge transformation (4.5) such that the new fields ψ satisfy periodic boundary conditions. With respect to the action (4.13) the gauge transformation (4.5) only shifts the hopping parameters according to $\{t,t'\} \to \{t,t'\}\,e^{-i\frac{\Phi}{L}(x-x')}$, while the remaining terms in (4.13) are left unchanged. The new action in momentum space, where the extended s-wave part has been dropped, reads

$$\mathcal{S} = \sum_k \bar{\psi}_{\sigma k}\left(-i\omega_n + \epsilon^{\Phi}_{\boldsymbol{k}}\right)\psi_{\sigma k} - g\,\frac{T}{L^2}\sum_q \bar{\mathsf{B}}_q\mathsf{B}_q\,,$$

with $\epsilon_{\boldsymbol{k}}^{\Phi} = \epsilon_{\boldsymbol{k}-\frac{\Phi}{L}\boldsymbol{e}_x}$. We use the notation $k = (i\omega_n, \boldsymbol{k})$ and $q = (i\nu_m, \boldsymbol{q})$ denoting fermionic and bosonic Matsubara frequencies, respectively. Next, we decouple the interaction part by means of a Hubbard-Stratonovich transformation,

$$e^{g\frac{T}{L^2}\sum_q \bar{\mathsf{B}}_q \mathsf{B}_q} = \int \mathcal{D}[\bar{\Delta}, \Delta] e^{-\frac{1}{g}\sum_q \bar{\Delta}_q \Delta_q + \sqrt{\frac{T}{L^2}}\sum_q \left\{\bar{\Delta}_q \mathsf{B}_q + \Delta_q \bar{\mathsf{B}}_q\right\}},$$

which introduces the superconducting pairing field Δ. The action becomes

$$S = \frac{1}{g}\sum_q \bar{\Delta}_q \Delta_q - \sum_{k,k'} \Psi_k^\dagger \left[\hat{\mathcal{G}}^{-1,\Phi}\right]_{k,k'} \Psi_{k'} , \tag{4.15}$$

with the Nambu-Gorkov Green's function

$$\left[\hat{\mathcal{G}}^{-1,\Phi}\right]_{k,k'} = \begin{pmatrix} \left(i\omega_n - \epsilon_{\boldsymbol{k}}^{\Phi}\right)\delta_{k,k'} & \sqrt{\frac{T}{L^2}}\gamma_{\frac{\boldsymbol{k}}{2}+\frac{\boldsymbol{k}'}{2}}\Delta_{k-k'} \\ \sqrt{\frac{T}{L^2}}\gamma_{\frac{\boldsymbol{k}}{2}+\frac{\boldsymbol{k}'}{2}}\bar{\Delta}_{k'-k} & \left(i\omega_n + \epsilon_{\boldsymbol{k}}^{-\Phi}\right)\delta_{k,k'} \end{pmatrix}, \tag{4.16}$$

and the Nambu spinor $\Psi_k = (\psi_{\uparrow k}, \bar{\psi}_{\downarrow -k})^T$. Since the action (B.4) is bilinear in the fermionic fields, the corresponding Gaussian integration in the partition function can be performed, yielding

$$\begin{aligned} Z(\Phi) &= \int \mathcal{D}[\psi, \bar{\psi}]\mathcal{D}[\bar{\Delta}, \Delta]\, e^{-S[\psi,\bar{\psi},\bar{\Delta},\Delta,\Phi]} \\ &= \int \mathcal{D}[\bar{\Delta}, \Delta]\, e^{-\mathcal{S}^{eff}[\bar{\Delta},\Delta,\Phi]}, \end{aligned} \tag{4.17}$$

with the effective action

$$\mathcal{S}^{eff} = \frac{1}{g}\sum_q \bar{\Delta}_q \Delta_q - \operatorname{tr}\ln\left[\hat{\mathcal{G}}^{-1,\Phi}\right]. \tag{4.18}$$

Here, the trace refers to a summation over spin indices as well as momenta and Matsubara frequencies. In the following, we use the saddle-point approximation and we treat the superconducting fluctuations as small, i.e. we formally expand the action in terms of small bosonic fluctuations. The minimization of the action (4.18) with respect to the pairing field Δ yields the well-known BCS gap equation in the d-wave channel

$$\frac{1}{g} = \frac{T}{L^2\Delta_0}\sum_k \gamma_{\boldsymbol{k}} F_k^{\Phi} , \tag{4.19}$$

with the anomalous Green's function in the presence of the phase twist F_k^{Φ} defined in (D.3). In a next step, we expand the superconducting order parameter around its mean-field value $\Delta_q = \Delta_0\sqrt{\frac{T}{L^2}}\delta_{q,0} + \delta\Delta_q + \mathsf{i}\theta_q$, where $\delta\Delta_q$ and θ_q are the amplitude and phase field, respectively. The Nambu-Gorkov

Green's function (4.16) can be decomposed as $[\hat{\mathcal{G}}^{-1}]_{k,k'} = \hat{G}_k^{-1}\delta_{k,k'} + \hat{\Lambda}^{(1)}_{k,k'}$, with the mean-field Nambu-Gorkov Green's function

$$\hat{G}_k^{-1,\Phi} = \begin{pmatrix} \mathrm{i}\omega_n - \epsilon_{\boldsymbol{k}}^{\Phi} & \gamma_{\boldsymbol{k}}\Delta_0 \\ \gamma_{\boldsymbol{k}}\Delta_0 & \mathrm{i}\omega_n + \epsilon_{\boldsymbol{k}}^{-\Phi} \end{pmatrix}, \tag{4.20}$$

and the fluctuation part $\hat{\Lambda}^{(1)}_{k,k'} = \sqrt{\frac{T}{L^2}}\gamma_{\frac{\boldsymbol{k}}{2}+\frac{\boldsymbol{k}'}{2}}(\delta\Delta_{k-k'}\hat{\tau}_x - \theta_{k-k'}\hat{\tau}_y)$ where the Pauli matrices $\hat{\tau}_{x,y}$ act in the spinor space. Expanding the action (4.18) up to second order yields $\mathcal{S}^{eff} = \mathcal{S}_0^{\Phi} + \mathcal{S}_2^{\Phi}$ with

$$\begin{aligned}
\mathcal{S}_0^{\Phi} =& \frac{1}{g}\frac{L^2}{T}\Delta_0^2 - \operatorname{tr}\ln\left[-\hat{G}^{-1,\Phi}\right] , \\
\mathcal{S}_2^{\Phi} =& \frac{1}{g}\sum_q \left(\delta\Delta_{-q}\delta\Delta_q + \theta_{-q}\theta_q\right) + \frac{1}{2}\mathrm{tr}\left[\left(\hat{G}^{\Phi}\hat{\Lambda}^{(1)}\right)^2\right] \qquad = \frac{1}{2}\sum_q \begin{pmatrix} \delta\Delta_{-q} \\ \theta_{-q} \end{pmatrix}^T \hat{M}_q^{\Phi} \begin{pmatrix} \delta\Delta_q \\ \theta_q \end{pmatrix}.
\end{aligned}$$

The inverse matrix pair fluctuation propagator $\hat{M}_q^{\Phi}$ for a current-carrying superfluid is given by

$$\hat{M}_q^{\Phi} = \begin{pmatrix} \Gamma_q^{(\Delta\Delta),\Phi} & \mathrm{i}\Gamma_q^{(\Delta\theta),\Phi} \\ -\mathrm{i}\Gamma_q^{(\Delta\theta),\Phi} & \Gamma_q^{(\theta\theta),\Phi} \end{pmatrix}, \tag{4.21}$$

with the matrix elements defined in the appendix D.1. Eventually, the bosonic Gaussian field integration can be performed and the partition function (4.17) becomes

$$Z(\Phi) = e^{-\mathcal{S}_0^{\Phi}} \int \mathcal{D}[\delta\Delta,\theta]\, e^{-\mathcal{S}_2^{\Phi}} \; = e^{-\mathcal{S}_0^{\Phi}} \prod_q \left[\det\, \hat{M}_q^{\Phi}\right]^{-\frac{1}{2}}. \tag{4.22}$$

In the last line, constant factors have been neglected since they do not contribute to the phase stiffness. The ensuing grand canonical potential reads

$$\Omega(\Phi) = \Omega_F(\Phi) + \Omega_B(\Phi),$$

with the fermionic and bosonic contributions

$$\Omega_F(\Phi) = \frac{L^2}{g}\,\Delta_0^2 - T\operatorname{tr}\ln\left[-\hat{G}^{-1,\Phi}\right], \tag{4.23}$$

$$\Omega_B(\Phi) = \frac{1}{2}\,T\sum_q \ln\det\, \hat{M}_q^{\Phi}. \tag{4.24}$$

These expressions allow for the calculation of the phase stiffness (4.10) which is explicitly done in the next two sections.

4.4 Fermionic part of the phase stiffness

In this part, we study the fermionic contribution $\rho_s^{(F)}$ to the phase stiffness (4.10). The evaluation of the derivative of equation (4.10) and (4.23) at zero temperature yields after performing the summation over Matsubara frequencies

$$\rho_s^{(F)} = \left.\frac{\partial^2 \Omega_F}{\partial \Phi^2}\right|_{\Delta,\mu} = \frac{1}{L^2}\sum_{\boldsymbol{k}} \frac{\partial^2 \epsilon_{\boldsymbol{k}}}{\partial k_x^2}\left(1 - \frac{\epsilon_{\boldsymbol{k}}}{\lambda_{\boldsymbol{k}}}\right), \tag{4.25}$$

with $\lambda_{\boldsymbol{k}} = \sqrt{\epsilon_{\boldsymbol{k}}^2 + \gamma_{\boldsymbol{k}}^2 \Delta_0^2}$. It is instructive to first revisit Leggett's theorem which, once again, says that the entire electronic system contributes to a Galilean invariant superfluid, cf. Eq. (4.1). In such a Galilean invariant system, it holds $(\partial^2 \epsilon_{\boldsymbol{k}})/(\partial k_x^2) = 1/m$ and thus, one can easily derive the equation $\rho_s^{(F)} = \frac{N_F}{L^2 m}$, with N_F defined in (4.12) and (D.11). Moreover, in the case of Galilean invariance one obtains for the bosonic contribution that it holds $N_B = \rho_s^{(B)} = 0$, see the appendix D.3 for details. Consequently, no matter how strong the BCS coupling strength, in a Galilean invariant flow the superfluid density $n_s = n$ always equals the electron density at zero temperature as is sketched in Fig. 4.1. If however, Galilean invariance is broken, for example, via the underlying lattice, i.e. $\epsilon_{\boldsymbol{k}} \neq \boldsymbol{k}^2/(2m) - \mu$, the superfluid density changes. We have numerically analyzed the fermionic part to the phase stiffness (4.25) for our cuprate lattice model (4.14) for three distinct cases, as shown in Fig. 4.3. Apart from the actual model (4.14), we have also studied the system at perfect nesting in both, s-wave and d-wave pairing channels. The results show a similar behavior for all three cases. The decrease of the fermionic part $\rho_s^{(F)}$ is moderate and does not change significantly as a function of the coupling strength g.

4.5 Bosonic part of the phase stiffness

The aim of this section is to evaluate the bosonic contribution $\rho_s^{(B)}$ to the phase stiffness (4.10). A priori, it is not clear how large $\rho_s^{(B)}$ can become in a lattice model. The bosonic contribution reads

$$\rho_s^{(B)} = \left.\frac{\partial^2 \Omega_B}{\partial \Phi^2}\right|_{\Delta,\mu} + \left.\frac{\partial \Omega_B}{\partial \Delta}\right|_{\Delta,\mu} \left.\frac{\partial^2 \Delta}{\partial \Phi^2}\right|_{\mu}. \tag{4.26}$$

Unpacking the expression (4.26) with the aid of (4.24) yields

$$\begin{aligned}\rho_s^{(B)} = \frac{T}{2L^2}\sum_q \Bigg\{ &- \frac{\left(\Gamma_q^{(\theta\theta)}\Gamma_q^{(\Delta\Delta 1)} + \Gamma_q^{(\Delta\Delta)}\Gamma_q^{(\theta\theta 1)} - 2\Gamma_q^{(\Delta\theta)}\Gamma_q^{(\Delta\theta 1)}\right)^2}{\left(\det \hat{M}_q^0\right)^2} \\ &+ \frac{\Gamma_q^{(\theta\theta)}\Gamma_q^{(\Delta\Delta 2)} + \Gamma_q^{(\Delta\Delta)}\Gamma_q^{(\theta\theta 2)} + 2\Gamma_q^{(\Delta\Delta 1)}\Gamma_q^{(\theta\theta 1)} - 2\Gamma_q^{(\Delta\theta)}\Gamma_q^{(\Delta\theta 2)} - 2\left(\Gamma_q^{(\Delta\theta 1)}\right)^2}{\det \hat{M}_q^0}\Bigg\},\end{aligned} \tag{4.27}$$

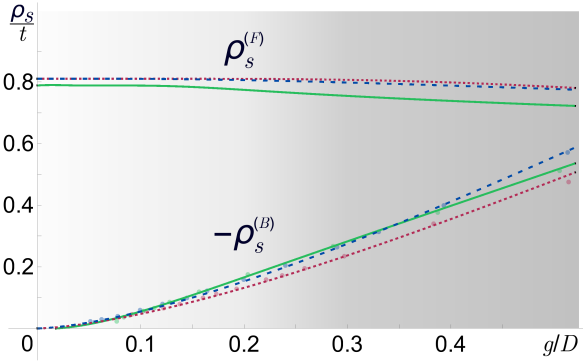

Figure 4.3: The plot shows the fermionic $\rho_s^{(F)}$ and the **negative** bosonic $\rho_s^{(B)}$ contribution to the phase stiffness as a function of the BCS coupling strength for three cases. Solid green: the lattice model (4.14) with the chosen values $t'/t = -0.2749$ and $\mu/t = -0.8772$. Dashed blue: the model (4.14) at perfect nesting ($t' = \mu = 0$) with d-wave pairing. Dotted red: the model (4.14) at perfect nesting ($t' = \mu = 0$) with s-wave ($\gamma_{\boldsymbol{k}} = 1$) pairing. In all three cases the phase stiffness exhibits the same behavior. While the fermionic contribution is roughly unchanged, the bosonic contribution rises significantly in its magnitude as the coupling strength increases. The shaded gray background indicates the limit of applicability of the weak-coupling theory. Results in the dark region should not be considered trustworthy. Plotted are the dimensionless quantities ρ_s/t and g/D with $D = 4t$. The small solid circles in the bosonic curves denote the numerically computed points.

where we defined

$$\Gamma_q^{(\zeta)} = \Gamma_q^{(\zeta),0}\,, \qquad \Gamma_q^{(\zeta 1)} = L\frac{\partial \Gamma_q^{(\zeta),\Phi}}{\partial \Phi}\bigg|_{\Delta,\mu}\,, \qquad \Gamma_q^{(\zeta 2)} = L^2\frac{\partial^2 \Gamma_q^{(\zeta),\Phi}}{\partial \Phi^2}\bigg|_{\Delta,\mu} + L^2\frac{\partial^2 \Delta}{\partial \Phi^2}\bigg|_{\mu}\frac{\partial \Gamma_q^{(\zeta),\Phi}}{\partial \Delta}\bigg|_{\mu}\,,$$

with $\zeta = \{\Delta\Delta, \theta\theta, \Delta\theta\}$. The propagators $\Gamma_q^{(\zeta),\Phi}$ and the derivative of the gap $\frac{\partial^2\Delta}{\partial\Phi^2}|_\mu$ are calculated in the appendix D. The figure 4.3 shows the bosonic contribution (4.27) to the phase stiffness—multiplied by -1 for clarity—as a function of the BCS coupling strength at zero temperature. Similarly to the previous section, we have investigated the same three scenarios and again, we find that the overall behavior is the same for all three of them. In contrast to the fermionic contribution, the bosonic part heavily depends on the coupling strength. Its magnitude increases significantly and becomes comparable to the fermionic part already for a small BCS coupling strength.

4.6 Conclusion of chapter 4

In this work, we have studied how the superfluid phase stiffness ρ_s changes in a clean system as Galilean invariance is broken by a periodic lattice potential. In particular, we focus on systems with a flat-band electronic dispersion in the vicinity of the Fermi energy, i.e. on systems with a van-Hove singularity nearby. Our findings might be of relevance for the over-doped cuprate superconductors. Compared to Galilean invariant systems where fluctuations do not contribute to the phase stiffness, we have found these fluctuations to generate a significant downward renormalization in such a lattice model. The dominant source of momentum relaxation in the case of a periodic lattice are the umklapp scattering events. The renormalization effect can already for a rather moderate interaction strength be as pronounced as to make the fluctuation and the mean-field driven contributions similar in size. The resulting suppression of the phase stiffness is depicted in Fig.4.3. In the case of the cuprate superconductors, our analysis does not provide a controlled description of the physics revolving around the quantum critical point. Nonetheless, our theory may provide an insight into the understanding of the phase stiffness reduction and the strong role played by phase fluctuations and inhomogeneities.

Chapter 5
5 Conclusion

In this thesis two aspects that revolve around the role of fluctuations in unconventional superconductors have been studied, and will be summarized in the following.

Vestigial nematic phase Having introduced the doped topological insulator Bi_2Se_3 and discussed its superconducting properties in chapter 2, we exploit three of its main characteristics in chapter 3: (i) the pairing state is two-dimensional, which is consistent with a C_{3z} rotational symmetry breaking [15, 17, 94–103], (ii) the low carrier density $n \sim 10^{20}\,\mathrm{cm}^{-3}$ and small ratio of coherence length over Fermi wavelength $\xi_0/\lambda_F = 2..4$ significantly enhances superconducting fluctuations [14, 18, 19], and (iii) the Fermi surface displays a strong anisotropy with increased doping level [92].

These three observations are a prerequisite for the study we have conducted: a possible fluctuation-induced phase that precedes the superconducting state. On the basis of a large-N theory—with the parameters being chosen compatibly with doped Bi_2Se_3—we predict the existence of such a vestigial nematic phase. As a consequence, the C_{3z} rotational and the $U(1)$ symmetry are separately broken at temperatures T_{nem} and $T_c < T_{\mathrm{nem}}$. A characteristic of the vestigial nematic phase is the presence of strong anisotropic fluctuations that inflict their anisotropy on various observables such as the ones explicitly computed, i.e. the conductivity and the diamagnetic susceptibility. The nematic phase transition falls into the universality class of the Z_3-Potts model and thus, the onset at T_{nem} is a first-order transition. Additionally, the ground state is three-fold degenerate which manifests itself in three distinct domains. The balance among these domains is particularly vulnerable as the nematic order parameter couples to both, in-plane $(\epsilon_{xx} - \epsilon_{yy}, \epsilon_{xy})$ and out-of-plane $(\epsilon_{yz}, \epsilon_{zx})$ strain fields. Focusing on in-plane strain only, we have illustrated the lattice deformation caused by the nematicity. The nematic susceptibility signals the approaching nematic phase transition, yet owed to the first-order transition, it does not diverge. We have studied the associated lattice softening and thereby, we analyzed the renormalization of the E_g elastic constants and determined the directions of vanishing sound velocity. The condensation of a vestigial phase enhances the superconducting transition temperature as compared to the T_c suppression caused by trivial fluctuations. While T_c should still be smaller than the mean-field temperature, it may offer an explanation for the comparably large transition temperature in doped Bi_2Se_3, given the small carrier concentration. A controversial issue raised by the experimental findings in doped Bi_2Se_3 concerns the orientation of the in-plane upper critical field H_{c2} [104]. In this regard the vestigial nematic scenario unambiguously confines the large H_{c2} axis to be aligned with the crystal x-axis. In a doping range where the z-anisotropy is less pronounced, the two transitions merge and undergo a joint first-order transition. We show that in this case—depending on the microscopic

parameters—a magnetic field in the z-direction can give rise to split phase transitions where the system first enters a chiral phase with the C_{3z} rotational symmetry still being intact. Only below a second transition, the system acquires its nematic character.

Strong experimental evidence which is consistent with a vestigial nematic scenario has been provided by Rolf Lortz and collaborators [20]. They have probed the thermal expansion of Nb and Cu doped Bi_2Se_3 samples and detected an onset of in-plane anisotropy at a temperature $T_{\mathrm{nem}} = 3.8\,\mathrm{K}$ above the superconducting transition $T_c = 3.25\,\mathrm{K}$. The observed step-like transition is characteristic of a first-order transition, and magnetostriction data has demonstrated that the inflicted lattice distortion vanishes at the offset of superconductivity. In addition, the observed enhanced signals in the magnetization and in the resistivity roughly coincide with the nematic transition temperature.

The structure of the superconducting ground state in doped Bi_2Se_3 is still a topic of debate; either the fully-gapped $\boldsymbol{\Delta}^{E_u} \sim (1,0)$ or the nodal state $\boldsymbol{\Delta}^{E_u} \sim (0,1)$ is realized. While this has essentially no consequences for the above prediction, our microscopic analysis suggests that the fully-gapped state is favored by the system. This tendency is found in both contributing channels, the discriminating mean-field interaction parameter and the fluctuation-induced nematic order parameter.

The framework of the presented theory can equally be applied to any other fluctuation-induced correlation function. The concept may potentially be useful for the identification of yet unknown phases in unconventional superconductors.

Phase stiffness suppression In chapter 4 we have addressed a fundamental question: can scattering processes in a clean lattice system cause a significant reduction of the phase stiffness? It is known from Leggett's theorem that in a Galilean invariant system at zero temperature the value of the phase stiffness $\rho_s \sim n$ involves the entire electronic density. Similar to disorder, the lattice manifestly breaks the Galilean invariance and thus, causes a phase stiffness suppression. In this work, we have aimed at quantifying the extent of the corresponding suppression. We have focused on a system with a flat-band electronic dispersion where a van-Hove singularity is located in the vicinity of the Fermi surface. In a periodic lattice, umklapp scattering events are the dominant source of momentum relaxation. While the fluctuation contribution to the phase stiffness vanishes in a Galilean invariant system, we have found these superconducting fluctuations to generate a significant downward renormalization in such a lattice system. For moderate values of the coupling strength the renormalization can already be as pronounced as to make the fluctuation and the mean-field driven contributions similar in size. This finding may be of direct relevance for some cuprate superconductors in the over-doped regime where a phase stiffness suppression has been reported. In particular, evidence has been given in [23, 159, 160, 163] that the observed suppression should not exclusively be due to disorder.

Appendix A

A Symmetry-based deductions

A.1 Time-reversal symmetry constraint on pairing function

In section 1.3.4 we have introduced the matrices $\Lambda^{n,\mu} = \mathcal{U}_{\mathcal{T}}\lambda^{n,\mu}$, and exploited the relations

$$\left(\chi^{n,\mu}_{\boldsymbol{k},\boldsymbol{q}}\Lambda^{n,\mu}\right)^{\dagger} = \left(\chi^{\bar{n},\mu}_{\boldsymbol{k},-\boldsymbol{q}}\Lambda^{\bar{n},\mu}\right) , \qquad \Delta^{n,\mu}_{\boldsymbol{q}} = \left(\Delta^{\bar{n},\mu}_{-\boldsymbol{q}}\right)^{*} . \tag{A.1}$$

Here, we want to illustrate their validity. For a real proof we refer to Ref. [56, 171]. Our illustration follows the lines in Ref. [56] and starts from the BCS interaction Hamiltonian, i.e. the expression before the mean-field decoupling has been carried out. The Hamiltonian reads

$$\mathcal{H}_{int} = -V\sum g^{\mu\mu'}_{nn'}\left\{\hat{\boldsymbol{c}}^{\dagger,T}_{\boldsymbol{k}+\frac{\boldsymbol{q}}{2}}\left(\chi^{n,\mu}_{\boldsymbol{k},\boldsymbol{q}}\Lambda^{n,\mu}\right)^{\dagger}\mathcal{U}_{\mathcal{T}}\,\hat{\boldsymbol{c}}^{\dagger}_{-\boldsymbol{k}+\frac{\boldsymbol{q}}{2}}\right\}\left\{\hat{\boldsymbol{c}}^{T}_{-\boldsymbol{k}'+\frac{\boldsymbol{q}}{2}}\,\mathcal{U}^{\dagger}_{\mathcal{T}}\left(\chi^{n',\mu'}_{\boldsymbol{k}',\boldsymbol{q}}\Lambda^{n',\mu'}\right)\,\hat{\boldsymbol{c}}_{\boldsymbol{k}'+\frac{\boldsymbol{q}}{2}}\right\} , \tag{A.2}$$

with the notation being identical to what has been used in chapter 1. The rotated matrix $\Lambda^{n,\mu} = \mathcal{U}_{\mathcal{T}}\lambda^{n,\mu}$ transforms under the point group symmetry elements in a sesquilinear form

$$\mathcal{U}_g\left(\chi^{n,\mu}_{\mathcal{R}^{\dagger}_v(g)\boldsymbol{k},\mathcal{R}^{\dagger}_v(g)\boldsymbol{q}}\Lambda^{n,\mu}\right)^{\dagger}\mathcal{U}^{\dagger}_g = \mathcal{U}_g\left(\chi^{n,\mu}_{\mathcal{R}^{\dagger}_v(g)\boldsymbol{k},\mathcal{R}^{\dagger}_v(g)\boldsymbol{q}}\lambda^{n,\mu}\right)^{\dagger}\mathcal{U}^{T}_g\mathcal{U}^{\dagger}_{\mathcal{T}} \overset{(A.5)}{=} \mathcal{R}^{T}_n(g)_{\mu\mu'}\left(\chi^{n,\mu'}_{\boldsymbol{k},\boldsymbol{q}}\Lambda^{n,\mu'}\right)^{\dagger} , \tag{A.3}$$

$$\text{H.c.:}\qquad \mathcal{U}_g\left(\chi^{n,\mu}_{\mathcal{R}^{\dagger}_v(g)\boldsymbol{k},\mathcal{R}^{\dagger}_v(g)\boldsymbol{q}}\Lambda^{n,\mu}\right)\mathcal{U}^{\dagger}_g = \mathcal{R}^{\dagger}_n(g)_{\mu\mu'}\left(\chi^{n,\mu'}_{\boldsymbol{k},\boldsymbol{q}}\Lambda^{n,\mu'}\right) , \tag{A.4}$$

where the transformation property

$$\mathcal{U}_g\left(\chi^{n,\mu}_{\mathcal{R}^{\dagger}_v(g)\boldsymbol{k},\mathcal{R}^{\dagger}_v(g)\boldsymbol{q}}\lambda^{n,\mu}\right)^{\dagger}\mathcal{U}^{T}_g = \mathcal{R}^{T}_n(g)_{\mu\mu'}\left(\chi^{n,\mu'}_{\boldsymbol{k},\boldsymbol{q}}\lambda^{n,\mu'}\right)^{\dagger} , \tag{A.5}$$

has been inserted. The time-reversal operation commutes with each lattice element $[\mathcal{T},\mathcal{U}_g] = 0$, such that it holds $\mathcal{U}_{\mathcal{T}}\mathcal{U}^{T}_g = \mathcal{U}^{\dagger}_g\mathcal{U}_{\mathcal{T}}$ and $\mathcal{U}^{\dagger}_{\mathcal{T}}\mathcal{U}^{\dagger}_g = \mathcal{U}^{T}_g\mathcal{U}^{\dagger}_{\mathcal{T}}$. As a first step, the invariance upon point group elements is imposed on the Hamiltonian (A.2) which leads to a the diagonalization of the coupling

parameter $g^{\mu\mu'}_{nn'} \equiv g_n \delta_{\mu\mu'}\delta_{nn'}$, see Sec. 1.3.5.[1] Next, the action of the time-reversal is considered where we allow for complex conjugated pairs of IRs n and $\bar{n}$. For the time-reversed Hamiltonian one computes (using (1.23) and $\mathcal{U}_\mathcal{T}^T = -\mathcal{U}_\mathcal{T}$)

$$\begin{aligned}\mathcal{H}_{int} = &-g_n V \left\{ \hat{\mathbf{c}}^{\dagger,T}_{\boldsymbol{k}+\frac{\boldsymbol{q}}{2}} \left(\chi^{n,\mu}_{\boldsymbol{k},\boldsymbol{q}}\Lambda^{n,\mu}\right)^\dagger \mathcal{U}_\mathcal{T}\, \hat{\mathbf{c}}^\dagger_{-\boldsymbol{k}+\frac{\boldsymbol{q}}{2}} \right\} \left\{ \hat{\mathbf{c}}^T_{-\boldsymbol{k}'+\frac{\boldsymbol{q}}{2}} \mathcal{U}_\mathcal{T}^\dagger \left(\chi^{n,\mu}_{\boldsymbol{k}',\boldsymbol{q}}\Lambda^{n,\mu}\right) \hat{\mathbf{c}}_{\boldsymbol{k}'+\frac{\boldsymbol{q}}{2}} \right\} \\ &- g_{\bar{n}} V \left\{ \hat{\mathbf{c}}^{\dagger,T}_{\boldsymbol{k}+\frac{\boldsymbol{q}}{2}} \left(\chi^{\bar{n},\mu}_{\boldsymbol{k},\boldsymbol{q}}\Lambda^{\bar{n},\mu}\right)^\dagger \mathcal{U}_\mathcal{T}\, \hat{\mathbf{c}}^\dagger_{-\boldsymbol{k}+\frac{\boldsymbol{q}}{2}} \right\} \left\{ \hat{\mathbf{c}}^T_{-\boldsymbol{k}'+\frac{\boldsymbol{q}}{2}} \mathcal{U}_\mathcal{T}^\dagger \left(\chi^{\bar{n},\mu}_{\boldsymbol{k}',\boldsymbol{q}}\Lambda^{\bar{n},\mu}\right) \hat{\mathbf{c}}_{\boldsymbol{k}'+\frac{\boldsymbol{q}}{2}} \right\} \end{aligned} \tag{A.6}$$

$$\begin{aligned}\hat{\mathcal{T}}\mathcal{H}_{int}\hat{\mathcal{T}}^\dagger = &-g_n V \left\{ \hat{\mathbf{c}}^{\dagger,T}_{\boldsymbol{k}+\frac{\boldsymbol{q}}{2}} \left(\chi^{n,\mu}_{\boldsymbol{k},-\boldsymbol{q}}\Lambda^{n,\mu}\right) \mathcal{U}_\mathcal{T}\, \hat{\mathbf{c}}^\dagger_{-\boldsymbol{k}+\frac{\boldsymbol{q}}{2}} \right\} \left\{ \hat{\mathbf{c}}^T_{-\boldsymbol{k}'+\frac{\boldsymbol{q}}{2}} \mathcal{U}_\mathcal{T}^\dagger \left(\chi^{n,\mu}_{\boldsymbol{k}',-\boldsymbol{q}}\Lambda^{n,\mu}\right)^\dagger \hat{\mathbf{c}}_{\boldsymbol{k}'+\frac{\boldsymbol{q}}{2}} \right\} \\ &- g_{\bar{n}} V \left\{ \hat{\mathbf{c}}^{\dagger,T}_{\boldsymbol{k}+\frac{\boldsymbol{q}}{2}} \left(\chi^{\bar{n},\mu}_{\boldsymbol{k},-\boldsymbol{q}}\Lambda^{\bar{n},\mu}\right) \mathcal{U}_\mathcal{T}\, \hat{\mathbf{c}}^\dagger_{-\boldsymbol{k}+\frac{\boldsymbol{q}}{2}} \right\} \left\{ \hat{\mathbf{c}}^T_{-\boldsymbol{k}'+\frac{\boldsymbol{q}}{2}} \mathcal{U}_\mathcal{T}^\dagger \left(\chi^{\bar{n},\mu}_{\boldsymbol{k}',-\boldsymbol{q}}\Lambda^{\bar{n},\mu}\right)^\dagger \hat{\mathbf{c}}_{\boldsymbol{k}'+\frac{\boldsymbol{q}}{2}} \right\}. \end{aligned} \tag{A.7}$$

In case of a real IR ($n = \bar{n}$) the time-reversal symmetry requires the partner functions to satisfy the condition $(\chi^{n,\mu}_{\boldsymbol{k},\boldsymbol{q}}\Lambda^{n,\mu})^\dagger = (\chi^{n,\mu}_{\boldsymbol{k},-\boldsymbol{q}}\Lambda^{n,\mu})$. The IRs of a complex conjugated pair are mixed upon application of point group symmetry operations on (A.6) and (A.7). Using (A.3),(A.4) we note that the first g_n term in (A.6) transforms exactly like the first $g_{\bar{n}}$ term in (A.7), namely

$$\left(\chi^{n,\mu}_{\boldsymbol{k},\boldsymbol{q}}\Lambda^{n,\mu}\right)^\dagger \to \mathcal{R}^T_n(g)_{\mu\mu'} \left(\chi^{n,\mu'}_{\boldsymbol{k},\boldsymbol{q}}\Lambda^{n,\mu'}\right)^\dagger , \qquad \left(\chi^{\bar{n},\mu}_{\boldsymbol{k},-\boldsymbol{q}}\Lambda^{\bar{n},\mu}\right) \to \mathcal{R}^T_n(g)_{\mu\mu'} \left(\chi^{\bar{n},\mu'}_{\boldsymbol{k},-\boldsymbol{q}}\Lambda^{\bar{n},\mu'}\right) , \tag{A.8}$$

where we have used the defining property $\mathcal{R}_{\bar{n}}(g) = \mathcal{R}^*_n(g)$. Since the two terms supposedly belong to different IRs, this equivalence only makes sense if, in fact, the two IRs n and $\bar{n}$ transform as a doublet. Then, it must hold

$$\left(\chi^{n,\mu}_{\boldsymbol{k},\boldsymbol{q}}\Lambda^{n,\mu}\right)^\dagger = e^{\mathrm{i}\zeta^{n,\mu}} \left(\chi^{\bar{n},\mu}_{\boldsymbol{k},-\boldsymbol{q}}\Lambda^{\bar{n},\mu}\right) , \qquad \text{and} \qquad g_{\bar{n}} = g_n ,$$

with an arbitrary phase factor $e^{\mathrm{i}\zeta^{n,\mu}}$ that can be chosen to unity. Thus, the IRs of a complex conjugated pair, n and $\bar{n}$, effectively transform like a $2\dim n$-dimensional IR.

Next, we derive the action of the time-reversal operation on the pairing field

$$\Delta(\boldsymbol{k},\boldsymbol{q}) = \sum_{n,\mu} \Delta^{n,\mu}_{\boldsymbol{q}} \left(\chi^{n,\mu}_{\boldsymbol{k},\boldsymbol{q}}\Lambda^{n,\mu}\right)^\dagger \mathcal{U}_\mathcal{T} .$$

The time-reversed pairing field $\Delta_\mathcal{T}(\boldsymbol{k},\boldsymbol{q}) = \mathcal{U}_\mathcal{T}\,\Delta^*(-\boldsymbol{k},-\boldsymbol{q})\,\mathcal{U}_\mathcal{T}^T$ (1.26) can be simplified according to

[1] One has to apply the point group symmetry constraint similar to Eq.(1.27), apply the transformation behavior of the partner functions (1.32), sum over all group elements and apply the *grand orthogonality theorem* (cf. Sec.1.3.5).

$$\begin{aligned}\Delta_{\mathcal{T}}(\boldsymbol{k},\boldsymbol{q}) &= \sum_{n,\mu}\left(\Delta^{n,\mu}_{-\boldsymbol{q}}\right)^{*}\mathcal{U}_{\mathcal{T}}\left(\chi^{n,\mu}_{-\boldsymbol{k},-\boldsymbol{q}}\Lambda^{n,\mu}\right)^{T}\mathcal{U}^{*}_{\mathcal{T}}\mathcal{U}^{T}_{\mathcal{T}}\\ &\overset{(A.1)}{=}\sum_{n,\mu}\left(\Delta^{n,\mu}_{-\boldsymbol{q}}\right)^{*}\mathcal{U}_{\mathcal{T}}\left(\chi^{\bar{n},\mu}_{-\boldsymbol{k},\boldsymbol{q}}\Lambda^{\bar{n},\mu}\right)^{*}\\ &\overset{(A.9)}{=}\sum_{n,\mu}\left(\Delta^{n,\mu}_{-\boldsymbol{q}}\right)^{*}\left(\chi^{\bar{n},\mu}_{\boldsymbol{k},\boldsymbol{q}}\Lambda^{\bar{n},\mu}\right)^{\dagger}\mathcal{U}_{\mathcal{T}}\\ &=\sum_{n,\mu}\left(\Delta^{\bar{n},\mu}_{-\boldsymbol{q}}\right)^{*}\left(\chi^{n,\mu}_{\boldsymbol{k},\boldsymbol{q}}\Lambda^{n,\mu}\right)^{\dagger}\mathcal{U}_{\mathcal{T}}\,,\end{aligned}$$

and hence, the condition (A.1) has to hold in the presence of time-reversal symmetry. In the third line, we have inserted the anti-symmetry constraint

$$\Delta(\boldsymbol{k},\boldsymbol{q})=\sum_{n,\mu}\Delta^{n,\mu}_{\boldsymbol{q}}\left(\chi^{n,\mu}_{\boldsymbol{k},\boldsymbol{q}}\Lambda^{n,\mu}\right)^{\dagger}\mathcal{U}_{\mathcal{T}}=-\Delta^{T}(-\boldsymbol{k},\boldsymbol{q})=\sum_{n,\mu}\Delta^{n,\mu}_{\boldsymbol{q}}\mathcal{U}_{\mathcal{T}}\left(\chi^{n,\mu}_{-\boldsymbol{k},\boldsymbol{q}}\Lambda^{n,\mu}\right)^{*}\,. \tag{A.9}$$

A.2 Trilinear forms and sixth-order terms of the free energy

In section 1.3.5, the interaction contributions to the free energy up to fourth order have been computed. Here, we apply the same logic to derive the sixth-order terms. Due to the $U(1)$ symmetry constraint (1.42), a generic sixth-order term has to be of the form

$$\mathcal{F}^{(6)}_{int}\left[(\Delta^{n_0,\mu})^{*},\Delta^{n_0,\mu},\mathbf{0}\right]=v_{\mu_1\mu_2\mu_3\mu_4\mu_5\mu_6}(\Delta^{n_0,\mu_1})^{*}(\Delta^{n_0,\mu_2})^{*}(\Delta^{n_0,\mu_3})^{*}\Delta^{n_0,\mu_4}\Delta^{n_0,\mu_5}\Delta^{n_0,\mu_6}. \tag{A.10}$$

In this context, the central objects are the trilinear combinations

$$T^{n,i,l}=\Delta^{n_0,\mu_1}\Delta^{n_0,\mu_2}\Delta^{n_0,\mu_3}\,\lambda^{n,i,l}_{\mu_1\mu_2\mu_3}\,, \tag{A.11}$$

with the IRs n and its component $l=1,..,\dim(n)$ and possible multiplicities denoted by i. The respective tensors $\lambda^{n,i,l}_{\mu_1\mu_2\mu_3}$ are determined such that they satisfy the transformation condition

$$\lambda^{n,i,l}_{\nu_1\nu_2\nu_3}\,\mathcal{R}^{\dagger}_{n_0}(g)_{\nu_1\mu_1}\mathcal{R}^{\dagger}_{n_0}(g)_{\nu_2\mu_2}\mathcal{R}^{\dagger}_{n_0}(g)_{\nu_3\mu_3}=\mathcal{R}^{-1}_{n}(g)_{ll'}\,\lambda^{n,i,l'}_{\mu_1\mu_2\mu_3}\,, \tag{A.12}$$

and thus, the trilinear combinations transform according to

$$T^{n,i,l}=\mathcal{R}^{-1}_{n}(g)_{ll'}T^{n,i,l'}\,. \tag{A.13}$$

The occurring IRs n have to be part of the set $\{n_a,n_b,\dots\}$ that results from the decomposition

$$\Gamma_{n_0}\otimes\Gamma_{n_0}\otimes\Gamma_{n_0}=\#_{n_a}\Gamma_{n_a}\oplus\#_{n_b}\Gamma_{n_b}\oplus\dots\,,\qquad\qquad \#_{n_a},\#_{n_b}\in\mathbb{N}^{+}\,, \tag{A.14}$$

where $i = 1, .., \#_n$. Using the trilinear representation (A.11), the free energy (A.10) can be conveniently compressed to

$$\mathcal{F}^{(6)}_{int}\left[(\Delta^{n_0,\mu})^*, \Delta^{n_0,\mu}, \mathbf{0}\right] = v^{n',i',l'}_{n,i,l}\, T^{n,i,l}\, \left(T^{n',i',l'}\right)^* . \tag{A.15}$$

Upon application of the point group symmetry constraint (1.43), we obtain the condition for the interaction parameters

$$v^{n',i',l'}_{n,i,l} = \mathcal{R}^*_n(g)_{l\ell} v^{n',i',\ell'}_{n,i,\ell}\, \mathcal{R}_{n'}(g)_{l'\ell'} \qquad\qquad \forall g \in \mathcal{G}_p\,, \tag{A.16}$$

where we have used $\mathcal{R}^*_n(g) = \mathcal{R}_{\bar{n}}(g)$. The summation of Eq. (A.16) over all the group elements g and the subsequent application of the *grand orthogonality theorem* (1.47) yields

$$v^{n',i',l'}_{n,i,l} == \delta_{nn'}\delta_{ll'}\delta_{\ell\ell'}\frac{1}{d_n}\, v^{n,i',\ell'}_{n,i,\ell} \equiv \delta_{nn'}\delta_{ll'} v^{i,i'}_n\,.$$

Thus,—similarly to the quadratic and quartic terms—the sixth-order term diagonalizes with respect to the IRs n and becomes

$$\mathcal{F}^{(6)}_{int}\left[(\Delta^{n_0,\mu})^*, \Delta^{n_0,\mu}, \mathbf{0}\right] = \sum_n \sum_{i,i'} v^{i,i'}_n \sum_l T^{n,i,l}\, \left(T^{n,i',l}\right)^* . \tag{A.17}$$

Superconducting E_u order parameter of $\mathsf{D_{3d}}$ Let us consider a superconducting order parameter that belongs to the two-dimensional IR $n_0 = E_u$ of the point group $\mathsf{D_{3d}}$, see Tab.1.1. The corresponding bilinear and trilinear decompositions (A.14) read

$$\Gamma_{E_u} \otimes \Gamma_{E_u} = \Gamma_{A_{1g}} \oplus \Gamma_{A_{2g}} \oplus \Gamma_{E_g}\,, \qquad \Gamma_{E_u} \otimes \Gamma_{E_u} \otimes \Gamma_{E_u} = \Gamma_{A_{1u}} \oplus \Gamma_{A_{2u}} \oplus 3\Gamma_{E_u}\,. \tag{A.18}$$

The tensor elements $\lambda^{n,i,l}_{\mu_1\mu_2\mu_3}$ of the trinlinear form are determined via (A.12) with the results listed in table A.1. Explicitly, the sixth-order contribution to the free energy reads

$$\begin{aligned}
\mathcal{F}^{(6)}_{int} &= v_{A_{1u}} \left[\left(\Delta^{E_u,1}\right)^3 - 3\Delta^{E_u,1}\left(\Delta^{E_u,2}\right)^2\right]\left[\left(\Delta^{E_u,1}\right)^3 - 3\Delta^{E_u,1}\left(\Delta^{E_u,2}\right)^2\right]^* && \text{(A.19)}\\
&+ v_{A_{2u}} \left[3\left(\Delta^{E_u,1}\right)^2\Delta^{E_u,2} - \left(\Delta^{E_u,2}\right)^3\right]\left[3\left(\Delta^{E_u,1}\right)^2\Delta^{E_u,2} - \left(\Delta^{E_u,2}\right)^3\right]^* && \text{(A.20)}\\
&+ v_{E_u} \left[\left(\Delta^{E_u,1}\right)^2 + \left(\Delta^{E_u,2}\right)^2\right]\left[\left(\Delta^{E_u,1}\right)^2 + \left(\Delta^{E_u,2}\right)^2\right]^* \left[|\Delta^{E_u,1}|^2 + |\Delta^{E_u,2}|^2\right] && \text{(A.21)}\\
&= \nu_+ \mathsf{B}_0\left(\mathsf{B}_0^2 + 3\mathsf{B}_y^2\right) + \nu_- \mathsf{B}_z\left(\mathsf{B}_z^2 - 3\mathsf{B}_x^2\right) + v_{E_u}\mathsf{B}_0\left(\mathsf{B}_x^2 + \mathsf{B}_z^2\right)\,, && \text{(A.22)}
\end{aligned}$$

where we introduced $v_\pm = (v_{A_{1u}} \pm v_{A_{2u}})/2$ and the bilinear forms $\mathsf{B}_j = \left(\mathbf{\Delta}^{E_u}\right)^\dagger \tau^j \mathbf{\Delta}^{E_u}$. Upon decomposition of the order parameter $(\mathbf{\Delta}^{E_u})^T = \Delta_0 e^{\mathrm{i}\varphi_1}\left(\sin(\theta), \cos(\theta)e^{\mathrm{i}\delta\varphi}\right)$ with $\Delta_0 > 0$, $\varphi_1, \delta\varphi, \theta \in [0, 2\pi]$, the free energy can be rewritten as

$$\mathcal{F}^{(6)}_{int} = \Delta_0^6\left[v_+ + v_{E_u} - v_-\cos\left(6\theta\right) + \sin^2\left(\delta\varphi\right)\sin^2\left(2\theta\right)\left(3v_+ - v_{E_u} - 3v_-\cos\left(2\theta\right)\right)\right].$$

$\mathsf{D_{3d}}$	tensors $\lambda^{n,i,l}$	trilinear forms $T^{n,i,l}$
A_{1u}	$\lambda^{A_{1u},1,1}_{111} = -\lambda^{A_{1u},1,1}_{122} = -\lambda^{A_{1u},1,1}_{212} = -\lambda^{A_{1u},1,1}_{221} = 1$	$(\Delta^{E_u,1})^3 - 3\Delta^{E_u,1}(\Delta^{E_u,2})^2$
A_{2u}	$\lambda^{A_{2u},1,1}_{112} = \lambda^{A_{2u},1,1}_{121} = \lambda^{A_{2u},1,1}_{211} = -\lambda^{A_{2u},1,1}_{222} = 1$	$3(\Delta^{E_u,1})^2\Delta^{E_u,2} - (\Delta^{E_u,2})^3$
E_u	$\left(\lambda^{E_u,1,1}_{111} = \lambda^{E_u,1,1}_{221} = \lambda^{E_u,1,2}_{112} = \lambda^{E_u,1,2}_{222} = 1\right)$	$(\boldsymbol{\Delta}^{E_u})^2\boldsymbol{\Delta}^{E_u}$
	$\left(\lambda^{E_u,2,1}_{122} = -\lambda^{E_u,2,1}_{221} = -\lambda^{E_u,2,2}_{112} = \lambda^{E_u,2,2}_{211} = 1\right)$	$(0,0)$
	$\left(\lambda^{E_u,3,1}_{212} = -\lambda^{E_u,3,1}_{221} = -\lambda^{E_u,3,2}_{112} = \lambda^{E_u,3,2}_{121} = 1\right)$	$(0,0)$

Table A.1: Trilinear analysis for the IR $n_0 = E_u$ of the point group $\mathsf{D_{3d}}$. The tensors $\lambda^{n,i,l}$ associated with the IRs $n = \{A_{1u}, A_{2u}, E_u\}$ as they result from the condition (A.12). Only the shown elements are non-zero. Note that (A.18) explains the multiplicity $i = 1, 2, 3$ in the $n = E_u$ case. On the right column we have explicitly stated the corresponding trilinear combinations (A.11).

$\mathsf{D_{3d}}$	tensors $\lambda^{n,i,l}$	trilinear forms $T^{n,i,l}$
A_{1g}	$\lambda^{A_{1g},1,1}_{111} = -\lambda^{A_{1g},1,1}_{122} = -\lambda^{A_{1g},1,1}_{212} = -\lambda^{A_{1g},1,1}_{221} = 1$	$(\mathsf{C}^{E_g,1})^3 - 3\mathsf{C}^{E_g,1}(\mathsf{C}^{E_g,2})^2$
A_{2g}	$\lambda^{A_{2g},1,1}_{112} = \lambda^{A_{2g},1,1}_{121} = \lambda^{A_{2g},1,1}_{211} = -\lambda^{A_{2g},1,1}_{222} = 1$	$3(\mathsf{C}^{E_g,1})^2\mathsf{C}^{E_g,2} - (\mathsf{C}^{E_g,2})^3$
E_g	$\left(\lambda^{E_g,1,1}_{111} = \lambda^{E_g,1,1}_{221} = \lambda^{E_g,1,2}_{112} = \lambda^{E_g,1,2}_{222} = 1\right)$	$(\mathbf{C}^{E_g})^2\mathbf{C}^{E_g}$
	$\left(\lambda^{E_g,2,1}_{122} = -\lambda^{E_g,2,1}_{221} = -\lambda^{E_g,2,2}_{112} = \lambda^{E_g,2,2}_{211} = 1\right)$	$(0,0)$
	$\left(\lambda^{E_g,3,1}_{212} = -\lambda^{E_g,3,1}_{221} = -\lambda^{E_g,3,2}_{112} = \lambda^{E_g,3,2}_{121} = 1\right)$	$(0,0)$

Table A.2: Trilinear analysis for the IR $n_0 = E_g$ of the point group $\mathsf{D_{3d}}$.

Composite E_g order parameter of $\mathsf{D_{3d}}$ In this part, we consider a real two-dimensional IR $n_0 = E_g$ of the point group $\mathsf{D_{3d}}$, and for convenience, we denote the order parameter as $\mathsf{C}^{E_g,l}$. Then, the trilinear form reads

$$T^{n,i,\ell} = \mathsf{C}^{E_g,l_1}\mathsf{C}^{E_g,l_2}\mathsf{C}^{E_g,l_3}\,\lambda^{n,i,\ell}_{l_1l_2l_3}\,, \tag{A.23}$$

and with regards to Eq. (3.14) it is apt to determine $\lambda^{n,i,\ell}_{l_1l_2l_3}$ via

$$\mathcal{R}^{\dagger}_{E_g}(g)_{l_1l_1'}\mathcal{R}^{\dagger}_{E_g}(g)_{l_2l_2'}\mathcal{R}^{\dagger}_{E_g}(g)_{l_3l_3'}\lambda^{n,i,\ell}_{l_1'l_2'l_3'} = \mathcal{R}_n(g)_{\ell\ell'}\,\lambda^{n,i,\ell'}_{l_1l_2l_3}\,, \tag{A.24}$$

such that the trilinear transforms as $T^{n,i,l} = \mathcal{R}_n(g)_{\ell\ell'}T^{n,i,\ell'}$. In table A.2 we show the resulting association.

A.3 Lattice-compliant spatial functions

In section 2.2.1 we have derived the model Hamiltonian for the Bi_2Se_3 topological insulator family. The two important orbitals that reside close to the Fermi energy at the Γ- point have been found [84, 85] to transform according to the representation $E_{3g} \oplus E_{3u}$ of the crystal double group $\mathsf{D}'_{\mathsf{3d}}$, cf. table 2.2. With the transformation matrices 2.6 we want to determine the fully symmetry-compliant momentum functions that satisfy

$$\omega^{n,i,\mu}(\mathcal{R}_v^\dagger(g)\boldsymbol{k}) = \omega^{n,i,\mu'}(\boldsymbol{k})\mathcal{R}_n(g)_{\mu'\mu} \,, \tag{A.25}$$

with the vector representation reading $\mathcal{R}_v(g) = \mathcal{R}_{E_u}(g) \oplus \mathcal{R}_{A_{2u}}(g)$. The condition (A.25) does not depend on the properties of the associated fields such that the resulting classification can be used for both, the model Hamiltonian and the free energy expansion. For the D_{3d} (or the $\mathsf{D}'_{\mathsf{3d}}$ double group) we find spatial functions in the five symmetry channels A_{1g}, E_g, A_{1u}, A_{2u} and E_u which read

$$A_{1g}: \qquad f_{\boldsymbol{k}}^{A_{1g}} = \mathsf{d}_1^{A_{1g}} g_{x^2+y^2}(\tilde{\boldsymbol{k}}) + \mathsf{d}_2^{A_{1g}} 2\left(1 - \cos\left(\tilde{k}_z\right)\right) \tag{A.26}$$

$$A_{1u}: \qquad f_{\boldsymbol{k}}^{C_3} = R_1 g_y^{C_3}(\tilde{\boldsymbol{k}}) \tag{A.27}$$

$$A_{2u}: \qquad f_{\boldsymbol{k}}^{z} = v_z \sin\left(\tilde{k}_z\right) + R_2 g_x^{C_3}(\tilde{\boldsymbol{k}}) \tag{A.28}$$

$$E_g: \qquad \begin{pmatrix} f_{\boldsymbol{k}}^{E_g,1} \\ f_{\boldsymbol{k}}^{E_g,2} \end{pmatrix} = \sin\left(\tilde{k}_z\right) \begin{pmatrix} \mathsf{d}_{1a}^{E_g} g_y^{(1)}(\tilde{\boldsymbol{k}}) + \mathsf{d}_{1b}^{E_g} g_y^{(2)}(\tilde{\boldsymbol{k}}) \\ -\mathsf{d}_{1a}^{E_g} g_x^{(1)}(\tilde{\boldsymbol{k}}) - \mathsf{d}_{1b}^{E_g} g_x^{(2)}(\tilde{\boldsymbol{k}}) \end{pmatrix} + \mathsf{d}_2^{E_g} \cos\left(\tilde{k}_z\right) \begin{pmatrix} g_{x^2-y^2}(\tilde{\boldsymbol{k}}) \\ -g_{2xy}(\tilde{\boldsymbol{k}}) \end{pmatrix} \tag{A.29}$$

$$E_u: \qquad \begin{pmatrix} f_{\boldsymbol{k}}^{x} \\ f_{\boldsymbol{k}}^{y} \end{pmatrix} = \cos\left(\tilde{k}_z\right) \begin{pmatrix} \mathsf{d}_{1a}^{E_u} g_x^{(1)}(\tilde{\boldsymbol{k}}) + \mathsf{d}_{1b}^{E_u} g_x^{(2)}(\tilde{\boldsymbol{k}}) \\ \mathsf{d}_{1a}^{E_u} g_y^{(1)}(\tilde{\boldsymbol{k}}) + \mathsf{d}_{1b}^{E_u} g_y^{(2)}(\tilde{\boldsymbol{k}}) \end{pmatrix} + \mathsf{d}_2^{E_u} \sin\left(\tilde{k}_z\right) \begin{pmatrix} g_{2xy}(\tilde{\boldsymbol{k}}) \\ g_{x^2-y^2}(\tilde{\boldsymbol{k}}) \end{pmatrix}, \tag{A.30}$$

where the functions

$$\begin{aligned}
g_{2xy} &= \frac{8}{\sqrt{3}} \sin\left(\frac{\sqrt{3}}{2}\tilde{k}_y\right) \sin\left(\frac{\tilde{k}_x}{2}\right), & g_x^{(1)} &= \frac{2}{3} \cos\left(\frac{\sqrt{3}}{2}\tilde{k}_y\right) \sin\left(\frac{\tilde{k}_x}{2}\right) + \frac{2}{3} \sin\left(\tilde{k}_x\right), \\
g_{x^2-y^2} &= \frac{8}{3}\left(\cos\left(\frac{\sqrt{3}}{2}\tilde{k}_y\right) \cos\left(\frac{\tilde{k}_x}{2}\right) - \cos\left(\tilde{k}_x\right)\right), & g_y^{(1)} &= \frac{2}{\sqrt{3}} \sin\left(\frac{\sqrt{3}}{2}\tilde{k}_y\right) \cos\left(\frac{\tilde{k}_x}{2}\right), \\
g_{x^2+y^2} &= \frac{4}{3} - \frac{8}{9} \cos\left(\frac{3}{2}\tilde{k}_x\right) \cos\left(\frac{\sqrt{3}}{2}\tilde{k}_y\right) - \frac{4}{9} \cos\left(\sqrt{3}\tilde{k}_y\right), & g_x^{(2)} &= \frac{2}{3} \sin\left(\frac{3}{2}\tilde{k}_x\right) \cos\left(\frac{\sqrt{3}}{2}\tilde{k}_y\right), \\
g_x^{C_3} &= \frac{8}{3\sqrt{3}}\left(2\cos\left(\frac{3}{2}\tilde{k}_x\right) \sin\left(\frac{\sqrt{3}}{2}\tilde{k}_y\right) - \sin\left(\sqrt{3}\tilde{k}_y\right)\right), & g_y^{(2)} &= \frac{2}{3\sqrt{3}}\left(\cos\left(\frac{3}{2}\tilde{k}_x\right) \sin\left(\frac{\sqrt{3}}{2}\tilde{k}_y\right) + \sin\left(\sqrt{3}\tilde{k}_y\right)\right), \\
g_y^{C_3} &= 8\left(2\cos\left(\frac{\sqrt{3}}{2}\tilde{k}_y\right) \sin\left(\frac{\tilde{k}_x}{2}\right) - \sin\left(\tilde{k}_x\right)\right),
\end{aligned}$$

and the dimensionless momenta $\tilde{\boldsymbol{k}} = (k_x a, k_y a, k_z c)$ have been introduced. Note that the functions (A.26)-(A.30) reproduce the long wavelength limit shown in the main part (2.11)-(2.15) with $v_0 = \mathsf{d}_{1a}^{E_u} + \mathsf{d}_{1b}^{E_u}$ and $2\mathsf{d}_1^{E_g} = \mathsf{d}_{1a}^{E_g} + \mathsf{d}_{1b}^{E_g}$.

B Appendix B

Derivation of the E_u Ginzburg-Landau parameters

In this part, we derive the Ginzburg-Landau parameters for the two-component E_u pairing state, cf. Sec. 2.3.3. We start from the generalized BCS Hamiltonian

$$\hat{\mathcal{H}} = V \sum_{\boldsymbol{k}} (\hat{\boldsymbol{c}}^\dagger_{\boldsymbol{k}})^T h(\boldsymbol{k}) \hat{\boldsymbol{c}}_{\boldsymbol{k}} + V \sum_{\boldsymbol{kq}} \left((\hat{\boldsymbol{c}}^\dagger_{\boldsymbol{k}+\frac{\boldsymbol{q}}{2}})^T \Delta(\boldsymbol{k}, \boldsymbol{q}) \hat{\boldsymbol{c}}^\dagger_{-\boldsymbol{k}+\frac{\boldsymbol{q}}{2}} + H.c. \right) , \tag{B.1}$$

where the single-particle Hamiltonian has been derived in (2.16). We use the field integral approach, where the partition function

$$Z = \int \mathcal{D}\left[c, \bar{c}\right] \, \exp\left(-\beta \mathcal{S}\left[c, \bar{c}\right]\right) \tag{B.2}$$

is evaluated in the basis of coherent states. In this basis the former fermionic operators $\hat{c}, \hat{c}^\dagger$ directly become Graßman fields $c, \bar{c}$ which necessarily respect the Graßman algebra [40]. The integration in (B.2) involves all possible field configurations with the integration measure reading $\mathcal{D}[c, \bar{c}] = \lim_{N\to\infty} \prod_{i=1}^{N} d(c_i, \bar{c}_i)$. The exponent consists of the inverse temperature $\beta = T^{-1}$, and the action in imaginary time τ representation

$$\mathcal{S}\left[c, \bar{c}, \Delta, \Delta^*\right] = T \int_\tau \left(\int_{\boldsymbol{r}} \bar{\boldsymbol{c}}^T(\boldsymbol{r}, \tau) \partial_\tau \sigma^0 \mathfrak{s}^0 \boldsymbol{c}(\boldsymbol{r}, \tau) + \mathcal{H}(c, \bar{c}, \Delta, \Delta^*, \tau) \right) ,$$

with the real-space Hamiltonian function $\mathcal{H}(c, \bar{c}, \Delta, \Delta^*, \tau)$ deduced from (B.1). Additionally, we apply a magnetic field via a minimal coupling $-i\partial_{\boldsymbol{r}} \to -i\partial_{\boldsymbol{r}} - e\boldsymbol{A}$ method in real-space, and by a Zeeman coupling $\mu_0 \boldsymbol{B} \cdot \boldsymbol{\mathfrak{s}}$. The additional term $h^{\boldsymbol{A}}$ in the Hamiltonian results from $h(\boldsymbol{k}) \to h(\boldsymbol{k}) + h^{\boldsymbol{A}}(k, k')$. Then, the corresponding action becomes

$$\begin{aligned} \mathcal{S}\left[c, c^*, \Delta, \Delta^*\right] = V \sum_{k,k'} \bar{\boldsymbol{c}}^T_k \left(\left\{ -i\omega_n \sigma^0 \mathfrak{s}^0 + h(\boldsymbol{k}) + \mu_0 \boldsymbol{B} \cdot \boldsymbol{\mathfrak{s}} \sigma^0 \right\} \delta_{k,k'} + h^{\boldsymbol{A}}(k, k') \right) \boldsymbol{c}_{k'} \\ + V \sum_{k,k'} \left(\bar{\boldsymbol{c}}^T_k \Delta(\frac{k-k'}{2}, k+k') \boldsymbol{c}^*_{k'} + H.c. \right) + \frac{V}{g_{E_u}} \sum_q \sum_\mu |\Delta^{E_u,\mu}_q|^2, \end{aligned} \tag{B.3}$$

where $k = (\omega_n, \boldsymbol{k})$ and $q = (\nu_m, \boldsymbol{q})$ comprises momenta $\boldsymbol{k}$ and $\boldsymbol{q}$ together with the fermionic $\omega_n = (2n+1)\pi T$ and bosonic $\nu_m = 2m\pi T$ Matsubara frequencies.[1]The second line in (B.3) originates from the Hubbard-Stratonovich decoupling of the BCS interaction Hamiltonian (A.2). In the course of this procedure, the new paring field $\Delta(k,q) = \sum_\mu \Delta_q^{E_u,\mu}(\chi_{\boldsymbol{k},\boldsymbol{q}}^{E_u,\mu}\Lambda^{E_u,\mu})^\dagger$ gets associated with $\Delta_q^{E_u,\mu} \sim \langle \hat{\mathbf{c}}_{-k+\frac{q}{2}}^T (\chi_{\boldsymbol{k},\boldsymbol{q}}^{E_u,\mu}\lambda^{E_u,\mu})\, \hat{\boldsymbol{c}}_{k+\frac{q}{2}}\rangle$. In a first step, we switch into the pseudo-spin band basis $\boldsymbol{\psi}_k = (\boldsymbol{\psi}_{+,k}^c, \boldsymbol{\psi}_{-,k}^c, \boldsymbol{\psi}_{+,k}^v, \boldsymbol{\psi}_{-,k}^v) = U_b^\dagger(\boldsymbol{k})\boldsymbol{c}_{\boldsymbol{k}}$ (cf. Eq. 2.18) yielding

$$\begin{aligned}\mathcal{S}\left[\psi,\bar{\psi},\Delta,\Delta^*\right] = V\sum_{k,k'}\bar{\boldsymbol{\psi}}_k^T\left(\left\{-i\omega_n\tilde{\sigma}^0\tilde{\mathfrak{s}}^0 + h_b(\boldsymbol{k}) + h_b^{\boldsymbol{B}}(k)\right\}\delta_{k,k'} + h_b^{\boldsymbol{A}}(k,k')\right)\boldsymbol{\psi}_{k'} \\ + V\sum_{k,k'}\left(\bar{\boldsymbol{\psi}}_k^T\Delta_b(\frac{k-k'}{2},k+k')\bar{\boldsymbol{\psi}}_{k'} + H.c.\right) + \frac{V}{g_{E_u}}\sum_q|\boldsymbol{\Delta}_q^{E_u}|^2 \qquad \text{(B.4)}\end{aligned}$$

with

$$\begin{aligned} h_b^{\boldsymbol{A}}(k,k') &= U_b^\dagger(\boldsymbol{k})h^{\boldsymbol{A}}(k,k')U_b(\boldsymbol{k}')\,, & \Delta_b(\frac{k-k'}{2},k+k') &= U_b^\dagger(\boldsymbol{k})\Delta(\frac{k-k'}{2},k+k')U_b^*(\boldsymbol{k}'),\\ h_b^{\boldsymbol{B}}(k) &= U_b^\dagger(\boldsymbol{k})\mu_0\boldsymbol{B}\cdot\mathfrak{s}\sigma^0U_b(\boldsymbol{k})\,, & h_b(\boldsymbol{k}) &= \mathrm{diag}(E_{\boldsymbol{k}}^+,E_{\boldsymbol{k}}^+,E_{\boldsymbol{k}}^-,E_{\boldsymbol{k}}^-).\end{aligned}$$

Since the Cu doping [92] pushes the chemical potential into the conduction band ($\mu > |M_0|$), we focus only on the conduction band subspace $\boldsymbol{\psi}_k^{cc} = (\boldsymbol{\psi}_{+,k}^c, \boldsymbol{\psi}_{-,k}^c)$ in the following. More formally, we assume that the valence band is far away from the Fermi surface, and that there is no substantial coupling between the valence and the conduction band. Then, we extract the corresponding pairing field $\Delta_{cc}(k,q)$ from $\Delta_b(k,q) = \Delta_{cc}(k,q)\mathrm{i}\tilde{\mathfrak{s}}^y\frac{\tilde{\sigma}^0+\tilde{\sigma}^z}{2} + \dots$. Furthermore, we switch into Nambu space with the Nambu spinor $\boldsymbol{\psi}_k^{\mathrm{Nb}} = (\boldsymbol{\psi}_k^{cc}, \mathrm{i}\tilde{\mathfrak{s}}^y\bar{\boldsymbol{\psi}}_{-k}^{cc})^T$ where the action (B.4) reads

$$\mathcal{S}\left[\psi,\bar{\psi},\Delta,\Delta^*\right] = \frac{V}{g_{E_u}}\sum_q|\boldsymbol{\Delta}_q^{E_u}|^2 - \frac{V}{2}\sum_{k,k'}\left(\boldsymbol{\psi}_k^{\mathrm{Nb}}\right)^\dagger\mathcal{G}_{k,k'}^{-1}[\boldsymbol{A}]\,\boldsymbol{\psi}_{k'}^{\mathrm{Nb}}, \qquad \text{(B.5)}$$

and the Green's function matrix becomes

$$\begin{aligned}\mathcal{G}_{k,k'}^{-1}[\boldsymbol{A}] = \left\{i\omega_n\tilde{\tau}^0\tilde{\mathfrak{s}}^0 - E_{\boldsymbol{k}}^+\tilde{\tau}^z\tilde{\mathfrak{s}}^0 - \tilde{\tau}^0h_{cc}^{\boldsymbol{B}}(k)\right\}\delta_{k,k'} - \tilde{\tau}^0h_{cc}^{\boldsymbol{A}}(k,k') \\ - 2\tilde{\tau}^+\Delta_{cc}(\frac{k+k'}{2},k-k') - 2\tilde{\tau}^-\Delta_{cc}^\dagger(\frac{k+k'}{2},-k+k')\,. \qquad \text{(B.6)}\end{aligned}$$

Pairing state The corresponding pairing field in the pseudo-spin basis reads

$$\Delta_{cc}(k,q) = \left(d_{k,q}^{0,E_u} + \boldsymbol{d}_{k,q}^{E_u}\cdot\left(\tilde{\mathfrak{s}}^x,\tilde{\mathfrak{s}}^y,\tilde{\mathfrak{s}}^z\right)\right)\mathrm{i}\tilde{\mathfrak{s}}^y\,.$$

The complete d-functions read

$$\frac{-\mathrm{i}d_{k,q}^{0,E_u}}{\mathrm{sign}(M_{\boldsymbol{2}})} = F_{\boldsymbol{k},\boldsymbol{q}}^{x,-}\Delta_{\boldsymbol{q}}^{E_u,1} + F_{\boldsymbol{k},\boldsymbol{q}}^{y,-}\Delta_{\boldsymbol{q}}^{E_u,2} + F_{\boldsymbol{k},\boldsymbol{q}}^{C_3}\left(\hat{f}_{\boldsymbol{2}}^z\hat{f}_{\boldsymbol{1}}^y - \hat{f}_{\boldsymbol{1}}^z\hat{f}_{\boldsymbol{2}}^y\right)\Delta_{\boldsymbol{q}}^{E_u,1} - F_{\boldsymbol{k},\boldsymbol{q}}^{C_3}\left(\hat{f}_{\boldsymbol{2}}^z\hat{f}_{\boldsymbol{1}}^x - \hat{f}_{\boldsymbol{1}}^z\hat{f}_{\boldsymbol{2}}^x\right)\Delta_{\boldsymbol{q}}^{E_u,2} \qquad \text{(B.7)}$$

[1]We use the Fourier transforms $c(\boldsymbol{r},\tau) = \sum_{n,\boldsymbol{k}} e^{-i(\omega_n\tau - \boldsymbol{r}\boldsymbol{k})}c_k$ and $c_k = \frac{T}{V}\int_{\boldsymbol{r},\tau} e^{i(\omega_n\tau-\boldsymbol{r}\boldsymbol{k})}c(\boldsymbol{r},\tau)$.

$$\frac{\boldsymbol{d}^{E_u}_{k,q}}{\mathrm{sign}(M_{\mathbf{2}})} = \begin{pmatrix} F^{z,+}_{\boldsymbol{k},\boldsymbol{q}}\Delta^{E_u,2}_q \\ -F^{z,+}_{\boldsymbol{k},\boldsymbol{q}}\Delta^{E_u,1}_q \\ F^{y,+}_{\boldsymbol{k},\boldsymbol{q}}\Delta^{E_u,1}_q - F^{x,+}_{\boldsymbol{k},\boldsymbol{q}}\Delta^{E_u,2}_q \end{pmatrix} + F^{C_3}_{\boldsymbol{k},\boldsymbol{q}}\left(\frac{M_{\mathbf{1}}M_{\mathbf{2}}}{|M_{\mathbf{1}}M_{\mathbf{2}}|}\left(1+|\hat{M}_{\mathbf{1}}|\right)\left(1+|\hat{M}_{\mathbf{2}}|\right) - \hat{\boldsymbol{f}}_{\mathbf{1}}\cdot\hat{\boldsymbol{f}}_{\mathbf{2}}\right)\begin{pmatrix}\Delta^{E_u,1}_q \\ \Delta^{E_u,2}_q \\ 0\end{pmatrix}$$
$$+ F^{C_3}_{\boldsymbol{k},\boldsymbol{q}}\left(\left(\hat{f}^x_{\mathbf{1}}\Delta^{E_u,1}_q + \hat{f}^y_{\mathbf{1}}\Delta^{E_u,2}_q\right)\hat{\boldsymbol{f}}_{\mathbf{2}} + \left(\hat{f}^x_{\mathbf{2}}\Delta^{E_u,1}_q + \hat{f}^y_{\mathbf{2}}\Delta^{E_u,2}_q\right)\hat{\boldsymbol{f}}_{\mathbf{1}}\right) \tag{B.8}$$

where for brevity, we use the notation $\mathbf{1}\hat{=}\boldsymbol{k}+\frac{\boldsymbol{q}}{2}$, $\mathbf{2}\hat{=}\boldsymbol{k}-\frac{\boldsymbol{q}}{2}$ together with

$$F^{j,\pm}_{\boldsymbol{k},\boldsymbol{q}} = \left(\alpha^+_{\mathbf{1}}\alpha^-_{\mathbf{2}} + \alpha^-_{\mathbf{1}}\alpha^+_{\mathbf{2}}\right)\frac{\left(1+|\hat{M}_{\mathbf{2}}|\right)\mathrm{sign}(M_{\mathbf{2}})\hat{f}^j_{\mathbf{1}} \pm \left(1+|\hat{M}_{\mathbf{1}}|\right)\mathrm{sign}(M_{\mathbf{1}})\hat{f}^j_{\mathbf{2}}}{4\sqrt{1+|\hat{M}_{\mathbf{1}}|}\sqrt{1+|\hat{M}_{\mathbf{2}}|}},$$
$$F^{C_3}_{\boldsymbol{k},\boldsymbol{q}} = \left(\alpha^+_{\mathbf{1}}\alpha^+_{\mathbf{2}} + \alpha^-_{\mathbf{1}}\alpha^-_{\mathbf{2}}\right)\frac{1}{4\sqrt{1+|\hat{M}_{\mathbf{1}}|}\sqrt{1+|\hat{M}_{\mathbf{2}}|}}.$$

It is useful to decompose the d-functions according to

$$\boldsymbol{d}^{E_u}_{k,q} = \sum_\mu \Delta^{E_u,\mu}_q \boldsymbol{d}^{E_u,\mu}_{\boldsymbol{k},\boldsymbol{q}}, \qquad\qquad d^{0,E_u}_{\boldsymbol{k},\boldsymbol{q}} = \sum_\mu \Delta^{E_u,\mu}_q d^{0,E_u,\mu}_{\boldsymbol{k},\boldsymbol{q}}. \tag{B.9}$$

Effective action The Graßmann Nambu fields in (B.5) are bilinear and can, in principle, be integrated out. Yet, the components of the Nambu spinor $\boldsymbol{\psi}^{\mathrm{Nb}}_k = (\boldsymbol{\psi}^{cc}_k, \mathrm{i}\tilde{\mathfrak{s}}^y\bar{\boldsymbol{\psi}}^{cc}_{-k})$ are not independent variables. In the box below, we demonstrate the integration.

The Graßmann integration can be carried out upon usage of the integral $\int d\boldsymbol{\eta}\exp(-\frac{1}{2}\boldsymbol{\eta}^T A\boldsymbol{\eta}) = \sqrt{\det A}$ with a quadratic matrix A and Graßmann variables $\eta, \bar{\eta}$ [172, 173]. Note that for a singlet pairing state, one can directly apply the integral $\int d\left(\boldsymbol{\eta},\bar{\boldsymbol{\eta}}\right)\exp\left(-\bar{\boldsymbol{\eta}}^T A\boldsymbol{\eta}\right) = \det A$. Noting that the 'conjugated' Nambu spinor in (B.5) can be expressed by the 'non-conjugated' one via $(\boldsymbol{\psi}^{\mathrm{Nb}}_k)^\dagger = (\boldsymbol{\psi}^{\mathrm{Nb}}_{-k})^T\mathrm{i}\tilde{\mathfrak{s}}^y\tilde{\tau}^x \equiv (\boldsymbol{\psi}^{\mathrm{Nb}}_{k'})^T O_{k'k}$ with the matrix $O_{k'k} = \mathrm{i}\tilde{\tau}^x\tilde{\mathfrak{s}}^y\delta_{k',-k}$. Then, the above integral can be used which leads to $\int d\boldsymbol{\psi}^{\mathrm{Nb}}\exp\Big(-\frac{1}{2}(\boldsymbol{\psi}^{\mathrm{Nb}})^T\Big(-\beta\tilde{\mathcal{G}}^{-1}[\boldsymbol{A}]\Big)\boldsymbol{\psi}^{\mathrm{Nb}}\Big) = \sqrt{\det(-\beta\tilde{\mathcal{G}}^{-1}[\boldsymbol{A}])}$ with $\tilde{\mathcal{G}}^{-1}[\boldsymbol{A}] = O\mathcal{G}^{-1}[\boldsymbol{A}]$, see (B.10). The additional constant in (B.11) vanishes since $\mathrm{tr}\log\left(O\right) = \log\det\left(O\right) = 0$. The zero results from $\det\left(\mathrm{i}\tilde{\tau}^x\tilde{\mathfrak{s}}^y\right) = 1$, and the internal k structure of the matrix O which leads to $\det\left(O\right) = \det\left(\mathrm{i}\tilde{\tau}^x\tilde{\mathfrak{s}}^y\right)\det^{2(N_1+N_2+N_3)}\begin{pmatrix}0 & \mathrm{i}\tilde{\tau}^x\tilde{\mathfrak{s}}^y \\ \mathrm{i}\tilde{\tau}^x\tilde{\mathfrak{s}}^y & 0\end{pmatrix} = 1$ where $k_i = -k_{N_1},\ldots,k_{N_i}$. Including the Matsubara summation gives the same structure and it still holds $\det\left(O\right) = 1$.

The resulting effective action becomes

$$\mathcal{S}\left[\Delta,\Delta^*\right] = \frac{V}{g_{E_u}}\sum_q|\boldsymbol{\Delta}^{E_u}_q|^2 - \frac{T}{2}\mathrm{tr}\log\left(-\beta O\mathcal{G}^{-1}[\boldsymbol{A}]\right), \tag{B.10}$$
$$= \frac{V}{g_{E_u}}\sum_q|\boldsymbol{\Delta}^{E_u}_q|^2 - \frac{T}{2}\mathrm{tr}\log\left(O\right) - \frac{T}{2}\mathrm{tr}\log\left(-\beta\mathcal{G}^{-1}[\boldsymbol{A}]\right). \tag{B.11}$$

The action (B.11) encapsulates the full microscopic information, and will be expanded around T_c in the next section. For later convenience, we derive the BCS mean-field equations from (B.11) which

[using $\Delta_q^{E_u,\mu} = \Delta^\mu \delta_{q,0}$] read

$$\frac{\delta \mathcal{S}}{\delta \bar{\Delta}_q^{E_u,\mu}}\Big|_{\Delta_q^{E_u,\mu}=\Delta^\mu\delta_{q,0}} = 0 = \frac{V}{g_{E_u}}\Delta^\mu + T\sum_{k,k'} \mathrm{tr}\left(\mathcal{G}_{k,k}[\boldsymbol{A}]\tilde{\tau}^- \boldsymbol{d}_{k,0}^{E_u,\mu}\cdot\tilde{\mathfrak{s}}\right) . \tag{B.12}$$

Useful relations and identities For clarity we use $\bar{\Delta}_q^{E_u,\mu} := (\Delta_q^{E_u,\mu})^*$ and $\bar{\boldsymbol{d}}_{k,q}^{E_u} := (\boldsymbol{d}_{k,q}^{E_u})^*$ in the following. The upcoming equations can be conveniently expressed via the functions

$$\begin{aligned} D_{\boldsymbol{k},\boldsymbol{q}}^{(\{0,z\})} &= \frac{1}{2}\left(\left(\boldsymbol{d}_{\boldsymbol{k},\boldsymbol{q}}^{E_u,1}\right)^2 \pm \left(\boldsymbol{d}_{\boldsymbol{k},\boldsymbol{q}}^{E_u,2}\right)^2 - \left(\left(d_{\boldsymbol{k},\boldsymbol{q}}^{0,E_u,1}\right)^2 \pm \left(d_{\boldsymbol{k},\boldsymbol{q}}^{0,E_u,2}\right)^2\right)\right) , \\ D_{\boldsymbol{k},\boldsymbol{q}}^{(x)} &= -\boldsymbol{d}_{\boldsymbol{k},\boldsymbol{q}}^{E_u,1}\cdot\boldsymbol{d}_{\boldsymbol{k},\boldsymbol{q}}^{E_u,2} + d_{\boldsymbol{k},\boldsymbol{q}}^{0,E_u,1} d_{\boldsymbol{k},\boldsymbol{q}}^{0,E_u,2} \\ \boldsymbol{D}_{\boldsymbol{k},\boldsymbol{q}}^{(y)} &= \boldsymbol{d}_{\boldsymbol{k},\boldsymbol{q}}^{E_u,1}\times\boldsymbol{d}_{\boldsymbol{k},\boldsymbol{q}}^{E_u,2} + \mathsf{i}\left(d_{\boldsymbol{k},\boldsymbol{q}}^{0,E_u,2}\boldsymbol{d}_{\boldsymbol{k},\boldsymbol{q}}^{E_u,1} - d_{\boldsymbol{k},\boldsymbol{q}}^{0,E_u,1}\boldsymbol{d}_{\boldsymbol{k},\boldsymbol{q}}^{E_u,2}\right) , \end{aligned} \tag{B.13}$$

where it holds $\left(\boldsymbol{D}_{\boldsymbol{k},\boldsymbol{q}}^{(y)}\right)^2 = \left(D_{\boldsymbol{k},\boldsymbol{q}}^{(0)}\right)^2 - \left(D_{\boldsymbol{k},\boldsymbol{q}}^{(z)}\right)^2 - \left(D_{\boldsymbol{k},\boldsymbol{q}}^{(x)}\right)^2$. In case of zero external momentum $\boldsymbol{q} = 0$, the expressions simplify to

$$D_{\boldsymbol{k},\boldsymbol{0}}^{(\{0,z\})} = \frac{1\pm 1}{2} + \frac{1}{2}\left(\left(\hat{f}_{\mathbf{k}}^{C_3}\right)^2 - 1\right)\left(\hat{M}_{\mathbf{k}}^2 \pm \hat{M}_{\mathbf{k}}^2 + \left(\hat{f}_{\mathbf{k}}^{x}\right)^2 \pm \left(\hat{f}_{\mathbf{k}}^{y}\right)^2\right) \tag{B.14}$$

$$D_{\boldsymbol{k},\boldsymbol{0}}^{(x)} = \hat{f}_{\mathbf{k}}^{x}\hat{f}_{\mathbf{k}}^{y}\left(1 - \left(\hat{f}_{\mathbf{k}}^{C_3}\right)^2\right) \tag{B.15}$$

$$\left(\boldsymbol{D}_{\boldsymbol{k},\boldsymbol{0}}^{(y)}\right)^2 = \left(\left(\hat{f}_{\mathbf{k}}^{z}\right)^2\left(1 - \left(\hat{f}_{\mathbf{k}}^{C_3}\right)^2\right) + \left(\hat{f}_{\mathbf{k}}^{C_3}\right)^2\right)\left(\hat{\boldsymbol{f}}_{\mathbf{k}}^2 + \hat{M}_{\mathbf{k}}^2\left(\hat{f}_{\mathbf{k}}^{C_3}\right)^2\right) ,$$

and we can deduce the properties

$$\int_{\boldsymbol{k}} D_{\boldsymbol{k},\boldsymbol{0}}^{(z)} H_{\boldsymbol{k}} = \int_{\boldsymbol{k}} D_{\boldsymbol{k},\boldsymbol{0}}^{(x)} H_{\boldsymbol{k}} = 0 , \quad \int_{\boldsymbol{k}} \left(D_{\boldsymbol{k},\boldsymbol{0}}^{(z)}\right)^2 H_{\boldsymbol{k}} = \int_{\boldsymbol{k}} \left(D_{\boldsymbol{k},\boldsymbol{0}}^{(x)}\right)^2 H_{\boldsymbol{k}} , \quad \int_{\boldsymbol{k}} \left(D_{\boldsymbol{k},\boldsymbol{0}}^{(z)}\right)^3 H_{\boldsymbol{k}} = -\int_{\boldsymbol{k}} D_{\boldsymbol{k},\boldsymbol{0}}^{(z)}\left(D_{\boldsymbol{k},\boldsymbol{0}}^{(x)}\right)^2 , \tag{B.16}$$

valid for a function $H_{\boldsymbol{k}} = H_{\boldsymbol{k}}\left(\left(\hat{f}_{\boldsymbol{k}}^{x}\right)^2 + \left(\hat{f}_{\boldsymbol{k}}^{y}\right)^2, \left(\hat{f}_{\boldsymbol{k}}^{z}\right)^2, \hat{f}_{\boldsymbol{k}}^{C_3}, \hat{M}_{\boldsymbol{k}}\right)$ that transforms trivially under a C_{3z} rotation.[2]

[2] To check the identities, first note that any integral that is odd in k_x vanishes. Then, considering the transformation under a C_{3z} rotation (2.5) of the function $(\hat{f}_{\boldsymbol{k}}^{x})^2 - (\hat{f}_{\boldsymbol{k}}^{y})^2$ and the square thereof, one finds the other relations.

B.1 Ginzburg-Landau parameters

A Ginzburg-Landau theory aims to describe a system around a second-order phase transition where the order parameter is assumed to be small. To this end, we decompose the inverse Green's function matrix (B.6) according to $\mathcal{G}^{-1}_{k,k'}[\boldsymbol{A}] = G^{-1}_{k,k'}[\boldsymbol{A}] + \hat{\Delta}_{k,k'}$ with

$$\begin{aligned} G^{-1}_{k,k'}[\boldsymbol{A}] &\equiv \left(G^0_k\right)^{-1}\delta_{kk'} + \left(G^B_k\right)^{-1}[\boldsymbol{B}]\delta_{kk'} + \left(G^A\right)^{-1}_{k,k'}[\boldsymbol{A}]\,, \\ \hat{\Delta}_{k,k'} &\equiv -2\tilde{\tau}^+\Delta_{cc}(\frac{k+k'}{2}, k-k') - 2\tilde{\tau}^-\Delta^\dagger_{cc}(\frac{k+k'}{2}, -k+k')\,, \end{aligned} \tag{B.17}$$

and

$$\left(G^0_k\right)^{-1} = i\omega_n\tilde{\tau}^0\tilde{\mathfrak{s}}^0 - E^+_{\boldsymbol{k}}\tilde{\tau}^z\tilde{\mathfrak{s}}^0\,, \qquad \left(G^B_k\right)^{-1}[\boldsymbol{B}] = -\tilde{\tau}^0 h^{\boldsymbol{B}}_{cc}(\boldsymbol{k})\,, \qquad \left(G^A\right)^{-1}_{k,k'}[\boldsymbol{A}] = -\tilde{\tau}^0 h^{\boldsymbol{A}}_{cc}(\boldsymbol{k},\boldsymbol{k}')\,.$$

Using $\log\left(1+A\right) = -\sum_{j=1}^{\infty}(-A)^j/j$ we expand the action (B.11) for small Δ, Δ^* which leads to

$$\mathcal{S}\left[\Delta,\Delta^*\right] = \frac{V}{g_{E_u}}\sum_q |\boldsymbol{\Delta}^{E_u}_q|^2 + \mathcal{S}_0 - \frac{T}{2}\mathrm{tr}\log\left(1+G[\boldsymbol{A}]\hat{\Delta}\right) \approx \frac{V}{g_{E_u}}\sum_q |\boldsymbol{\Delta}^{E_u}_q|^2 + \mathcal{S}_0 + \sum_{j\in 2\mathbb{N}}\frac{T}{2j}\mathrm{tr}\left(G[\boldsymbol{A}]\hat{\Delta}\right)^j \tag{B.18}$$

with $\mathcal{S}_0 = -\frac{T}{2}\mathrm{tr}\log\left(-\beta G^{-1}[\boldsymbol{A}]\right)$ describing the normal state properties. The internal Nambu structure forces the odd expansion powers to vanish. To calculate the Green's function matrix $G[\boldsymbol{A}]$ from (B.17) we treat the magnetic field as a small perturbation which yields

$$\begin{aligned} G[\boldsymbol{A}] &= \left(\left(G^0\right)^{-1}\left\{\mathbb{1} + G^0\left(G^B\right)^{-1}[\boldsymbol{B}] + G^0\left(G^A\right)^{-1}[\boldsymbol{A}]\right\}\right)^{-1} \\ &= \left\{\mathbb{1} + G^0\left(G^B\right)^{-1}[\boldsymbol{B}] + G^0\left(G^A\right)^{-1}[\boldsymbol{A}]\right\}^{-1}G^0 \\ &\approx G^0 - G^0\left(G^B\right)^{-1}[\boldsymbol{B}]G^0 - G^0\left(G^A\right)^{-1}[\boldsymbol{A}]G^0\,, \end{aligned} \tag{B.19}$$

with $G^0_k = \left(\begin{smallmatrix}\mathrm{g}_k & 0\\ 0 & -\mathrm{g}_{-k}\end{smallmatrix}\right)\tilde{\mathfrak{s}}^0$ and $\mathrm{g}_k = (\mathrm{i}\omega_n - E^+_{\boldsymbol{k}})^{-1}$. Thus, the quadratic term in (B.18) can be decomposed into $\mathcal{S}^{(2)} = \mathcal{S}^{(2)}_0 + \mathcal{S}^{(2)}_B + \mathcal{S}^{(2)}_A$ with

$$\mathcal{S}^{(2)}_0 = \frac{V}{g_{E_u}}\sum_q |\boldsymbol{\Delta}^{E_u}_q|^2 + \frac{T}{4}\mathrm{tr}\left(G^0\hat{\Delta}G^0\hat{\Delta}\right)\,, \qquad \mathcal{S}^{(2)}_B = -\frac{T}{2}\mathrm{tr}\left(G^0\hat{\Delta}G^0\left(G^B\right)^{-1}[\boldsymbol{B}]G^0\hat{\Delta}\right)\,, \tag{B.20}$$

$$\mathcal{S}^{(2)}_A = -\frac{T}{2}\mathrm{tr}\left(G^0\hat{\Delta}G^0\left(G^A\right)^{-1}[\boldsymbol{A}]G^0\hat{\Delta}\right)\,, \tag{B.21}$$

where contributions of the order $\mathcal{O}(\boldsymbol{A}^2)$ have been neglected.

B.1.1 Non-magnetic contributions

In the following, we will subsequently study the individual contributions, beginning with the quadratic non-magnetic contributions. Here, the trace can be evaluated according to

$$\frac{T}{4}\mathrm{tr}\left(G^0\hat{\Delta}G^0\hat{\Delta}\right) = -4T\sum_{k,q}\mathrm{g}_{k+\frac{q}{2}}\mathrm{g}_{-k+\frac{q}{2}}\left(d^{0,E_u}_{\boldsymbol{k},\boldsymbol{q}}\bar{d}^{0,E_u}_{\boldsymbol{k},\boldsymbol{q}} + \boldsymbol{d}^{E_u}_{\boldsymbol{k},\boldsymbol{q}}\cdot\bar{\boldsymbol{d}}^{E_u}_{\boldsymbol{k},\boldsymbol{q}}\right) = -\frac{4}{T}\sum_{\boldsymbol{k},q}\eta_{\boldsymbol{k},\boldsymbol{q}}\sum_{j=0,x,z}\bar{\boldsymbol{\Delta}}^{E_u}_{q}\tau^j D^{(j)}_{\boldsymbol{k},\boldsymbol{q}}\boldsymbol{\Delta}^{E_u}_{q} \tag{B.22}$$

with $\eta_{k,q} = T^2\sum_{\omega_n}\mathrm{g}_{k+\frac{q}{2}}\mathrm{g}_{-k+\frac{q}{2}}$. To determine the gradient terms, we expand $\eta_{k,q}\approx\eta_{\boldsymbol{k},0}+\Sigma^{ij}_{\boldsymbol{k}}\tilde{q}_i\tilde{q}_j$ where we are mostly interested in the second derivatives. Due to the smallness of T_c, the derivatives $\partial_{q_i}\eta_{k,q}$ yield a factor $1/T$ which will yield the respective dominant contribution. It holds

$$\eta_{k,q} = \frac{T}{2}\frac{\tanh\left(\frac{E^+_{\boldsymbol{k}+\frac{\boldsymbol{q}}{2}}}{2T}+\frac{\mathrm{i}\nu_m}{4T}\right)+\tanh\left(\frac{E^+_{\boldsymbol{k}-\frac{\boldsymbol{q}}{2}}}{2T}+\frac{\mathrm{i}\nu_m}{4T}\right)}{E^+_{\boldsymbol{k}+\boldsymbol{q}/2}+E^+_{\boldsymbol{k}-\boldsymbol{q}/2}+\mathrm{i}\nu_m},\quad \Sigma^{ij}_{\boldsymbol{k}} = \frac{1}{16T^2}\left\{\left(\eta^{a2}_{\boldsymbol{k}}+\frac{E^+_{\boldsymbol{k}}}{8\lambda_{\boldsymbol{k}}}\eta^a_{\boldsymbol{k}}\right)\frac{F^i_{\boldsymbol{k}}F^j_{\boldsymbol{k}}}{\lambda^2_{\boldsymbol{k}}}-\frac{E^+_{\boldsymbol{k}}}{4\lambda_{\boldsymbol{k}}}\eta^a_{\boldsymbol{k}}F^{ij}_{\boldsymbol{k}}\right\},$$

with $F^i_{\boldsymbol{k}} = \partial\lambda^2_{\boldsymbol{k}}/\partial\tilde{k}_i$, $F^{ij}_{\boldsymbol{k}} = \partial^2\lambda^2_{\boldsymbol{k}}/\partial\tilde{k}_i\partial\tilde{k}_j$ and the dimensionless momenta $\tilde{\boldsymbol{k}} = \left(k_xa, k_ya, k_zc\right)$. We have also introduced the temperature weights

$$\eta^a_{\boldsymbol{k}} = 8T^4\sum_{\omega_n}\mathrm{g}^2_k\mathrm{g}^2_{-k} = -\frac{T^2}{\left(E^+_{\boldsymbol{k}}\right)^2}\frac{E^+_{\boldsymbol{k}}-T\sinh\left(E^+_{\boldsymbol{k}}/T\right)}{E^+_{\boldsymbol{k}}\cosh^2\left(E^+_{\boldsymbol{k}}/2T\right)},\qquad \eta^{a2}_{\boldsymbol{k}} = -\frac{T}{8E^+_{\boldsymbol{k}}}\frac{\tanh\left(E^+_{\boldsymbol{k}}/2T\right)}{\cosh^2\left(E^+_{\boldsymbol{k}}/2T\right)}.$$

Mass term In the $\boldsymbol{q}=0$ case, the expansion term (B.22) provides only a finite value in the τ^0 channel. Together with the coupling constant in (B.12) we can derive the mass parameter as

$$r_0 = \frac{1}{g_{E_u}}-\frac{4}{TV}\sum_{\boldsymbol{k}}\eta_{\boldsymbol{k},0}D^{(0)}_{\boldsymbol{k},\boldsymbol{0}} \qquad = \frac{1}{V}\sum_{\boldsymbol{k}}\frac{2}{E^+_{\boldsymbol{k}}}\left[\tanh\left(\frac{E^+_{\boldsymbol{k}}}{2T_c}\right)-\tanh\left(\frac{E^+_{\boldsymbol{k}}}{2T}\right)\right]D^{(0)}_{\boldsymbol{k},\boldsymbol{0}}.$$

Using $\tanh\left(\frac{E_{\mathbf{k}}}{2T}\right)\approx\tanh\left(\frac{E_{\mathbf{k}}}{2T_c}\right)-\frac{E_{\boldsymbol{k}}(T-T_c)}{2T_c^2\cosh^2(E_{\boldsymbol{k}}/2T_c)}$ we can also identify a_0 in $r_0 = a_0(T-T_c)$ as

$$a_0 = \frac{1}{T_c^2V}\sum_{\boldsymbol{k}}\frac{D^{(0)}_{\boldsymbol{k},\boldsymbol{0}}}{\cosh^2(E_{\boldsymbol{k}}/2T_c)}.$$

Gradient terms The computation of the gradient terms d_0,d',d_z and $\tilde{\mathsf{d}}$ from (2.38) is straightforward, albeit a bit tedious. We focus on the main contributions stemming from the second derivative of $\eta_{k,q}$ which are parametrical large in terms of $\left(v_0/T_c\right)$. Thus, we can identify

$$\mathsf{d}_0 = -\frac{2}{TV}\sum_{\boldsymbol{k}}\left(\Sigma^{xx}_{\boldsymbol{k}}+\Sigma^{yy}_{\boldsymbol{k}}\right)D^{(0)}_{\boldsymbol{k},\boldsymbol{0}},\qquad \mathsf{d}' = -\frac{4}{TV}\sum_{\boldsymbol{k}}\Sigma^{xy}_{\boldsymbol{k}}D^{(x)}_{\boldsymbol{k},\boldsymbol{0}}, \tag{B.23}$$

$$\mathsf{d}_z = -\frac{4}{TV}\sum_{\boldsymbol{k}}\Sigma^{zz}_{\boldsymbol{k}}D^{(0)}_{\boldsymbol{k},\boldsymbol{0}},\qquad \tilde{\mathsf{d}} = -\frac{4}{TV}\sum_{\boldsymbol{k}}\Sigma^{xz}_{\boldsymbol{k}}D^{(x)}_{\boldsymbol{k},\boldsymbol{0}}, \tag{B.24}$$

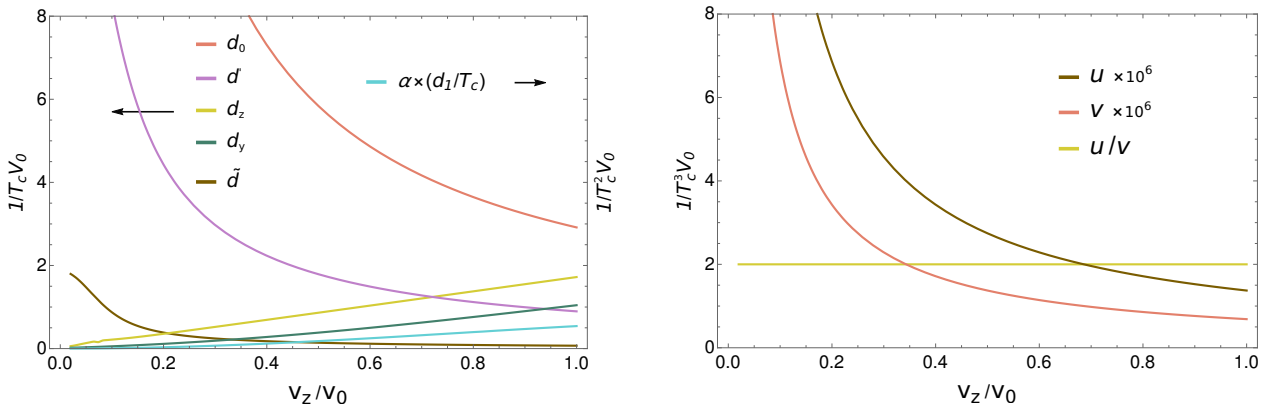

Figure B.1: (a) The gradient parameters d_0,d',d_z,d_y and $\tilde{\mathsf{d}}$ from (B.23)-(B.24). Moreover, we show the Zeeman caused magnetic prefactor α calculated from the the expression (B.41). The Ginzburg-Landau parameters are evaluated for $C_0 = C_1 = C_2 = R_1 = \mathsf{d}_2^{E_u} = R_2 = 0$. Only the parameter $\tilde{\mathsf{d}}$ has to be computed at finite $\mathsf{d}_2^{E_u}$ and R_2 since it would vanish otherwise. (b) The interaction parameter u and v from Eq. (B.29).

where in the $\boldsymbol{q} = 0$ the functions are given in (B.14) and (B.15). The gradient terms are evaluated and plotted in figure B.1.

Frequency term To compute the leading Matsubara frequency-dependent expansion term, we have to take a slightly different route. In particular, the order of integration in (B.22) is important. We first carry out the momentum summation, before the Matsubara summation. Let us denote the summation over $\boldsymbol{k}$ of the τ^0 term in (B.22) by $I_0(\nu_m, \boldsymbol{q})$ reading

$$\begin{aligned} I_0(\nu_m, \mathbf{0}) &= -4T \sum_n \sum_{\boldsymbol{k}} D^{(0)}_{\boldsymbol{k},\mathbf{0}} \left(\frac{1}{\left(E^+_{\boldsymbol{k}} - \mathrm{i}\frac{\nu_m}{2}\right)^2 + \omega_n^2} - \frac{1}{\left(E^+_{\boldsymbol{k}}\right)^2 + \omega_n^2} \right). \\ &= I_0^{(i)}(\nu_m, \mathbf{0}) + I_0^{(ii)}(\nu_m, \mathbf{0}) + I_0^{(iii)}(\nu_m, \mathbf{0}), \end{aligned}$$

We decompose the expression $I_0(\nu_m, \mathbf{0}) = I_0^{(i)}(\nu_m, \mathbf{0}) + I_0^{(ii)}(\nu_m, \mathbf{0}) + I_0^{(iii)}(\nu_m, \mathbf{0})$ into a manifestly particle-hole symmetric contribution

$$I_0^{(i)}(\nu_m, \mathbf{0}) = -4TV\nu(0) D^{(0)}_{\boldsymbol{k}_F,\mathbf{0}} \sum_n \int d\epsilon \left(\frac{1}{\left(\epsilon - \mathrm{i}\frac{\nu_m}{2}\right)^2 + \omega_n^2} - \frac{1}{\epsilon^2 + \omega_n^2} \right), \tag{B.25}$$

with $I_0^{(i)}(-\nu_m,\mathbf{0}) = I_0^{(i)}(\nu_m,\mathbf{0})$, and the two terms compensating for it

$$I_0^{(ii)}(\nu_m,\mathbf{0}) = -4TVD^{(0)}_{\boldsymbol{k}_F,\mathbf{0}}\sum_n \int d\epsilon\delta\nu(\epsilon)\left(\frac{1}{\left(\epsilon - \mathsf{i}\frac{\nu_m}{2}\right)^2+\omega_n^2} - \frac{1}{\epsilon^2+\omega_n^2}\right) \tag{B.26}$$

$$I_0^{(iii)}(\nu_m,\mathbf{0}) = -4T\sum_n\sum_{\boldsymbol{k}}\delta D^{(0)}_{\boldsymbol{k},\mathbf{0}}\left(\frac{1}{\left(E^+_{\boldsymbol{k}} - \mathsf{i}\frac{\nu_m}{2}\right)^2+\omega_n^2} - \frac{1}{\left(E^+_{\boldsymbol{k}}\right)^2+\omega_n^2}\right), \tag{B.27}$$

with $\delta D^{(0)}_{\boldsymbol{k},\mathbf{0}} = D^{(0)}_{\boldsymbol{k},\mathbf{0}} - D^{(0)}_{\boldsymbol{k}_F,\mathbf{0}}$, the density of states $\nu(\epsilon) = \frac{1}{V}\sum_{\boldsymbol{k}}\delta(\epsilon - E^+_{\boldsymbol{k}})$ and $\nu(\epsilon) = \nu(0) + \delta\nu(\epsilon)$. Focusing on the first term (B.25), we compute (after having shifted the external Matsubara frequency)

$$\begin{aligned}
I_0^{(i)}(\nu_m,\mathbf{0}) &= -4TV\nu(0)D^{(0)}_{\boldsymbol{k}_F,\mathbf{0}}\sum_n\int d\epsilon\left(\frac{1}{(-\mathsf{i}\omega_n-\epsilon)(\mathsf{i}\omega_n+\mathsf{i}\nu_m-\epsilon)} - \frac{1}{\left(\epsilon^2+\omega_n^2\right)}\right)\\
&= 4\pi TV\nu(0)D^{(0)}_{\boldsymbol{k}_F,\mathbf{0}}\sum_{n\geq 0}\left(\frac{\frac{\nu_m}{2}}{\omega_n(\omega_n+\frac{\nu_m}{2})} + \frac{\theta(m-1-n)}{\omega_n}\right)\\
&= -2V\nu(0)D^{(0)}_{\boldsymbol{k}_F,\mathbf{0}}\left(\psi_D\left(\frac{1}{2}\right) - \frac{1}{2}\psi_D\left(\frac{1}{2}+\frac{\nu_m}{2\pi T}\right) - \frac{1}{2}\psi_D\left(\frac{1}{2}+\frac{\nu_m}{4\pi T}\right)\right)\\
&\approx V\gamma_0|\nu_m|,
\end{aligned} \tag{B.28}$$

with $\gamma_0 = \frac{3\pi}{8T}\nu(0)D^{(0)}_{\boldsymbol{k}_F,\mathbf{0}}$ and the digamma function $\psi_D(x)$. In the last line we have expanded for small Matsubara frequencies and we have applied the modulus due to the property $I_0^{(i)}(-\nu_m,\mathbf{0}) = I_0^{(i)}(\nu_m,\mathbf{0})$. The contributions (B.26) and (B.27) may on a linear level well modify γ_0 and produce a term proportional to ν_m. However, since both terms describe deviations from the particle-hole symmetric contribution, we consider their influence as negligible, and will treat the term (B.28) as the dominant frequency dependence. Note, that the Fourier relations hold

$$\frac{-T}{2\pi}\int_0^\beta\int_0^\beta d\tau d\tau' \frac{e^{i\nu_m\tau}e^{-i\nu_{m'}\tau'}}{(\tau-\tau')^2} = \frac{-1}{2\pi}\delta_{m,m'}\int_{-\beta}^\beta d\tau\frac{e^{i\nu_m\tau}}{(\tau+i0)(\tau-i0)} = \delta_{m,m'}|\nu_m|.$$

Quartic interaction contribution For the higher order expansion terms, we ignore gradient terms and magnetic field coupling. For the fourth-order term $\mathcal{S}_0^{(4)} = \frac{T}{8}\mathrm{tr}\left(G^0\hat{\Delta}G^0\hat{\Delta}G^0\hat{\Delta}G^0\hat{\Delta}\right)$ we compute

$$\mathcal{S}_0^{(4)} = 4T\sum_{k,q_1,q_3,q}\mathrm{g}_k^2\mathrm{g}_{-k}^2\mathrm{tr}'\left(\Delta_{cc}(k,q_1+q)\Delta^\dagger_{cc}(k,q_1)\Delta_{cc}(k,q_3-q)\Delta^\dagger_{cc}(k,q_3)\right) \qquad = Tu_j\int_x \mathtt{B}_j^2,$$

where we have introduced $u_j = \frac{1}{VT^3}\sum_{\boldsymbol{k}}\eta^a_{\boldsymbol{k}}(D^{(j)}_{\boldsymbol{k},\mathbf{0}})^2$. From (B.16) we know that it holds $u_x = u_z$. Using the Fierz identity, we can absorb the x,z terms into the other two terms according to

$$u = u_0 + u_z = \frac{1}{VT^3}\sum_{\boldsymbol{k}}\eta^a_{\boldsymbol{k}}\left[\left(D^{(y)}_{\boldsymbol{k},\mathbf{0}}\right)^2 + 3\left(D^{(x)}_{\boldsymbol{k},\mathbf{0}}\right)^2\right], \quad v = u_y - u_x = \frac{1}{VT^3}\sum_{\boldsymbol{k}}\eta^a_{\boldsymbol{k}}\left[\left(D^{(y)}_{\boldsymbol{k},\mathbf{0}}\right)^2 - \left(D^{(x)}_{\boldsymbol{k},\mathbf{0}}\right)^2\right], \tag{B.29}$$

where we have used the identities (B.13) and (B.16). The parameter are plotted in figure B.1(b).

Sixth-order interaction contribution Using the same assumptions as in the quartic part above, we simplify the contribution $\mathcal{S}_0^{(6)} = \frac{T}{12}\mathrm{tr}\left(G^0\hat{\Delta}G^0\hat{\Delta}G^0\hat{\Delta}G^0\hat{\Delta}G^0\hat{\Delta}G^0\hat{\Delta}\right)$ according to

$$\begin{aligned}\mathcal{S}_0^{(6)} &= -\frac{32}{3}T\sum_{k,q_1,..,q_5}\mathrm{g}_k^3\mathrm{g}_{-k}^3\mathrm{tr}'\left(\Delta_{cc}(k,q_1)\Delta_{cc}^\dagger(k,-q_2)\Delta_{cc}(k,q_3)\Delta_{cc}^\dagger(k,-q_4)\Delta_{cc}(k,q_5)\Delta_{cc}^\dagger(k,\sum_i q_i)\right)\\ &= \nu_- T\int_x \mathtt{B}_z\left(\mathtt{B}_z^2-3\mathtt{B}_x^2\right)+\nu_+ T\int_x \mathtt{B}_0\left(\mathtt{B}_0^2+3\mathtt{B}_y^2\right)+\nu_{E_u}T\int_x\mathtt{B}_0\left(\mathtt{B}_x^2+\mathtt{B}_z^2\right),\end{aligned}$$

where we have introduced

$$\nu_- = -\frac{2}{3VT^5}\sum_{\boldsymbol{k}}\eta_{\boldsymbol{k}}^e\left(D_{\boldsymbol{k},\mathbf{0}}^{(z)}\right)^3, \qquad \nu_+ = -\frac{2}{3VT^5}\sum_{\boldsymbol{k}}\eta_{\boldsymbol{k}}^e D_{\boldsymbol{k},\mathbf{0}}^{(0)}\left(\left(D_{\boldsymbol{k},\mathbf{0}}^{(0)}\right)^2-\frac{1}{2}\left(D_{\boldsymbol{k},\mathbf{0}}^{(z)}\right)^2\right) \tag{B.30}$$

$$\nu_{E_u} = -\frac{7}{3VT^5}\sum_{\boldsymbol{k}}\eta_{\boldsymbol{k}}^e D_{\boldsymbol{k},\mathbf{0}}^{(0)}\left(D_{\boldsymbol{k},\mathbf{0}}^{(z)}\right)^2, \tag{B.31}$$

and $\eta_{\boldsymbol{k}}^e = 32T^6\sum_{\omega_n}\mathrm{g}_k^3\mathrm{g}_{-k}^3$. For the role it plays in discriminating between the nematic ground states A and B (2.43), it is worth examining the parameter ν_- a little closer. It only gets non-zero if there is a finite hexagonal warping term with $R_1 \neq 0$, or if there is a finite coupling between the basal plane and the z-direction with $\mathtt{d}_2^{E_u} \neq 0$. If we employ the continuum limit, we find the leading contributions to be

$$\nu_- = -\frac{v_0^4}{12VT^5}\frac{3}{16\pi^2}\int dk_\parallel k_\parallel^9\int dk_z\eta_{\boldsymbol{k}}^e\left(5(\mathtt{d}_2^{E_u})^2k_z^2+\frac{1}{4}\frac{R_1^2v_0^2k_\parallel^4}{M_{\boldsymbol{k}}^2+v_0^2k_\parallel^2+v_z^2k_z^2}\right), \tag{B.32}$$

which yields $\mathrm{sign}(\nu_-) < 0$ regardless of the individual signs of $\mathtt{d}_2^{E_u}$ or R_1.

B.1.2 Magnetic contributions

The magnetic terms we consider in (B.3) are on the one hand, the Zeeman coupling term $h^{\boldsymbol{B}}(\boldsymbol{k}) = \mu_0 \boldsymbol{B}\cdot\mathfrak{s}\sigma^0$ and on the other hand, the orbital coupling term $h^{\boldsymbol{A}}(\boldsymbol{k},\boldsymbol{k}')$ that formally results from a Peierls substitution and which is of the form

$$h^{\boldsymbol{A}}(\boldsymbol{k},\boldsymbol{k}') = -e\frac{\partial h(\boldsymbol{p})}{\partial \boldsymbol{p}}\Big|_{\boldsymbol{p}=\frac{\boldsymbol{k}+\boldsymbol{k}'}{2}}\cdot \boldsymbol{A}_{\boldsymbol{k}-\boldsymbol{k}'}\,. \tag{B.33}$$

We assume the magnetic field $\boldsymbol{B} = \boldsymbol{\nabla}\times\boldsymbol{A}(\boldsymbol{r})$ to be constant such that the vector potential $\boldsymbol{A}(\boldsymbol{r})$ becomes an odd function both, in position $\boldsymbol{A}(-\boldsymbol{r}) = -\boldsymbol{A}(\boldsymbol{r})$ and in momentum space $\boldsymbol{A}_{-\boldsymbol{q}} = -\boldsymbol{A}_{\boldsymbol{q}}$. Note that we only include linear magnetic contributions to the Ginzburg-Landau action, such that the linear term (B.33) is sufficient. On the basis of the Hamiltonian (2.16) we can write

$$h^{\boldsymbol{A}}(\boldsymbol{k},\boldsymbol{k}') = \sigma^z\mathfrak{s}^0 M^A_{\boldsymbol{k},\boldsymbol{k}'} + \sigma^x\left(\mathfrak{s}^y f^{Ax}_{\boldsymbol{k},\boldsymbol{k}'} - \mathfrak{s}^x f^{Ay}_{\boldsymbol{k},\boldsymbol{k}'}\right) - \sigma^y\mathfrak{s}^0 f^{Az}_{\boldsymbol{k},\boldsymbol{k}'} \tag{B.34}$$

where we have defined

$$M^A_{\boldsymbol{k},\boldsymbol{k}'} = -e\frac{\partial M_{\boldsymbol{p}}}{\partial p_\alpha}\Big|_{\boldsymbol{p}=\frac{\boldsymbol{k}+\boldsymbol{k}'}{2}} A^\alpha_{\boldsymbol{k}-\boldsymbol{k}'},\quad f^{A\{x,y\}}_{\boldsymbol{k},\boldsymbol{k}'} = -e\frac{\partial f^{\{x,y\}}_{\boldsymbol{p}}}{\partial p_\alpha}\Big|_{\boldsymbol{p}=\frac{\boldsymbol{k}+\boldsymbol{k}'}{2}} A^\alpha_{\boldsymbol{k}-\boldsymbol{k}'},\quad f^{Az}_{\boldsymbol{k},\boldsymbol{k}'} = -e\frac{\partial f^z_{\boldsymbol{p}}}{\partial p_\alpha}\Big|_{\boldsymbol{p}=\frac{\boldsymbol{k}+\boldsymbol{k}'}{2}} A^\alpha_{\boldsymbol{k}-\boldsymbol{k}'}. \tag{B.35}$$

For simplicity and brevity, we set $f^{C_3}_{\boldsymbol{k}} = f^0_{\boldsymbol{k}} = 0$ in this part. Yet, they could be straightforwardly included if need be. The expressions (B.35) are odd under momentum exchange $M^A_{\boldsymbol{k}',\boldsymbol{k}} = -M^A_{\boldsymbol{k},\boldsymbol{k}'}$, $\boldsymbol{f}^A_{\boldsymbol{k}',\boldsymbol{k}} = -\boldsymbol{f}^A_{\boldsymbol{k},\boldsymbol{k}'}$ and transform under inversion as $M^A_{-\boldsymbol{k},-\boldsymbol{k}'} = M^A_{\boldsymbol{k},\boldsymbol{k}'}$, $\boldsymbol{f}^A_{-\boldsymbol{k},-\boldsymbol{k}'} = -\boldsymbol{f}^A_{\boldsymbol{k},\boldsymbol{k}'}$ with $\boldsymbol{f}^A_{\boldsymbol{k},\boldsymbol{k}'} = (f^{Ax}_{\boldsymbol{k},\boldsymbol{k}'}, f^{Ay}_{\boldsymbol{k},\boldsymbol{k}'}, f^{Az}_{\boldsymbol{k},\boldsymbol{k}'})$. After a switch into the band basis (B.4), the magnetic terms (B.34) and $h^{\boldsymbol{B}}(\boldsymbol{k})$ become

$$h^{\boldsymbol{A}}_{cc}(\boldsymbol{k},\boldsymbol{k}') = \mathfrak{a}^0(\boldsymbol{k},\boldsymbol{k}')\cdot\tilde{\mathfrak{s}} + \mathfrak{a}(\boldsymbol{k},\boldsymbol{k}')\cdot\tilde{\mathfrak{s}}\,,\qquad\qquad h^{\boldsymbol{B}}_{cc}(\boldsymbol{k}) = \mathfrak{b}_{\boldsymbol{k}}\cdot\tilde{\mathfrak{s}}\,, \tag{B.36}$$

where we have only kept the respective conduction band part, e.g. $h^{\boldsymbol{A}}_b(\boldsymbol{k},\boldsymbol{k}') = h^{\boldsymbol{A}}_{cc}(\boldsymbol{k},\boldsymbol{k}')\frac{\tilde\sigma^0+\tilde\sigma^z}{2} + \ldots$. The individual components read

$$\frac{\mathfrak{b}_{\boldsymbol{k}}}{\operatorname{sign}(M_{\boldsymbol{k}})} = \mu_0\begin{pmatrix} B_x \\ B_y \\ \hat{M}_{\boldsymbol{k}}B_z\end{pmatrix} - \mu_0\frac{\left(B_x\hat{f}^x_{\boldsymbol{k}} + B_y\hat{f}^y_{\boldsymbol{k}}\right) - \operatorname{sign}(M_{\boldsymbol{k}})B_z\hat{f}^z_{\boldsymbol{k}}}{1+|\hat{M}_{\boldsymbol{k}}|}\,\hat{\boldsymbol{f}}_{\boldsymbol{k}}\,,$$

$$\begin{aligned}\mathfrak{a}^0(\boldsymbol{k},\boldsymbol{k}') = {}& \left(1+\frac{M_{\boldsymbol{k}}M_{\boldsymbol{k}'}}{|M_{\boldsymbol{k}}M_{\boldsymbol{k}'}|}\right)\left(\frac{\beta^+_{\boldsymbol{k}}}{4\beta^+_{\boldsymbol{k}'}}\hat{\boldsymbol{f}}_{\boldsymbol{k}'}\cdot\boldsymbol{f}^A_{\boldsymbol{k},\boldsymbol{k}'} + \frac{\beta^+_{\boldsymbol{k}'}}{4\beta^+_{\boldsymbol{k}}}\hat{\boldsymbol{f}}_{\boldsymbol{k}}\cdot\boldsymbol{f}^A_{\boldsymbol{k},\boldsymbol{k}'}\right) + \left(\frac{M_{\boldsymbol{k}}}{|M_{\boldsymbol{k}}|} - \frac{M_{\boldsymbol{k}'}}{|M_{\boldsymbol{k}'}|}\right)\frac{\left(\hat{\boldsymbol{f}}_{\boldsymbol{k}}\times\hat{\boldsymbol{f}}_{\boldsymbol{k}'}\right)\cdot\boldsymbol{f}^A_{\boldsymbol{k},\boldsymbol{k}'}}{16\beta^+_{\boldsymbol{k}}\beta^+_{\boldsymbol{k}'}} \\ &+ \left(\frac{M_{\boldsymbol{k}}}{|M_{\boldsymbol{k}}|} + \frac{M_{\boldsymbol{k}'}}{|M_{\boldsymbol{k}'}|}\right)\left(M^A_{\boldsymbol{k},\boldsymbol{k}'}\beta^+_{\boldsymbol{k}}\beta^+_{\boldsymbol{k}'} - \frac{M^A_{\boldsymbol{k},\boldsymbol{k}'}\hat{\boldsymbol{f}}_{\boldsymbol{k}}\cdot\hat{\boldsymbol{f}}_{\boldsymbol{k}'}}{16\beta^+_{\boldsymbol{k}}\beta^+_{\boldsymbol{k}'}}\right),\end{aligned}$$

$$\begin{aligned}\mathfrak{a}(\boldsymbol{k},\boldsymbol{k}') = \mathsf{i}M^A_{\boldsymbol{k},\boldsymbol{k}'}\left(1-\frac{M_{\boldsymbol{k}}M_{\boldsymbol{k}'}}{|M_{\boldsymbol{k}}M_{\boldsymbol{k}'}|}\right)\left(\frac{\beta^+_{\boldsymbol{k}}}{4\beta^+_{\boldsymbol{k}'}}\hat{\boldsymbol{f}}_{\boldsymbol{k}'}-\frac{\beta^+_{\boldsymbol{k}'}}{4\beta^+_{\boldsymbol{k}}}\hat{\boldsymbol{f}}_{\boldsymbol{k}}\right)-\mathsf{i}M^A_{\boldsymbol{k},\boldsymbol{k}'}\left(\frac{M_{\boldsymbol{k}}}{|M_{\boldsymbol{k}}|}+\frac{M_{\boldsymbol{k}'}}{|M_{\boldsymbol{k}'}|}\right)\frac{\hat{\boldsymbol{f}}_{\boldsymbol{k}}\times\hat{\boldsymbol{f}}_{\boldsymbol{k}'}}{16\beta^+_{\boldsymbol{k}}\beta^+_{\boldsymbol{k}'}}\\ +\mathsf{i}\left(1+\frac{M_{\boldsymbol{k}}M_{\boldsymbol{k}'}}{|M_{\boldsymbol{k}}M_{\boldsymbol{k}'}|}\right)\left(\frac{\beta^+_{\boldsymbol{k}'}}{4\beta^+_{\boldsymbol{k}}}\hat{\boldsymbol{f}}_{\boldsymbol{k}}\times\boldsymbol{f}^A_{\boldsymbol{k},\boldsymbol{k}'}-\frac{\beta^+_{\boldsymbol{k}}}{4\beta^+_{\boldsymbol{k}'}}\hat{\boldsymbol{f}}_{\boldsymbol{k}'}\times\boldsymbol{f}^A_{\boldsymbol{k},\boldsymbol{k}'}\right)+\mathsf{i}\left(\frac{M_{\boldsymbol{k}}}{|M_{\boldsymbol{k}}|}-\frac{M_{\boldsymbol{k}'}}{|M_{\boldsymbol{k}'}|}\right)\beta^+_{\boldsymbol{k}}\beta^+_{\boldsymbol{k}'}\boldsymbol{f}^A_{\boldsymbol{k},\boldsymbol{k}'}\\ +\mathsf{i}\left(\frac{M_{\boldsymbol{k}}}{|M_{\boldsymbol{k}}|}-\frac{M_{\boldsymbol{k}'}}{|M_{\boldsymbol{k}'}|}\right)\frac{\left(\hat{\boldsymbol{f}}_{\boldsymbol{k}}\left(\boldsymbol{f}^A_{\boldsymbol{k},\boldsymbol{k}'}\cdot\hat{\boldsymbol{f}}_{\boldsymbol{k}'}\right)+\hat{\boldsymbol{f}}_{\boldsymbol{k}'}\left(\boldsymbol{f}^A_{\boldsymbol{k},\boldsymbol{k}'}\cdot\hat{\boldsymbol{f}}_{\boldsymbol{k}}\right)-\boldsymbol{f}^A_{\boldsymbol{k},\boldsymbol{k}'}\left(\hat{\boldsymbol{f}}_{\boldsymbol{k}}\cdot\hat{\boldsymbol{f}}_{\boldsymbol{k}'}\right)\right)}{16\beta^+_{\boldsymbol{k}}\beta^+_{\boldsymbol{k}'}}.\end{aligned}$$

Due to the properties $\mathfrak{a}^0(-\boldsymbol{k},-\boldsymbol{k}')=\mathfrak{a}^0(\boldsymbol{k},\boldsymbol{k}')$, $\mathfrak{a}^0(\boldsymbol{k}',\boldsymbol{k})=-\mathfrak{a}^0(\boldsymbol{k},\boldsymbol{k}')$, $\mathfrak{a}(-\boldsymbol{k},-\boldsymbol{k}')=\mathfrak{a}(\boldsymbol{k},\boldsymbol{k}')$, $\mathfrak{a}(\boldsymbol{k}',\boldsymbol{k})=\mathfrak{a}(\boldsymbol{k},\boldsymbol{k}')$ and $\mathfrak{b}_{-\boldsymbol{k}}=\mathfrak{b}_{\boldsymbol{k}}$ both Hamiltonians (B.36) couple via the τ^0 matrix in Nambu space as is used in (B.6). Eventually, we have all prerequisites to compute the Ginzburg-Landau parameters α, d_y in the magnetic contribution

$$\mathcal{S}_B = T\int_x \underbrace{\left(\alpha\mu_0+2ea^2d_y\right)}_{\equiv\alpha'} B_z\bar{\boldsymbol{\Delta}}^{E_u}\tau^y\boldsymbol{\Delta}^{E_u}, \tag{B.37}$$

which originate from the microscopic Zeeman coupling and the orbital coupling, respectively.

Zeeman term The Zeeman term causes the contribution related to α that can be computed from the expanded action (B.20) yielding

$$\begin{aligned}\mathcal{S}^{(2)}_B &= 2T\mathrm{tr}\left(\left(\mathrm{g}_k\mathrm{g}_{-k}^2\Delta_{cc}(k,q)h^{\boldsymbol{B}}_{cc}(\boldsymbol{k})\Delta^\dagger_{cc}(k,q)-\mathrm{g}_k\mathrm{g}_{-k}^2\Delta^\dagger_{cc}(-k,q)h^{\boldsymbol{B}}_{cc}(\boldsymbol{k})\Delta_{cc}(-k,q)\right)\right) &\text{(B.38)}\\ &= -\frac{1}{T^2}\sum_{\boldsymbol{k},q}\eta^{(4)}_{\mathbf{k}}\mathfrak{b}_{\boldsymbol{k}}\cdot\boldsymbol{D}^{(y)}_{\boldsymbol{k},\mathbf{0}}\bar{\boldsymbol{\Delta}}^{E_u}_q\tau^y\boldsymbol{\Delta}^{E_u}_q &\text{(B.39)}\\ &= V\mu_0B_z\alpha\sum_q\bar{\boldsymbol{\Delta}}^{E_u}_q\tau^y\boldsymbol{\Delta}^{E_u}_q &\text{(B.40)}\end{aligned}$$

with $\eta^{(4)}_{\mathbf{k}}=8T^3\sum_{\omega_n}\mathrm{g}_k\mathrm{g}_{-k}^2=\frac{E_{\boldsymbol{k}}}{T}\eta^a_{\boldsymbol{k}}$, $\boldsymbol{D}^{(y)}_{\boldsymbol{k},\mathbf{0}}=\hat{f}^z_{\boldsymbol{k}}\hat{\boldsymbol{f}}_{\boldsymbol{k}}$ and

$$\alpha = -\frac{1}{\mu_0B_zVT^2}\sum_{\boldsymbol{k},q}\eta^{(4)}_{\boldsymbol{k}}\mathfrak{b}_{\boldsymbol{k}}\cdot\boldsymbol{D}^{(y)}_{\boldsymbol{k},\mathbf{0}} \qquad = -\frac{1}{VT^2}\sum_{\boldsymbol{k},q}\frac{E_{\boldsymbol{k}}}{T}\eta^a_{\boldsymbol{k}}\left(\hat{f}^z_{\boldsymbol{k}}\right)^2. \tag{B.41}$$

The parameter is plotted in figure B.1(a), and we see that it is parametrically (T_c/v_0) smaller than the gradient parameters.

Orbital coupling Now, we address the orbital coupling term (B.21) and in particular, we focus on the part related to d_y which leads to the $B_z\mathsf{B}^{A_{2g}}$ term, according to

$$i\sum_{q'}\left(q'_xA^y_{q'}-q'_yA^x_{q'}\right)\sum_q\bar{\boldsymbol{\Delta}}^{E_u}_q\tau^y\boldsymbol{\Delta}^{E_u}_q \to B_z\sum_q\bar{\boldsymbol{\Delta}}^{E_u}_q\tau^y\boldsymbol{\Delta}^{E_u}_q. \tag{B.42}$$

The corresponding action can be simplified to

$$\mathcal{S}_A^{(2)} = \frac{1}{2T^2} \sum_{\boldsymbol{k},q,q'} \eta^{(5)}_{\boldsymbol{k},\boldsymbol{q}'} \left(\bar{\boldsymbol{\Delta}}_q^{E_u} \tau^y \boldsymbol{\Delta}_q^{E_u} \right) \left(\mathfrak{a}^0(\boldsymbol{k}, \boldsymbol{k}-\boldsymbol{q}') \tilde{D}^y_{\boldsymbol{k},\boldsymbol{q}'} - 2\boldsymbol{\mathfrak{a}}(\boldsymbol{k}, \boldsymbol{k}-\boldsymbol{q}') \cdot \boldsymbol{D}^{(y)}_{\boldsymbol{k},\boldsymbol{0}} \right) , \tag{B.43}$$

with

$$\begin{aligned} \tilde{D}^y_{\boldsymbol{k},\boldsymbol{q}'} &= -\mathsf{i} \left(\boldsymbol{d}^{E_u,1}_{\boldsymbol{k},\boldsymbol{0}} \cdot \boldsymbol{d}^{E_u,2}_{\boldsymbol{k}-\frac{\boldsymbol{q}'}{2},-\boldsymbol{q}'} - \boldsymbol{d}^{E_u,2}_{\boldsymbol{k},\boldsymbol{0}} \cdot \boldsymbol{d}^{E_u,1}_{\boldsymbol{k}-\frac{\boldsymbol{q}'}{2},-\boldsymbol{q}'} \right) , \\ \boldsymbol{D}^{(y)}_{\boldsymbol{k},\boldsymbol{q}} &= \boldsymbol{d}^{E_u,1}_{\boldsymbol{k},\boldsymbol{q}} \times \boldsymbol{d}^{E_u,2}_{\boldsymbol{k},\boldsymbol{q}} + \mathsf{i} \left(d^{0,E_u,2}_{\boldsymbol{k},\boldsymbol{q}} \boldsymbol{d}^{E_u,1}_{\boldsymbol{k},\boldsymbol{q}} - d^{0,E_u,1}_{\boldsymbol{k},\boldsymbol{q}} \boldsymbol{d}^{E_u,2}_{\boldsymbol{k},\boldsymbol{q}} \right) , \end{aligned} \tag{B.44}$$

and $\eta^{(5)}_{\boldsymbol{k},\boldsymbol{q}'} = 8T^3 \sum_{\omega_n} \mathrm{g}_{-k} \mathrm{g}^2_{k-q'}$ with $\eta^{(5)}_{\boldsymbol{k},\boldsymbol{0}} = \frac{E_{\boldsymbol{k}}}{T} \eta^a_{\boldsymbol{k}}$. It holds $\tilde{D}^y_{\boldsymbol{k},\boldsymbol{q}'} \sim q'_i$ and $\boldsymbol{\mathfrak{a}}(\boldsymbol{k}, \boldsymbol{k}-\boldsymbol{q}') \sim q'_i$ such that the deduction of the $B_z \mathsf{B}^{A_{2g}}$ term (B.42) requires the respective accompanying terms to be evaluated at $\boldsymbol{q}' = 0$. Then, the action (B.43) can be expanded with respect to $\boldsymbol{q}'$ yielding $\mathcal{S}_A^{(2)} = V(2ea^2 B_z) \mathsf{d}_y \sum_q (\bar{\boldsymbol{\Delta}}_q^{E_u} \tau^y \boldsymbol{\Delta}_q^{E_u})$ with

$$\mathsf{d}_y = -\frac{v_0^2}{16VT^2} \sum_{\boldsymbol{k}} \frac{E_{\boldsymbol{k}}}{T} \eta^a_{\boldsymbol{k}} \frac{\left(f^y_{\boldsymbol{k}}\right)^2 + \left(f^x_{\boldsymbol{k}}\right)^2 + 4\left(f^z_{\boldsymbol{k}}\right)^2}{\left(M^2_{\boldsymbol{k}} + \boldsymbol{f}^2_{\boldsymbol{k}}\right)^{3/2}} . \tag{B.45}$$

The parameter d_y is plotted in figure B.1(a), where we note that it is of the same order as the other gradient parameters. In particular, this means that the α' action contribution (B.37) is not negligible.

Appendix C

C Vestigial nematicity

In this part, we provide further details on relations used in chapter 3.

C.1 Large-N theory in the primary ordered phase

Here, we want to discuss how the superconducting ordered phase can be described in the context of vestigial phases. While the actual number in the present problem is $N = 2$ ($\hat{=}$real- and imaginary part of $\mathbf{\Delta}^{E_u}$), systematically the number has to be treated as the largest scale in the problem. We present two possible methods which conceptually slightly differ.

Condensation along a given direction The first approach is based on the textbook [49]. We explain the key elements in the language of the real field $\boldsymbol{\phi} = (\phi^1, \phi^2, \ldots, \phi^N)^T$ with N components. The corresponding action is of the form $\mathcal{S} = \frac{1}{2}\boldsymbol{\phi}^T \hat{A}\boldsymbol{\phi} + c\boldsymbol{\lambda}^2$ with the positive definite diagonal matrix $\hat{A} = \mathrm{diag}(A_1, A_2, .., A_N)$, and the composite field being $\boldsymbol{\lambda}$. Now, one decomposes the field $\boldsymbol{\phi} = \phi_L \boldsymbol{e}_L + \boldsymbol{\pi}$ into one longitudinal ϕ_L, and $N-1$ transverse components $\boldsymbol{\pi}$, where the longitudinal component is assumed to condense in the primary phase. Note that the longitudinal component has to be chosen in this approach and is fixed. The $N-1$ components $\boldsymbol{\pi}$ are purely fluctuating and can be integrated out. For concreteness, we choose $\boldsymbol{e}_L = \boldsymbol{e}_1$ such that the action becomes

$$\mathcal{S} = \frac{1}{2} A_1 \phi_L^2 + \frac{1}{2}\boldsymbol{\pi}^T \hat{A}\boldsymbol{\pi} + c\boldsymbol{\lambda}^2 \,. \tag{C.1}$$

After integration of the $N-1$ finite components of $\boldsymbol{\pi}$, the effective action reads

$$\mathcal{S} = \frac{1}{2} A_1 \phi_L^2 + \frac{N-1}{2} \underbrace{\frac{1}{N-1} \log\Big(\prod_{i=2}^{N} A_i\Big)}_{\equiv \log \tilde{A}} + c\boldsymbol{\lambda}^2 \,, \tag{C.2}$$

where we have identified the new matrix $\log \tilde{A}$. For as long as not too many of the eigenvalues $A_i \approx 1$ equal one, it holds $\log \tilde{A} = \mathcal{O}(1)$ and not $\mathcal{O}(1/N)$. The statement is in particular true for $A_i = A_0$ all eigenvalues being identical. Thus, the second term in (C.2) is of order $\mathcal{O}(N)$, where it holds $N-1 \approx N$. Then, one needs to rescale the condensed component according to $\phi_L \to \phi_L \sqrt{N}$ to establish the same order in N. Eventually, the action (C.2) has an overall prefactor N.

In the present superconducting model, the large number N arises from the two complex components, i.e. real- and imaginary part of the order parameter $\boldsymbol{\Delta}^{E_u}$. Moreover, due to the two-dimensional IR, the longitudinal and the transverse components individually have a two-dimensional structure, such that the Green's function $\left(\mathcal{G}\left[\boldsymbol{A}\right]\right)^{-1}$ embodies a $2N \times 2N$ matrix in the large-N language. The first task is to find a longitudinal direction which is chosen such that the action between the longitudinal and transverse components decouples similar to (C.1). Starting from the action (3.7)

$$\mathcal{S} = \mathcal{S}_{\mathsf{C}} + V \sum_{q,q'} \left(\boldsymbol{\Delta}_q^{E_u}\right)^\dagger \left(\mathcal{G}\left[\boldsymbol{A}\right]\right)^{-1}_{q,q'} \boldsymbol{\Delta}_{q'}^{E_u}\,, \tag{C.3}$$

we decompose the order parameter according to

$$\boldsymbol{\Delta}_q^{E_u} = \underbrace{\begin{pmatrix} \operatorname{Re}\Delta_q^{E_u,1} \\ \zeta \operatorname{Re}\Delta_q^{E_u,2} + \mathsf{i}\left(1-\zeta\right)\operatorname{Im}\Delta_q^{E_u,2} \end{pmatrix}}_{=\boldsymbol{\Delta}_q^{c.A}} + \mathsf{i}\underbrace{\begin{pmatrix} \operatorname{Im}\Delta_q^{E_u,1} \\ \zeta \operatorname{Im}\Delta_q^{E_u,2} - \mathsf{i}\left(1-\zeta\right)\operatorname{Re}\Delta_q^{E_u,2} \end{pmatrix}}_{=\boldsymbol{\Delta}_q^{c.B}}, \tag{C.4}$$

with $\zeta = \{0,1\}$. Then, the action (C.3) becomes

$$\begin{aligned}\mathcal{S} = \mathcal{S}_{\mathsf{C}} &+ V \sum_{j=\{A,B\}} \sum_{q,q'} \left(\boldsymbol{\Delta}_q^{c.j}\right)^\dagger \left(\mathcal{G}\left[\boldsymbol{A}\right]\right)^{-1}_{q,q'} \boldsymbol{\Delta}_{q'}^{c.j} \\ &+ 2V \sum_{q,q'} \begin{pmatrix} \operatorname{Re}\Delta_q^{E_u,1} \\ \operatorname{Im}\Delta_q^{E_u,1} \end{pmatrix} \left(\left(1-\zeta\right)\tau^0 \operatorname{tr}\left[\left(\mathcal{G}\left[\boldsymbol{A}\right]\right)^{-1}_{q,q'}\tau^x\right] + \mathsf{i}\zeta\tau^y \operatorname{tr}\left[\left(\mathcal{G}\left[\boldsymbol{A}\right]\right)^{-1}_{q,q'}\tau^y\right]\right) \begin{pmatrix} \operatorname{Re}\Delta_{q'}^{E_u,2} \\ \operatorname{Im}\Delta_{q'}^{E_u,2} \end{pmatrix},\end{aligned} \tag{C.5}$$

with

$$\begin{aligned}\operatorname{tr}\left[\left(\mathcal{G}\left[\boldsymbol{A}\right]\right)^{-1}_{q,q'}\tau^x\right] &= -2f_{\boldsymbol{q}}^{E_g,2}\delta_{qq'} - 2\zeta \mathsf{C}_{q-q'}^{E_g,2} + \frac{2e\partial f_{\boldsymbol{p}}^{E_g,2}}{\partial p_\alpha}\Big|_{\boldsymbol{p}=\frac{\boldsymbol{q}+\boldsymbol{q}'}{2}} A_{q\text{-}q'}^\alpha - \sum_{\boldsymbol{q}_1} \frac{e^2\partial^2 f_{\boldsymbol{p}}^{E_g,2}}{\partial p_\alpha \partial p_\beta}\Big|_{\boldsymbol{p}=\frac{\boldsymbol{q}+\boldsymbol{q}'}{2}} A_{q_1}^\alpha A_{q\text{-}q'\text{-}q_1}^\beta, \\ \operatorname{tr}\left[\left(\mathcal{G}\left[\boldsymbol{A}\right]\right)^{-1}_{q,q'}\tau^y\right] &= 2\left(1-\zeta\right)\mathsf{C}_{q-q'}^{A_{2g}} + 2B_z\,.\end{aligned}$$

Aiming for a uniform solution $\boldsymbol{\Delta}_q^{c.j} = \boldsymbol{\Delta}_0^{c.j}\delta_{q,0}$, we note that the coupling term (C.5) only vanishes if both holds, $\zeta = \{0,1\}$ and the external field is zero. These are the constraints we have to impose on the system in the superconducting state such that the action decouples in line with the large-N approach (C.1). Now, we assign $\boldsymbol{\Delta}^{c.A}$ as the longitudinal component, and we integrate out the remaining $N-1$ components, yielding[1]

$$\mathcal{S}_- = \mathcal{S}_{\mathsf{C}} + V\left(\boldsymbol{\Delta}_0^{c.A}\right)^\dagger \left(\mathcal{G}\left[0\right]\right)^{-1}_{0,0} \boldsymbol{\Delta}_0^{c.A} + \beta^{-1}\frac{N-1}{2}\operatorname{tr}\log\left(2V\beta^{-1}\left(\mathcal{G}\left[0\right]\right)^{-1}\right), \tag{C.6}$$

[1]The integration runs over a N-component real vector $\boldsymbol{v}$ and reads $\int d\boldsymbol{v}\exp\left(-\frac{1}{2}\boldsymbol{v}^T A\boldsymbol{v}\right) = \sqrt{2\pi}^N/\sqrt{\det A}$, where the symmetric part of the matrix A has to be positive definite. In the cases $\zeta = 1$ and $\zeta = 0$ the matrices read $A = (\mathcal{G}[0])^{-1}$ and $A = O^\dagger(\mathcal{G}[0])^{-1}O$, respectively. The matrix $O = \left(\begin{smallmatrix} 1 & 0 \\ 0 & \mathsf{i} \end{smallmatrix}\right)$ does not change the integrals outcome as $\det\left(O^\dagger(\mathcal{G}[0])^{-1}O\right) = \det\left((\mathcal{G}[0])^{-1}\right)$.

and eventually, we approximate $N-1 \approx N$. If the temperature is above the superconducting transition, the purely fluctuating superconducting field in Eq. (C.3) can directly be integrated out with the result reading

$$\mathcal{S}_+ = \mathcal{S}_\mathsf{C} + \beta^{-1}\frac{N}{2}\mathrm{tr}\log\left(2V\beta^{-1}\left(\mathcal{G}\left[\boldsymbol{A}\right]\right)^{-1}\right).$$

In the large-N limit the two actions are smoothly connected.

Condensation along an arbitrary direction Again, we begin by considering a $(\boldsymbol{\phi}^2)^2$ theory with the real field $\boldsymbol{\phi} = (\phi^1, \phi^2, \ldots, \phi^N)^T$ having N components. The corresponding action is of the form $\mathcal{S} = \frac{1}{2}\boldsymbol{\phi}^T\hat{A}\boldsymbol{\phi} + c\boldsymbol{\lambda}^2$ where $\hat{A}$ is an arbitrary positive definite matrix, and the composite field reads $\boldsymbol{\lambda}$. Now, we define a condensed direction $\boldsymbol{\phi}_0$ as the solution of the equation

$$\frac{\delta\mathcal{S}}{\delta\boldsymbol{\phi}}\Big|_{\boldsymbol{\phi}=\boldsymbol{\phi}_0} = 0\,.$$

We express the field $\boldsymbol{\phi} = \boldsymbol{\phi}_0 + \delta\boldsymbol{\phi}$ via the condensed component $\boldsymbol{\phi}_0$, and the fluctuations $\delta\boldsymbol{\phi}$ in all N components. By construction, the corresponding action decomposes according to

$$\tilde{\mathcal{S}} = \frac{1}{2}\boldsymbol{\phi}_0^T\hat{A}\boldsymbol{\phi}_0 + \frac{1}{2}\delta\boldsymbol{\phi}^T\hat{A}\delta\boldsymbol{\phi} + c\boldsymbol{\lambda}^2\,, \tag{C.7}$$

and the $\delta\boldsymbol{\phi}$ can be integrated out. The corresponding effective action reads

$$\mathcal{S} = \frac{1}{2}\boldsymbol{\phi}_0^T\hat{A}\boldsymbol{\phi}_0 + \frac{N}{2}\underbrace{\frac{1}{N}\log\Big(\prod_{i=1}^{N}A_i\Big)}_{\equiv\log\tilde{A}} + c\boldsymbol{\lambda}^2\,, \tag{C.8}$$

with the eigenvalues A_i of the matrix $\hat{A}$. Again, we have defined the matrix $\log\tilde{A}$ which is of the order $\mathcal{O}(1)$ unless too many eigenvalues $A_i \approx 1$ yield one. After rescaling the condensed component $\boldsymbol{\phi}_0 \to \boldsymbol{\phi}_0\sqrt{N}$, the resulting action looks similar to (C.2). However, the key difference is that the present approach did not require the matrix $\hat{A}$ to be diagonal, nor did one have to specify the direction of the condensed component in the first place.

To employ this method on the present superconductor, we start from the action (3.7)

$$\mathcal{S}_\Delta = \mathcal{S}_\mathsf{C} + V\sum_{q,q'}\left(\boldsymbol{\Delta}_q^{E_u}\right)^\dagger\left(\mathcal{G}\left[\boldsymbol{A}\right]\right)^{-1}_{q,q'}\boldsymbol{\Delta}_{q'}^{E_u}\,, \tag{C.9}$$

and define the ordered field $\boldsymbol{\Delta}_q^{\circ,E_u}$ via the solution of the equation

$$\frac{\delta\mathcal{S}_\Delta}{\delta\bar{\boldsymbol{\Delta}}_q^{E_u}}\Big|_{\boldsymbol{\Delta}_q^{E_u}=\boldsymbol{\Delta}_q^{\circ,E_u}} = 0\,. \tag{C.10}$$

Next, we decompose the order parameter $\boldsymbol{\Delta}_q^{E_u} = \boldsymbol{\Delta}_q^{\circ,E_u} + \delta\boldsymbol{\Delta}_q^{E_u}$ around its ordered component $\boldsymbol{\Delta}_q^{\circ,E_u}$,

we insert the ansatz and integrate out the fluctuating fields, yielding

$$\mathcal{S}_f = \mathcal{S}_{\mathsf{C}} + V\sum_{q,q'}\left(\boldsymbol{\Delta}_q^{\circ,E_u}\right)^\dagger\left(\mathcal{G}\left[\boldsymbol{A}\right]\right)^{-1}_{q,q'}\boldsymbol{\Delta}_{q'}^{\circ,E_u} + \beta^{-1}\frac{N}{2}\mathrm{tr}\log\left(2V\beta^{-1}\left(\mathcal{G}\left[\boldsymbol{A}\right]\right)^{-1}\right).$$

Eventually, we rescale the superconducting field $\boldsymbol{\Delta}_q^{\circ,E_u}\to\boldsymbol{\Delta}_q^{\circ,E_u}\sqrt{N}$, and the action looks the same as in the previous method, yet the condensation direction is left unspecified.

C.2 Derivation of the C^{E_g} free energy expansion

In this part, we derive the Ginzburg-Landau parameter r_{c},g_{c} and u_{c} of the composite order parameter $\mathbf{C}_0^{E_g}$. We start from the mean-field equations valid above the superconducting transition

$$0 = -\frac{V}{2u'}\left(R_0-\delta r_0-r_0^c\right)+T\frac{1}{2}\sum_q\mathrm{tr}_\tau\left(\mathcal{G}_q\left[R_0,\mathsf{C}_0^{E_g,l}\right]\tau^0\right) \tag{C.11}$$

$$0 = \frac{V}{2v}\mathsf{C}_0^{E_g,l}+T\frac{1}{2}\sum_q\mathrm{tr}_\tau\left(\mathcal{G}_q\left[R_0,\mathsf{C}_0^{E_g,l}\right]\tau^{E_g,l}\right), \tag{C.12}$$

where we have introduced the notation $u'=u+v$, $R_0=r_0+\mathsf{C}_0^{A_{1g}}$, $\delta r_0=r_0-r_0^c$ and $\hat{r}_0^c$ according to Eq. (3.43). For clarity, the matrix Green's function (C.13) reads

$$\mathcal{G}_q\left[R_0,\mathsf{C}_0^{E_g,l}\right]=\frac{\left(R_0+f_q^{(0)}\right)\tau^0-\left(f_{\boldsymbol{q}}^{E_g,l}+\mathsf{C}_0^{E_g,l}\right)\tau^{E_g,l}}{\left(R_0+f_q^{(0)}\right)^2-\left(\boldsymbol{f}_{\boldsymbol{q}}^{E_g}+\mathbf{C}_0^{E_g}\right)^2}. \tag{C.13}$$

The goal is to expand the above equations with respect to $\mathbf{C}_0^{E_g}$, yet because of Eq. (C.12), the renormalized mass $R_0(\mathbf{C}_0^{E_g})$ has to be treated as a function of $\mathbf{C}_0^{E_g}$ as well. For this purpose, we expand R_0 around its value in the para-nematic phase R_p according to

$$R_0 = R_p+\kappa_l^{(1)}\mathsf{C}_0^{E_g,l}+\kappa_{ll'}^{(2)}\mathsf{C}_0^{E_g,l}\mathsf{C}_0^{E_g,l'}. \tag{C.14}$$

It proves useful to first expand the matrix (C.13) for small $\mathsf{C}_0^{E_g,l}$ which provides the expression

$$\begin{aligned}\mathcal{G}_q\Big[R_0,\mathsf{C}_0^{E_g,l}\Big]\approx{}&\mathcal{G}_q^p-\left(\mathcal{G}_q^p\mathcal{G}_q^p\,\kappa_l^{(1)}+\mathcal{G}_q^p\tau^{E_g,l}\mathcal{G}_q^p\right)\mathsf{C}_0^{E_g,l}+\left(\mathcal{G}_q^p\mathcal{G}_q^p\mathcal{G}_q^p\,\kappa_l^{(1)}\kappa_{l'}^{(1)}-\mathcal{G}_q^p\mathcal{G}_q^p\,\kappa_{ll'}^{(2)}\right)\mathsf{C}_0^{E_g,l}\mathsf{C}_0^{E_g,l'}\\&+\frac{1}{2}\left(\mathcal{G}_q^p\left(\mathcal{G}_q^p\tau^{E_g,l'}+\tau^{E_g,l'}\mathcal{G}_q^p\right)\mathcal{G}_q^p\,\kappa_l^{(1)}+\mathcal{G}_q^p\left(\mathcal{G}_q^p\tau^{E_g,l}+\tau^{E_g,l}\mathcal{G}_q^p\right)\mathcal{G}_q^p\,\kappa_{l'}^{(1)}\right)\mathsf{C}_0^{E_g,l}\mathsf{C}_0^{E_g,l'}\\&+\frac{1}{2}\mathcal{G}_q^p\left(\tau^{E_g,l'}\mathcal{G}_q^p\tau^{E_g,l}+\tau^{E_g,l}\mathcal{G}_q^p\tau^{E_g,l'}\right)\mathcal{G}_q^p\mathsf{C}_0^{E_g,l}\mathsf{C}_0^{E_g,l'},\end{aligned} \tag{C.15}$$

where we have introduced $\mathcal{G}_q^p=\mathcal{G}_q[R_p,0]$ and employed the derivatives

$$\frac{\partial\mathcal{G}_q[R_0,\mathsf{C}_0^{E_g,l}]}{\partial R_0}=-\mathcal{G}_q[R_0,\mathsf{C}_0^{E_g,l}]\mathcal{G}_q[R_0,\mathsf{C}_0^{E_g,l}],\quad \frac{\partial\mathcal{G}_q[R_0,\mathsf{C}_0^{E_g,l}]}{\partial\mathsf{C}_0^{E_g,l}}=-\mathcal{G}_q[R_0,\mathsf{C}_0^{E_g,l}]\tau^{E_g,l}\mathcal{G}_q[R_0,\mathsf{C}_0^{E_g,l}].$$

The insertion of the expansion (C.15) into (C.11) and sorting with respect to powers of $\mathsf{C}_0^{E_g,l}$ yields

$$R_p = \delta r_0 + r_0^c + u'\tilde{\Pi}_0, \tag{C.16}$$

$$\kappa_l^{(1)}\mathsf{C}_0^{E_g,l} = -u'\left(\tilde{\Pi}_{0,0}\,\kappa_l^{(1)} + \tilde{\Pi}_{0,l}\right)\mathsf{C}_0^{E_g,l}, \tag{C.17}$$

$$\kappa_{ll'}^{(2)}\mathsf{C}_0^{E_g,l}\mathsf{C}_0^{E_g,l'} = u'\left(\tilde{\Pi}_{0,0,0}\,\kappa_l^{(1)}\kappa_{l'}^{(1)} - \tilde{\Pi}_{0,0}\,\kappa_{ll'}^{(2)} + \tilde{\Pi}_{0,0,l'}\,\kappa_l^{(1)} + \tilde{\Pi}_{0,0,l}\,\kappa_{l'}^{(1)} + \frac{\tilde{\Pi}_{0,l',l} + \tilde{\Pi}_{0,l,l'}}{2}\right)\mathsf{C}_0^{E_g,l}\mathsf{C}_0^{E_g,l'}. \tag{C.18}$$

Here, we have introduced the notation

$$\tilde{\Pi}_{\mathtt{i}} = \frac{T}{V}\sum_q \mathrm{tr}_\tau\left(\mathcal{G}_q^p\tau^{\mathtt{i}}\right), \qquad \tilde{\Pi}_{\mathtt{i},\mathtt{j}} = \frac{T}{V}\sum_q \mathrm{tr}_\tau\left(\mathcal{G}_q^p\tau^{\mathtt{i}}\mathcal{G}_q^p\tau^{\mathtt{j}}\right), \tag{C.19}$$

$$\tilde{\Pi}_{\mathtt{i},\mathtt{j},\mathtt{k}} = \frac{T}{V}\sum_q \mathrm{tr}_\tau\left(\mathcal{G}_q^p\tau^{\mathtt{i}}\mathcal{G}_q^p\tau^{\mathtt{j}}\mathcal{G}_q^p\tau^{\mathtt{k}}\right), \qquad \tilde{\Pi}_{\mathtt{i},\mathtt{j},\mathtt{k},\mathtt{l}} = \frac{T}{V}\sum_q \mathrm{tr}_\tau\left(\mathcal{G}_q^p\tau^{\mathtt{i}}\mathcal{G}_q^p\tau^{\mathtt{j}}\mathcal{G}_q^p\tau^{\mathtt{k}}\mathcal{G}_q^p\tau^{\mathtt{l}}\right), \tag{C.20}$$

with $\{\mathtt{i},\mathtt{j},\mathtt{k},\mathtt{l}\} \in \{0,1,2\}$ where $\{1,2\} \hat{=} \{(E_g,1),(E_g,2)\}$. For $l = 1,2$ it is easily proven that the expressions $\tilde{\Pi}_l = \tilde{\Pi}_{0,l} = 0$ have to vanish and $\tilde{\Pi}_{0,l,l'} = \tilde{\Pi}_{0,z,z}\delta_{l,l'}$ owed to the symmetry behavior of $f_{\boldsymbol{q}}^{E_g,l}$. In particular, the following identities are useful for the upcoming derivation $\int_{\boldsymbol{q}} f_{\boldsymbol{q}}^{E_g,1}H_{\boldsymbol{q}} = \int_{\boldsymbol{q}} f_{\boldsymbol{q}}^{E_g,2}H_{\boldsymbol{q}} = 0$,

$$\int_{\boldsymbol{q}} (\boldsymbol{f}_{\boldsymbol{q}}^{E_g})^T\sigma^z\boldsymbol{f}_{\boldsymbol{q}}^{E_g}H_{\boldsymbol{q}} = \int_{\boldsymbol{q}} (\boldsymbol{f}_{\boldsymbol{q}}^{E_g})^T\sigma^x\boldsymbol{f}_{\boldsymbol{q}}^{E_g}H_{\boldsymbol{q}} = 0\,, \quad \int_{\boldsymbol{q}}\left((\boldsymbol{f}_{\boldsymbol{q}}^{E_g})^T\sigma^z\boldsymbol{f}_{\boldsymbol{q}}^{E_g}\right)^2 H_{\boldsymbol{q}} = \int_{\boldsymbol{q}}\left((\boldsymbol{f}_{\boldsymbol{q}}^{E_g})^T\sigma^x\boldsymbol{f}_{\boldsymbol{q}}^{E_g}\right)^2 H_{\boldsymbol{q}}\,, \tag{C.21}$$

which are valid for any function $H_{\boldsymbol{q}} = H_{\boldsymbol{q}}((\boldsymbol{f}_{\boldsymbol{q}}^{E_g})^2, f_{\boldsymbol{q}}^{A_{1g}})$ that transforms trivially.[2] The equation (C.17) only allows for the solution $\kappa_l^{(1)} = 0$ and thus, equation (C.18) is solved for

$$\kappa_{ll'}^{(2)} = \frac{\tilde{\Pi}_{0,z,z}}{\frac{1}{u'} + \tilde{\Pi}_{0,0}}\,\delta_{l,l'} \equiv \kappa_0^{(2)}\,\delta_{l,l'}\,.$$

Next, we expand the action (3.9) with respect to $\mathbf{C}^{E_g}$ to derive the desired free energy expansion. To this end, we separate the Green's function matrix according to

$$\left(\mathcal{G}^{\mathsf{C}}\right)^{-1}_{q,q} = \underbrace{\left(R_0^p + f_q^{(0)}\right)\tau^0 + f_{\boldsymbol{q}}^{E_g,l}\tau^{E_g,l}}_{(\mathcal{G}_q^p)^{-1}} + \underbrace{\kappa_0^{(2)}\left(\mathbf{C}_0^{E_g}\right)^2\tau^0 + \mathsf{C}_0^{E_g,l}\tau^{E_g,l}}_{\hat{\mathrm{C}}},$$

[2] The identities can be proven in a similar way as in Eq. (B.16) with the transformation properties (2.5) of $f_{\boldsymbol{q}}^{E_g,l}$ under the C_{3z} and C_{2x} rotations.

and insert it, together with (C.14) into the action (3.9) and expand

$$\begin{aligned}\frac{\mathcal{S}}{NV} &= -\frac{1}{4u'}\left(R_0-\delta r_0-r_0^c\right)^2+\frac{1}{4v}\left(\mathsf{C}_0^{E_g}\right)^2+T\frac{1}{2V}\mathrm{tr}\log\left(2V\beta^{-1}\left(\mathcal{G}^p\right)^{-1}\right)+T\frac{1}{2V}\mathrm{tr}\log\left(1+\mathcal{G}^p\hat{\mathrm{C}}\right)\\ &\approx \mathcal{S}_p+r_{\mathsf{c}}\left(\mathsf{C}_0^{E_g}\right)^2+g_{\mathsf{c}}\left(\left(\mathsf{C}_0^{E_g,1}\right)^3-3\mathsf{C}_0^{E_g,1}\left(\mathsf{C}_0^{E_g,2}\right)^2\right)+u_{\mathsf{c}}\left(\mathsf{C}_0^{E_g}\right)^4. \end{aligned} \tag{C.22}$$

The para-nematic part reads $\mathcal{S}_p=\frac{T}{2V}\mathrm{tr}\log(2V\beta^{-1}\left(\mathcal{G}^p\right)^{-1})-\frac{1}{4u'}(R_p-\delta r_0-r_0^c)^2$ and we have identified the desired parameters as

$$r_{\mathsf{c}}=\frac{1}{4}\left(\frac{1}{v}-\tilde{\Pi}_{z,z}\right),\qquad g_{\mathsf{c}}=\frac{1}{6}\tilde{\Pi}_{z,z,z},\qquad u_{\mathsf{c}}=\frac{1}{8}\left(\frac{2(\tilde{\Pi}_{0,z,z})^2}{\frac{1}{u'}+\tilde{\Pi}_{0,0}}-\tilde{\Pi}_{z,z,z,z}\right). \tag{C.23}$$

The traces that were involved in the expansion of (C.22) can be simplified to

$$\begin{aligned}&\frac{T}{V}\mathrm{tr}\left(\mathcal{G}^p\hat{\mathrm{C}}\right)=\kappa_0^{(2)}(\mathsf{C}_0^{E_g})^2\tilde{\Pi}_0,\quad \frac{T}{V}\mathrm{tr}\left(\mathcal{G}^p\hat{\mathrm{C}}\right)^2=(\kappa_0^{(2)})^2(\mathsf{C}_0^{E_g})^4\tilde{\Pi}_{0,0}+(\mathsf{C}_0^{E_g})^2\tilde{\Pi}_{z,z},\\ &\frac{T}{V}\mathrm{tr}\left(\mathcal{G}^p\hat{\mathrm{C}}\right)^4=(\mathsf{C}_0^{E_g})^4\tilde{\Pi}_{z,z,z,z},\quad \frac{T}{V}\mathrm{tr}\left(\mathcal{G}^p\hat{\mathrm{C}}\right)^3=\mathsf{C}_0^{E_g,1}\left((\mathsf{C}_0^{E_g,1})^2-3(\mathsf{C}_0^{E_g,2})^2\right)\tilde{\Pi}_{z,z,z}+3\kappa_0^{(2)}(\mathsf{C}_0^{E_g})^4\tilde{\Pi}_{0,z,z},\end{aligned}$$

where it has been used $\tilde{\Pi}_{l,l'}=\tilde{\Pi}_{z,z}\delta_{l,l'}$. Explicitly, the integrals read

$$\begin{aligned}\tilde{\Pi}_0&=2\frac{T}{V}\sum_q\frac{(R_p+f_q^{(0)})}{\det\left(\mathcal{G}^p\right)_q^{-1}},&\tilde{\Pi}_{0,z,z}&=2\frac{T}{V}\sum_q(R_p+f_q^{(0)})\frac{(R_p+f_q^{(0)})^2+(\boldsymbol{f}_{\boldsymbol{q}}^{E_g})^2}{(\det\left(\mathcal{G}^p\right)_q^{-1})^3},\\ \tilde{\Pi}_{0,0}&=2\frac{T}{V}\sum_q\frac{(R_p+f_q^{(0)})^2+(\boldsymbol{f}_{\boldsymbol{q}}^{E_g})^2}{(\det\left(\mathcal{G}^p\right)_q^{-1})^2},&\tilde{\Pi}_{z,z,z}&=-2\frac{T}{V}\sum_q f_{\boldsymbol{q}}^{E_g,1}\frac{(f_{\boldsymbol{q}}^{E_g,1})^2-3(f_{\boldsymbol{q}}^{E_g,2})^2}{(\det\left(\mathcal{G}^p\right)_q^{-1})^3},\\ \tilde{\Pi}_{z,z}&=2\frac{T}{V}\sum_q\frac{(R_p+f_q^{(0)})^2}{(\det\left(\mathcal{G}^p\right)_q^{-1})^2},&\tilde{\Pi}_{z,z,z,z}&=2\frac{T}{V}\sum_q(R_p+f_q^{(0)})^2\frac{(R_p+f_q^{(0)})^2+4(\boldsymbol{f}_{\boldsymbol{q}}^{E_g})^2}{(\det\left(\mathcal{G}^p\right)_q^{-1})^4}.\end{aligned}$$

C.3 Conductivity and magnetic susceptibility

In this part, we provide more details on the calculations involved in the derivations carried out in section 3.3. In the free energy expansion in (3.69) we have omitted the two terms

$$\frac{\delta \log Z\left[\boldsymbol{H},\boldsymbol{A}\right]}{\delta A^{\alpha}_{q}}\Big|_{\boldsymbol{H}}\Big|_{\boldsymbol{A}=\boldsymbol{H}=0}=0, \qquad \frac{\delta}{\delta H^{\alpha}_{q}}\left[\frac{\delta \log Z\left[\boldsymbol{H},\boldsymbol{A}\right]}{\delta A^{\beta}_{-q}}\Big|_{\boldsymbol{H}}\right]\Big|_{\boldsymbol{A}}\Big|_{\boldsymbol{A}=\boldsymbol{H}=0}=0\,,$$

which vanish due to the fact that a single $\boldsymbol{A}$ derivative leads to expressions which are odd upon the inversion symmetry. Central for the derivation of the conductivity and the susceptibility are the correlation functions $Q^{A}_{\alpha\beta}(q)$ and $Q^{H}_{\alpha\beta}(q)$. With the definitions given in (3.70) the correlation function $Q^{A}_{\alpha\beta}(q)$ evaluates for our system (3.9) to

$$\begin{aligned}
Q^{A}_{\alpha\beta}(q)&=\frac{T}{V}\frac{\delta^2 \log Z[\boldsymbol{H},\boldsymbol{A}]}{\delta A^{\beta}_{q}\delta A^{\alpha}_{-q}}\Big|_{\boldsymbol{H}}\Big|_{\boldsymbol{A}=\boldsymbol{H}=0}=-\frac{T}{V}\frac{\delta}{\delta A^{\beta}_{q}}\mathrm{tr}\left(\mathcal{G}\left[\boldsymbol{A}\right]\frac{\delta\mathcal{G}\left[\boldsymbol{A}\right]^{-1}}{\delta A^{\alpha}_{-q}}\right)\Big|_{\boldsymbol{A}=0}\\
&=\frac{Te^2}{V}\sum_{p'}\mathrm{tr}_{\tau}\left(\mathcal{G}^{\mathsf{C}}_{q+p'}\hat{V}^{\beta}_{\boldsymbol{p}'+\frac{\boldsymbol{q}}{2}}\mathcal{G}^{\mathsf{C}}_{p'}\hat{V}^{\alpha}_{\boldsymbol{p}'+\frac{\boldsymbol{q}}{2}}\right)-\frac{Te^2}{V}\sum_{p}\mathrm{tr}_{\tau}\left(\mathcal{G}^{\mathsf{C}}_{p}\hat{O}_{\alpha\beta}(p)\right)\\
&=K_{\alpha\beta}(q)-K_{\alpha\beta}(0)\,,
\end{aligned}\tag{C.24}$$

where we have exploited the identity $\frac{\delta\mathcal{G}[\boldsymbol{A}]}{\delta A^{\beta}_{q}}=-\mathcal{G}\left[\boldsymbol{A}\right]\frac{\delta\mathcal{G}[\boldsymbol{A}]^{-1}}{\delta A^{\beta}_{q}}\mathcal{G}\left[\boldsymbol{A}\right]$ and we have integrated by parts in the last line, using $\hat{O}_{\alpha\beta}(p)=\partial_{\alpha}\hat{V}^{\beta}_{\boldsymbol{p}}$. Eventually, the task amounts to the computation of the function

$$K_{\alpha\beta}(q)=\frac{Te^2}{V}\sum_{p}\mathrm{tr}_{\tau}\left(\mathcal{G}^{\mathsf{C}}_{p+\frac{q}{2}}\hat{V}^{\beta}_{\boldsymbol{p}}\mathcal{G}^{\mathsf{C}}_{p-\frac{q}{2}}\hat{V}^{\alpha}_{\boldsymbol{p}}\right)\,.\tag{C.25}$$

The second correlation function $Q^{H}_{\alpha\beta}(q)$ can be written as

$$\begin{aligned}
Q^{H}_{\alpha\beta}(q)&=\frac{T}{V\mu_0^2}\frac{\delta^2 \log Z\left[\boldsymbol{H},\boldsymbol{A}\right]}{\delta H^{\beta}_{-q}\delta H^{\alpha}_{q}}\Big|_{\boldsymbol{A}}\Big|_{\boldsymbol{A}=\boldsymbol{H}=0}=-\frac{T}{V\mu_0^2}\frac{\delta}{\delta H^{\beta}_{-q}}\mathrm{tr}\left(\mathcal{G}\left[\boldsymbol{A}\right]\frac{\delta\mathcal{G}\left[\boldsymbol{A}\right]^{-1}}{\delta H^{\alpha}_{q}}\right)\Big|_{\boldsymbol{A}}\Big|_{\boldsymbol{A}=\boldsymbol{H}=0}\\
&=\frac{T(\alpha')^2}{V}\delta_{q,0}\delta_{\alpha,z}\delta_{\beta,z}\mathrm{tr}\left(\mathcal{G}^{\mathsf{C}}_{p}\tau^{y}\mathcal{G}^{\mathsf{C}}_{p}\tau^{y}\right)>0\,,
\end{aligned}$$

where the positivity leads to a purely para-magnetic contribution to the susceptibility, cf. Eq. (3.76).

Magnetic susceptibility In order to derive the static DC susceptibility, we expand the response kernel (C.24) to second order in the momentum $\boldsymbol{q}$, reading $Q^{A}_{\alpha\beta}(q)\approx\frac{1}{2}\Gamma^{\gamma\delta}_{a\beta}q_{\gamma}q_{\delta}$. The expansion coefficients obey the relations $\Gamma^{\gamma\delta}_{a\beta}=\Gamma^{\gamma\delta}_{\beta\alpha}=\Gamma^{\delta\gamma}_{a\beta}$. The explicit expression can be cast as $\Gamma^{\gamma\delta}_{a\beta}=D^{\beta\gamma}_{\alpha\delta}+D^{\alpha\delta}_{\beta\gamma}+D^{\alpha\gamma}_{\beta\delta}+D^{\beta\delta}_{\alpha\gamma}+2P_{\alpha\delta\beta\gamma}$ with

$$D^{\gamma\delta}_{\alpha\beta}=\frac{Te^2}{8V}\sum_{p}\mathrm{tr}_{\tau}\Big[\mathcal{G}^{\mathsf{C}}_{p}\left(\hat{V}^{\alpha}_{\boldsymbol{p}}\mathcal{G}^{\mathsf{C}}_{p}\hat{V}^{\beta}_{\boldsymbol{p}}+\hat{V}^{\beta}_{\boldsymbol{p}}\mathcal{G}^{\mathsf{C}}_{p}\hat{V}^{\alpha}_{\boldsymbol{p}}\right)\mathcal{G}^{\mathsf{C}}_{p}\hat{O}^{\gamma\delta}_{\boldsymbol{p}}\Big],\quad P_{\alpha\delta\beta\gamma}=\frac{-Te^2}{2V}\sum_{p}\mathrm{tr}_{\tau}\Big[\mathcal{G}^{\mathsf{C}}_{p}\hat{V}^{\alpha}_{\boldsymbol{p}}\mathcal{G}^{\mathsf{C}}_{p}\hat{V}^{\delta}_{\boldsymbol{p}}\mathcal{G}^{\mathsf{C}}_{p}\hat{V}^{\beta}_{\boldsymbol{p}}\,\mathcal{G}^{\mathsf{C}}_{p}\hat{V}^{\gamma}_{\boldsymbol{p}}\Big].$$

From the above expression it can be deduced that the coefficients $\Gamma^{\gamma\delta}_{a\beta}$ are also identical upon pairwise exchange of indices $\Gamma^{\gamma\delta}_{a\beta} = \Gamma^{a\beta}_{\gamma\delta}$. Using these symmetries, the diagonal elements of the susceptibility can be expressed as [using $\hat{q}_\alpha = q_\alpha/|\boldsymbol{q}|$]

$$\begin{aligned}
\chi_{xx}(0,0) &= \frac{\mu_0}{2}\left(\Gamma^{\delta\delta'}_{yy}\,\hat{q}_\delta\hat{q}_{\delta'}\hat{q}_z\hat{q}_z + \Gamma^{\delta\delta'}_{zz}\,\hat{q}_\delta\hat{q}_{\delta'}\hat{q}_y\hat{q}_y - 2\Gamma^{\delta\delta'}_{yz}\,\hat{q}_\delta\hat{q}_{\delta'}\hat{q}_z\hat{q}_y\right)\\
&= \frac{\mu_0}{2}\left(\hat{q}_y^2\hat{q}_z^2\left(\Gamma^{yy}_{yy} + \Gamma^{zz}_{zz} - 4\Gamma^{yz}_{yz}\right) + (\hat{q}_y^4 + \hat{q}_z^4)\Gamma^{zz}_{yy} + 2\hat{q}_y\hat{q}_z(\hat{q}_z^2 - \hat{q}_y^2)\left(\Gamma^{yz}_{yy} - \Gamma^{zz}_{yz}\right)\right)\\
&\overset{(*)}{=} \frac{\chi_0}{2}\,\hat{c}^2\,\tilde{\Gamma}^{zz}_{yy}\,,\\
\chi_{yy}(0,0) &= \frac{\mu_0}{2}\left(\Gamma^{\delta\delta'}_{zz}\,\hat{q}_\delta\hat{q}_{\delta'}\hat{q}_x\hat{q}_x + \Gamma^{\delta\delta'}_{xx}\,\hat{q}_\delta\hat{q}_{\delta'}\hat{q}_z\hat{q}_z - 2\Gamma^{\delta\delta'}_{zx}\,\hat{q}_\delta\hat{q}_{\delta'}\hat{q}_x\hat{q}_z\right)\\
&= \frac{\mu_0}{2}\left(\hat{q}_x^2\hat{q}_z^2\left(\Gamma^{xx}_{xx} + \Gamma^{zz}_{zz} - 4\Gamma^{xz}_{xz}\right) + (\hat{q}_x^4 + \hat{q}_z^4)\Gamma^{zz}_{xx} + 2\hat{q}_x\hat{q}_z(\hat{q}_x^2 - \hat{q}_z^2)\left(\Gamma^{xz}_{zz} - \Gamma^{xz}_{xx}\right)\right)\\
&\overset{(*)}{=} \frac{\chi_0}{2}\,\hat{c}^2\,\tilde{\Gamma}^{zz}_{xx}\,,\\
\chi_{zz}(0,0) &= \mu_0 Q^H_{zz}(0) + \frac{\mu_0}{2}\left(-2\Gamma^{\delta\delta'}_{xy}\,\hat{q}_\delta\hat{q}_{\delta'}\hat{q}_y\hat{q}_x + \Gamma^{\delta\delta'}_{xx}\,\hat{q}_\delta\hat{q}_{\delta'}\hat{q}_y\hat{q}_y + \Gamma^{\delta\delta'}_{yy}\,\hat{q}_\delta\hat{q}_{\delta'}\hat{q}_x\hat{q}_x\right)\\
&= \mu_0 Q^H_{zz}(0) + \frac{\mu_0}{2}\left(\hat{q}_x^2\hat{q}_y^2\left(\Gamma^{xx}_{xx} + \Gamma^{yy}_{yy} - 4\Gamma^{xy}_{xy}\right) + (\hat{q}_x^4 + \hat{q}_y^4)\Gamma^{yy}_{xx} + 2\hat{q}_x\hat{q}_y(\hat{q}_x^2 - \hat{q}_y^2)\left(\Gamma^{xy}_{yy} - \Gamma^{xy}_{xx}\right)\right)\\
&\overset{(*)}{=} \chi_0\tilde{Q}^H_{zz}(0) + \frac{\chi_0}{2}\tilde{\Gamma}^{yy}_{xx}\,.
\end{aligned}$$

where we have reinstalled $\hbar$ and introduced $\chi_0 = \mu_0 T e^2 a^4/V_0\hbar^2$, as well as the dimensional quantities $\tilde{\Gamma}^{\gamma\delta}_{\alpha\beta} = \frac{V_0}{T}\frac{\hbar^2}{e^2}\frac{1}{a_\alpha a_\beta a_\gamma a_\delta}\,\Gamma^{\gamma\delta}_{\alpha\beta}$ and $\tilde{Q}^H_{zz}(0) = \frac{V_0\hbar^2}{Te^2a^4}\,Q^H_{zz}(0)$ with $a_1 = a_2 = a$, $a_3 = c$ and $\hat{c} = c/a$. The quest of finding symmetry arguments of why the following identities

$$\begin{aligned}
&\Gamma^{yy}_{yy} + \Gamma^{zz}_{zz} - 4\Gamma^{yz}_{yz} \overset{(*)}{=} 2\Gamma^{zz}_{yy}\,, && \Gamma^{yz}_{yy} \overset{(*)}{=} \Gamma^{zz}_{yz}\,,\\
&\Gamma^{xx}_{xx} + \Gamma^{zz}_{zz} - 4\Gamma^{xz}_{xz} \overset{(*)}{=} 2\Gamma^{zz}_{xx}\,, && \Gamma^{yz}_{yy} \overset{(*)}{=} \Gamma^{zz}_{yz} \overset{(*)}{=} 0\,,\\
&\Gamma^{xx}_{xx} + \Gamma^{yy}_{yy} - 4\Gamma^{xy}_{xy} \overset{(*)}{=} 2\Gamma^{yy}_{xx}\,, && \Gamma^{xy}_{yy} \overset{(*)}{=} \Gamma^{xy}_{xx} \overset{(*)}{=} 0\,,
\end{aligned}$$

should hold has proven to be a tedious business. The numerical evaluations clearly suggest the above relations to hold. (The asterisk marks that they have not been proven analytically.) From a physical point of view, they should hold since otherwise the static DC values $\chi_{xx}(0,0)$, $\chi_{yy}(0,0)$ and $\chi_{zz}(0,0)$ would depend on the direction $\hat{q}_\alpha$ from which zero is approached.

C.3.1 Conductivity

For the evaluation of the conductivity the internal Matsubara summation of $K_{\alpha\beta}(\boldsymbol{q}, \mathrm{i}\nu_m)$ (C.25) has to be taken seriously, and fully accounted for. We rewrite the expression according to

$$\begin{aligned} K_{\alpha\beta}(\mathrm{i}\nu_m, \boldsymbol{q}) &= \frac{Te^2}{V} \sum_{\boldsymbol{p}} \sum_{\nu_n} \mathrm{tr}_\tau \Big(\mathcal{G}^{\mathsf{C}}_{\boldsymbol{p}+\frac{\boldsymbol{q}}{2}}(\mathrm{i}\nu_n) \hat{V}^\beta_{\boldsymbol{p}} \mathcal{G}^{\mathsf{C}}_{\boldsymbol{p}-\frac{\boldsymbol{q}}{2}}(\mathrm{i}\nu_n - \mathrm{i}\nu_m) \hat{V}^\alpha_{\boldsymbol{p}} \Big) \\ &= \frac{e^2}{V} \sum_{\boldsymbol{p}} \oint_C \frac{dz}{2\pi\mathrm{i}}\, n(z)\, \mathrm{tr}_\tau \Big(\mathcal{G}^{\mathsf{C}}_{\boldsymbol{p}+\frac{\boldsymbol{q}}{2}}(z) \hat{V}^\beta_{\boldsymbol{p}} \mathcal{G}^{\mathsf{C}}_{\boldsymbol{p}-\frac{\boldsymbol{q}}{2}}(z - \mathrm{i}\nu_m) \hat{V}^\alpha_{\boldsymbol{p}} \Big) \\ &= \frac{e^2}{\pi V} \sum_{\boldsymbol{p}} \int_{-\infty}^{\infty} d\epsilon\, n(\epsilon)\, \mathrm{tr}_\tau \Big(\mathrm{Im} \Big[\mathcal{G}^{\mathsf{C}}_{\boldsymbol{p}+\frac{\boldsymbol{q}}{2}}(\epsilon + \mathrm{i}0) \Big] \hat{V}^\beta_{\boldsymbol{p}} \mathcal{G}^{\mathsf{C}}_{\boldsymbol{p}-\frac{\boldsymbol{q}}{2}}(\epsilon - \mathrm{i}\nu_m) \hat{V}^\alpha_{\boldsymbol{p}} \\ &\quad + \mathcal{G}^{\mathsf{C}}_{\boldsymbol{p}+\frac{\boldsymbol{q}}{2}}(\epsilon + \mathrm{i}\nu_m) \hat{V}^\beta_{\boldsymbol{p}} \mathrm{Im} \Big[\mathcal{G}^{\mathsf{C}}_{\boldsymbol{p}-\frac{\boldsymbol{q}}{2}}(\epsilon + \mathrm{i}0) \Big] \hat{V}^\alpha_{\boldsymbol{p}} \Big) \Big), \end{aligned}$$

with the Bose function $n(\epsilon) = 1/(e^{\beta\epsilon} - 1)$. In the second line we have deformed the integration contour C to the integration contours $\epsilon \pm \mathrm{i}0$ above and below the real axis, and we have identified $2\mathrm{i}\,\mathrm{Im}\,\mathcal{G}^{\mathsf{C}}_{\boldsymbol{p}}(\epsilon + \mathrm{i}0) = \mathcal{G}^{\mathsf{C}}_{\boldsymbol{p}}(\epsilon + \mathrm{i}0) - \mathcal{G}^{\mathsf{C}}_{\boldsymbol{p}}(\epsilon - \mathrm{i}0)$. In a next step, we perform an analytical continuation $\mathrm{i}\nu_m \to \nu + \mathrm{i}0$ and write the imaginary part of the above function as

$$\mathrm{Im}\, K_{\alpha\beta}(\nu + \mathrm{i}0, \boldsymbol{q}) = \frac{e^2}{\pi V} \sum_{\boldsymbol{p}} \int_{-\infty}^{\infty} d\epsilon\, \delta n(\epsilon, \nu)\, \mathrm{tr}_\tau \Big(\mathrm{Im} \Big[\mathcal{G}^{\mathsf{C}}_{\boldsymbol{p}+\frac{\boldsymbol{q}}{2}}(\epsilon + \nu + \mathrm{i}0) \Big] \hat{V}^\beta_{\boldsymbol{p}}\, \mathrm{Im} \Big[\mathcal{G}^{\mathsf{C}}_{\boldsymbol{p}-\frac{\boldsymbol{q}}{2}}(\epsilon + \mathrm{i}0) \Big] \hat{V}^\alpha_{\boldsymbol{p}} \Big),$$

with $\delta n(\epsilon, \nu) = n(\epsilon) - n(\epsilon + \nu)$. If we approximate $\delta n(\epsilon, \nu) \approx \nu T/\epsilon(\epsilon + \nu)$, we can conveniently express the conductivity (3.67) by

$$\mathrm{Re}\, \sigma_{\alpha\beta}(\nu + \mathrm{i}0, \boldsymbol{q}) = \frac{\mathrm{Im}\, Q^A_{\alpha\beta}(\nu + \mathrm{i}0, \boldsymbol{q})}{\nu} \tag{C.26}$$

$$\approx \frac{Te^2}{\pi V} \sum_{\boldsymbol{p}} \int_{-\infty}^{\infty} d\epsilon\, \mathrm{tr}_\tau \Big(\frac{\mathrm{Im} \Big[\mathcal{G}^{\mathsf{C}}_{\boldsymbol{p}+\frac{\boldsymbol{q}}{2}}(\epsilon + \nu + \mathrm{i}0) \Big]}{\epsilon + \nu} \hat{V}^\beta_{\boldsymbol{p}} \frac{\mathrm{Im} \Big[\mathcal{G}^{\mathsf{C}}_{\boldsymbol{p}-\frac{\boldsymbol{q}}{2}}(\epsilon + \mathrm{i}0) \Big]}{\epsilon} \hat{V}^\alpha_{\boldsymbol{p}} \Big). \tag{C.27}$$

Note that the above result holds for any Green's function matrix $\mathcal{G}^{\mathsf{C}}_{\boldsymbol{p}}(\epsilon)$. In the following, we carry out the ϵ integration which requires the actual frequency dependence of the present Green's function matrix. After the analytical continuation the Green's function reads

$$\Big(\mathcal{G}^{\mathsf{C}}_{\boldsymbol{p}} \Big)^{-1} (\nu + \mathrm{i}0) = \Big(r_0 + \mathrm{i}\gamma_0 \nu + f^{A_{1g}}_{\boldsymbol{p}} + \mathsf{C}^{A_{1g}}_0 \Big) \tau^0 + \Big(\boldsymbol{f}^{E_g}_{\boldsymbol{p}} + \mathbf{C}^{E_g}_0 \Big) \cdot \boldsymbol{\tau}^{E_g}.$$

We diagonalize this matrix

$$\Big(\mathcal{G}^{\mathsf{C}}_{\boldsymbol{p}} \Big)^{-1} (\nu + \mathrm{i}0) = U^\sigma_{\boldsymbol{p}} \begin{pmatrix} \lambda^{\sigma-}_{\boldsymbol{p}} + \mathrm{i}\gamma_0\nu & 0 \\ 0 & \lambda^{\sigma+}_{\boldsymbol{p}} + \mathrm{i}\gamma_0\nu \end{pmatrix} \Big(U^\sigma_{\boldsymbol{p}} \Big)^\dagger, \tag{C.28}$$

using the unitary matrix

$$U_{\boldsymbol{p}}^{\sigma} = \begin{pmatrix} \beta_{\boldsymbol{p}}^{\sigma-} & -\mathrm{sign}(f_{\boldsymbol{p}}^{E_g,2} + \mathsf{C}_0^{E_g,2})\beta_{\boldsymbol{p}}^{\sigma+} \\ \mathrm{sign}(f_{\boldsymbol{p}}^{E_g,2} + \mathsf{C}_0^{E_g,2})\beta_{\boldsymbol{p}}^{\sigma+} & \beta_{\boldsymbol{p}}^{\sigma-} \end{pmatrix},$$

with $\beta_{\boldsymbol{p}}^{\sigma\pm} = \sqrt{1 \pm (f_{\boldsymbol{p}}^{E_g,1} + \mathsf{C}_0^{E_g,1})/|\boldsymbol{f}_{\boldsymbol{p}}^{E_g} + \boldsymbol{\mathsf{C}}_0^{E_g}|}$ and the eigenvalues $\lambda_{\boldsymbol{p}}^{\sigma\pm} = r_0 + f_{\boldsymbol{p}}^{A_{1g}} + \mathsf{C}_0^{A_{1g}} \pm |\boldsymbol{f}_{\boldsymbol{p}}^{E_g} + \boldsymbol{\mathsf{C}}_0^{E_g}|$. Then, the imaginary part of the inverse of (C.28) becomes

$$\frac{\mathrm{Im}\,\mathcal{G}_{\boldsymbol{p}}^{\mathsf{C}}(\nu + \mathrm{i}0)}{\nu} = -\gamma_0 U_{\boldsymbol{p}}^{\sigma} \begin{pmatrix} \frac{1}{(\lambda_{\boldsymbol{p}}^{\sigma-})^2 + \gamma_0^2\nu^2} & 0 \\ 0 & \frac{1}{(\lambda_{\boldsymbol{p}}^{\sigma+})^2 + \gamma_0^2\nu^2} \end{pmatrix} \left(U_{\boldsymbol{p}}^{\sigma}\right)^{\dagger},$$

and the ϵ integration in (C.27) can be carried out, yielding

$$\begin{aligned} \mathrm{Re}\,\sigma_{\alpha\beta}(\nu + \mathrm{i}0, \boldsymbol{0}) = \frac{2Te^2}{V}\gamma_0 \sum_{\boldsymbol{p}} \Bigg(& \frac{1}{\lambda_{\boldsymbol{p}}^{\sigma-}} \frac{\tilde{V}_{1,1,\boldsymbol{p}}^{\alpha} \tilde{V}_{1,1,\boldsymbol{p}}^{\beta}}{(2\lambda_{\boldsymbol{p}}^{\sigma-})^2 + \gamma_0^2\nu^2} + \frac{1}{\lambda_{\boldsymbol{p}}^{\sigma+}} \frac{\tilde{V}_{2,2,\boldsymbol{p}}^{\alpha} \tilde{V}_{2,2,\boldsymbol{p}}^{\beta}}{(2\lambda_{\boldsymbol{p}}^{\sigma+})^2 + \gamma_0^2\nu^2} \\ & + \frac{1}{2}\left(\frac{1}{\lambda_{\boldsymbol{p}}^{\sigma-}} + \frac{1}{\lambda_{\boldsymbol{p}}^{\sigma+}}\right) \frac{\tilde{V}_{1,2,\boldsymbol{p}}^{\alpha} \tilde{V}_{2,1,\boldsymbol{p}}^{\beta} + \tilde{V}_{2,1,\boldsymbol{p}}^{\alpha} \tilde{V}_{1,2,\boldsymbol{p}}^{\beta}}{(\lambda_{\boldsymbol{p}}^{\sigma+} + \lambda_{\boldsymbol{p}}^{\sigma-})^2 + \gamma_0^2\nu^2} \Bigg) \end{aligned} \tag{C.29}$$

with the introduced velocity matrix $\tilde{V}_{\boldsymbol{p}}^{\beta} = \left(U_{\boldsymbol{p}}^{\sigma}\right)^{\dagger} \hat{V}_{\boldsymbol{p}}^{\beta} U_{\boldsymbol{p}}^{\sigma}$. The involved integrals were of the kind

$$\int_{-\infty}^{\infty} \frac{d\epsilon}{2\pi} \frac{1}{\mu_1^2 + \epsilon^2} \frac{1}{\mu_2^2 + (\epsilon + \nu)^2} = \frac{\mu_1 + \mu_2}{2\mu_1\mu_2} \frac{1}{\left(\nu^2 + (\mu_1 + \mu_2)^2\right)}.$$

C.4 Nematic susceptibility and renormalized elastic constants

In the first part of this section, we derive a rigorous relation between the nematic susceptibility and the renormalized elastic constants. Since they are linearly coupled, also their response functions must be somehow related. In the second part, we deduce an explicit expression for the nematic susceptibility. We start from an action where the fluctuating superconductor is coupled to its elastic degrees of freedom characterized by the strain tensor $\boldsymbol{\epsilon}^{\mathsf{D}_{3\mathsf{d}}}$. We use the notation developed in section 3.4.1. Additionally, we couple the nematic degrees of freedom to the external field $\mathbf{h}^{E_g} = (\mathsf{h}^{E_g,1}, \mathsf{h}^{E_g,2})$ via $\sum_q \mathbf{B}_q^{E_g} \cdot \mathbf{h}_{-q}^{E_g}$, and the dilatation related components via $\sum_q \mathsf{B}_q^{A_{1g}} \mathsf{h}_{-q}^{A_{1g}}$. The bilinear forms are defined as $\mathsf{B}_q^{n,l} = \sum_{q_1} (\boldsymbol{\Delta}_{q_1}^{E_u})^\dagger \tau^{n,l} \boldsymbol{\Delta}_{q_1+q}^{E_u}$. We also apply an external stress tensor $\boldsymbol{\sigma}^{\mathsf{D}_{3\mathsf{d}}}$ via $\mathcal{S}_\sigma = -\sum_q \boldsymbol{\sigma}_{-q}^{\mathsf{D}_{3\mathsf{d}}} \boldsymbol{\epsilon}_q^{\mathsf{D}_{3\mathsf{d}}}$ with $\boldsymbol{\sigma}^{\mathsf{D}_{3\mathsf{d}}} = ((\boldsymbol{\sigma}^{A_{1g}})^T, (\boldsymbol{\sigma}^{E_g})^T)^T$. Then, the action $\mathcal{S} = \mathcal{S}[\mathsf{h}^{n,l}, \boldsymbol{\sigma}^{\mathsf{D}_{3\mathsf{d}}}]$ depends on the external fields, and the expectation values can be computed via

$$\langle \mathsf{B}_q^{n,l} \rangle = T \frac{\delta \log Z[\mathsf{h}^{n,l}, \boldsymbol{\sigma}^{\mathsf{D}_{3\mathsf{d}}}]}{\delta \mathsf{h}_{-q}^{n,l}}, \quad \langle \epsilon_q^{A_{1g},j} \rangle = T \frac{\delta \log Z[\mathsf{h}^{n,l}, \boldsymbol{\sigma}^{\mathsf{D}_{3\mathsf{d}}}]}{\delta \sigma_{-q}^{A_{1g},j}}, \quad \langle \epsilon_q^{E_g,\alpha} \rangle = T \frac{\delta \log Z[\mathsf{h}^{n,l}, \boldsymbol{\sigma}^{\mathsf{D}_{3\mathsf{d}}}]}{\delta \sigma_{-q}^{E_g,\alpha}}, \tag{C.30}$$

with $i,j = \{1,2\}$ and $\alpha,\beta = \{1,\dots,4\}$. As is usual, we define the corresponding susceptibilities, the nematic susceptibility χ_{nem} and the renormalized elastic tensor $\mathcal{C}^r$, as the second derivatives evaluated at zero field, i.e.

$$\chi_{\mathrm{nem},ij}(q) = T \frac{\delta^2 \log Z[\mathsf{h}^{n,l}, \boldsymbol{\sigma}^{\mathsf{D}_{3\mathsf{d}}}]}{\delta \mathsf{h}_q^{E_g,i} \delta \mathsf{h}_{-q}^{E_g,j}}\Big|_{\mathsf{h}^{n,l}=\boldsymbol{\sigma}^{\mathsf{D}_{3\mathsf{d}}}=0}, \qquad \left(\mathcal{C}_q^{r,E_g}\right)^{-1}_{\alpha,\beta} = T \frac{\delta^2 \log Z[\mathsf{h}^{n,l}, \boldsymbol{\sigma}^{\mathsf{D}_{3\mathsf{d}}}]}{\delta \sigma_q^{E_g,\alpha} \delta \sigma_{-q}^{E_g,\beta}}\Big|_{\mathsf{h}^{n,l}=\boldsymbol{\sigma}^{\mathsf{D}_{3\mathsf{d}}}=0}.$$

Apart from the two above response functions which are the most relevant for our application, we also define the remaining correlation functions for completeness,

$$\left(\mathcal{C}_q^{r,A_{1g}}\right)^{-1}_{i,j} = T \frac{\delta^2 \log Z[\mathsf{h}^{n,l}, \boldsymbol{\sigma}^{\mathsf{D}_{3\mathsf{d}}}]}{\delta \sigma_q^{A_{1g},i} \delta \sigma_{-q}^{A_{1g},j}}\Big|_{\mathsf{h}^{n,l}=\boldsymbol{\sigma}^{\mathsf{D}_{3\mathsf{d}}}=0}, \quad \left(\mathcal{C}_q^{r,A_{1g}E_g}\right)^{-1}_{i,\beta} = T \frac{\delta^2 \log Z[\mathsf{h}^{n,l}, \boldsymbol{\sigma}^{\mathsf{D}_{3\mathsf{d}}}]}{\delta \sigma_q^{A_{1g},i} \delta \sigma_{-q}^{E_g,\beta}}\Big|_{\mathsf{h}^{n,l}=\boldsymbol{\sigma}^{\mathsf{D}_{3\mathsf{d}}}=0},$$

$$\chi_{A_{1g}}(q) = T \frac{\delta^2 \log Z[\mathsf{h}^{n,l}, \boldsymbol{\sigma}^{\mathsf{D}_{3\mathsf{d}}}]}{\delta \mathsf{h}_q^{A_{1g}} \delta \mathsf{h}_{-q}^{A_{1g}}}\Big|_{\mathsf{h}^{n,l}=\boldsymbol{\sigma}^{\mathsf{D}_{3\mathsf{d}}}=0}, \qquad \chi_{A_{1g}E_g,j}(q) = T \frac{\delta^2 \log Z[\mathsf{h}^{n,l}, \boldsymbol{\sigma}^{\mathsf{D}_{3\mathsf{d}}}]}{\delta \mathsf{h}_q^{E_g,j} \delta \mathsf{h}_{-q}^{A_{1g}}}\Big|_{\mathsf{h}^{n,l}=\boldsymbol{\sigma}^{\mathsf{D}_{3\mathsf{d}}}=0}.$$

Another way, the susceptibilities can be expressed is via

$$\chi_{\mathrm{nem},ij}(q) = \frac{\delta \langle \mathsf{B}_q^{E_g,j} \rangle_{\mathsf{h}}}{\delta \mathsf{h}_{i,q}}\Big|_0, \qquad \chi_{A_{1g}}(q) = \frac{\delta \langle \mathsf{B}_q^{A_{1g}} \rangle}{\delta \mathsf{h}_q^{A_{1g}}}\Big|_0, \qquad \chi_{A_{1g}E_g,j}(q) = \frac{\delta \langle \mathsf{B}_q^{A_{1g}} \rangle}{\delta \mathsf{h}_q^{E_g,j}} = \frac{\delta \langle \mathsf{B}_{-q}^{E_g,j} \rangle}{\delta \mathsf{h}_{-q}^{A_{1g}}}\Big|_0.$$

The explicit action is a combination of (3.7) and (3.89) with the additional elasto-nematic coupling terms $\sum_q \mathbf{B}_q^{E_g} \cdot (\kappa_{\mathsf{c}1} \boldsymbol{\epsilon}_{-q}^{E_g,1} + \kappa_{\mathsf{c}2} \boldsymbol{\epsilon}_{-q}^{E_g,2})$ and $\sum_q \mathsf{B}_q^{A_{1g}} (\kappa_{A1} \boldsymbol{\epsilon}_{-q}^{A_{1g},1} + \kappa_{A2} \boldsymbol{\epsilon}_{-q}^{A_{1g},2})$. It reads

$$\frac{\mathcal{S}_{\mathrm{kin}}}{NV} = \mathcal{S}_{\mathsf{C}} + \sum_{q,q'} \left(\boldsymbol{\Delta}_q^{E_u}\right)^\dagger \left(\mathcal{G}^{\mathsf{C}}\right)^{-1}_{q,q'} \boldsymbol{\Delta}_{q'}^{E_u} + \frac{1}{2} \sum_q \left(\boldsymbol{\epsilon}_{-q}^{\mathsf{D}_{3\mathsf{d}}}\right)^T \mathcal{C}^{\mathsf{D}_{3\mathsf{d}}} \boldsymbol{\epsilon}_q^{\mathsf{D}_{3\mathsf{d}}} \tag{C.31}$$

$$\frac{\mathcal{S}_{\mathrm{coupl}}}{NV} = \sum_q \begin{pmatrix} \tilde{\mathbf{B}}_{-q}^{A_{1g}} \\ \tilde{\mathbf{B}}_{-q}^{E_g} \end{pmatrix}^T \begin{pmatrix} \epsilon_q^{A_{1g}} \\ \epsilon_q^{E_g} \end{pmatrix} - \sum_q (\mathbf{h}_{-q}^{E_g})^T \cdot \mathbf{B}_q^{E_g} - \sum_q \mathsf{h}_{-q}^{A_{1g}} \mathsf{B}_q^{A_{1g}} - \sum_q (\boldsymbol{\sigma}_{-q}^{\mathsf{D}_{3\mathsf{d}}})^T \cdot \boldsymbol{\epsilon}_q^{\mathsf{D}_{3\mathsf{d}}}, \tag{C.32}$$

with

$$\left(\mathcal{G}^{\mathsf{C}}\right)^{-1}_{q,q'} = \left(\left(r_0 + \gamma_0|\nu_m| + f_{\boldsymbol{q}}^{A_{1g}}\right)\delta_{qq'} + \mathsf{C}^{A_{1g}}_{q-q'}\right)\tau^0 + \left(\boldsymbol{f}_{\boldsymbol{q}}^{E_g}\delta_{qq'} + \mathbf{C}^{E_g}_{q-q'}\right)\cdot\boldsymbol{\tau}^{E_g}\,,$$

and the vectors

$$\tilde{\mathbf{B}}_q^{A_{1g}} = \begin{pmatrix}\kappa_{A1}\mathsf{B}_q^{A_{1g}}\\ \kappa_{A2}\mathsf{B}_q^{A_{1g}}\end{pmatrix} = \underbrace{\begin{pmatrix}\kappa_{A1} & 0\\ 0 & \kappa_{A2}\end{pmatrix}}_{\hat{\kappa}_A}\begin{pmatrix}\mathsf{B}_q^{A_{1g}}\\ \mathsf{B}_q^{A_{1g}}\end{pmatrix}, \qquad \tilde{\mathbf{B}}_q^{E_g} = \begin{pmatrix}\kappa_{\mathsf{c}1}\mathbf{B}_q^{E_g}\\ \kappa_{\mathsf{c}2}\mathbf{B}_q^{E_g}\end{pmatrix} = \underbrace{\begin{pmatrix}\kappa_{\mathsf{c}1}\mathbb{1}_2 & 0\\ 0 & \kappa_{\mathsf{c}2}\mathbb{1}_2\end{pmatrix}}_{\hat{\kappa}_{\mathsf{c}}}\begin{pmatrix}\mathbf{B}_q^{E_g}\\ \mathbf{B}_q^{E_g}\end{pmatrix}.$$

In this notation, the partition function has to be evaluated as

$$Z\left[\mathsf{h}^{n,l},\boldsymbol{\sigma}^{\mathsf{D}_{3\mathsf{d}}}\right] = \int D\boldsymbol{\epsilon}_q^{\mathsf{D}_{3\mathsf{d}}} D\mathbf{C}_q^{E_g} D\mathbf{C}_q^{A_{1g}} D\left(\bar{\boldsymbol{\Delta}}_q^{E_u},\boldsymbol{\Delta}_q^{E_u}\right)\; e^{-\beta\mathcal{S}\left[\mathsf{h}^{n,l},\boldsymbol{\sigma}^{\mathsf{D}_{3\mathsf{d}}}\right]}$$

with $\mathcal{S}[\mathsf{h}^{n,l},\boldsymbol{\sigma}^{\mathsf{D}_{3\mathsf{d}}}] = \mathcal{S}_{\text{kin}} + \mathcal{S}_{\text{coupl}}$. For brevity, we will comprise all the integration variables in $\mathcal{D} = D\boldsymbol{\epsilon}_q^{\mathsf{D}_{3\mathsf{d}}} D\mathbf{C}_q^{E_g} D\mathbf{C}_q^{A_{1g}} D\left(\bar{\boldsymbol{\Delta}}_q^{E_u},\boldsymbol{\Delta}_q^{E_u}\right)$ in the following. As a first, step we remove the direct coupling $\boldsymbol{\epsilon}_q^{\mathsf{D}_{3\mathsf{d}}}\boldsymbol{\sigma}_{-q}^{\mathsf{D}_{3\mathsf{d}}}$ in the above action by shifting the integration variable to $(\boldsymbol{\epsilon}_q^{\mathsf{D}_{3\mathsf{d}}})' = \boldsymbol{\epsilon}_q^{\mathsf{D}_{3\mathsf{d}}} - (\mathcal{C}^{\mathsf{D}_{3\mathsf{d}}})^{-1}\boldsymbol{\sigma}_q^{\mathsf{D}_{3\mathsf{d}}}$. To explicitly state the variable shift let us first compute the inverse bare elastic tensor from (3.90) yielding

$$\left(\mathcal{C}^{\mathsf{D}_{3\mathsf{d}}}\right)^{-1} = \begin{pmatrix}\left(\mathcal{C}^{\mathsf{A}_{1\mathsf{g}}}\right)^{-1} & 0\\ 0 & \left(\mathcal{C}^{E_g}\right)^{-1}\end{pmatrix},$$

with

$$\left(\mathcal{C}^{\mathsf{A}_{1\mathsf{g}}}\right)^{-1} = \begin{pmatrix}\hat{c}_{A_{1g},2} & -\hat{c}_{A_{1g},3}\\ -\hat{c}_{A_{1g},3} & \hat{c}_{A_{1g},1}\end{pmatrix}, \qquad \left(\mathcal{C}^{E_g}\right)^{-1} = \begin{pmatrix}\hat{c}_{E_g,2} & -\hat{c}_{E_g,3}\\ -\hat{c}_{E_g,3} & \hat{c}_{E_g,1}\end{pmatrix}\otimes\mathbb{1}_2\,,$$

and $\hat{c}_{A_{1g},i} = c_{A_{1g},i}/(c_{A_{1g},1}c_{A_{1g},2} - (c_{A_{1g},3})^2)$ and $\hat{c}_{E_g,i} = c_{E_g,i}/(c_{E_g,1}c_{E_g,2} - (c_{E_g,3})^2)$. Then, we can express the variable shift as

$$\boldsymbol{\epsilon}_q^{\mathsf{D}_{3\mathsf{d}}} = \left(\boldsymbol{\epsilon}_q^{\mathsf{D}_{3\mathsf{d}}}\right)' + \begin{pmatrix}\left(\mathcal{C}^{\mathsf{A}_{1\mathsf{g}}}\right)^{-1}\boldsymbol{\sigma}_q^{A_{1g}}\\ \left(\mathcal{C}^{E_g}\right)^{-1}\boldsymbol{\sigma}_q^{E_g}\end{pmatrix}$$

which turns the action into (we replace $\epsilon' \to \epsilon$ afterwards)

$$\frac{\mathcal{S}_{\text{kin}}}{NV} = \mathcal{S}_{\mathsf{C}} + \sum_{q,q'}\left(\boldsymbol{\Delta}_q^{E_u}\right)^{\dagger}\left(\mathcal{G}^{\mathsf{C}}\right)^{-1}_{q,q'}\boldsymbol{\Delta}_{q'}^{E_u} + \frac{1}{2}\sum_q\left(\boldsymbol{\epsilon}_{-q}^{\mathsf{D}_{3\mathsf{d}}}\right)^T\mathcal{C}^{\mathsf{D}_{3\mathsf{d}}}\boldsymbol{\epsilon}_q^{\mathsf{D}_{3\mathsf{d}}} - \frac{1}{2}\sum_q\left(\boldsymbol{\sigma}_{-q}^{\mathsf{D}_{3\mathsf{d}}}\right)^T\left(\mathcal{C}^{\mathsf{D}_{3\mathsf{d}}}\right)^{-1}\boldsymbol{\sigma}_q^{\mathsf{D}_{3\mathsf{d}}}$$

$$\frac{\mathcal{S}_{\text{coupl}}}{NV} = \sum_q\begin{pmatrix}\tilde{\mathbf{B}}_{-q}^{A_{1g}}\\ \tilde{\mathbf{B}}_{-q}^{E_g}\end{pmatrix}^T\begin{pmatrix}\boldsymbol{\epsilon}_q^{A_{1g}} + \left(\mathcal{C}^{\mathsf{A}_{1\mathsf{g}}}\right)^{-1}\boldsymbol{\sigma}_q^{A_{1g}}\\ \boldsymbol{\epsilon}_q^{E_g} + \left(\mathcal{C}^{E_g}\right)^{-1}\boldsymbol{\sigma}_q^{E_g}\end{pmatrix} - \sum_q(\mathbf{h}_{-q}^{E_g})^T\cdot\mathbf{B}_q^{E_g} - \sum_q\mathsf{h}_{-q}^{A_{1g}}\mathsf{B}_q^{A_{1g}}\,.$$

Now, we perform the derivatives in (C.30) explicitly to obtain

$$\langle \mathsf{B}_q^{n,j}\rangle = T\frac{\delta \log Z[\mathsf{h}^{n,l},\boldsymbol{\sigma}^{\mathsf{D}_{3\mathsf{d}}}]}{\delta \mathsf{h}_{-q}^{n,j}} = \frac{1}{Z[\mathsf{h}^{n,l},\boldsymbol{\sigma}^{\mathsf{D}_{3\mathsf{d}}}]}\int \mathcal{D}\ \mathsf{B}_q^{n,j} e^{-\frac{1}{T}\mathcal{S}\left[\mathsf{h}^{n,l},\boldsymbol{\sigma}^{\mathsf{D}_{3\mathsf{d}}}\right]},$$

$$\begin{aligned}\langle \epsilon_q^{E_g,\beta}\rangle &= T\frac{\delta \log Z[\mathsf{h}^{n,l},\boldsymbol{\sigma}^{\mathsf{D}_{3\mathsf{d}}}]}{\delta \sigma_{-q}^{E_g,\beta}} = \int\mathcal{D}\ \frac{e^{-\frac{1}{T}\mathcal{S}\left[\mathsf{h}^{n,l},\boldsymbol{\sigma}^{\mathsf{D}_{3\mathsf{d}}}\right]}}{Z[\mathsf{h}^{n,l},\boldsymbol{\sigma}^{\mathsf{D}_{3\mathsf{d}}}]}\left(\sigma_q^{E_g,\beta'}\left(\mathcal{C}^{E_g}\right)^{-1}_{\beta'\beta} - \hat{\kappa}_{\mathsf{c}}^{\beta'\beta''}\mathsf{B}_q^{E_g,2-\beta''\mathrm{mod}(2)}\left(\mathcal{C}^{E_g}\right)^{-1}_{\beta'\beta}\right)\\ &= \sigma_q^{E_g,\beta'}\left(\mathcal{C}^{E_g}\right)^{-1}_{\beta'\beta} - \hat{\kappa}_{\mathsf{c}}^{\beta'\beta''}T\frac{\delta \log Z[\mathsf{h}^{n,l},\boldsymbol{\sigma}^{\mathsf{D}_{3\mathsf{d}}}]}{\delta \mathsf{h}_{-q}^{E_g,2-\beta''\mathrm{mod}(2)}}\left(\mathcal{C}^{E_g}\right)^{-1}_{\beta'\beta}, \end{aligned} \tag{C.33}$$

$$\begin{aligned}\langle \epsilon_q^{A_{1g},j}\rangle &= T\frac{\delta \log Z[\mathsf{h}^{n,l},\boldsymbol{\sigma}^{\mathsf{D}_{3\mathsf{d}}}]}{\delta \sigma_{-q}^{A_{1g},j}} = \int\mathcal{D}\ \frac{e^{-\frac{1}{T}\mathcal{S}\left[\mathsf{h}^{n,l},\boldsymbol{\sigma}^{\mathsf{D}_{3\mathsf{d}}}\right]}}{Z[\mathsf{h}^{n,l},\boldsymbol{\sigma}^{\mathsf{D}_{3\mathsf{d}}}]}\left(\sigma_q^{A_{1g},i}\left(\mathcal{C}^{A_{1g}}\right)^{-1}_{ij} - \hat{\kappa}_A^{ii'}\mathsf{B}_q^{A_{1g}}\left(\mathcal{C}^{A_{1g}}\right)^{-1}_{ij}\right)\\ &= \sigma_q^{A_{1g},i}\left(\mathcal{C}^{A_{1g}}\right)^{-1}_{ij} - \hat{\kappa}_A^{ii'}\left(\mathcal{C}^{A_{1g}}\right)^{-1}_{ij}T\frac{\delta \log Z[\mathsf{h}^{n,l},\boldsymbol{\sigma}^{\mathsf{D}_{3\mathsf{d}}}]}{\delta \mathsf{h}_{-q}^{A_{1g}}}. \end{aligned} \tag{C.34}$$

Next,we compute the second derivative

$$\begin{aligned}T\frac{\delta^2 \log Z[\mathsf{h}^{n,l},\boldsymbol{\sigma}^{\mathsf{D}_{3\mathsf{d}}}]}{\delta\sigma_q^{E_g,\alpha}\delta\sigma_{-q}^{E_g,\beta}} &= \left(\mathcal{C}^{E_g}\right)^{-1}_{\alpha\beta} - \left(\mathcal{C}^{E_g}\right)^{-1}_{\beta\beta'}\hat{\kappa}_{\mathsf{c}}^{\beta'\beta''}T\frac{\delta^2 \log Z[\mathsf{h}^{n,l},\boldsymbol{\sigma}^{\mathsf{D}_{3\mathsf{d}}}]}{\delta \mathsf{h}_{-q}^{E_g,2-\beta''\mathrm{mod}(2)}\delta\sigma_q^{E_g,\alpha}}\\ &= \left(\mathcal{C}^{E_g}\right)^{-1}_{\alpha\beta} + \left(\mathcal{C}^{E_g}\right)^{-1}_{\alpha'\alpha}\left(\mathcal{C}^{E_g}\right)^{-1}_{\beta\beta'}\hat{\kappa}_{\mathsf{c}}^{\beta'\beta''}\hat{\kappa}_{\mathsf{c}}^{\alpha'\alpha''}T\frac{\delta^2 \log Z[\mathsf{h}^{n,l},\boldsymbol{\sigma}^{\mathsf{D}_{3\mathsf{d}}}]}{\delta \mathsf{h}_{-q}^{E_g,2-\beta''\mathrm{mod}(2)}\delta \mathsf{h}_{q}^{E_g,2-\alpha''\mathrm{mod}(2)}}, \end{aligned}$$

which becomes the eventual relation

$$\left(\mathcal{C}_q^{r,E_g}\right)^{-1}_{\alpha,\beta} = \left(\mathcal{C}^{E_g}\right)^{-1}_{\alpha\beta} + \left(\mathcal{C}^{E_g}\right)^{-1}_{\alpha'\alpha}\left(\mathcal{C}^{E_g}\right)^{-1}_{\beta\beta'}\hat{\kappa}_{\mathsf{c}}^{\beta'\beta''}\hat{\kappa}_{\mathsf{c}}^{\alpha'\alpha''}\chi_{\mathrm{nem},2-\alpha''\mathrm{mod}(2),2-\beta''\mathrm{mod}(2)}(q).$$

In matrix representation the equation reads

$$\left(\mathcal{C}_q^{r,E_g}\right)^{-1} = \left(\mathcal{C}^{E_g}\right)^{-1} + \left(\mathcal{C}^{E_g}\right)^{-1}\hat{\kappa}_{\mathsf{c}}\hat{\chi}_{\mathrm{nem}}(q)\hat{\kappa}_{\mathsf{c}}\left(\mathcal{C}^{E_g}\right)^{-1} \tag{C.35}$$

with

$$\hat{\chi}_{\mathrm{nem}}(q) = \begin{pmatrix}\chi_{\mathrm{nem}}(q) & \chi_{\mathrm{nem}}(q)\\ \chi_{\mathrm{nem}}(q) & \chi_{\mathrm{nem}}(q)\end{pmatrix}.$$

While the above relation (C.35) is the one, we are most interested in, we can also relate the remaining elastic constants to the respective correlation functions, and eventually study the renormalization thereof due to approaching superconducting instability. Taking the other second derivatives of (C.34)

and (C.33) yields

$$T\frac{\delta^2 \log Z[\mathsf{h}^{n,l},\boldsymbol{\sigma}^{\mathsf{D}_{3\mathsf{d}}}]}{\delta\sigma_q^{A_{1g},i}\delta\sigma_{-q}^{A_{1g},j}} = \left(\mathcal{C}^{A_{1g}}\right)^{-1}_{ij} + \hat{\kappa}_A^{j'j''}\left(\mathcal{C}^{A_{1g}}\right)^{-1}_{j'j}\hat{\kappa}_A^{i'i''}\left(\mathcal{C}^{A_{1g}}\right)^{-1}_{i'i} T\frac{\delta^2 \log Z[\mathsf{h}^{n,l},\boldsymbol{\sigma}^{\mathsf{D}_{3\mathsf{d}}}]}{\delta\mathsf{h}_q^{A_{1g}}\delta\mathsf{h}_{-q}^{A_{1g}}}$$
$$T\frac{\delta^2 \log Z[\mathsf{h}^{n,l},\boldsymbol{\sigma}^{\mathsf{D}_{3\mathsf{d}}}]}{\delta\sigma_q^{A_{1g},i}\delta\sigma_{-q}^{E_g,\beta}} = \left(\mathcal{C}^{E_g}\right)^{-1}_{\beta'\beta}\hat{\kappa}_{\mathsf{c}}^{\beta'\beta''}\hat{\kappa}_A^{i'j'}\left(\mathcal{C}^{A_{1g}}\right)^{-1}_{i'i} T\frac{\delta^2 \log Z[\mathsf{h}^{n,l},\boldsymbol{\sigma}^{\mathsf{D}_{3\mathsf{d}}}]}{\delta\mathsf{h}_{-q}^{E_g,2-\beta''\mathrm{mod}(2)}\delta\mathsf{h}_q^{A_{1g}}}$$

and thus, the relations

$$\left(\mathcal{C}_q^{r,A_{1g}}\right)^{-1}_{i,j} = \left(\mathcal{C}^{A_{1g}}\right)^{-1} + \left(\mathcal{C}^{A_{1g}}\right)^{-1}\hat{\chi}_{A_{1g}}(q)\left(\mathcal{C}^{A_{1g}}\right)^{-1},$$
$$\left(\mathcal{C}_q^{r,A_{1g}E_g}\right)^{-1} = \left(\mathcal{C}^{A_{1g}}\right)^{-1}\hat{\chi}_{A_{1g}E_g}(-q)\hat{\kappa}_{\mathsf{c}}\left(\mathcal{C}^{E_g}\right)^{-1},$$

with

$$\hat{\chi}_{A_{1g}}(q) = \begin{pmatrix} \kappa_{A1}^2 & \kappa_{A1}\kappa_{A2} \\ \kappa_{A1}\kappa_{A2} & \kappa_{A2}^2 \end{pmatrix}\chi_{A_{1g}}(q), \qquad \hat{\chi}_{A_{1g}E_g}(q) = \begin{pmatrix} \kappa_{A1} & \kappa_{A1} \\ \kappa_{A2} & \kappa_{A2} \end{pmatrix}\otimes\chi_{A_{1g}E_g}(q).$$

C.4.1 Computation of the nematic susceptibility

We derive the nematic susceptibility conveniently from the saddle-point equations above T_c in the presence of the external fields $\mathbf{h}^{E_g}$ and $\mathsf{h}^{A_{1g}}$. The corresponding action is given in (C.31), and after the Hubbard-Stratonovich transformation, we shift the composite fields $\tilde{\mathsf{C}}_q^{n,l} = \mathsf{C}_q^{n,l} - \mathsf{h}_q^{n,l}$ such that the external field dependence is moved into the kinetic term

$$\mathcal{S}_{\mathsf{C}} = \frac{-1}{4u'}V\sum_q(\tilde{\boldsymbol{C}}_q^{A_{1g}} + \mathsf{h}_q^{A_{1g}})(\tilde{\boldsymbol{C}}_{-q}^{A_{1g}} + \mathsf{h}_{-q}^{A_{1g}}) + \frac{1}{4v}V\sum_q(\tilde{\boldsymbol{C}}_q^{E_g} + \mathbf{h}_q^{E_g})(\tilde{\boldsymbol{C}}_{-q}^{E_g} + \mathbf{h}_{-q}^{E_g}).$$

Similarly to Eq.(3.63) the susceptibilities can be derived via

$$\chi_{\mathrm{nem},lj}(q) = -\frac{1}{2v}\left(\frac{\delta\langle\tilde{\mathsf{C}}_q^{E_g,l}\rangle_{\mathsf{h}}}{\delta\mathsf{h}_q^{E_g,j}}\bigg|_{\mathbf{h}=0} + \delta_{lj}\right), \qquad \chi_{E_gA_{1g},l}(q) = -\frac{1}{2v}\frac{\delta\langle\tilde{\mathsf{C}}_q^{E_g,l}\rangle_{\mathsf{h}}}{\delta\mathsf{h}_q^{A_{1g}}}\bigg|_{\mathbf{h}=0},$$
$$\chi_{A_{1g}}(q) = \frac{1}{2u'}\left(\frac{\delta\langle\tilde{\mathsf{C}}_q^{A_{1g}}\rangle_{\mathsf{h}}}{\delta\mathsf{h}_q^{A_{1g}}}\bigg|_{\mathbf{h}=0} + 1\right), \qquad \chi_{E_gA_{1g},l}(q) = \frac{1}{2u'}\frac{\delta\langle\tilde{\mathsf{C}}_q^{A_{1g}}\rangle_{\mathsf{h}}}{\delta\mathsf{h}_q^{E_g,l}}\bigg|_{\mathbf{h}=0}.$$

Then, we obtain the saddle-point equations

$$0 = -\frac{1}{2u'}\left(\tilde{\mathsf{C}}_0^{A_{1g}} + \mathsf{h}_0^{A_{1g}}\right) + \frac{T}{2V}\sum_q \mathrm{tr}_\tau\left(\mathcal{G}_{q,q}^{\tilde{\mathsf{C}}}\tau^0\right), \quad 0 = \frac{1}{2v}\left(\tilde{\mathsf{C}}_0^{E_g,l} + \mathsf{h}_0^{E_g,l}\right) + \frac{T}{2V}\sum_q \mathrm{tr}_\tau\left(\mathcal{G}_{q,q}^{\tilde{\mathsf{C}}}\tau^{E_g,l}\right).$$

The variation of the above equations with respect to $\mathsf{h}_0^{E_g,j}$ and $h_0^{A_{1g}}$ yields

$$0 = -\chi_{E_gA_{1g},j}(0) + \chi^{(0)}_{A_{1g}E_g,j}(0) - 2u'\chi^{(0)}_{A_{1g}}(0)\chi_{E_gA_{1g},j}(0) + 2v\chi^{(0)}_{A_{1g}E_g,i}(0)\chi_{\mathrm{nem},ij}(0), \tag{C.36}$$

$$0 = -\chi_{\mathrm{nem},lj}(0) - 2u'\chi^{(0)}_{A_{1g}E_g,l}(0)\chi_{E_gA_{1g},j}(0) + 2v\chi^{(0)}_{\mathrm{nem},li}(0)\chi_{\mathrm{nem},ij}(0) + \chi^{(0)}_{\mathrm{nem},lj}(0). \tag{C.37}$$

$$0 = -\chi_{A_{1g}}(0) - 2u'\chi^{(0)}_{A_{1g}}(0)\chi_{A_{1g}}(0) + \chi^{(0)}_{A_{1g}}(0) + 2v\chi^{(0)}_{A_{1g}E_g,i}(0)\chi_{E_gA_{1g},i}(0), \tag{C.38}$$

$$0 = -\chi_{E_gA_{1g},l}(0) - 2u'\chi^{(0)}_{A_{1g}E_g,l}(0)\chi_{A_{1g}}(0) + \chi^{(0)}_{A_{1g}E_g,l}(0) + 2v\chi^{(0)}_{\mathrm{nem},li}(0)\chi_{E_gA_{1g},i}(0). \tag{C.39}$$

with

$$\chi^{(0)}_{A_{1g}}(0) = \frac{T}{2V}\sum_q \mathrm{tr}_\tau\left(\mathcal{G}_q\tau^0\mathcal{G}_q\tau^0\right)\Big|_{\mathsf{h}^{n,l}=0}, \qquad \chi^{(0)}_{\mathrm{nem},lj}(0) = \frac{T}{2V}\sum_q \mathrm{tr}_\tau\left(\mathcal{G}_q\tau^{E_g,l}\mathcal{G}_q\tau^{E_g,j}\right)\Big|_{\mathsf{h}^{n,l}=0},$$
$$\chi^{(0)}_{A_{1g}E_g,l}(0) = \frac{T}{2V}\sum_q \mathrm{tr}_\tau\left(\mathcal{G}_q\tau^{E_g,l}\mathcal{G}_q\tau^0\right)\Big|_{\mathsf{h}^{n,l}=0}.$$

In the para-nematic regime, i.e. $T > T_{\mathrm{nem}}$, the bare susceptibilities become

$$\chi^{(0)}_{A_{1g}}(0) = \frac{1}{2}\tilde{\Pi}_{0,0}, \qquad \chi^{(0)}_{\mathrm{nem},lj}(0) = \frac{1}{2}\tilde{\Pi}_{l,j}, \qquad \chi^{(0)}_{A_{1g}E_g,l}(0) = \frac{1}{2}\tilde{\Pi}_{0,l} = 0,$$

with the definitions (C.19). With the vanishing $\chi^{(0)}_{A_{1g}E_g,l}(0) = 0$ the equations (C.36)-(C.39) are solved by $\chi_{E_gA_{1g},j}(0) = 0$ and

$$\chi_{\mathrm{nem}}(0) = \chi^{(0)}_{\mathrm{nem}}(0)\left(\mathbb{1} - 2v\chi^{(0)}_{\mathrm{nem}}(0)\right)^{-1}, \qquad \chi_{A_{1g}}(0) = \frac{\chi^{(0)}_{A_{1g}}(0)}{1 + 2u'\chi^{(0)}_{A_{1g}}(0)}.$$

Inserting the identity $\tilde{\Pi}_{l,l'} = \tilde{\Pi}_{z,z}\delta_{l,l'}$ (see Sec.C.2), we can further simplify the nematic susceptibility to

$$\chi_{\mathrm{nem}}(0) = \frac{\frac{1}{2}\tilde{\Pi}_{z,z}}{1 - v\tilde{\Pi}_{z,z}}\mathbb{1}.$$

C.5 Derivation of the upper critical field

In this section, we redo the analysis of Sec. 3.5.1, yet with the magnetic field being applied within the basal plane $\boldsymbol{B} = |\boldsymbol{B}|(\cos\varphi_B e_x + \sin\varphi_B e_y)$. The aim of this part is to determine the angle dependence of the upper critical field $H_{c2}(\varphi_B)$. It is convenient to rotate the coordinate system such that one axis, say the new x-axis, coincides with the magnetic field direction. Hence, we rotate the coordinates according to

$$\boldsymbol{r} = R_{SO(3)}(\varphi_B, e_z)\boldsymbol{r'}, \quad \nabla_{\boldsymbol{r}} = R_{SO(3)}(\varphi_B, e_z)\nabla_{\boldsymbol{r'}}, \quad \boldsymbol{A'}(\boldsymbol{r'}) = R^{-1}_{SO(3)}(\varphi_B, e_z)\boldsymbol{A}(\boldsymbol{r}) = \frac{|\boldsymbol{B}|}{2}\begin{pmatrix}0\\ -z'\\ y'\end{pmatrix}$$

with the representation of the rotation matrix (1.18)

$$R_{SO(3)}(\varphi_B, e_z) = \begin{pmatrix} \cos\varphi_B & -\sin\varphi_B & 0 \\ \sin\varphi_B & \cos\varphi_B & 0 \\ 0 & 0 & 1 \end{pmatrix}.$$

Then, the canonical momenta transform as $(D_x, D_y, D_z)^T = R_{SO(3)}(\varphi_B, e_z)(D_{x'}, D_{y'}, D_{z'})^T$ and it holds $[D_{x'}, D_{y'}] = [D_{x'}, D_{z'}] = 0$ and $[D_{y'}, D_{z'}] = \mathrm{i}e|\boldsymbol{B}|$. Thus, the x'-direction is aligned with the magnetic field, while $D_{y'}, D_{z'}$ fulfill the harmonic oscillator algebra. Similarly to section 3.5.1, we neglect modulations along the vortex axis, such that $D_{x'}\Delta^{E_u,\pm} = 0$. In the rotated frame, the two saddle-point equations become

$$0 = \Big(R_0 + \mathsf{d}_0 D_{y'}^2 + \mathsf{d}_z D_{z'}^2\Big)\Delta^{E_u,+} - \Big(\mathsf{d}' e^{2\mathrm{i}\varphi_B} D_{y'}^2 - \tilde{\mathsf{d}} e^{-\mathrm{i}\varphi_B} \left\{D_{z'}, D_{y'}\right\}_+ - \mathsf{C}^{E_g,-}\Big)\Delta^{E_u,-} \tag{C.40}$$

$$0 = \Big(R_0 + \mathsf{d}_0 D_{y'}^2 + \mathsf{d}_z D_{z'}^2\Big)\Delta^{E_u,-} - \Big(\mathsf{d}' e^{-2\mathrm{i}\varphi_B} D_{y'}^2 - \tilde{\mathsf{d}} e^{\mathrm{i}\varphi_B} \left\{D_{z'}, D_{y'}\right\}_+ - \mathsf{C}^{E_g,+}\Big)\Delta^{E_u,+}. \tag{C.41}$$

With the annihilation and creation operators

$$a = \frac{1}{\sqrt{2e|\boldsymbol{B}|\sqrt{\mathsf{d}_0\mathsf{d}_z}}}\left(\sqrt{\mathsf{d}_0} D_{y'} + \mathrm{i}\sqrt{\mathsf{d}_z} D_{z'}\right), \qquad a^\dagger = \frac{1}{\sqrt{2e|\boldsymbol{B}|\sqrt{\mathsf{d}_0\mathsf{d}_z}}}\left(\sqrt{\mathsf{d}_0} D_{y'} - \mathrm{i}\sqrt{\mathsf{d}_z} D_{z'}\right),$$

satisfying $[a, a^\dagger] = 1$, the above equations transform into

$$0 = \Big(R_0 + a^\dagger a + \frac{1}{2}\Big)\Delta^{E_u,+} - \Big(\frac{\hat{\mathsf{d}}' e^{2\mathrm{i}\varphi_B}}{4}\Big(a^2 + (a^\dagger)^2 + 2a^\dagger a + 1\Big) - \frac{\hat{\tilde{\mathsf{d}}} e^{-\mathrm{i}\varphi_B}}{2}\Big((a^\dagger)^2 - a^2\Big) - \mathsf{C}^{E_g,-}\Big)\Delta^{E_u,-},$$

$$0 = \Big(R_0 + a^\dagger a + \frac{1}{2}\Big)\Delta^{E_u,-} - \Big(\frac{\hat{\mathsf{d}}' e^{-2\mathrm{i}\varphi_B}}{4}\Big(a^2 + (a^\dagger)^2 + 2a^\dagger a + 1\Big) - \frac{\hat{\tilde{\mathsf{d}}} e^{\mathrm{i}\varphi_B}}{2}\Big((a^\dagger)^2 - a^2\Big) - \mathsf{C}^{E_g,+}\Big)\Delta^{E_u,+},$$

where we have defined $\{\hat{R}_0, \hat{\mathsf{C}}^{E_g,+}\} = \{R_0, \mathsf{C}^{E_g,+}\}/2e|\boldsymbol{B}|\sqrt{\mathsf{d}_0\mathsf{d}_z}$, $\hat{\alpha} = \alpha'/2e\mathsf{d}_0$, $\hat{\mathsf{d}}' = \mathsf{d}'/\mathsf{d}_0$ and $\hat{\tilde{\mathsf{d}}} = \tilde{\mathsf{d}}/\sqrt{\mathsf{d}_0\mathsf{d}_z}$. Using again the ansatz (3.100), we find the recursion formula

$$\begin{aligned}\hat{R}_0 a_n = {} & -a_n\left(n + \frac{1}{2}\right) + \frac{1}{4}\left(\hat{\mathsf{d}}' e^{2\mathrm{i}\varphi_B} + 2\mathrm{i}\hat{\tilde{\mathsf{d}}} e^{-\mathrm{i}\varphi_B}\right) b_{n+2}\sqrt{(n+2)(n+1)} \\ & + \frac{1}{4}\left(\hat{\mathsf{d}}' e^{2\mathrm{i}\varphi_B} - 2\mathrm{i}\hat{\tilde{\mathsf{d}}} e^{-\mathrm{i}\varphi_B}\right) b_{n-2}\sqrt{n(n-1)} + \left(\frac{1}{4}\hat{\mathsf{d}}' e^{2\mathrm{i}\varphi_B}\ (2n+1) - \hat{\mathsf{C}}^{E_g,-}\right) b_n, \end{aligned} \tag{C.42}$$

$$\begin{aligned}\hat{R}_0 b_n = {} & -b_n\left(n + \frac{1}{2}\right) + \frac{1}{4}\left(\hat{\mathsf{d}}' e^{-2\mathrm{i}\varphi_B} + 2\mathrm{i}\hat{\tilde{\mathsf{d}}} e^{\mathrm{i}\varphi_B}\right) a_{n+2}\sqrt{(n+2)(n+1)} \\ & + \frac{1}{4}\left(\hat{\mathsf{d}}' e^{-2\mathrm{i}\varphi_B} - 2\mathrm{i}\hat{\tilde{\mathsf{d}}} e^{\mathrm{i}\varphi_B}\right) a_{n-2}\sqrt{n(n-1)} + \left(\frac{1}{4}\hat{\mathsf{d}}' e^{-2\mathrm{i}\varphi_B}\ (2n+1) - \mathsf{C}^{E_g,+}\right) a_n, \end{aligned} \tag{C.43}$$

valid for $n = 0, 1, 2, \ldots$. For the reasons outlined in Sec. 3.5.1, we focus on the even subspace and introduce the vector $\boldsymbol{\zeta} = (b_0, a_0, b_2, a_2, b_4, a_4, \ldots)^T$, which transforms the above condition into the eigenwert problem $\hat{R}_0\boldsymbol{\zeta} = M\boldsymbol{\zeta}$. For clarity, we do not show the matrix M explicitly. Yet, the resulting angle dependence of $H_{c2}(\varphi_B)$— i.e. the H_{c2} contour in the x, y-plane which yields a fixed maximum eigenvalue—is plotted in Fig. 3.13, with and without a nematic order parameter present.

D Appendix D

Phase stiffness

In this part, we provide the calculations and proofs that were exploited in chapter 4.

D.1 Individual propagators and Matsubara summation

In this part of the appendix, we provide the explicit expressions for both, the individual Green's functions hidden in (4.20) and the matrix elements (4.21). The Green's function matrix, i.e. the inverse of (4.20), reads

$$\hat{G}_k^{\Phi} = \begin{pmatrix} G_k^{\Phi} & F_k^{\Phi} \\ F_k^{\Phi} & -G_{-k}^{\Phi} \end{pmatrix}, \tag{D.1}$$

where the normal and anomalous Green's functions in the presence of an external flux are given by

$$G_k^{\Phi} = \frac{-(i\omega_n + \epsilon_{-\boldsymbol{k}}^{\Phi})}{\omega_n^2 + \epsilon_{\boldsymbol{k}}^{\Phi}\epsilon_{-\boldsymbol{k}}^{\Phi} + \gamma_{\boldsymbol{k}}^2\Delta_0^2 + i\omega_n(\epsilon_{\boldsymbol{k}}^{\Phi} - \epsilon_{-\boldsymbol{k}}^{\Phi})} = \frac{(u_{\boldsymbol{k}}^{\Phi})^2}{i\omega_n - a_{\boldsymbol{k}}^{\Phi} - \lambda_{\boldsymbol{k}}^{\Phi}} + \frac{(v_{\boldsymbol{k}}^{\Phi})^2}{i\omega_n - a_{\boldsymbol{k}}^{\Phi} + \lambda_{\boldsymbol{k}}^{\Phi}}, \tag{D.2}$$

$$F_k^{\Phi} = \frac{\gamma_{\boldsymbol{k}}\Delta_0}{\omega_n^2 + \epsilon_{\boldsymbol{k}}^{\Phi}\epsilon_{-\boldsymbol{k}}^{\Phi} + \gamma_{\boldsymbol{k}}^2\Delta_0^2 + i\omega_n(\epsilon_{\boldsymbol{k}}^{\Phi} - \epsilon_{-\boldsymbol{k}}^{\Phi})} = \frac{\gamma_{\boldsymbol{k}}\Delta_0}{2\lambda_{\boldsymbol{k}}^{\Phi}}\left(\frac{-1}{i\omega_n - a_{\boldsymbol{k}}^{\Phi} - \lambda_{\boldsymbol{k}}^{\Phi}} + \frac{1}{i\omega_n - a_{\boldsymbol{k}}^{\Phi} + \lambda_{\boldsymbol{k}}^{\Phi}}\right). \tag{D.3}$$

Here, we have defined $\lambda_{\boldsymbol{k}}^{\Phi} = \sqrt{(\xi_{\boldsymbol{k}}^{\Phi})^2 + \gamma_{\boldsymbol{k}}^2\Delta_0^2}$, $u_{\boldsymbol{k}}^{\Phi} = \sqrt{\frac{1}{2}(1 + \xi_{\boldsymbol{k}}^{\Phi}/\lambda_{\boldsymbol{k}}^{\Phi})}$, $v_{\boldsymbol{k}}^{\Phi} = \sqrt{\frac{1}{2}(1 - \xi_{\boldsymbol{k}}^{\Phi}/\lambda_{\boldsymbol{k}}^{\Phi})}$, as well as

$$\xi_{\boldsymbol{k}}^{\Phi} = \epsilon_{\boldsymbol{k}} + 2\cos(k_x)\sin^2(\frac{\Phi}{2L})\left(t + 2t'\cos\left(k_y\right)\right), \qquad a_{\boldsymbol{k}}^{\Phi} = -2\sin(k_x)\sin(\frac{\Phi}{L})\left(t + 2t'\cos\left(k_y\right)\right).$$

Using this notation, the matrix elements of $\hat{M}^{\Phi}$ (4.21) become

$$\Gamma_q^{(\Delta\Delta),\Phi} = \frac{2}{g} + 2\Gamma_q^{(FF),\Phi} + \Gamma_q^{(GG),\Phi} + \Gamma_{-q}^{(GG),\Phi}$$
$$= \frac{1}{L^2}\sum_{\boldsymbol{k}} \left\{ \frac{\gamma_{\boldsymbol{k}}^2}{\lambda_{\boldsymbol{k}}^\Phi} + \left(1 + \frac{\xi_{\boldsymbol{k}}^\Phi \xi_{\boldsymbol{k}+\boldsymbol{q}}^\Phi - \gamma_{\boldsymbol{k}}\gamma_{\boldsymbol{k}+\boldsymbol{q}}\Delta_0^2}{\lambda_{\boldsymbol{k}}^\Phi \lambda_{\boldsymbol{k}+\boldsymbol{q}}^\Phi}\right) \frac{\gamma_{\boldsymbol{k}+\frac{\boldsymbol{q}}{2}}^2 (\lambda_{\boldsymbol{k}+\boldsymbol{q}}^\Phi + \lambda_{\boldsymbol{k}}^\Phi)}{(i\nu_m - \delta a_{\boldsymbol{k},\boldsymbol{q}}^\Phi)^2 - (\lambda_{\boldsymbol{k}+\boldsymbol{q}}^\Phi + \lambda_{\boldsymbol{k}}^\Phi)^2} \right\}, \tag{D.4}$$

$$\Gamma_q^{(\theta\theta),\Phi} = \frac{2}{g} - 2\Gamma_q^{(FF),\Phi} + \Gamma_q^{(GG),\Phi} + \Gamma_{-q}^{(GG),\Phi}$$
$$= \frac{1}{L^2}\sum_{\boldsymbol{k}} \left\{ \frac{\gamma_{\boldsymbol{k}}^2}{\lambda_{\boldsymbol{k}}^\Phi} + \left(1 + \frac{\xi_{\boldsymbol{k}}^\Phi \xi_{\boldsymbol{k}+\boldsymbol{q}}^\Phi + \gamma_{\boldsymbol{k}}\gamma_{\boldsymbol{k}+\boldsymbol{q}}\Delta_0^2}{\lambda_{\boldsymbol{k}}^\Phi \lambda_{\boldsymbol{k}+\boldsymbol{q}}^\Phi}\right) \frac{\gamma_{\boldsymbol{k}+\frac{\boldsymbol{q}}{2}}^2 (\lambda_{\boldsymbol{k}+\boldsymbol{q}}^\Phi + \lambda_{\boldsymbol{k}}^\Phi)}{(i\nu_m - \delta a_{\boldsymbol{k},\boldsymbol{q}}^\Phi)^2 - (\lambda_{\boldsymbol{k}+\boldsymbol{q}}^\Phi + \lambda_{\boldsymbol{k}}^\Phi)^2} \right\}, \tag{D.5}$$

$$\Gamma_q^{(\Delta\theta),\Phi} = \Gamma_q^{(GG),\Phi} - \Gamma_{-q}^{(GG),\Phi}$$
$$= \frac{1}{L^2}\sum_{\boldsymbol{k}} \left(\frac{\xi_{\boldsymbol{k}}^\Phi}{\lambda_{\boldsymbol{k}}^\Phi} + \frac{\xi_{\boldsymbol{k}+\boldsymbol{q}}^\Phi}{\lambda_{\boldsymbol{k}+\boldsymbol{q}}^\Phi} \right) \frac{\gamma_{\boldsymbol{k}+\frac{\boldsymbol{q}}{2}}^2 (i\nu_m - \delta a_{\boldsymbol{k},\boldsymbol{q}}^\Phi)}{(i\nu_m - \delta a_{\boldsymbol{k},\boldsymbol{q}}^\Phi)^2 - (\lambda_{\boldsymbol{k}+\boldsymbol{q}}^\Phi + \lambda_{\boldsymbol{k}}^\Phi)^2}\,, \tag{D.6}$$

where the Matsubara summations have been performed and the zero-temperature limit $T = 0$ has been applied. We have defined the quantity $\delta a_{\boldsymbol{k},\boldsymbol{q}}^\Phi = a_{\boldsymbol{k}+\boldsymbol{q}}^\Phi - a_{\boldsymbol{k}}^\Phi$. Furthermore, the gap equation (4.19) has been used and the expressions

$$\Gamma_q^{(FF),\Phi} = \frac{T}{L^2}\sum_k \gamma_{\boldsymbol{k}+\frac{\boldsymbol{q}}{2}}^2 F_k^\Phi F_{k+q}^\Phi = \frac{\text{-}1}{L^2}\sum_{\boldsymbol{k}} \gamma_{\boldsymbol{k}+\frac{\boldsymbol{q}}{2}}^2 \frac{\gamma_{\boldsymbol{k}}\gamma_{\boldsymbol{k}+\boldsymbol{q}}\Delta_0^2}{2\lambda_{\boldsymbol{k}}^\Phi \lambda_{\boldsymbol{k}+\boldsymbol{q}}^\Phi} \frac{(\lambda_{\boldsymbol{k}+\boldsymbol{q}}^\Phi + \lambda_{\boldsymbol{k}}^\Phi)}{(i\nu_m - \delta a_{\boldsymbol{k},\boldsymbol{q}}^\Phi)^2 - (\lambda_{\boldsymbol{k}+\boldsymbol{q}}^\Phi + \lambda_{\boldsymbol{k}}^\Phi)^2},$$

$$\Gamma_q^{(GG),\Phi} = \frac{\text{-}T}{L^2}\sum_k \gamma_{\boldsymbol{k}+\frac{\boldsymbol{q}}{2}}^2 G_{-k}^\Phi G_{k+q}^\Phi = \frac{\text{-}1}{2L^2}\sum_{\boldsymbol{k}} \gamma_{\boldsymbol{k}+\frac{\boldsymbol{q}}{2}}^2 \frac{(i\nu_m - \delta a_{\boldsymbol{k},\boldsymbol{q}}^\Phi)\left(\frac{\xi_{\boldsymbol{k}}^\Phi}{\lambda_{\boldsymbol{k}}^\Phi} + \frac{\xi_{\boldsymbol{k}+\boldsymbol{q}}^\Phi}{\lambda_{\boldsymbol{k}+\boldsymbol{q}}^\Phi}\right) + (\lambda_{\boldsymbol{k}+\boldsymbol{q}}^\Phi + \lambda_{\boldsymbol{k}}^\Phi)\left(1 + \frac{\xi_{\boldsymbol{k}}^\Phi \xi_{\boldsymbol{k}+\boldsymbol{q}}^\Phi}{\lambda_{\boldsymbol{k}}^\Phi \lambda_{\boldsymbol{k}+\boldsymbol{q}}^\Phi}\right)}{(i\nu_m - \delta a_{\boldsymbol{k},\boldsymbol{q}}^\Phi)^2 - (\lambda_{\boldsymbol{k}+\boldsymbol{q}}^\Phi + \lambda_{\boldsymbol{k}}^\Phi)^2},$$

have been inserted. All the above equations are evaluated at zero-temperature. Note that by having set the Fermi functions $f(\pm\lambda_{\boldsymbol{k}}^\Phi + a_{\boldsymbol{k}}^\Phi) = \theta(\mp 1)$, we ignore integral contributions from the derivatives $f'(\pm\lambda_{\boldsymbol{k}}^\Phi + a_{\boldsymbol{k}}^\Phi) = f''(\pm\lambda_{\boldsymbol{k}}^\Phi + a_{\boldsymbol{k}}^\Phi)$ which would occur during the computation of the phase stiffness. In other words, we neglect additional integral contributions from the single points in the Brillouin zone where $\lambda_{\boldsymbol{k}} = 0$.

The calculation of the derivatives of the matrix elements (D.4-D.6) with respect to Φ or Δ as required in section 4.5 is tedious but straightforward. We refrain from showing these lengthy expressions.

D.2 Derivatives of the gap and the chemical potential

This part deals with the response of the superconducting gap and the chemical potential on the applied external flux Φ. To be more precise, we want to prove that the first-order derivatives of the superconducting gap, and the chemical potential indeed vanish. Afterwards, we compute the required higher order derivatives. All the occurring derivatives are implicitly assumed to be evaluated at $\Phi \to 0$. At the core of the proof is the identity

$$\frac{\partial\Omega}{\partial\Phi}\Big|_{\Delta,\mu}\Big|_{\Phi\to 0} = 0\,, \tag{D.7}$$

which is quickly checked upon exploitation of the mirror symmetry $M_x : q_x \to -q_x$ after the derivative has been carried out. Now, we express the number and the gap equation by

$$N = -\frac{\partial \Omega}{\partial \mu} \equiv f_N\left(\mu(\Phi), \Delta\left(\mu(\Phi), \Phi\right), \Phi\right), \qquad g^{-1} = \frac{\partial \Omega_F}{\partial \Delta} \equiv f_\Delta\left(\mu(\Phi), \Delta\left(\mu(\Phi), \Phi\right), \Phi\right). \tag{D.8}$$

The application of $\frac{\partial}{\partial \Phi}|_{\Delta,\mu}$ on (D.8) allows for a respective interchange of the order of variation and hence, the identity (D.7) can be employed yielding $\frac{\partial f_N}{\partial \Phi}|_{\Delta,\mu} = \frac{\partial f_\Delta}{\partial \Phi}|_{\Delta,\mu} = 0$. This, however, means that the total derivatives of (D.8) with respect to the phase twist read

$$0 = \frac{\partial f_N}{\partial \Delta}\Big|_\mu \frac{\partial \Delta}{\partial \Phi}\Big|_\mu + \left(\frac{\partial f_N}{\partial \Delta}\Big|_\mu \frac{\partial \Delta}{\partial \mu} + \frac{\partial f_N}{\partial \mu}\Big|_\Delta\right)\frac{\partial \mu}{\partial \Phi}, \quad 0 = \frac{\partial f_\Delta}{\partial \Delta}\Big|_\mu \frac{\partial \Delta}{\partial \Phi}\Big|_\mu + \left(\frac{\partial f_\Delta}{\partial \Delta}\Big|_\mu \frac{\partial \Delta}{\partial \mu} + \frac{\partial f_\Delta}{\partial \mu}\Big|_\Delta\right)\frac{\partial \mu}{\partial \Phi}, \tag{D.9}$$

which only allow for the trivial solution

$$\frac{\partial \Delta}{\partial \Phi}\Big|_\mu = \frac{\partial \mu}{\partial \Phi} = 0\,. \tag{D.10}$$

Let us now compute the functions in (D.8) and the derivatives at zero temperature explicitly. The bosonic part N_B of the number equation (4.12) is considered as a higher order term in the weak coupling limit. The mean-field part of the number of electrons (4.12) and the gap equation (4.19) at zero temperature become

$$N_F = 2T\sum_k G_k^\Phi = \sum_{\boldsymbol{k}}\left(1 - \frac{\epsilon_{\boldsymbol{k}}^\Phi}{\lambda_{\boldsymbol{k}}^\Phi}\right), \qquad \frac{1}{g} = \frac{T}{L^2\Delta_0}\sum_k \gamma_{\boldsymbol{k}} F_k^\Phi = \frac{1}{L^2}\sum_{\boldsymbol{k}} \frac{\gamma_{\boldsymbol{k}}^2}{2\lambda_{\boldsymbol{k}}^\Phi}\,. \tag{D.11}$$

For the two functions one computes the derivatives

$$\frac{\partial f_N}{\partial \Delta}\Big|_\mu = \Delta_0 c_1\,, \quad \frac{\partial f_N}{\partial \mu}\Big|_\Delta = \Delta_0^2 c_2\,, \quad \frac{\partial f_\Delta}{\partial \Delta}\Big|_\mu = -\frac{\Delta_0 c_0}{2}\,, \quad \frac{\partial f_\Delta}{\partial \mu}\Big|_\Delta = \frac{c_1}{2}\,, \quad \frac{\partial^2 f_\Delta}{\partial \Phi^2}\Big|_{\Delta,\mu} = \frac{c_3}{L^2}\,,$$

where we have introduced the functions $c_0 = L^{-2}\sum_{\boldsymbol{k}} \gamma_{\boldsymbol{k}}^4/\lambda_{\boldsymbol{k}}^3$, $c_1 = L^{-2}\sum_{\boldsymbol{k}} \gamma_{\boldsymbol{k}}^2\epsilon_{\boldsymbol{k}}/\lambda_{\boldsymbol{k}}^3$, $c_2 = L^{-2}\sum_{\boldsymbol{k}} \gamma_{\boldsymbol{k}}^2/\lambda_{\boldsymbol{k}}^3$ and $c_3 = -L^{-2}\sum_{\boldsymbol{k}} \frac{\partial^2 \epsilon_{\boldsymbol{k}}}{\partial k_x^2}\gamma_{\boldsymbol{k}}^2\epsilon_{\boldsymbol{k}}/\lambda_{\boldsymbol{k}}^3$. For the second derivative of the gap function we obtain

$$0 = \frac{\partial^2 f_\Delta}{\partial \Phi^2}|_{\Delta,\mu} + \frac{\partial f_\Delta}{\partial \Delta}\Big|_\mu \frac{\partial^2 \Delta}{\partial \Phi^2}\Big|_\mu + \underbrace{\left(\frac{\partial f_\Delta}{\partial \Delta}\Big|_\mu \frac{\partial \Delta}{\partial \mu} + \frac{\partial f_\Delta}{\partial \mu}\Big|_\Delta\right)}_{=0}\frac{\partial^2 \mu}{\partial \Phi^2}\,.$$

The second term vanishes because the gap equation (D.8) has to hold for any value of Φ, in particular also for $\Phi = 0$. In this case, the derivative of the gap equation (D.8) with respect to the chemical potential exactly yields the term in the bracket. Hence, the required second derivative of the gap function becomes

$$\frac{\partial^2 \Delta}{\partial \Phi^2}\Big|_\mu = \frac{1}{L^2}\frac{2c_3}{\Delta_0 c_0}\,. \tag{D.12}$$

D.3 Limit of a Galilean invariant system

In the limit of a Galilean invariant system, i.e. $\epsilon_{\boldsymbol{k}} = \boldsymbol{k}^2/2m - \mu$, it must hold $\rho_s^{(B)} = 0$. In the present formalism, this is not obviously recovered. Following Ref.[167], we prove the identity by carrying out the external Matsubara integration. In the limit of Galilean invariance the form of the propagators (D.4)-(D.6) allows that the derivative with respect to Φ at constant Δ and μ can be recast as a derivative with respect to $\mathrm{i}\nu_m$. As an example, it holds

$$\left.\frac{\partial^2 \Gamma_q^{(\zeta),\Phi}}{\partial \Phi^2}\right|_{\Delta,\mu} = \frac{\partial^2}{\partial(\mathrm{i}\nu_m)^2}\tilde{\Gamma}_q^{(\zeta),0}\,,$$

where the integrand in $\tilde{\Gamma}_q^{(\zeta),0}$ is multiplied by an extra factor k_x^2/m^2L^2. Similar relations hold for the remaining propagators. Additionally, it holds $\frac{\partial^2\Delta}{\partial\Phi^2}|_\mu = 0$. The core result is that the derivative of the matrix $\hat{M}^\Phi$ (4.21) can be recast into

$$\left.\frac{\partial^2 \ln\det\,\hat{M}_q^\Phi}{\partial \Phi^2}\right|_{\Delta,\mu} = \frac{\partial^2 \ln\det\,\tilde{M}_q^0}{\partial(\mathrm{i}\nu_m)^2}\,,$$

and the external Matsubara integration can be carried out yielding

$$\int_{-\infty}^{\infty} d\nu\, \frac{\partial^2 \ln\det\,\tilde{M}_q^0}{\partial\nu^2} = \left.\frac{\partial \ln\det\,\tilde{M}_q^0}{\partial\nu}\right|_{-\infty}^{+\infty} = 0\,.$$

It is clear from Eqs. (D.4)-(D.6) that the first-order derivatives vanish in the limit $\nu \to \pm\infty$ while the original propagators stay finite. This completes the proof that the bosonic contribution in the Galilean invariant system is equal to zero.

Bibliography

[1] H. K. Onnes, *The resistance of pure mercury at helium temperatures*, Commun. Phys. Lab. Univ. Leiden **120b**, 1 (1911).

[2] J. Bardeen, L. N. Cooper, and J. R. Schrieffer, *Theory of superconductivity*, Physical review **108**, 1175 (1957).

[3] J. Bardeen, L. N. Cooper, and J. R. Schrieffer, *Microscopic theory of superconductivity*, Physical Review **106**, 162 (1957).

[4] W. Meissner and R. Ochsenfeld, *Ein neuer Effekt bei Eintritt der Supraleitfähigkeit*, Naturwissenschaften **21**, 787 (1933).

[5] J. G. Bednorz and K. A. Müller, *Possible high T_c superconductivity in the Ba- La- Cu- O system*, Zeitschrift für Physik B Condensed Matter **64**, 189 (1986).

[6] G. Sun, K. Wong, B. Xu, Y. Xin, and D. Lu, *T_c enhancement of $HgBa_2Ca_2Cu_3O_{8+\delta}$ by Tl substitution*, Physics Letters A **192**, 122 (1994).

[7] Y. Kamihara, T. Watanabe, M. Hirano, and H. Hosono, *Iron-based layered superconductor $La[O_{1-x}F_x]FeAs$ ($x = 0.05 - 0.12$) with $T_c = 26\,\mathrm{K}$*, Journal of the American Chemical Society **130**, 3296 (2008).

[8] T. Timusk and B. Statt, *The pseudogap in high-temperature superconductors: an experimental survey*, Reports on Progress in Physics **62**, 61 (1999).

[9] M. Sutherland, D. G. Hawthorn, R. W. Hill, F. Ronning, S. Wakimoto, H. Zhang, C. Proust, E. Boaknin, C. Lupien, L. Taillefer, R. Liang, D. A. Bonn, W. N. Hardy, R. Gagnon, N. E. Hussey, T. Kimura, M. Nohara, and H. Takagi, *Thermal conductivity across the phase diagram of cuprates: Low-energy quasiparticles and doping dependence of the superconducting gap*, Phys. Rev. B **67**, 174520 (2003).

[10] S. Hüfner, M. Hossain, A. Damascelli, and G. Sawatzky, *Two gaps make a high-temperature superconductor?*, Reports on Progress in Physics **71**, 062501 (2008).

[11] K. v. Klitzing, G. Dorda, and M. Pepper, *New method for high-accuracy determination of the fine-structure constant based on quantized hall resistance*, Physical Review Letters **45**, 494 (1980).

[12] Y. Ando, *Topological insulator materials*, Journal of the Physical Society of Japan **82**, 102001 (2013).

[13] L. Fu and C. L. Kane, *Superconducting proximity effect and Majorana fermions at the surface of a topological insulator*, Phys. Rev. Lett. **100**, 096407 (2008).

[14] Y. S. Hor, A. J. Williams, J. G. Checkelsky, P. Roushan, J. Seo, Q. Xu, H. W. Zandbergen, A. Yazdani, N. P. Ong, and R. J. Cava, *Superconductivity in $Cu_xBi_2Se_3$ and its implications for pairing in the undoped topological insulator*, Phys. Rev. Lett. **104**, 057001 (2010).

[15] K. Matano, M. Kriener, K. Segawa, Y. Ando, and G.-q. Zheng, *Spin-rotation symmetry breaking in the superconducting state of $Cu_xBi_2Se_3$*, Nature Physics **12**, 852 (2016).

[16] L. Fu and E. Berg, *Odd-parity topological superconductors: theory and application to $Cu_xBi_2Se_3$*, Physical review letters **105**, 097001 (2010).

[17] R. Tao, Y.-J. Yan, X. Liu, Z.-W. Wang, Y. Ando, Q.-H. Wang, T. Zhang, and D.-L. Feng, *Direct visualization of the nematic superconductivity in $Cu_xBi_2Se_3$*, Physical Review X **8**, 041024 (2018).

[18] M. Kriener, K. Segawa, Z. Ren, S. Sasaki, S. Wada, S. Kuwabata, and Y. Ando, *Electrochemical synthesis and superconducting phase diagram of $Cu_xBi_2Se_3$*, Physical Review B **84**, 054513 (2011).

[19] M. Kriener, K. Segawa, Z. Ren, S. Sasaki, and Y. Ando, *Bulk superconducting phase with a full energy gap in the doped topological insulator $Cu_xBi_2Se_3$*, Phys. Rev. Lett. **106**, 127004 (2011).

[20] C.-w. Cho, J. Shen, J. Lyu, O. Atanov, Q. Chen, S. H. Lee, Y. San Hor, D. J. Gawryluk, E. Pomjakushina, M. Bartkowiak, M. Hecker, J. Schmalian, and R. Lortz, *Z_3-vestigial nematic order due to superconducting fluctuations in the doped topological insulator $Nb_xBi_2Se_3$ and $Cu_xBi_2Se_3$*, Nature communications **11**, 1 (2020).

[21] A. J. Leggett, *On the superfluid fraction of an arbitrary many-body system at $T = 0$*, Journal of statistical physics **93**, 927 (1998).

[22] Y. Uemura, A. Keren, L. Le, G. Luke, W. Wu, Y. Kubo, T. Manako, Y. Shimakawa, M. Subramanian, J. Cobb *et al.*, *Magnetic-field penetration depth in $TI_2Ba_2CuO_{6+\delta}$ in the overdoped regime*, Nature **364**, 605 (1993).

[23] I. Božović, X. He, J. Wu, and A. Bollinger, *Dependence of the critical temperature in overdoped copper oxides on superfluid density*, Nature **536**, 309 (2016).

[24] H. K. Onnes, *The disappearance of the resistance of mercury*, Commun. Phys. Lab. Univ. Leiden **122b** (1911).

[25] H. K. Onnes, *On the sudden change in the rate at which the resistance of mercury disappears*, Commun. Phys. Lab. Univ. Leiden **124c** (1912).

[26] J. Schmalian, *Failed theories of superconductivity*, Modern Physics Letters B **24**, 2679 (2010).

[27] F. London and H. London, *The electromagnetic equations of the supraconductor*, Proceedings of the Royal Society A: Mathematical, Physical and Engineering Sciences **149** (1935).

[28] L. D. Landau, *On the theory of phase transitions*, Zh. Eksp. Teor. Fiz. **7**, 19 (1937).

[29] V. L. Ginzburg and L. D. Landau, *To the theory of superconductivity*, Zh. Eksp. Teor. Fiz. **20**, 1064 (1950).

[30] V. L. Ginzburg, *On the theory of superconductivity*, Il Nuovo Cimento (1955-1965) **2**, 1234 (1955).

[31] N. E. Phillips, *Heat capacity of aluminum between 0.1°K and 4.0°K*, Phys. Rev. **114**, 676 (1959).

[32] M. Tinkham, *Introduction to Superconductivity*, Dover Publications Inc (2004).

[33] P. G. D. Gennes, *Superconductivity Of Metals And Alloys*, Westview Press (1999).

[34] L. P. Gorkov, *Microscopic derivation of the Ginzburg-Landau equations in the theory of superconductivity*, Sov. Phys. JETP **9**, 1364 (1959).

[35] E. Maxwell, *Isotope effect in the superconductivity of mercury*, Physical Review **78**, 477 (1950).

[36] C. Reynolds, B. Serin, W. Wright, and L. Nesbitt, *Superconductivity of isotopes of mercury*, Physical Review **78**, 487 (1950).

[37] H. Fröhlich, *Theory of the superconducting state. i. the ground state at the absolute zero of temperature*, Physical Review **79**, 845 (1950).

[38] J. Bardeen, *Zero-point vibrations and superconductivity*, Physical Review **79**, 167 (1950).

[39] L. N. Cooper, *Bound electron pairs in a degenerate Fermi gas*, Physical Review **104**, 1189 (1956).

[40] A. Altland and B. D. Simons, *Condensed Matter Field Theory*, Cambridge University Press (2010).

[41] N. Bogoljubov, V. V. Tolmachov, and D. Širkov, *A new method in the theory of superconductivity*, Fortschritte der physik **6**, 605 (1958).

[42] G. Eliashberg, *Interactions between electrons and lattice vibrations in a superconductor*, Sov. Phys. JETP **11**, 696 (1960).

[43] G. Eliashberg, *Temperature green's function for electrons in a superconductor*, Sov. Phys. JETP **39**, 1437 (1961).

[44] A. Migdal, *Interaction between electrons and lattice vibrations in a normal metal*, Sov. Phys. JETP **7**, 996 (1958).

[45] F. Steglich, J. Aarts, C. D. Bredl, W. Lieke, D. Meschede, W. Franz, and H. Schäfer, *Superconductivity in the presence of strong Pauli paramagnetism: $CeCu_2Si_2$*, Phys. Rev. Lett. **43**, 1892 (1979).

[46] G. Stewart, Z. Fisk, J. Willis, and J. Smith, *Possibility of coexistence of bulk superconductivity and spin fluctuations in UPt_3*, in *Ten Years of Superconductivity: 1980–1990*, Springer, (85–88) (1984).

[47] D. Jérome, A. Mazaud, M. Ribault, and K. Bechgaard, *Superconductivity in a synthetic organic conductor $(TMTSF)_2PF_6$*, Journal de Physique Lettres **41**, 95 (1980).

[48] P. Coleman, *Introduction to Many-Body Physics*, Cambridge University Press (2015).

[49] J. Zinn-Justin, *Quantum Field Theory and Critical Phenomena*, Oxford University Press (2002).

[50] C. Weber, L. Capriotti, G. Misguich, F. Becca, M. Elhajal, and F. Mila, *Ising transition driven by frustration in a 2D classical model with continuous symmetry*, Phys. Rev. Lett. **91**, 177202 (2003).

[51] D. Loison and P. Simon, *Monte carlo analysis of the phase transitions in the two-dimensional $J_1 - J_2$XY model*, Phys. Rev. B **61**, 6114 (2000).

[52] M. Tinkham, *Group theory and quantum mechanics*, McGraw-Hill Book Company (1964).

[53] W. Hegert and M. Geilhufe, *Group Theory in Solid State Physics and Photonics*, Wiley-VCH (2018).

[54] M. Lax, *Symmetry principles in solid state and molecular physics*, John Wiley & Sons, Inc. (1974).

[55] B. A. Bernevig and T. Hughes, *Topological Insulators and Topological Superconductors*, Princeton University Press (2013).

[56] M. S. Scheurer, *Mechanism, symmetry and topology of ordered phase in correlated systems*, Ph.D. thesis, Karlsruhe Institute of Technology (2016).

[57] L. Fu, *Odd-parity topological superconductor with nematic order: Application to $Cu_xBi_2Se_3$*, Physical Review B **90**, 100509 (2014).

[58] P. Brydon, S. D. Sarma, H.-Y. Hui, and J. D. Sau, *Odd-parity superconductivity from phonon-mediated pairing: application to $Cu_xBi_2Se_3$*, Physical Review B **90**, 184512 (2014).

[59] P. Fulde and R. A. Ferrell, *Superconductivity in a strong spin-exchange field*, Phys. Rev. **135**, A550 (1964).

[60] A. Larkin and Y. N. Ovchinnikov, *Nonuniform state of superconductors*, Soviet Physics-JETP **20**, 762 (1965).

[61] E. Bauer and M. Sigrist, *Non-centrosymmetric Superconductors*, Springer (2012).

[62] A. Messiah, *Quantenmechanik: Quantenmechanik 2*, de Gruyter (1990).

[63] A. Altland and M. R. Zirnbauer, *Nonstandard symmetry classes in mesoscopic normal-superconducting hybrid structures*, Physical Review B **55**, 1142 (1997).

[64] M. R. Zirnbauer, *Riemannian symmetric superspaces and their origin in random-matrix theory*, Journal of Mathematical Physics **37**, 4986 (1996).

[65] É. Cartan, *Sur une classe remarquable d'espaces de Riemann*, Bulletin de la Société Mathématique de France **54**, 214 (1926).

[66] M. Z. Hasan and C. L. Kane, *Colloquium: Topological insulators*, Rev. Mod. Phys. **82**, 3045 (2010).

[67] A. P. Schnyder, S. Ryu, A. Furusaki, and A. W. Ludwig, *Classification of topological insulators and superconductors*, in *AIP Conference Proceedings*, vol. 1134, American Institute of Physics (2009), vol. 1134, (10–21).

[68] F. D. M. Haldane, *Model for a quantum hall effect without Landau levels: Condensed-matter realization of the "parity anomaly"*, Physical review letters **61**, 2015 (1988).

[69] C. L. Kane and E. J. Mele, *Quantum spin Hall effect in graphene*, Physical review letters **95**, 226801 (2005).

[70] C. L. Kane and E. J. Mele, *Z_2 topological order and the quantum spin Hall effect*, Physical review letters **95**, 146802 (2005).

[71] M. König, S. Wiedmann, C. Brüne, A. Roth, H. Buhmann, L. W. Molenkamp, X.-L. Qi, and S.-C. Zhang, *Quantum spin Hall insulator state in $HgTe$ quantum wells*, Science **318**, 766 (2007).

[72] B. A. Bernevig, T. L. Hughes, and S.-C. Zhang, *Quantum spin Hall effect and topological phase transition in $HgTe$ quantum wells*, science **314**, 1757 (2006).

[73] L. Fu and C. L. Kane, *Topological insulators with inversion symmetry*, Physical Review B **76**, 045302 (2007).

[74] L. Fu, C. L. Kane, and E. J. Mele, *Topological insulators in three dimensions*, Physical review letters **98**, 106803 (2007).

[75] J. C. Y. Teo and C. L. Kane, *Topological defects and gapless modes in insulators and superconductors*, Phys. Rev. B **82**, 115120 (2010).

[76] J. C. Y. Teo and T. L. Hughes, *Existence of Majorana-Fermion bound states on disclinations and the classification of topological crystalline superconductors in two dimensions*, Phys. Rev. Lett. **111**, 047006 (2013).

[77] K. Shiozaki and M. Sato, *Topology of crystalline insulators and superconductors*, Phys. Rev. B **90**, 165114 (2014).

[78] M. Sato, *Topological odd-parity superconductors*, Physical Review B **81**, 220504 (2010).

[79] A. P. Schnyder and P. M. Brydon, *Topological surface states in nodal superconductors*, Journal of Physics: Condensed Matter **27**, 243201 (2015).

[80] L. Trifunovic and P. W. Brouwer, *Higher-order bulk-boundary correspondence for topological crystalline phases*, Physical Review X **9**, 011012 (2019).

[81] M. Sato and Y. Ando, *Topological superconductors: a review*, Reports on Progress in Physics **80**, 076501 (2017).

[82] H. K. P. Eckerlin, *Structure Data of Elements and Intermetallic Phases · $BiOsSe - CaPb$*, Springer-Verlag Berlin Heidelberg (1971).

[83] S. Nakajima, *The crystal structure of $Bi_2Te_{3-x}Se_x$*, Journal of Physics and Chemistry of Solids **24**, 479 (1963).

[84] C.-X. Liu, X.-L. Qi, H. Zhang, X. Dai, Z. Fang, and S.-C. Zhang, *Model Hamiltonian for topological insulators*, Physical Review B **82**, 045122 (2010).

[85] H. Zhang, C.-X. Liu, X.-L. Qi, X. Dai, Z. Fang, and S.-C. Zhang, *Topological insulators in Bi_2Se_3, Bi_2Te_3 and Sb_2Te_3 with a single Dirac cone on the surface*, Nature physics **5**, 438 (2009).

[86] J. G. Analytis, J.-H. Chu, Y. Chen, F. Corredor, R. D. McDonald, Z. X. Shen, and I. R. Fisher, *Bulk Fermi surface coexistence with Dirac surface state in Bi_2Se_3 : A comparison of photoemission and Shubnikov–de Haas measurements*, Phys. Rev. B **81**, 205407 (2010).

[87] K. Wittel and R. Manne, *Atomic spin-orbit interaction parameters from spectral data for 19 elements*, Theoretica chimica acta **33**, 347 (1974).

[88] L. Fu, *Hexagonal warping effects in the surface states of topological insulator Bi_2Te_3*, Phys. Rev. Lett. **103**, 266801 (2009).

[89] M. Z. Hasan, H. Lin, and A. Bansil, *Warping the cone on a topological insulator*, Physics **2**, 108 (2009).

[90] Z. Liu, X. Yao, J. Shao, M. Zuo, L. Pi, S. Tan, C. Zhang, and Y. Zhang, *Superconductivity with topological surface state in $Sr_xBi_2Se_3$*, J. Am. Chem. Soc. **137**, 10512 (2015).

[91] Shruti, V. K. Maurya, P. Neha, P. Srivastava, and S. Patnaik, *Superconductivity by Sr intercalation in the layered topological insulator Bi_2Se_3*, Phys. Rev. B **92**, 020506 (2015).

[92] E. Lahoud, E. Maniv, M. S. Petrushevsky, M. Naamneh, A. Ribak, S. Wiedmann, L. Petaccia, Z. Salman, K. B. Chashka, Y. Dagan, and A. Kanigel, *Evolution of the Fermi surface of a doped topological insulator with carrier concentration*, Phys. Rev. B **88**, 195107 (2013).

[93] L. A. Wray, S.-Y. Xu, Y. Xia, Y. San Hor, D. Qian, A. V. Fedorov, H. Lin, A. Bansil, R. J. Cava, and M. Z. Hasan, *Observation of topological order in a superconducting doped topological insulator*, Nature Physics **6**, 855 (2010).

[94] S. Yonezawa, K. Tajiri, S. Nakata, Y. Nagai, Z. Wang, K. Segawa, Y. Ando, and Y. Maeno, *Thermodynamic evidence for nematic superconductivity in $Cu_xBi_2Se_3$*, Nature Physics **13**, 123 (2017).

[95] Y. Pan, A. Nikitin, G. Araizi, Y. Huang, Y. Matsushita, T. Naka, and A. De Visser, *Rotational symmetry breaking in the topological superconductor $Sr_xBi_2Se_3$ probed by upper-critical field experiments*, Scientific reports **6**, 28632 (2016).

[96] G. Du, Y. Li, J. Schneeloch, R. D. Zhong, G. Gu, H. Yang, H. Lin, and H.-H. Wen, *Superconductivity with two-fold symmetry in topological superconductor $Sr_xBi_2Se_3$*, Science China Physics, Mechanics & Astronomy **60**, 037411 (2017).

[97] M. Smylie, K. Willa, H. Claus, A. Koshelev, K. Song, W.-K. Kwok, Z. Islam, G. Gu, J. Schneeloch, R. Zhong *et al.*, *Superconducting and normal-state anisotropy of the doped topological insulator $Sr_{0.1}Bi_2Se_3$*, Scientific reports **8**, 1 (2018).

[98] A. Y. Kuntsevich, M. Bryzgalov, V. Prudkoglyad, V. Martovitskii, Y. G. Selivanov, and E. Chizhevskii, *Structural distortion behind the nematic superconductivity in $Sr_xBi_2Se_3$*, New Journal of Physics **20**, 103022 (2018).

[99] K. Willa, R. Willa, K. W. Song, G. D. Gu, J. A. Schneeloch, R. Zhong, A. E. Koshelev, W.-K. Kwok, and U. Welp, *Nanocalorimetric evidence for nematic superconductivity in the doped topological insulator* $Sr_{0.1}Bi_2Se_3$, Phys. Rev. B **98**, 184509 (2018).

[100] J. Shen, W.-Y. He, N. F. Q. Yuan, Z. Huang, C.-w. Cho, S. H. Lee, Y. San Hor, K. T. Law, and R. Lortz, *Nematic topological superconducting phase in Nb-doped* Bi_2Se_3, npj Quantum Materials **2**, 59 (2017).

[101] T. Asaba, B. J. Lawson, C. Tinsman, L. Chen, P. Corbae, G. Li, Y. Qiu, Y. S. Hor, L. Fu, and L. Li, *Rotational symmetry breaking in a trigonal superconductor Nb-doped* Bi_2Se_3, Phys. Rev. X **7**, 011009 (2017).

[102] A. M. Nikitin, Y. Pan, Y. K. Huang, T. Naka, and A. de Visser, *High-pressure study of the basal-plane anisotropy of the upper critical field of the topological superconductor* $Sr_xBi_2Se_3$, Phys. Rev. B **94**, 144516 (2016).

[103] M. P. Smylie, K. Willa, H. Claus, A. Snezhko, I. Martin, W.-K. Kwok, Y. Qiu, Y. S. Hor, E. Bokari, P. Niraula, A. Kayani, V. Mishra, and U. Welp, *Robust odd-parity superconductivity in the doped topological insulator* $Nb_xBi_2Se_3$, Phys. Rev. B **96**, 115145 (2017).

[104] S. Yonezawa, *Nematic superconductivity in doped* Bi_2Se_3 *topological superconductors*, Condensed Matter **4**, 2 (2019).

[105] S. Sasaki, M. Kriener, K. Segawa, K. Yada, Y. Tanaka, M. Sato, and Y. Ando, *Topological superconductivity in* $Cu_xBi_2Se_3$, Physical review letters **107**, 217001 (2011).

[106] J. W. Venderbos, V. Kozii, and L. Fu, *Odd-parity superconductors with two-component order parameters: Nematic and chiral, full gap, and Majorana node*, Physical Review B **94**, 180504 (2016).

[107] M. Hecker and J. Schmalian, *Vestigial nematic order and superconductivity in the doped topological insulator* $Cu_xBi_2Se_3$, npj Quantum Materials **3**, 1 (2018).

[108] L. Aslamazov and A. Larkin, *The influence of fluctuation pairing of electrons on the conductivity of normal metal*, Phys. Lett. A **26**, 238 (1968).

[109] L. Aslamazov and A. Larkin, *Effect of fluctuations on the properties of a superconductor above the critical temperature*, Sov. Phys. Solid State **10**, 875 (1968).

[110] H. Schmidt, *The onset of superconductivity in the time dependent Ginzburg-Landau theory*, Zeitschrift für Physik A Hadrons and nuclei **216**, 336 (1968).

[111] R. M. Fernandes, A. V. Chubukov, J. Knolle, I. Eremin, and J. Schmalian, *Preemptive nematic order, pseudogap, and orbital order in the iron pnictides*, Physical Review B **85**, 024534 (2012).

[112] R. M. Fernandes, P. P. Orth, and J. Schmalian, *Intertwined vestigial order in quantum materials: Nematicity and beyond*, Annual Review of Condensed Matter Physics **10**, 133 (2019).

[113] V. Ginzburg, *Some remarks on second order phase transitions and microscopic theory of ferroelectrics*, J. Exp. Theor. Phys. (1960).

[114] A. Levanyuk, *Contribution to the theory of light scattering near the second-order phase-transition points*, Sov. Phys. JETP (1959).

[115] J. P. Straley and M. E. Fisher, *Three-state Potts model and anomalous tricritical points*, Journal of Physics A: Mathematical, Nuclear and General **6**, 1310 (1973).

[116] Y. Gallais, R. Fernandes, I. Paul, L. Chauviere, Y.-X. Yang, M.-A. Méasson, M. Cazayous, A. Sacuto, D. Colson, and A. Forget, *Observation of incipient charge nematicity in* $Ba(Fe_{1-x}Co_x)_2As_2$, Physical review letters **111**, 267001 (2013).

[117] F. Kretzschmar, T. Böhm, U. Karahasanović, B. Muschler, A. Baum, D. Jost, J. Schmalian, S. Caprara, M. Grilli, C. Di Castro *et al.*, *Critical spin fluctuations and the origin of nematic order in* $Ba(Fe_{1-x}Co_x)_2As_2$, Nature Physics **12**, 560 (2016).

[118] R. A. Toupin, *Saint-venant's principle*, Archive for Rational Mechanics and Analysis **18**, 83 (1965).

[119] X. Gao, M. Zhou, Y. Cheng, and G. Ji, *First-principles study of structural, elastic, electronic and thermodynamic properties of topological insulator* Bi_2Se_3 *under pressure*, Philosophical Magazine **96**, 208 (2016).

[120] I. Kostylev, S. Yonezawa, Z. Wang, Y. Ando, and Y. Maeno, *Uniaxial-strain control of nematic superconductivity in* $Sr_xBi_2Se_3$.

[121] M. Yoshizawa, D. Kimura, T. Chiba, S. Simayi, Y. Nakanishi, K. Kihou, C.-H. Lee, A. Iyo, H. Eisaki, M. Nakajima *et al.*, *Structural quantum criticality and superconductivity in iron-based superconductor* $Ba(Fe_{1-x}Co_x)_2As_2$, Journal of the Physical Society of Japan **81**, 024604 (2012).

[122] A. E. Böhmer, P. Burger, F. Hardy, T. Wolf, P. Schweiss, R. Fromknecht, M. Reinecker, W. Schranz, and C. Meingast, *Nematic susceptibility of hole-doped and electron-doped* $BaFe_2As_2$ *iron-based superconductors from shear modulus measurements*, Phys. Rev. Lett. **112**, 047001 (2014).

[123] F. Weber, D. Parshall, L. Pintschovius, J.-P. Castellan, M. Kauth, M. Merz, T. Wolf, M. Schütt, J. Schmalian, R. M. Fernandes, and D. Reznik, *Soft phonons reveal the nematic correlation length in* $Ba(Fe_{0.94}Co_{0.06})_2As_2$, Phys. Rev. B **98**, 014516 (2018).

[124] A. A. Abrikosov, *On the magnetic properties of superconductors of the second group*, Sov. Phys. JETP **5**, 1174 (1957).

[125] W. Kleiner, L. Roth, and S. Autler, *Bulk solution of Ginzburg-Landau equations for type II superconductors: upper critical field region*, Physical Review **133**, A1226 (1964).

[126] D. F. Agterberg, *Square vortex lattices for two-component superconducting order parameters*, Phys. Rev. B **58**, 14484 (1998).

[127] D. F. Agterberg, *Vortex lattice structures of* Sr_2RuO_4, Phys. Rev. Lett. **80**, 5184 (1998).

[128] S. K. Sundaram and R. Joynt, *Superconducting* UPt_3 *in a magnetic field*, Phys. Rev. B **40**, 8780 (1989).

[129] I. Luk'yanchuk and M. Zhitomirsky, *Magnetic properties of unconventional superconductors*, arXiv preprint cond-mat/9501091 (1995).

[130] G. Volovik, *On the vortex lattice transition in heavy-fermionic UPt_3*, Journal of Physics C: Solid State Physics **21**, L221 (1988).

[131] M. Zhitomirskii, *Magnetic transitions in a superconducting UPt_3*, JETP LETTERS **49**, 379 (1989).

[132] J. W. Venderbos, V. Kozii, and L. Fu, *Identification of nematic superconductivity from the upper critical field*, Physical Review B **94**, 094522 (2016).

[133] A. Larkin, *Effect of collective excitations on the electrodynamics of superconductors*, Sov. Phys. JETP **19**, 1478 (1964).

[134] A. Leggett, *Quantum liquids: Bose condensation and Cooper pairing in condensed-matter systems*, Oxford University Press (2006).

[135] L. P. G. A. A. Abrikosov and I. E. Dzyaloshinski, *Methods of Quantum Field Theory in Statistical Physics*, DOVER PUBN INC (1975).

[136] Y. J. Uemura, G. M. Luke, B. J. Sternlieb, J. H. Brewer, J. F. Carolan, W. N. Hardy, R. Kadono, J. R. Kempton, R. F. Kiefl, S. R. Kreitzman, P. Mulhern, T. M. Riseman, D. L. Williams, B. X. Yang, S. Uchida, H. Takagi, J. Gopalakrishnan, A. W. Sleight, M. A. Subramanian, C. L. Chien, M. Z. Cieplak, G. Xiao, V. Y. Lee, B. W. Statt, C. E. Stronach, W. J. Kossler, and X. H. Yu, *Universal correlations between T_c and $\frac{n_s}{m^*}$ (carrier density over effective mass) in high-T_c cuprate superconductors*, Phys. Rev. Lett. **62**, 2317 (1989).

[137] V. Emery and S. Kivelson, *Importance of phase fluctuations in superconductors with small superfluid density*, Nature **374**, 434 (1995).

[138] J. Orenstein and A. Millis, *Advances in the physics of high-temperature superconductivity*, Science **288**, 468 (2000).

[139] R. Liang, D. A. Bonn, W. N. Hardy, and D. Broun, *Lower critical field and superfluid density of highly underdoped $YBa_2Cu_3O_{6+x}$ single crystals*, Phys. Rev. Lett. **94**, 117001 (2005).

[140] D. M. Broun, W. A. Huttema, P. J. Turner, S. Özcan, B. Morgan, R. Liang, W. N. Hardy, and D. A. Bonn, *Superfluid density in a highly underdoped $YBa_2Cu_3O_{6+y}$ superconductor*, Phys. Rev. Lett. **99**, 237003 (2007).

[141] P. A. Lee, N. Nagaosa, and X.-G. Wen, *Doping a Mott insulator: Physics of high-temperature superconductivity*, Reviews of modern physics **78**, 17 (2006).

[142] I. Hetel, T. R. Lemberger, and M. Randeria, *Quantum critical behaviour in the superfluid density of strongly underdoped ultrathin copper oxide films*, Nature Physics **3**, 700 (2007).

[143] B. Keimer, S. A. Kivelson, M. R. Norman, S. Uchida, and J. Zaanen, *From quantum matter to high-temperature superconductivity in copper oxides*, Nature **518**, 179 (2015).

[144] J. E. Sonier, *μSR studies of cuprate superconductors*, Journal of the Physical Society of Japan **85**, 091005 (2016).

[145] A. Steppke, L. Zhao, M. E. Barber, T. Scaffidi, F. Jerzembeck, H. Rosner, A. S. Gibbs, Y. Maeno, S. H. Simon, A. P. Mackenzie *et al.*, *Strong peak in T_c of Sr_2RuO_4 under uniaxial pressure*, Science **355**, eaaf9398 (2017).

[146] M. E. Barber, A. S. Gibbs, Y. Maeno, A. P. Mackenzie, and C. W. Hicks, *Resistivity in the vicinity of a van Hove singularity: Sr_2RuO_4 under uniaxial pressure*, Physical review letters **120**, 076602 (2018).

[147] C. A. Watson, A. S. Gibbs, A. P. Mackenzie, C. W. Hicks, and K. A. Moler, *Micron-scale measurements of low anisotropic strain response of local T_c in Sr_2RuO_4*, Physical Review B **98**, 094521 (2018).

[148] Y. Luo, A. Pustogow, P. Guzman, A. Dioguardi, S. M. Thomas, F. Ronning, N. Kikugawa, D. Sokolov, F. Jerzembeck, A. Mackenzie *et al.*, *Normal state O_{17} NMR studies of Sr_2RuO_4 under uniaxial stress*, Physical Review X **9**, 021044 (2019).

[149] A. Fujimori, A. Ino, T. Mizokawa, C. Kim, Z.-X. Shen, T. Sasagawa, T. Kimura, K. Kishio, M. Takaba, K. Tamasaku *et al.*, *Chemical potential shift, density of states and Fermi surfaces in overdoped and underdoped $La_{2-x}Sr_xCuO_4$*, Journal of Physics and Chemistry of Solids **59**, 1892 (1998).

[150] A. Ino, C. Kim, T. Mizokawa, Z.-X. Shen, A. Fujimori, M. Takaba, K. Tamasaku, H. Eisaki, and S. Uchida, *Fermi surface and band dispersion in $La_{2-x}Sr_xCuO_4$*, Journal of the Physical Society of Japan **68**, 1496 (1999).

[151] A. Ino, C. Kim, M. Nakamura, T. Yoshida, T. Mizokawa, A. Fujimori, Z.-X. Shen, T. Kakeshita, H. Eisaki, and S. Uchida, *Doping-dependent evolution of the electronic structure of $La_{2-x}Sr_xCuO_4$ in the superconducting and metallic phases*, Physical Review B **65**, 094504 (2002).

[152] T. Kondo, T. Takeuchi, T. Yokoya, S. Tsuda, S. Shin, and U. Mizutani, *Hole-concentration dependence of band structure in $(Bi, Pb)_2(Sr, La)_2CuO_{6+\delta}$ determined by the angle-resolved photoemission spectroscopy*, ICESS-9 Proceedings of the 9th International Conference on Electronic Spectroscopy and Structure **137-140**, 663 (2004).

[153] T. Yoshida, X. Zhou, K. Tanaka, W. Yang, Z. Hussain, Z.-X. Shen, A. Fujimori, S. Sahrakorpi, M. Lindroos, R. Markiewicz *et al.*, *Systematic doping evolution of the underlying Fermi surface of $La_{2-x}Sr_xCu_{O4}$*, Physical Review B **74**, 224510 (2006).

[154] A. Kaminski, S. Rosenkranz, H. Fretwell, M. Norman, M. Randeria, J. Campuzano, J. Park, Z. Li, and H. Raffy, *Change of Fermi-surface topology in $Bi_2Sr_2CaCu_2O_{8+\delta}$ with doping*, Physical Review B **73**, 174511 (2006).

[155] M. Platé, J. Mottershead, I. Elfimov, D. Peets, R. Liang, D. Bonn, W. Hardy, S. Chiuzbaian, M. Falub, M. Shi *et al.*, *Fermi surface and quasiparticle excitations of overdoped $Tl_2Ba_2CuO_{6+\delta}$*, Physical review letters **95**, 077001 (2005).

[156] A. Chubukov and P. J. Hirschfeld, *Iron-based*, Physics today **68**, 46 (2015).

[157] C. Niedermayer, C. Bernhard, U. Binninger, H. Glückler, J. Tallon, E. Ansaldo, and J. Budnick, *Muon spin rotation study of the correlation between T_c and n_s/m^* in overdoped $Tl_2Ba_2CuO_{6+\delta}$*, Physical review letters **71**, 1764 (1993).

[158] J. L. Tallon, J. W. Loram, J. R. Cooper, C. Panagopoulos, and C. Bernhard, *Superfluid density in cuprate high-T_c superconductors: A new paradigm*, Phys. Rev. B **68**, 180501 (2003).

[159] T. Lemberger, I. Hetel, A. Tsukada, and M. Naito, *Anomalously sharp superconducting transitions in overdoped $La_{2-x}Sr_xCuO_4$ films*, Physical Review B **82**, 214513 (2010).

[160] T. Lemberger, I. Hetel, A. Tsukada, M. Naito, and M. Randeria, *Superconductor-to-metal quantum phase transition in overdoped $La_{2-x}Sr_xCuO_4$*, Physical Review B **83**, 140507 (2011).

[161] N. Lee-Hone, V. Mishra, D. Broun, and P. Hirschfeld, *Optical conductivity of overdoped cuprate superconductors: Application to $La_{2-x}Sr_xCuO_4$*, Physical Review B **98**, 054506 (2018).

[162] N. R. Lee-Hone, J. S. Dodge, and D. M. Broun, *Disorder and superfluid density in overdoped cuprate superconductors*, Phys. Rev. B **96**, 024501 (2017).

[163] J. Loram, J. Luo, J. Cooper, W. Liang, and J. Tallon, *Evidence on the pseudogap and condensate from the electronic specific heat*, Journal of Physics and Chemistry of Solids **62**, 59 (2001).

[164] B. Spivak, P. Oreto, and S. Kivelson, *Theory of quantum metal to superconductor transitions in highly conducting systems*, Physical Review B **77**, 214523 (2008).

[165] M. E. Fisher, M. N. Barber, and D. Jasnow, *Helicity modulus, superfluidity, and scaling in isotropic systems*, Phys. Rev. A **8**, 1111 (1973).

[166] E. Taylor, A. Griffin, N. Fukushima, and Y. Ohashi, *Pairing fluctuations and the superfluid density through the BCS-BEC crossover*, Phys. Rev. A **74**, 063626 (2006).

[167] N. Fukushima, Y. Ohashi, E. Taylor, and A. Griffin, *Superfluid density and condensate fraction in the BCS-BEC crossover regime at finite temperatures*, Phys. Rev. A **75**, 033609 (2007).

[168] A. Paramekanti, M. Randeria, T. V. Ramakrishnan, and S. S. Mandal, *Effective actions and phase fluctuations in d-wave superconductors*, Phys. Rev. B **62**, 6786 (2000).

[169] V. N. Popov, *Functional Integrals and Collective Excitations*, Cambridge University Press (2011).

[170] D. J. Scalapino, S. R. White, and S. Zhang, *Insulator, metal, or superconductor: The criteria*, Physical Review B **47**, 7995 (1993).

[171] S. Yip and A. Garg, *Superconducting states of reduced symmetry: General order parameters and physical implications*, Physical Review B **48**, 3304 (1993).

[172] P. Hlobil, B. Narozhny, and J. Schmalian, *Strong coupling behavior of the neutron resonance mode in unconventional superconductors*, Physical Review B **88**, 205104 (2013).

[173] W. Greiner and J. Reinhardt, *Field Quantization*, Springer-Verlag Berlin Heidelberg (1996).

Acknowledgements

At last, I have the pleasure to thank everybody who made this thesis possible.

First of all, I have to mention Jörg Schmalian who made this entire endeavor possible in the first place. Without his ingenuity, his keen mind, his willingness to help, his encouragements in times of subtle frustrations, his humorous style (and his money), I would probably not have gotten this far. Thank you very much.

Second in line would be my second referee Markus Garst, who I thank for accepting this position, and who—I hope—is enjoying reading through the first chapters at the time of this writing.

I also want to express my deep gratitude to Erez Berg, who made my research stay at the University of Chicago possible, and who shared his ingenious and inspiring way of doing physics. Thanks for that. On the same note, I want to appreciate the financial support I received from the Karlsruhe House of Young Scientist (KHYS) as part of the program 'Research Travel Grant'.

Over the years, I have received so much intellectual support from so many present and former members of the Institute for Condensed Matter Physics, which I am sincerely thankful for. While I could mention the entire research group, I want to emphasize a few chosen ones who contributed vastly to the refinement of my physical comprehension: In the early days Bhilahari Jeevanesan and Mathias Scheurer embodied some kind of physical mentors—thanks for that. I have to thank Mareike Hoyer for her guidance, her technical finesse and her humorous manner. I thank Tim Ludwig, Markus Klug, Egor Kiselev, Matthias Bard and Lars Lauke for all the years we spent together, and the helpful discussions we had over one topic or the other. And, I thank Davide Valentinis and Roland Willa for the stimulating conversation and their sound advice.

On the note of proofreading, I have to express my gratitude to Tim Ludwig, Davide Valentinis, Kristin Willa, and especially to Roland Willa.

For taking care of my physical shape, I have to thank the members of the 'TKM Sport-team' Nefta Kanilmaz, Alexander Gawrilow, Mareike Hoyer, Matthias Bard and Sven Danz.

There are so many more people I could mention, which I do not have the space for. Yet, I hope they sense my appreciation.

At last, I have to thank my family for their eternal support and affection: my parents Bettina and Michael, my brother Christian and all of my grandparents. In particular, I want to mention Ottmar, who I owe so much for what I have become. Thank you, thank you all!